

NUCLEAR WASTE GLASS LEACHING  
IN A SIMULATED GRANITE REPOSITORY

BY

BINGFU ZHU

A DISSERTATION PRESENTED TO THE GRADUATE SCHOOL  
OF THE UNIVERSITY OF FLORIDA IN  
PARTIAL FULFILLMENT OF THE REQUIREMENTS  
FOR THE DEGREE OF DOCTOR OF PHILOSOPHY

UNIVERSITY OF FLORIDA

1987

To my mother and late father

## ACKNOWLEDGMENTS

The author acknowledges his gratitude to Dr. David E. Clark for guidance and encouragement throughout his research. He also is greatly indebted to Drs. Larry L. Hench, Lars Werme and George G. Wicks for their advice and encouragement. The author thanks Drs. Alexander Lodding, Christopher D. Batich, Stanley R. Bates and Gar B. Hoflund for their timely suggestions, helpful discussions and review of this dissertation.

The author wishes to thank Dr. Cheng Jijian for introducing him to the field of chemical durability of glasses. Without his guidance, the fulfillment of this research could not be possible. He also thanks his wife, Jisi, for her support and encouragement.

## TABLE OF CONTENTS

	<u>Page</u>
ACKNOWLEDGMENTS.....	iii
LIST OF TABLES.....	vi
LIST OF FIGURES.....	viii
ABSTRACT.....	xv
 CHAPTERS	
I INTRODUCTION.....	1
II PREVIOUS WORK ON NUCLEAR WASTE GLASS LEACHING.....	13
Laboratory Studies.....	13
General Considerations.....	13
Effect of Flow Rate.....	17
Surface Film Formation.....	20
Molecular Mechanism of Aqueous Dissolution.....	25
Systems Interaction Tests.....	29
Burial Studies.....	33
III RESEARCH OBJECTIVES, APPROACH AND SUMMARY OF CONCLUSIONS.....	36
Research Objectives and Approach.....	36
Major Conclusions.....	37
IV MATERIALS AND METHODS.....	39
Glass Compositions and Characterization.....	39
Burial Samples.....	39
Glass Quality.....	44
Laboratory Samples.....	48
Stripa Field Tests.....	48
Sample Assemblies, Minicans and Pineapple Slices...	48
Stripa Repository.....	51
Burial and Retrieval.....	55
Disadvantage of the Burial Test Method.....	60
Similar Tests Being Used in MIIT Studies at WIPP...	61
Laboratory Tests of Simulated Corrosion.....	62



	Analytical Techniques.....	67
	Solid State Analyses.....	67
	Solution Analyses.....	85
V	TEST RESULTS.....	87
	Field Test Results.....	87
	General Observation.....	87
	Results with ABS Glasses.....	89
	Results with SRL Glasses.....	116
	Effect of Glass Heterogeneities.....	125
	Laboratory Test Results.....	135
	Modified MCC-1 Static Leach Tests.....	135
	Single-Pass Flow Tests and Static Tests Using Rock Cups.....	140
VI	DISCUSSION.....	152
	ABS Glasses.....	152
	SRL Glasses.....	161
	A Model of Alkali Borosilicate Glass Leaching.....	168
	Effect of Glass Composition.....	179
	Influence of Repository Variables.....	185
	Ground Water Chemistry.....	185
	Effects of Repository Materials.....	188
	Effect of Temperature.....	193
	Comparison of Field and Laboratory Test Results.....	193
VII	SUMMARY.....	197
	REFERENCES.....	203
	BIOGRAPHICAL SKETCH.....	212

## LIST OF TABLES

<u>Table</u>	<u>Page</u>
1-1 Quantity and Radioactivity of High-Level Nuclear Wastes in Some Developed Countries.....	5
1-2 Candidate Waste Forms Considered for Geologic Disposal of High-Level Waste.....	8
4-1 Nominal Waste Glass Compositions (wt%) Used in the Stripa Burial.....	40
4-2 Sample Matrix of the Stripa Burial Tests.....	45
4-3 Variations in Spectral Characteristics of SRL Waste Glasses.....	46
4-4 Nominal Composition of Black Frit 165-Mobay Glass.....	49
4-5 Average Major/Minor Chemical and Mineral Constituents in Stripa Granite.....	54
4-6 Ground Water Composition and pH Measured in this Study within the 1-month Test Hole at Stripa. Concentration mg/L.....	58
4-7 Ground Water Composition for the Stripa Granite, Literature Values.....	59
4-8 Sample Matrix of the Laboratory Tests.....	68
4-9 Characteristics of Analytical Techniques.....	70
5-1 Composition of Ground Water Collected from the Boreholes where SRL Glass Pineapple Slice Assemblies Had Been Buried.....	91
5-2 Gram•Atoms of Elements Remaining at Gel Mid-Plateau and Outer Region of the Altered Glass Surface Based on 100 Gram•Atoms of Unleached ABS 118 Glass after 12-Month, 90°C Burial in Stripa.....	119

5-3	Relative Concentrations (Ratio to Si) at the Black Frit 165-Mobay Glass Surface after Static Leaching in the Rock Cup Test. Data Are from EDS Analysis.....	147
6-1	90°C Glass Leach Rates During 12- to 31-Month Period ( $\mu\text{m}/\text{year}$ ).....	155
6-2	SIMS Compositional Analysis of Glass/Glass, Glass/ Bentonite and Glass/Granite Interfaces for ABS 39, ABS 41 and ABS 118 after 12-Month, 90°C Stripa Burial (Gram•atoms Remaining Based on 100 Gram•atoms of Unleached Glass).....	158
6-3	Coordination Number and Bond Strength of Most Oxides in Alkali Borosilicate Nuclear Waste Glasses.....	170
6-4	90°C ABS Glass Leach Rates During 7-12 Month Period.....	191
7-1	Estimated Boron Depletion Depths ( $\mu\text{m}$ ) after 300 Years of the Thermal Period of Storage for the Six Nuclear Waste Glasses.....	201
7-2	Estimated Boron Depletion Depths ( $\mu\text{m}$ ) after $10^5$ Years of Storage for the Glass/Glass Interfaces of SRL Simulated Nuclear Waste Glasses.....	202

## LIST OF FIGURES

<u>Figure</u>	<u>Page</u>
1-1	Flow diagram showing the reprocessing of the spent nuclear fuel.....2
1-2	Schematic showing the glass waste form in a geological repository.....6
1-3	Glass structure containing dissolved wastes.....11
2-1	Research activities on leaching of nuclear waste glass.....14
2-2	Plot showing the total mass loss per unit area as a function of flow rate.....19
2-3	The five types of glass surfaces and six surface conditions resulting from glass-environment interactions...21
2-4	Ratio of normalized solubility to $NL_{Si}$ (20 g/m <sup>2</sup> ) for $CaCO_3$ , $SrCO_3$ , $Nd(OH)_3$ , $Fe(OH)_3$ and $Zn(OH)_2$ in MCC-1 28-day test at 90°C in solutions of different pH.....26
2-5	The Si leachability of a borosilicate glass immersed in a 5-day static 23°C solution buffered to various pH values.....27
2-6	Calculated Si concentrations in the surface layer and bulk solution based on the surface layer diffusion and pH as a function of leaching time. A diffusion coefficient of $10^{-9}$ cm <sup>2</sup> /sec was assumed.....30
4-1	Pineapple slices of glass, granite, stainless steel, Ti, Pb and compacted bentonite before burial.....43
4-2	Representative FT-IRRS spectra of SRL glass pineapple slices before burial.....47
4-3	A minican assembly.....50
4-4	A typical pineapple slice assembly.....52

4-5	Seven preburial pineapple slice assemblies with different sample stacking sequences for SRL simulated nuclear waste glasses.....	53
4-6	Location within Stripa where SRL samples were buried.....	56
4-7	Diagram illustrating the position of the samples in the Stripa mine during burial.....	57
4-8	Schematic of experimental configuration of static leach test.....	63
4-9	A corrosion cell in the flowing test.....	65
4-10	Schematic of experimental configuration of continuous flow test.....	66
4-11	Sampling depths with various techniques used in this study.....	69
4-12	Light micrograph of SRL 131 + 29.8% TDS glass with crystallites (100X).....	72
4-13	Light micrograph of a typical glass surface after polishing to 600 grit surface finish (100X).....	73
4-14	FT-IRRS analysis of SRL 165 + 29.8% TDS glass/glass interface prior to and after 2-year burial in Stripa.....	76
4-15	SEM micrograph of a typical glass surface after polishing to 600 grit prior to leaching.....	77
4-16	EDS analysis of an uncorroded SRL 131 + 29.8% TDS glass surface.....	78
4-17	SIMS depth profiles of ABS 118 glass/glass interface after 1-year, 90°C burial in Stripa. The atomic concentrations of all cations (except H) are summed up to 100%.....	80
4-18	SIMS depth profiles of ABS 118 glass/glass interface after 1-year, 90°C burial in Stripa. Data are presented as gram•atoms of various cations remaining in the leach layer at certain depth based on 100 gram•atoms of unleached glass.....	83
5-1	A typical assembly after burial in Stripa mine. Bentonite coating can be observed on the outer surface due to bentonite swelling.....	88

5-2	Schematic of glass/glass interface illustrating several types of surface areas resulting from water and/or bentonite intrusion.....	90
5-3	FT-IRRS spectra of glass ABS 39 (a) and ABS 41 (b) before and after 31-month, 90°C Stripa burial.....	92
5-4	SIMS depth profiles for (a) ABS 39 (Al-corrected) and (b) ABS 41 (Si-corrected) after 31-month, 90°C Stripa burial.....	94
5-5	Light micrographs (100X) of glass 39 (a) glass/glass, (b) glass/granite and (c) glass/bentonite interfaces and glass ABS 41 (d) glass/glass, (e) glass/granite and (f) glass/bentonite interfaces after 31-month, 90°C Stripa burial.....	97
5-6	SIMS depth profiles of boron for glass ABS 39 (a) and glass ABS 41 (b) after 31-month, 90°C Stripa burial....	99
5-7	FT-IRRS spectra of glass/glass, glass/granite and glass/bentonite interfaces for nuclear waste glass ABS 118 buried in Stripa at 90°C for (a) 2 months and (b) 12 months. Also shown is the spectrum of a preburial glass surface.....	100
5-8	Light micrographs (100X) of glass ABS 118 after 2-month burial, (a) glass/glass, (b) glass granite, and (c) glass/bentonite interfaces, and after 12-month burial, (d) glass/glass, (e) glass/granite, and (f) glass/bentonite interfaces at 90°C in Stripa.....	102
5-9	SIMS depth compositional profiles of (a) B; (b) Cs, Sr; and (c) Fe, U for ABS 118 glass/glass interface after 2- and 12-month, 90°C burial in Stripa. The data have been corrected using Al concentration.....	103
5-10	SIMS depth compositional profiles of (a) Si, H, Na, Li, K; (b) LD (including La, Ce, Pr, Nd and Y), P, Sn; (c) Ca, Zn, Ba; and (d) Zr, Mo, Ni, Cr, Si for ABS 118 glass/glass interface after 12-month, 90°C burial in Stripa.....	105
5-11	FT-IRRS analysis of ABS 118 glass/Pb, glass/Ti and glass/Cu interfaces after (a) 2-month and (b) 12-month 90°C burial in Stripa.....	108



5-12	Light micrographs of ABS 118 glass surfaces after 90°C Stripa burial for 2 months, (a) glass/Pb, (b) glass/Cu, and (c) glass/Ti interfaces, and for 12 months, (d) glass/Pb, (e) glass/Cu, and (f) glass/Ti interfaces.....	109
5-13	Boron profiles of ABS 118 (a) glass/Pb, (b) glass/Cu and (c) glass/Ti interfaces after 2- and 12-month, 90°C burial at Stripa.....	111
5-14	Cs and Sr profiles of ABS 118 (a) glass/Pb, (b) glass/Cu and (c) glass/Ti interfaces after 2- and 12-month, 90°C burial at Stripa.....	112
5-15	Fe and U profiles of ABS 118 (a) glass/Pb, (b) glass/Cu and (c) glass/Ti interfaces after 2- and 12-month, 90°C burial at Stripa.....	113
5-16	SIMS analysis of ABS 118 (a) glass/Pb, (b) glass/Cu and (c) glass/Ti interfaces after 12-month, 90°C Stripa burial, Si, H, Li, Na and K profiles.....	114
5-17	SIMS analysis of ABS 118 (a) glass/Pb, (b) glass/Cu and (c) glass/Ti interfaces after 12-month, 90°C Stripa burial, Ca, Zn and Ba profiles.....	115
5-18	SIMS analysis of ABS 118 (a) glass/Pb, (b) glass/Cu and (c) glass/Ti interfaces after 12-month, 90°C Stripa burial, LD, Pb, Cu and Ti profiles. LD stands for the sum of La, Ce, Pr, Nd and Y.....	117
5-19	SIMS analysis of ABS 118 (a) glass/Pb, (b) glass/Cu and (c) glass/Ti interfaces after 12-month, 90°C Stripa burial, Zr, Mo, Ni and Cr profiles.....	118
5-20	RBS analysis of ABS 118 glass/Pb, glass/Ti and glass/Cu interfaces after 12-month, 90°C burial in Stripa.....	120
5-21	FT-IRRS analysis of the glass/glass interface for three SRL glasses after 2 years of burial in Stripa.....	121
5-22	SEM micrographs of glass surfaces in contact with glass of the same composition during 2-year burial at 90°C in Stripa: (a) SRL 131 + 29.8% TDS, (b) SRL 165 + 29.8% TDS, (c) SRL 131 + 35% TDS and (d) an uncorroded glass surface.....	123
5-23	SIMS depth profiles of SRL glass surfaces after 2-year Stripa burial at 90°C.....	124

5-24	X-ray diffraction pattern for powders prepared from devitrified SRL 131 + 29.8% TDS glass.....	126
5-25	SEM-EDS analysis of preburial SRL 131 + 29.8% TDS glass: (a) homogeneous glass surface and (b) partially devitrified glass surface.....	127
5-26	SEM analysis of SRL 131 + 29.8% TDS glass surfaces in contact with bentonite, Stripa burial at 90°C: (a) homogeneous glass, 1-month burial; (b) partially devitrified glass, 1-month burial; (c) partially devitrified glass, 3-month burial; and (d) partially devitrified glass, 6-month burial.....	129
5-27	FT-IRRS analysis of SRL 131 + 29.8% TDS glass surfaces in contact with bentonite, Stripa burial at 90°C: (a) homogeneous glass, 1-month burial; and partially devitrified glass (b) 1-month burial; (c) 3-month burial; and (d) 6-month burial.....	131
5-28	EDS analysis of SRL 131 + 29.8% TDS glass surfaces in contact with bentonite, Stripa burial at 90°C: (a) homogeneous glass, 1-month burial; and glass matrix of partially devitrified glass, (b) 1-month burial; (c) 3-month burial; and (d) 6-month burial.....	133
5-29	EDS analysis of crystal areas of partially devitrified SRL 131 + 29.8% TDS glass surfaces in contact with bentonite, Stripa burial at 90°C: (a) for 1 month, (b) for 3 months and (c) for 6 months.....	134
5-30	FT-IRRS analysis of SRL 165 + 29.8% TDS glass before and after leaching for 28 days at 90°C in (a) deionized water with SA/V = 0.1 cm <sup>-1</sup> , (b) Stripa ground water with SA/V = 0.1 cm <sup>-1</sup> , (c) Stripa ground water with SA/V = 1.0 cm <sup>-1</sup> and (d) saturated Stripa ground water with SA/V = 0.1 cm <sup>-1</sup> . Also shown is a spectrum for the glass/glass interface after 3-month Stripa burial.....	136
5-31	SIMS analysis of SRL 165 + 29.8% TDS waste, laboratory-corroded, 1 month 90°C in Stripa water with SA/V = 1.0 cm <sup>-1</sup> .....	139
5-32	Solution pH vs time for Black Frit 165-Mobay glass corroded under static and flow conditions.....	141
5-33	Concentrations of Si, B, Al and Li in the single pass flowing ground water at 0.3 ml/hr as a function of leaching time for Black Frit 165-Mobay glass samples.....	142



5-34	Normalized leach rates of Li, B and Si as a function of time under flowing (at 0.3 ml/hr) conditions for Black Frit 165-Mobay glass with SA/V = 1.0 cm <sup>-1</sup> . Also shown are the weight losses for glass samples leached under static and flow conditions with SA/V = 1.0 cm <sup>-1</sup> .....	144
5-35	EDS analysis of Black Frit 165-Mobay glass leached in the rock cup test at 90°C with SA/V = 1.0 cm <sup>-1</sup> in ground water under static conditions.....	145
5-36	FT-IRRS analysis of Black Frit 165-Mobay glass leached in the granite rock cup test at 90°C under static conditions with SA/V = 1.0 cm <sup>-1</sup> .....	148
5-37	SIMS depth profiles for Frit 165-Mobay glass leached in the granite rock cup tests at 90°C with SA/V = 1.0 cm <sup>-1</sup> , (a) under static conditions and (b) under flow conditions (0.3 mL/hr).....	150
6-1	Time dependence of reaction layer thickness for glass ABS 39 (a) and ABS 41 (b) after 31-month, 90°C Stripa burial.....	153
6-2	Boron depletion depth vs burial time for the glass/glass, glass/granite and glass/bentonite interfaces. Three ABS glasses are compared.....	160
6-3	Penetration depth as a function of leaching time for the SRL glasses either buried in contact with glass, stainless steel, granite or bentonite in Stripa mine, or leached in Stripa ground water with SA/V = 0.1 or 1.0 cm <sup>-1</sup> in laboratory.....	162
6-4	SIMS compositional profiles of SRL 165 + 29.8% TDS glass/bentonite interface after 24-month, 90°C burial in Stripa.....	165
6-5	Five modes of corrosion in partially devitrified alkali borosilicate simulated nuclear waste glass: (a) leaching of the glass matrix; (b) enhanced attack of the glass-crystal interface; (c) pitting of the polycrystalline phase at grain boundaries; (d) surface films enriched in the less soluble multivalent species; and (e) crystallite stripping.....	167
6-6	Stability of B <sub>2</sub> O <sub>3</sub> and SiO <sub>2</sub> in aqueous solution at 25°C as a function of pH.....	173

6-7	Schematics showing (a) the altered alkali borosilicate glass surface and the compositional profiles after leaching based on the model proposed in this dissertation and (b) the altered glass surface based on Grambow's model.....	176
6-8	The density index curve for three SRL glasses after 2-year burial in Stripa at 90°C.....	180
6-9	Compositional ternary diagram showing the direction of increasing boron depletion depth. $R_2O$ represents alkali metal oxide, $Me_2O_3$ represents $Al_2O_3$ and $Fe_2O_3$ , and WP stands for waste products.....	181
6-10	The boron depletion depth as a function of $(SiO_2 + Al_2O_3)/(R_2O + B_2O_3)$ wt ratio in glasses.....	183
6-11	Schematic illustrating the relationship between concentration, contact time and leach rate.....	186
6-12	The boron depletion depth as a function of burial time for ABS 118 glass/glass, glass/granite, glass/Pb, glass/Cu and glass/Ti interfaces after 90°C Stripa burial.....	190
6-13	SIMS compositional profiles of SRL 165 + 29.8% TDS glass/glass interface after 8-10°C Stripa burial for 2 years.....	194

Abstract of Dissertation Presented to the Graduate School  
of the University of Florida in Partial Fulfillment of the  
Requirements for the Degree of Doctor of Philosophy

NUCLEAR WASTE GLASS LEACHING  
IN A SIMULATED GRANITE REPOSITORY

BY

BINGFU ZHU

May 1987

Chairman: Dr. David E. Clark  
Cochairman: Dr. Larry L. Hench  
Major Department: Materials Science and Engineering

Burial experiments of three Savannah River Laboratory (SRL) and three Swedish alkali borosilicate (ABS) simulated nuclear waste glasses were conducted to evaluate the resistance of these glasses to ground water attack under repository-like conditions. Glass samples were buried in the boreholes at a depth of about 350 meters below the surface in the Stripa granite at either ambient mine temperature (8-10°C) or 90°C. Included in the same boreholes were other potential waste package components. Glasses were also leached in the Stripa ground water contained in a leaching vessel under the laboratory simulation conditions. The leached surfaces were characterized using SEM-EDS, FT-IRRS, SIMS, RBS and optical microscopy. Differences in glass leach rate were observed among the six compositions with SRL 165 + 29.8% TDS being the lowest. Results show that durabilities of the SRL composite nuclear waste glasses

were increased by approximately six times when frit 131 was substituted by frit 165. An increase of waste loading of SRL 131 glass from 29.8 wt% to 35 wt% decreases the leachability by a factor of 2.

The leach rates of buried samples based on boron extraction at 90°C ranged from 0.3-3  $\mu\text{m}/\text{year}$  for the glass/glass interfaces of all glass formulations. These values are at least two orders of magnitude lower than those for glasses leached using MCC-1 static leaching procedures and deionized water. The Stripa repository-like conditions can be simulated in the laboratory using Stripa ground water and high SA/V ratios ( $\geq 1.0 \text{ cm}^{-1}$ ). Comparison of the laboratory test results with field test results indicates that the leaching mechanisms were similar under these test conditions. One of the advantages of the laboratory simulation testing is saving of time since glass leaches faster under the laboratory-controlled conditions than under field-leach environment.

A model, based on glass structure and thermodynamic considerations, is proposed to describe alkali borosilicate glass leaching under repository-like conditions.

## CHAPTER I INTRODUCTION

The increasing use of nuclear energy for electric power generation and the expanding application of radioisotopes in various fields are inevitably associated with the production of growing amounts of nuclear wastes. These wastes, which result from fabrication, use and reprocessing of nuclear fuels, contain a variety of hazardous materials. Hence, their disposal must ensure a low probability of human contact.

Major types of nuclear wastes include high-level (HLW), transuranic (TRU), low-level (LLW), uranium mine and mill tailings, decontamination and decommissioning wastes, and gaseous effluents. High-level wastes are usually further divided into those resulting from either weapons production (defense waste) or commercial power reactors.

Upon removal from the nuclear reactors, the depleted fuel is stored under water for several months to permit the short-lived fission products to decay. One of the options is to send the fuel pellets to a chemical-reprocessing plant to recover the uranium and plutonium, which are then available to make new fuel [1]. As shown in Fig. 1-1, the reprocessing generally consists of dismantling reactor fuel in a manner that permits dissolution of the core material of the nuclear fuel pellets without dissolving their

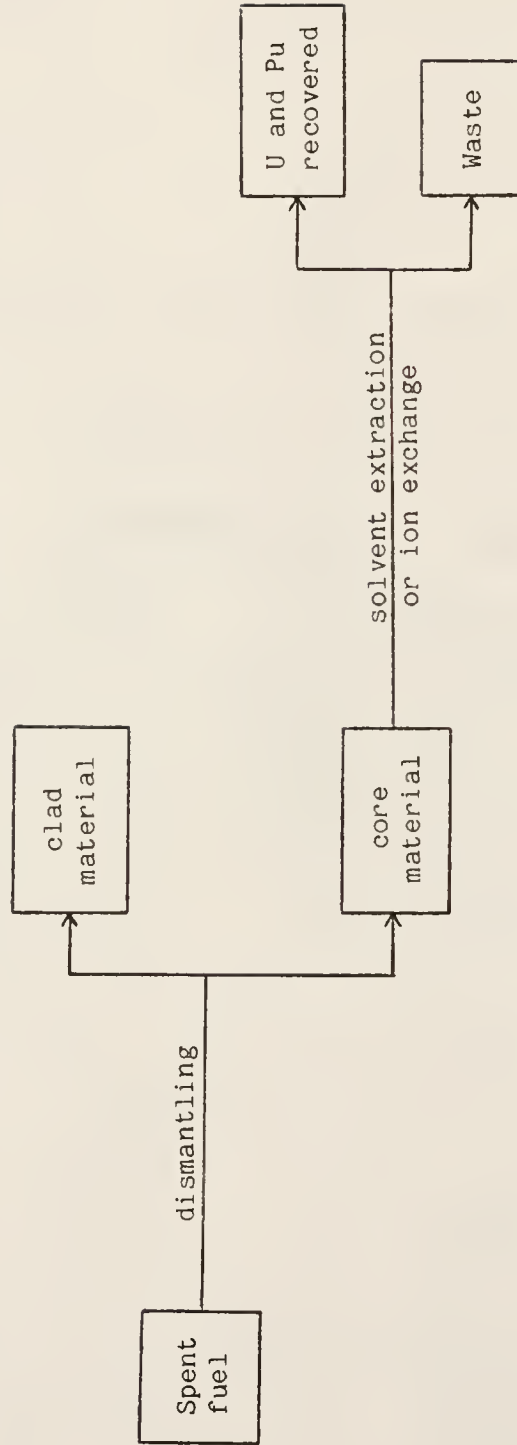


Fig. 1-1. Flow diagram showing the reprocessing of the spent nuclear fuel [1].

corrosion resistant cladding [1]. The resulting solution is subsequently treated by several cycles of solvent extraction or ion exchange to recover, separate and purify the residual uranium and plutonium. At Savannah River Plant, Aiken, South Carolina; in Hanford Reservation, Richland, Washington; and in Idaho National Engineering Laboratory, outskirts of Idaho Falls, Idaho, there are large facilities owned and operated by the United States government that reprocess spent fuel coming out of the reactors used for making weapons. However, only one commercial reprocessing plant, at West Valley, New York, was ever operated in the U.S. Currently there is no reprocessing of spent fuel coming out of commercial reactors in the United States.

High-level nuclear wastes, whether reprocessed or not, contain virtually all of the nonvolatile fission products, small amounts of uranium and plutonium and all the other actinides formed by transmutation of the uranium and plutonium in the reactors. They can be generally characterized by their very intense, penetrating radiation and their high heat-generation rates. The fission products and actinides are the major concern since they undergo spontaneous decay and emit radioactivity in the form of  $\alpha$  and  $\beta$  particles, and  $\gamma$ -rays. The two elements,  $\text{Cs}^{137}$  and  $\text{Sr}^{90}$ , are of most concern due to the relatively high concentration in the waste and their decay time (i.e., ~ 30 years)[2] and concern for their incorporation in body tissues, especially  $\text{Sr}^{90}$  in bones. When decaying, they give off both heat and radioactivity for about 700 years [2]. The actinides including U also emit radioactivity and



heat during decay--for example, about 25,000 years for  $\text{Pu}^{239}$ , the most abundant transuranium actinide [2].

Table 1-1 lists the quantity and radioactivity of high-level nuclear wastes in some developed countries [3-5]. There are over  $3 \times 10^5 \text{ m}^3$  defense HLW stored at three government sites in the United States. These defense wastes contain  $1.6 \times 10^9$  Curies of radioactivity (1 Curie =  $3.7 \times 10^{10}$  disintegrations per second)[3]. There are over  $2 \times 10^5 \text{ m}^3$  commercial HLW containing about  $1.1 \times 10^{10}$  Curies of radioactivity in the form of spent fuel in the United States [3]. The total amount of HLW in Europe, Japan, the United States and U.S.S.R. is estimated to be  $10.2 \times 10^5 \text{ m}^3$  containing about  $2.9 \times 10^{10}$  Curies.

One method for disposal of HLW is immobilization in a high-integrity solid waste form followed by emplacement in a mined cavern at a suitable geologic repository [6]. As shown in Fig. 1-2, this disposal system relies on multiple barriers to prevent the release of radionuclides. The system includes

- (1) solid waste form, a combination of host material (glass in the illustrated case) and waste. The waste is incorporated homogeneously in the host material to reduce the risk for dispersion.
- (2) a metal canister such as stainless steel, which is welded to form a hermetically sealed container after the waste form is placed in it.
- (3) a metallic overpack, of such materials as e.g., mild steel, ductile iron, pure titanium, or titanium alloy (Ti Code-12),



Table 1-1. Quantity and Radioactivity of High-Level Nuclear Wastes in Some Developed Countries.

	Form	Radioactivity (Ci)	Quantity (m <sup>3</sup> )	Source
U.S. Defense	slurry sludge	$1.6 \times 10^9$	$3 \times 10^5$	[3]
U.S. Commercial	spent fuel, sludge (West Valley, NY)	$1.1 \times 10^{10}$	$2 \times 10^5$	[3,4]
Europe Commercial	spent fuel	-	$2 \times 10^5$	estimated
Japan Commercial	spent fuel	-	$7 \times 10^4$	estimated
U.S.S.R.	slurry sludge	-	$2.5 \times 10^5$	estimated
Total		$2.9 \times 10^{10}$	$10.2 \times 10^5$	[5]

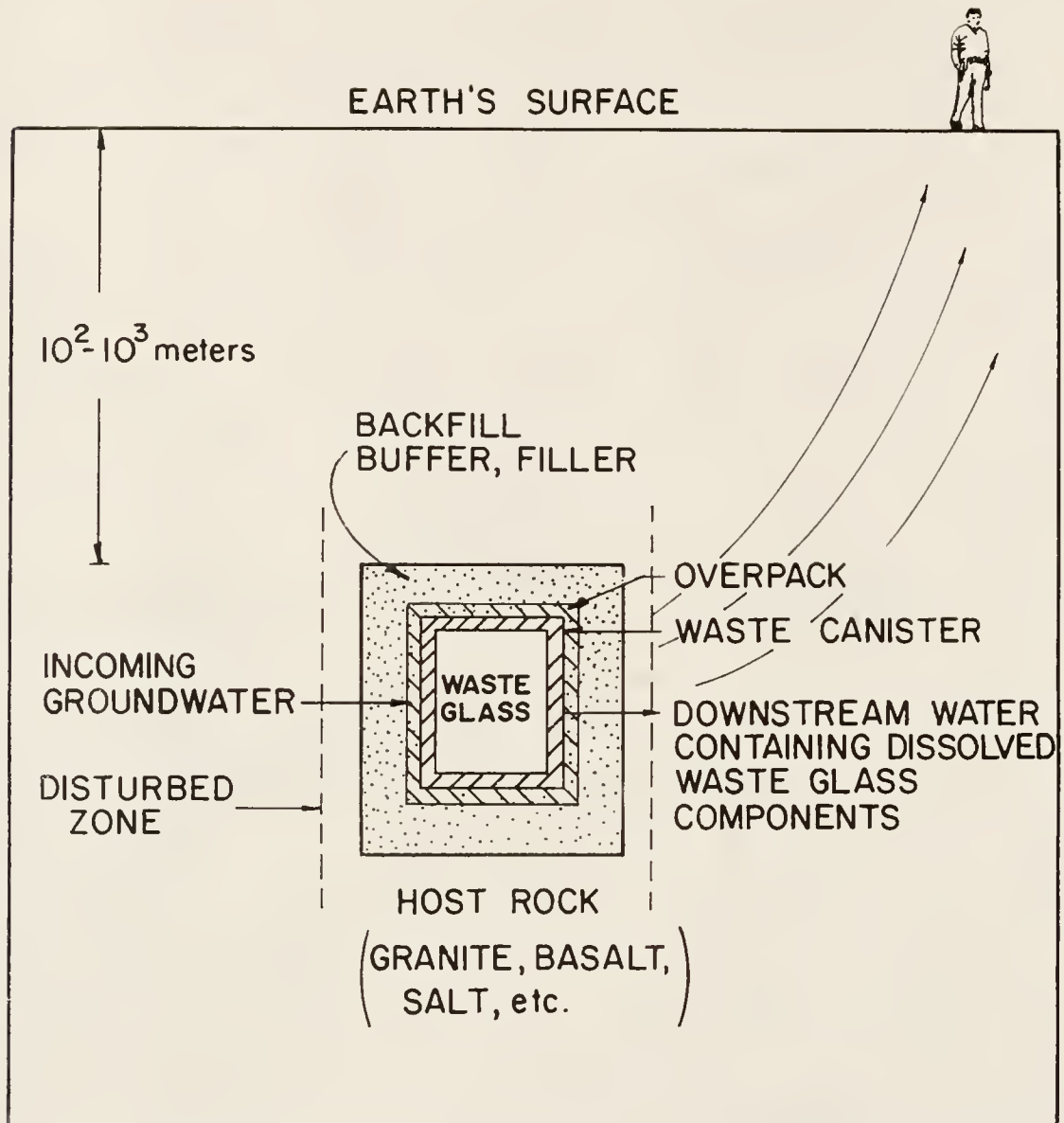


Fig. 1-2. Schematic showing the glass waste form in a geological repository.

and nickel alloys [7], which serves as an additional barrier for radionuclide containment.

- (4) a sleeve, when required, which is used to assure clearance for the retrievable package to facilitate its removal during the retrieval period. It provides structural support against geologic pressure forces and may also serve as a barrier for radionuclide containment.
- (5) backfill, the material contained between the other engineered waste package components and the host rock, which serves to facilitate heat transfer, load transfer and compatibility of the other engineered waste package components with the host rock. It may also serve as one of the barriers for radionuclide containment and a sorptive medium for radionuclide release. Swelling clays such as bentonite, alone or in a mixture with quartz or other minerals, are being considered as backfill materials.
- (6) a buffer, the material used to facilitate conditioning of the ground water, immobilization of radionuclides and compatibility of materials.
- (7) a filler, which is any material used to fill space between other components of the engineered waste package and may or may not have other specified functions.

Five years ago, there were seven candidate waste forms chosen for geologic disposal of HLW in the United States (Table 1-2). After a multifaceted assessment [8-11], borosilicate glass and Synroc (a titanate-based polyphase crystalline ceramic material) were selected

Table 1-2. Candidate Waste Forms Considered for Geologic Disposal of High Level Waste [8].

Waste Form	Comments
Borosilicate Glass	Primary Waste Form, U.S. Reference Waste Form
Synroc-C,D	Alternative U.S. Waste Form
Tailored Ceramic	Semi-finalist U.S. Alternative Waste Form
High-Silica Glass	Semi-finalist U.S. Alternative Waste Form
FUETAP Concrete	Semi-finalist U.S. Alternative Waste Form
Coated Sol-Gel Particles	Semi-finalist U.S. Alternative Waste Form
Glass Marbles in Lead Matrix	Semi-finalist U.S. Alternative Waste Form

from the seven as the primary waste form and first alternative, respectively. The focus of this work is on borosilicate nuclear waste glass.

There are two major reasons why glass was selected as the primary waste form. First, any material used for encapsulating radioactive wastes must be capable of surviving for at least 10,000 years in a wide range of severe environments. Glasses can meet this requirement. The existence of natural glasses, such as obsidians, basalts, or tektites, which are millions of years old, demonstrates that glass can be formulated which will survive long-term environmental exposures. Similarly, synthetic glasses of known longevity or performance, such as Roman glasses buried in the Mediterranean or exposed to ground water for nearly 2,000 years, also demonstrate the potential long-term performance of nuclear waste glass. Second, the process for producing nuclear waste glass is fairly simple. It involves feeding a slurry of waste sludge and glass frit to a continuous glass melter, from which the molten waste glass is poured into a canister. Such a simple fabrication method makes the remote control of the whole process possible, as demonstrated in the United States and France in full-scale operations [2,12].

In contrast, consolidation and synthesis of the mineral phases in synroc require hot isostatic processing or uniaxial hot processing, which complicates the remote production processes. Although the uranium leach rates are higher and the waste loading is lower for the glass form than for the crystalline ceramics,

borosilicate glass is currently the choice of most countries as the primary waste form due to simplicity of fabrication, moderate waste loading, intermediate product performance and radiation stability.

The list of candidate sites for the first repository in the United States has been narrowed to three locations--one in Nevada in volcanic tuff, one in Texas in salt, and one in Washington state in basalt [2]. Other rock formations such as granite in Sweden have been considered outside the United States [13]. A final decision on the site in the United States is still several years away and will require extensive testing and risk assessment.

The major concern when the waste is buried deep in the ground is that it might come into contact with water and be transported back to the earth's surface. Therefore, the resistance of the solid waste form to underground water attack is a problem of major concern, because the second innermost barrier (canister materials) is only expected to survive about 1,000 years in a geologic environment [14].

A nuclear waste glass is defined as a single phase amorphous material in which quantities of both radioactive and nonradioactive oxides are dissolved. The concept of using glass as a host for radioactive waste is based upon the radionuclides entering into and becoming part of the random three-dimensional glass network. Figure 1-3 schematically illustrates a portion of an alkali borosilicate glass network containing various radionuclides as constituents. The structural network of the glass is provided primarily by  $[\text{SiO}_4]^{4-}$ ,  $[\text{BO}_4]^{5-}$  and  $[\text{BO}_3]^{3-}$  polyhedra. Neighboring polyhedra are bonded together by sharing strong ionic-covalent bridging oxygen bonds.

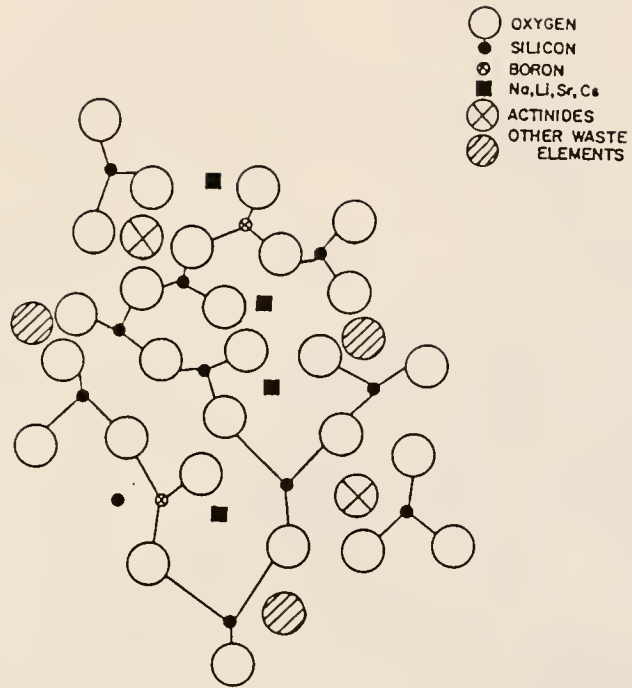


Fig. 1-3. Glass structure containing dissolved wastes (adapted from [15]).



Other multivalent species such as  $\text{Fe}^{+2,+3}$ , rare earths or actinides are also generally bonded within the network by bridging oxygen bonds. Low valence ions, such as  $\text{Na}^+$ ,  $\text{Cs}^+$ ,  $\text{Sr}^{+2}$ , etc., are bonded into the network by sharing various nonbridging oxygen bonds, depending upon size and valence of the ions. This difference in type of bonding in the glass network is responsible for the complex leach behavior of nuclear waste glasses.

To date, there are only few data available regarding the leaching behavior of nuclear waste glasses in the presence of a variety of disposal system components [16-23]. In order to test possible synergistic interactions of the materials in a nuclear waste disposal system under repository-like conditions, in situ burial experiments were designed. Such experiments approximated the physical conditions of the repository more closely than laboratory tests. Laboratory systems tests were also designed, when necessary, to evaluate the effects of individual system variables on glass leaching performance.

The primary objective of this dissertation was to determine the leaching performance of the glass containing high-level nuclear wastes\* under a simulated repository condition and to investigate how this is affected by the presence of other waste package components and geologic conditions. In the process of achieving this goal a new model of glass leaching was developed that satisfactorily describes the observed results from both laboratory and field studies.

---

\* The wastes used in this dissertation were simulated. It is assumed that isotopes of the same element have similar chemical behavior.



## CHAPTER II

### PREVIOUS WORK ON NUCLEAR WASTE GLASS LEACHING

Extensive laboratory tests and some field tests have been conducted using various combinations of reference materials in order to evaluate their effects on glass leaching. Figure 2-1 summarizes the research activities on nuclear waste glass leaching performances. The laboratory tests performed include static and flow experiments. In most of the laboratory tests, deionized water was used. Glasses were also leached in synthetic ground water, such as silicate water and brine, and/or in the presence of other waste package components. Relatively limited burial tests include a 15-year burial at Chalk River, Canada [24,25], a 9-year burial in England [26] and more recently an initiated burial study in Belgium [22]. More extensive work has been carried out in the Stripa mine in Sweden [16-20]. The major focus of this investigation is on the Stripa burial and laboratory systems interactions. The Waste Isolation Pilot Plant (WIPP) program was designed based on the experience from the Stripa burial test. This is the first burial test to be conducted in the United States.

#### Laboratory Studies

##### General Considerations

For some time, the primary issue of concern regarding glass and other HLW forms has been long-term stability in contact with hot

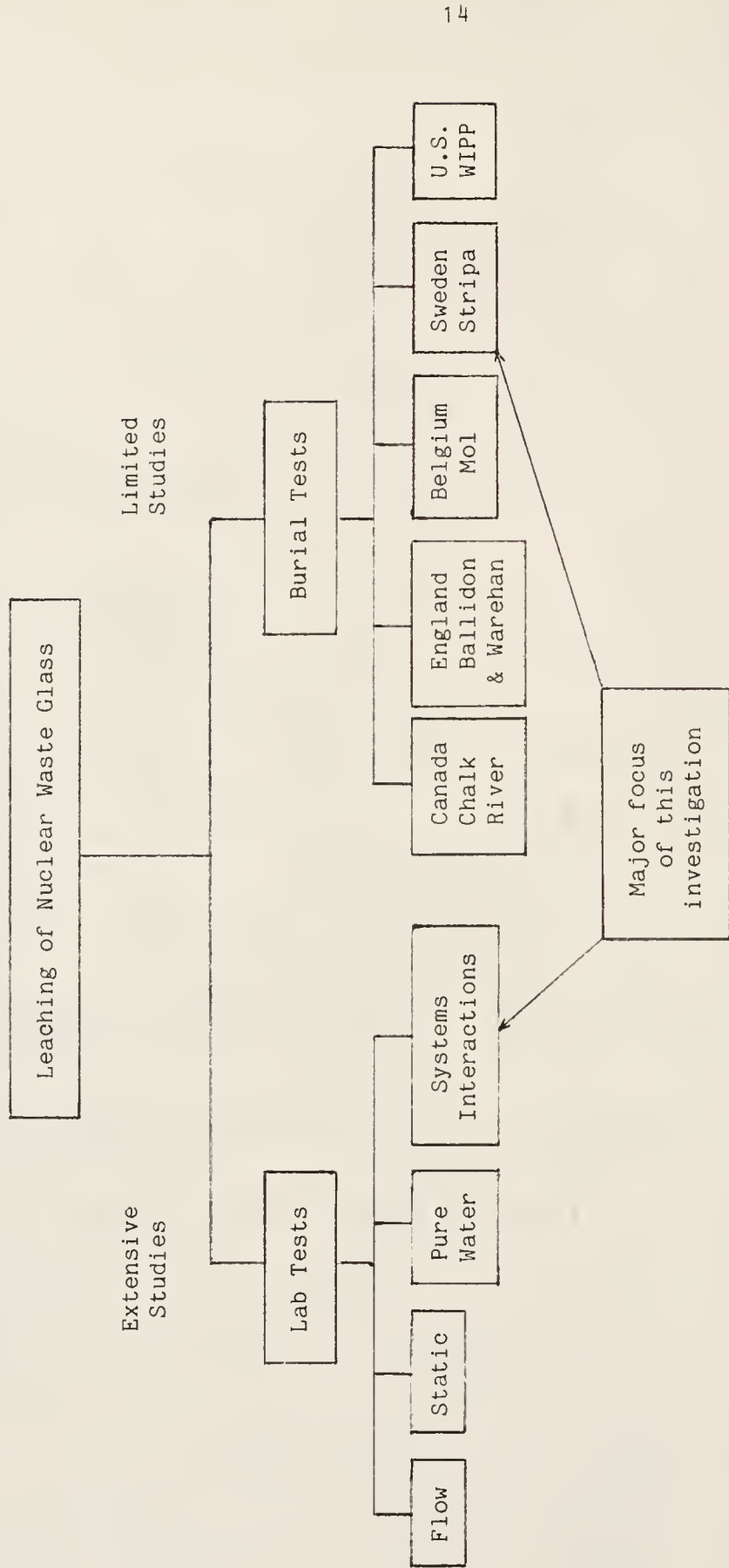


Fig. 2-1. Research activities on leaching of nuclear waste glass.

repository ground waters in the event a canister is breached. In the early 1980s, five tests were developed to determine the chemical durability of waste forms [27,28] under either static (MCC-1P\* and MCC-2P) or flowing (MCC-4S and MCC-5S) leaching environments. Maximum release by waste forms is determined using powders and stirred solutions (MCC-3S). General acceptance of these test methods, initiated by the Materials Characterization Center [27,28], reduced inconsistency, improved communication and made possible the comparison of data collected from different laboratories. This facilitated the accumulation of an extensive data base on glass leaching, including nuclear waste glasses.

In this paper, the term "leaching" is defined as release of glass component oxides or elements through glass-aqueous solution reactions without regard to mechanisms of release. The term "corrosion" is also associated with deterioration of glass surfaces due to the reactions that occur when water interacts with glass. Therefore, these terms are used synonymously in this dissertation.

Most leach test data are reported for short periods of time, i.e., 28 days or less. Such short-term data are frequently used to compare the relative stability of waste forms and to study effects of variables that control the rate of leaching. For example, Plodinec et al. [29] used the approach of Newton and Paul [30] to predict

---

\* Materials Characterization Center, Pacific Northwest Laboratory, Richland, WA.

nuclear waste glass leaching based on thermodynamic aspects of its chemical composition. They found a linear relationship between log normalized mass loss of Si ( $\text{g/m}^2$ , 28 days) and free energy of hydration (kcal/mol) for a number of natural and synthetic glasses, including simulated nuclear waste glasses. Comparing the corrosion resistance of nuclear waste glasses to natural glasses and ancient man-made glasses and/or relative thermodynamic stabilities allows extrapolation of waste glass corrosion resistance to geologic times [31,32].

Strachan [33] has reported results from a 1-year leach test using MCC-1 static test procedures. He found that a dramatic decrease in the rate of leaching occurred after approximately 91 days. The PNL76-68\* glass appeared to continue to alter, albeit at a significantly reduced rate, even though the solution concentrations of many elements were saturated or supersaturated with respect to alteration phases. In his studies, glasses were leached in deionized water, silicate water and brine at either 40°, 70° or 90°C with the ratio of glass surface area to volume of leachout (SA/V) of  $0.1 \text{ cm}^{-1}$ . Solid state analyses of the leached specimens indicated a steady growth of two layers. The outer layer grown by precipitation reactions on the original surface of the glass consisted predominantly of zinc and silicon, thus indicating a zinc silicate phase(s). An altered layer remained behind as the aqueous solution

---

\* A nuclear waste glass composition developed by Pacific Northwest Laboratories, Richland, WA.

leached soluble and moderately soluble material from the glass matrix. Thus, this layer was rich in Fe, Nd, La, Ti, and depleted in B, Cs, Na and Mo. The altered layer thicknesses for specimens leached in deionized water, silicate water, and brine at 90°C for up to 1 year ranged from 30 to 50  $\mu\text{m}$ .

The long-term data obtained by Bates et al. [34] using deionized water and MCC-1 test conditions agree qualitatively with those obtained by Strachan [33]. However, data of Bates et al. [34] indicate that the normalized elemental mass losses for most elements are constant after approximately 6 months of leaching, whereas Strachan's data indicate that leaching losses are continuing for several elements at the end of one year. The following equation defines the normalized elemental mass loss  $NL_i$  in  $\text{g}/\text{m}^2$ :

$$NL_i = \frac{m_i}{f_i \cdot SA} \quad (2-1)$$

where  $m_i$  = mass of element i in the leachate, g;

$f_i$  = mass fraction of element i in the unleached specimen, dimensionless;

SA = specimen surface area,  $\text{m}^2$ .

One important feature observed in results of Strachen [33] and Bates et al. [34] is the preferential leaching of B and Na. The normalized elemental mass losses for these two elements are larger than for Si.

#### Effect of Flow Rate

It is recognized that under certain conditions ground water will flow through a geological repository and react with its contents.

Strachan et al. [35] have reported increased leach rates for Si and Sr at a flow rate of 6 mL/h compared to static testing. Similar results have been found by other workers [36]. Based on weighing the samples before and after corrosion, the rate of leaching increased as the flow rate was increased from 0.1 to 10 mL/h. Little difference was observed between the static test and the test in which the flow rate was 0.1 mL/h during the first 28 days.

It has been found [36] that at sufficiently low flow rates (between 0.1 and 2 mL/h in Fig. 2-2) the total mass loss per unit area of waste glass matrix components surface is directly proportional to flow rate. The concentration of glass components in the leachate is nearly independent of flow rate. In the case of some matrix components (Si, Al), this concentration is determined by saturation with respect to the surface of the glass, as modified by the leaching process and possible alteration reactions. The modified surface forms a barrier against migration.

At sufficiently high flow rates ( $> 2$  mL/h in Fig. 2-2), the release rate becomes constant, limited by the kinetics of the leaching processes. In this case, corrosion products as well as potential surface-passivating species are removed from the leaching vessel, reducing the beneficial effects on both solution saturation and protective surface film formation.

Present indications are that high flow conditions ( $>10$  mL/h) are very unlikely in a geologic repository [37]. Low flow conditions are expected in the repository and the leach rate of the glass will be

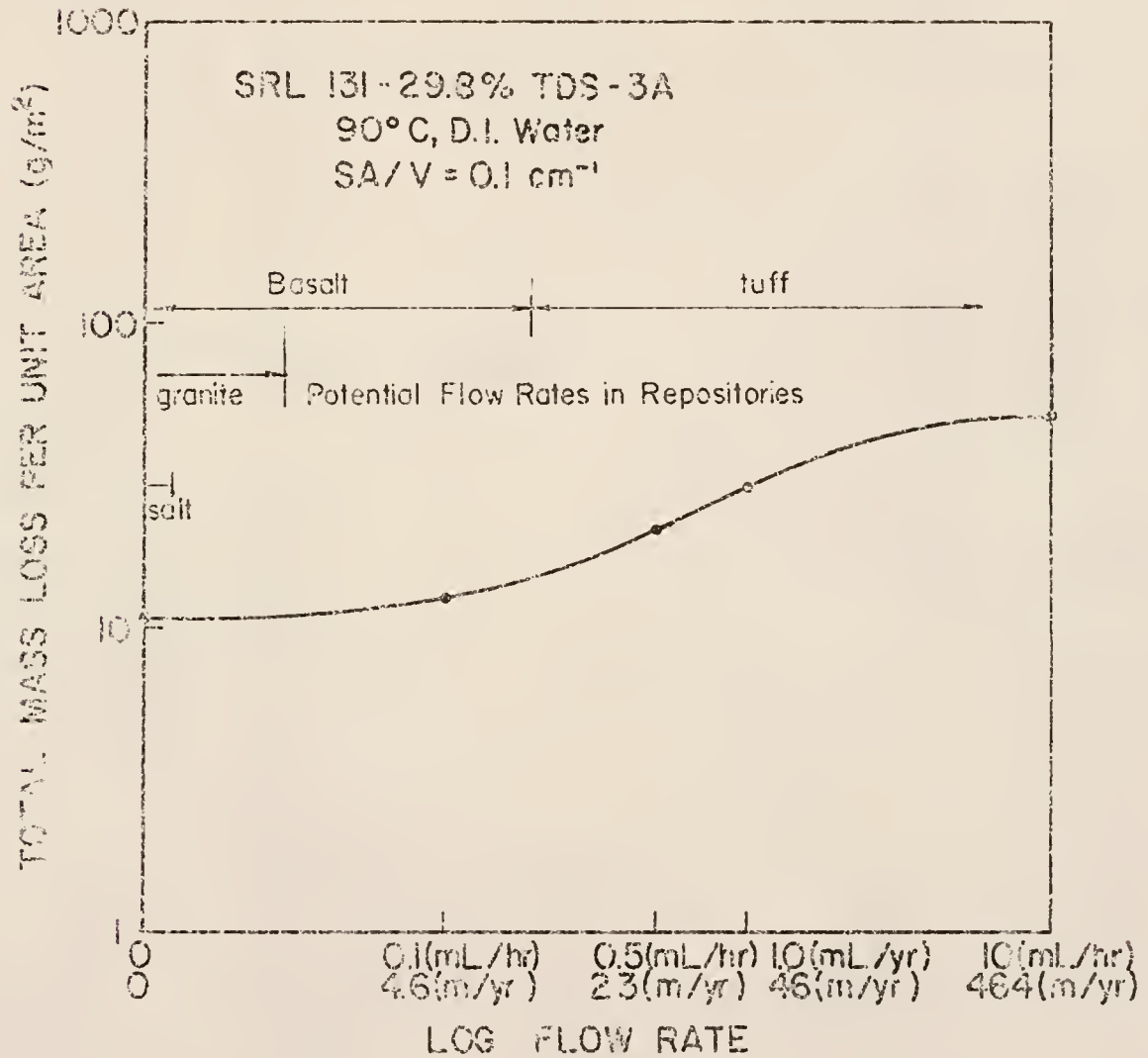


Fig. 2-2. Plot showing the total mass loss per unit area as a function of flow rate (adapted from [36]).



limited by the rate of transport of corrosion products from the repository.

#### Surface Film Formation

Previous efforts to generalize the surface behavior of silicate glasses proposed five types of glass surfaces and six surface conditions to represent a broad range of glass-environment interactions [38-40]. The type of surface is dependent on the environmental history of the glass and may be defined in terms of surface compositional profiles, as shown in Fig. 2-3. The ordinate in Fig. 2-3 represents the relative concentration of  $\text{SiO}_2$  (or oxides in Type IIIB surface) in the glass and the abscissa corresponds to the depth into the glass surface. If species are selectively dissolved from the glass surface, the relative  $\text{SiO}_2$  concentration will increase producing a  $\text{SiO}_2$ -rich surface layer. If all species in the glass are dissolved simultaneously (congruent dissolution), the relative concentration of  $\text{SiO}_2$  will remain the same as in the original glass. When combinations of selective dissolution, congruent dissolution and precipitation from solution occur, then any one of the six surface conditions shown in Fig. 2-3 is possible.

Hench [40] has pointed out earlier that low leach rates of complex nuclear waste glasses are due to Type IIIB surfaces, which are composed of multiple layers of oxides, hydroxides and hydrated silicates resulting from a sequence of solution-precipitation reactions between the glass surface and leaching solutions (Fig. 2-3). A number of alkali borosilicate nuclear waste glasses that exhibit Type IIIB surface behavior have elemental leach rates as low



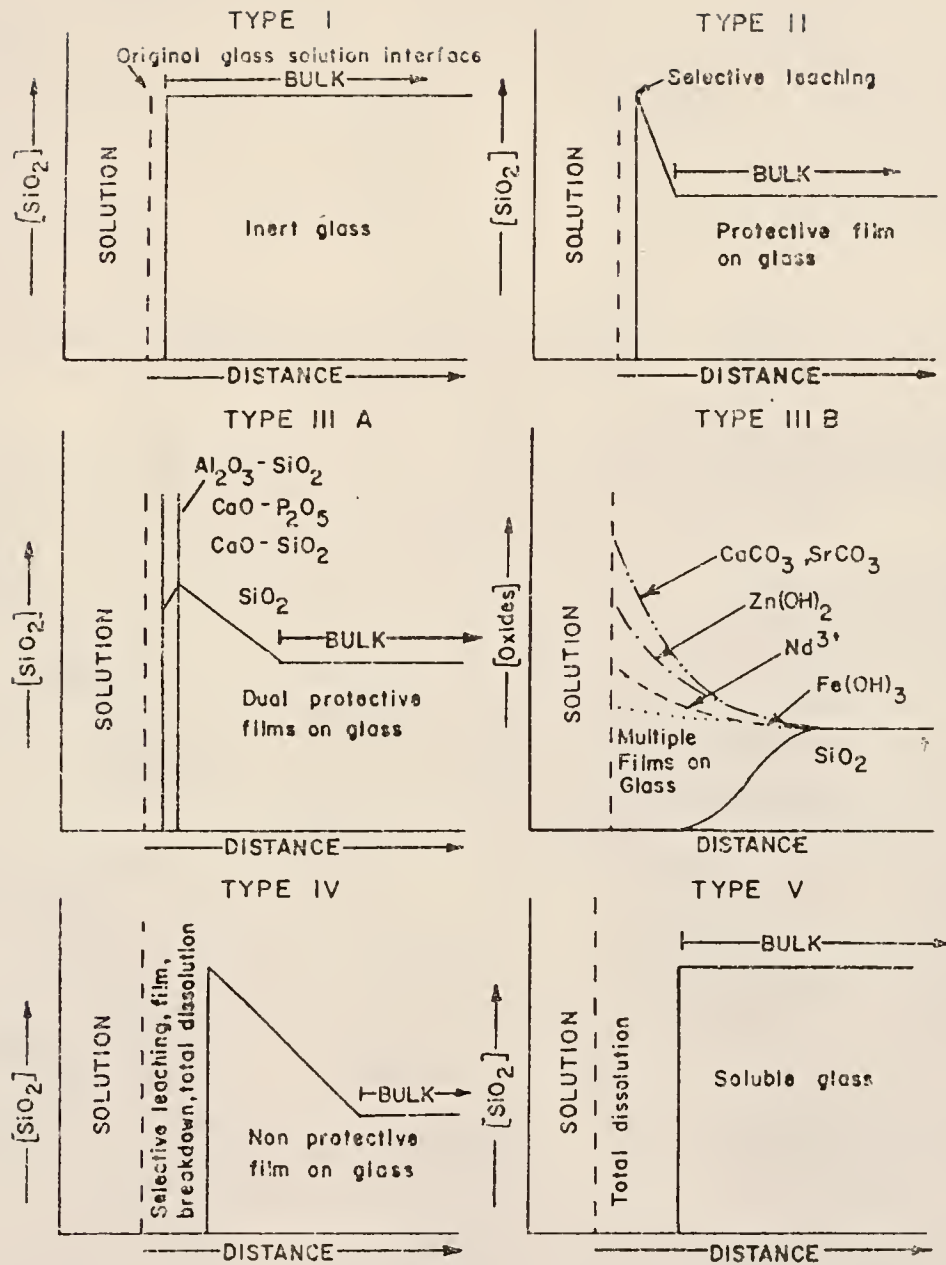


Fig. 2-3. The five types of glass surfaces and six surface conditions resulting from glass-environment interactions (adapted from [40]).

as 0.02 to 0.2 g/m<sup>2</sup>.day with a time dependence of static leaching of  $t^{0.5}$  to  $t^{0.2}$  or less after 28 days at 90°C.

In this work terms such as selective leaching and congruent dissolution are used in discussing the glass leaching mechanisms. Selective leaching includes ion exchange of the mobile species in the glass and selective dissolution of glass matrix, structural or network species with or without precipitation. Ion exchange involves a process in which exchange between mobile species such as Na from the glass and hydrogen or hydronium ions from the solution occurs. Ion exchange can also occur between Ca, Mg and K in ground water with mobile species from the glass. During this process, the remaining constituents of the glass are not altered. As mentioned in Chapter I, the structural network of the borosilicate glass is provided by  $[\text{SiO}_4]^{4-}$ ,  $[\text{BO}_4]^{5-}$  and  $[\text{BO}_3]^{3-}$  polyhedra. Since different glass network formers dissolve at different rates, selective dissolution of matrix, structural or network species is usually observed with a multicomponent glass containing two or more network formers. This may or may not be followed by precipitation depending on the composition of glass and solution. Congruent dissolution occurs when the species comprising the glass are dissolving into solution in the same ratios as they occur in the bulk glass. Without precipitation the composition in the glass surface is not changed by congruent dissolution. However, large dimensional changes often accompany such kinds of corrosion. Congruent dissolution may be followed by precipitation after certain less soluble species approach saturation. In this case, the composition of the glass surface

changes away from that of the bulk glass and less soluble constituents are enriched at the altered layer.

Although a short (several days) period of predominant alkali-hydrogen ion exchange may occur for Type IIIB glasses, the dominant, long-term mechanism controlling corrosion is a combination of more or less selective dissolution of glass matrix followed by precipitation. The extent of matrix dissolution and onset of surface and inner precipitation will depend on the time required for various species in the glass to reach saturation in solution. Saturation of a certain species will be a function of the initial solution pH, concentration of alkali species in the glass and their rates of release which change the solution pH, temperature, initial concentration of that species in the solution, the ratio of glass surface area to volume of leachant (SA/V) which influences solution concentration, and flow rate which also affects solution concentration.

The theoretical basis for Type IIIB glasses is the investigation of Grambow which predicts the formation of a series of insoluble reaction products on glass surfaces [41]. He concluded that reaction of the matrix is the fundamental process that occurs in the leaching of alkali borosilicate nuclear waste glasses. He pointed out that without solubility restrictions, congruent dissolution occurs at all pH values and leachant compositions. That is, the glass dissolves congruently at a rate proportional to  $kt^1$ . Even after saturation has occurred with respect to a certain species, the glass can continue to dissolve congruently with simultaneous precipitation of that species.

When solution saturation of species "i" is reached, there is no longer any driving force for that species to leave the glass surface. Consequently species i will accumulate at the glass-solution interface as the matrix dissolves. If matrix dissolution releases alkali ions, as will be the case for most glasses, there will be a concomitant rise in pH proportional to the flow rate or SA/V of the system. An increase in pH can have several simultaneous effects on the glass, the solution and the glass-solution interface. At the new pH, a second species "j" may reach solution saturation and subsequently be retained in the glass surface along with species "i." The extent of apparent incongruent dissolution of the glass is thereby increased. The sequence of events that occurs is predictable, based on the solubility limits of each species at a given pH, as shown by Grambow [41].

Figure 2-4 summarizes the behavior of various elements considered by Grambow [41]. Here, the ratio  $NS_i/NL_{Si}$  is used to present the solubility limits of these elements in solutions of different pH. The normalized solubility  $NS_i$  ( $g/m^2$ ) is given by

$$NS_i = \frac{C_{i,sat}}{f_i \cdot SA/V} \quad (2-2)$$

where  $C_{i,sat}$  = the solubility limited concentration in the leachate at the specified conditions, g/L;

$f_i$  = the mass fraction of element i in the glass;

SA = the specimen surface area,  $m^2$ ;

V = the volume of the leachage, L;

$NL_{Si}$  = the normalized elemental mass loss of Si,  $g/m^2$ , as defined in equation (2-1).

Therefore, in static leach tests, nuclear waste glass containing Fe oxides should concentrate Fe within surface layers. Zinc, Nd, Sr and Ca should be concentrated as well in nearly neutral or slightly alkaline solutions with Na and B depleted.

The low overall leachability of many nuclear waste glasses over a pH range from 4.5 to 9.5 is a consequence of the formation of the multiple barrier (Type IIIB) films. Figure 2-5 is a plot of Si leachability for an SRL composite waste glass immersed in a 5-day static 23°C solution buffered to various pH values from 3.5 to 10.7 [42]. These data show that over the pH range expected for repository ground waters, indicated by arrows, glass leachability is low, since the formation of less soluble reaction products lowers the solubility of silica in the solution [43].

One thing that Grambow did not explain with his leach data is why  $NL_i/NL_{Si}$ , where  $i$  is Ca, Fe, Zn, Nd or Ce, is usually larger than 1 when the solubility restrictions are removed. If  $NL_i/(NL_{Si}+NL_B)$  had been used, it may be much closer to 1, since  $B_2O_3$  is also a glass network former.

#### Molecular Mechanism of Aqueous Dissolution

In discussing the molecular mechanism of aqueous dissolution of alkali borosilicate glasses, Grambow [44] extended the idea of Aagaard and Helgeson [45] on the pure silica-water interactions, and interpreted the observed saturation effects as a local surface equilibrium process involving the critical activated surface

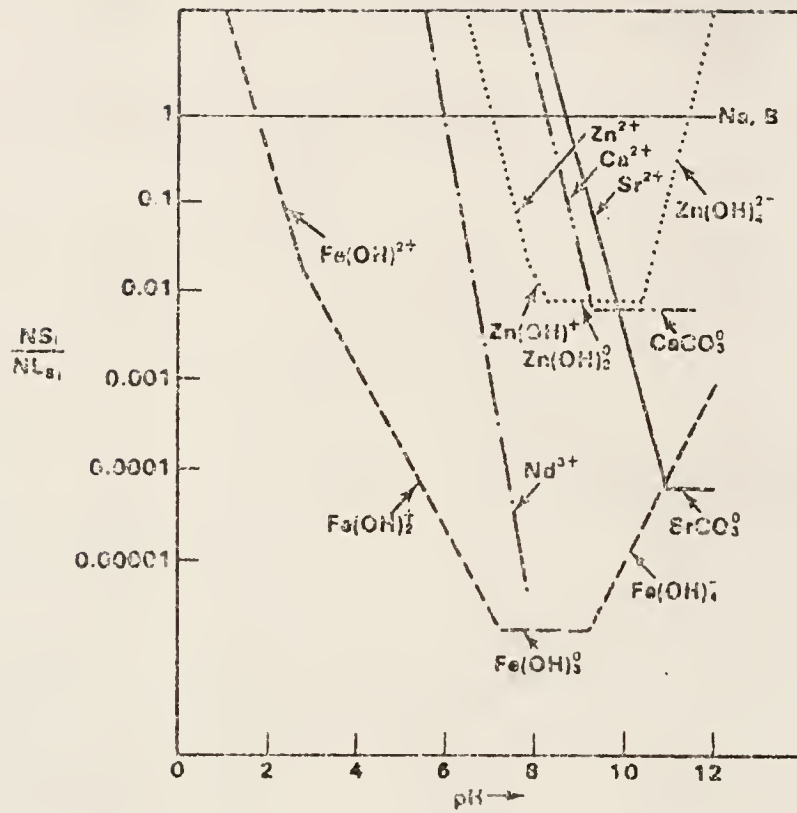


Fig. 2-4. Ratio of normalized solubility to  $NL_{Si}$  (20 g/m<sup>2</sup>) for  $CaCO_3$ ,  $SrCO_3$ ,  $Nd(OH)_3$ ,  $Fe(OH)_3$  and  $Zn(OH)_2$  in MCC-1 28-day test at 90°C in solutions of different pH (adapted from [41]).

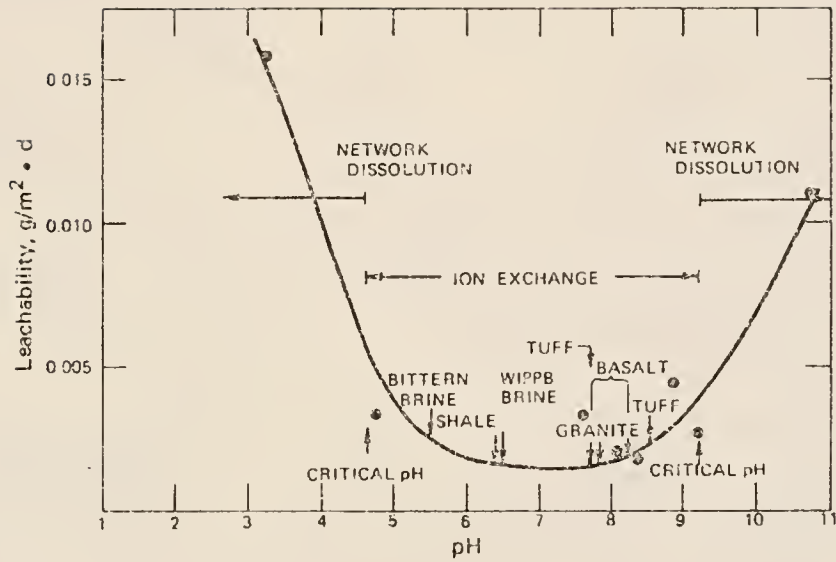


Fig. 2-5. The Si leachability of a borosilicate glass immersed in a 5-day static 23°C solution buffered to various pH values (adapted from [42]).



complex: for every complex desorbed from the glass matrix, another complex is adsorbed from solution (equal forward and back reactions). However, compared to the silica-water system, the waste glass-ground water system is much more complex; dozens of elements are involved in the system in addition to a dependence on variables such as Eh, pH, ground water composition. Furthermore, when using the approach of Aagaard and Helgeson, it is assumed that rates of hydrolysis are controlled primarily by reaction kinetics at activated sites on the surface of glass and not by diffusional transfer of material through a leached outer zone or a coherent surface layer of reaction products. Grambow [44] assumes that there exists a critical surface complex whose desorption controls the mobilization of various glass constituents. In contrast to saturation of Ca, Fe, Nd, and others, saturation of silica in solution has a major effect on the corrosion rate. Silica is the dominant constituent of the activated complex and, according to Grambow's arguments, its desorption (as silicic acid) from the glass network will limit the rate of release of other glass constituents, even when these elements are not solubility limited in solution. At saturation, condensation of silanol groups will stabilize the glass network against further attack of aqueous species.

Recent data from flow tests [46] as well as other investigations [47] indicate the importance of considering diffusion in the leached layer in addition to the reaction kinetics at the activated sites on the surface of glass. Data from flow tests [46] indicate an initial increase to a maximum of the solution concentration of various glass

constituents followed by a decrease with time. Grambow et al. [47] speculate that the leaching is controlled by the transport of silicic acid through a growing surface layer, as shown in Fig. 2-6. In this figure the saturation concentration is not a constant because the pH in the surface layer varies with time. Surface layer diffusion results from the difference between the silicic acid concentration in the bulk solution and at the surface layer. In the surface layer, saturation is reached after 200 days, whereas the solution concentration is still far below saturation. The same general trends are observed for other elements such as Na and B [46].

#### Systems Interaction Tests

A comprehensive systems interaction study was performed by Wicks et al. [48] in which they compared leaching behavior of a defense waste glass in deionized water, ground water and both waters containing rocks. Their analyses were based on the concentrations of species in solution and did not take into account the species adsorbed onto solids present in the leaching vessel. They found that the presence of salt (from Carlsbad and Avery Island), basalt, shale, granite and tuff all slightly decreased the concentrations of glass species in solution compared to those obtained when deionized water was used alone. Similar results were found with synthetic ground waters and with the same water containing the various rocks. Actual ground water yielded results comparable to the MCC reference waters and synthetic ground waters.

Clark and Maurer [49] have investigated the effects of several types of rocks, including basalt and granite, on the leaching of a

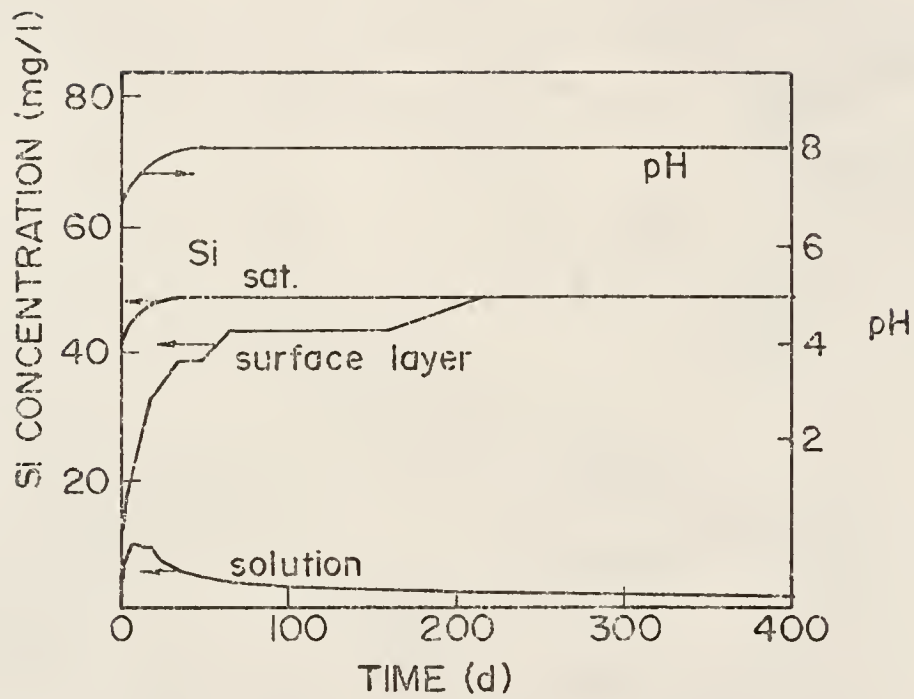


Fig. 2-6. Calculated silicon concentrations in the surface layer and bulk solution based on the surface layer diffusion and pH as a function of leaching time. A diffusion coefficient of  $10^{-9}$  cm<sup>2</sup>/sec was assumed [46,47].

borosilicate glass. With the possible exception of granite, the combination of glass and rocks in the same leaching vessel did not appear to have any significant effects in a 28-day test.

Brine solution generally decreases the rate of glass corrosion [48,50,51], with the possible exception of Sr, Ce and similar elements [35]. In the brine solutions, a protective magnesium chloride complex forms on the glass surface. Exposure of nuclear waste glass to tuffs results in a small decrease in corrosion rate, perhaps due to a buffering effect [48]. Autoclave tests of basalt-glass interactions [52] and granodiorite-glass [53] interactions show a decreasing rate of attack.

McVay and Buckwalter [54] investigated the effect of iron on nuclear waste glass leaching. They found that the presence of ductile iron in deionized, tuff and basalt ground waters containing PNL 76-68 borosilicate glass caused significant changes in the leaching characteristics of the glass. Formation of iron silicate precipitates effectively removes many elements from solution and therefore inhibits the saturation effects which normally cause decreases in elemental removal rate. Thus, basalt and tuff ground waters behave similarly to deionized water in the presence of ductile iron. The precipitates also retard saturation effects, resulting in high sustained leach rates and thus greater total elemental removal from the glass. A synergistic effect occurs between the two materials. The iron enhances glass leaching and the glass enhances iron corrosion.

The presence of a radiation field during storage and its effect on glass leaching is another consideration. Radiation may affect the glass-water system in several ways. Gamma radiation has been found to result in approximately three- to seven-fold increases in the leach rates of borosilicate glasses [55,56]. As reported by McVay and Pederson [55], some of the enhancement is due to nitric acid formation from air radiolysis in the presence of water. Nitric acid appears to preferentially attack zinc and lanthanides, both of which normally build up on the surface of the PNL 76-68 glass when leached in nonacidic solutions. The change of the solution chemistry by gamma radiation and generation of reactive species such as  $\text{OH}^-$  from water radiolysis also appear to be important. The principal effect of water radiolysis products is the increased silicate dissolution.

The leaching behavior of the radioactive glass has been investigated in comparison to that of the simulated glass [57]. In this case it was found that radiation, due to the low dose rate with the radionuclides (0.594 Ci per specimen), does not affect significantly the leaching rate. This conclusion includes the effects of radiation damage to the glass itself and the interaction of the radiation field from the glass with the water and air. Profiles of Pu and U behave similarly during leaching, both being enriched in the surface of the glass. Leaching of radioactive glass results in loss of B, Na, Li and Mo with about the same depth of leaching. The leaching mechanisms appear to be similar for radioactive and nonradioactive glasses [57].

### Burial Studies

Burial studies were started in the late 1950s and early 1960s. Merritt and Parsons [24,25] pioneered two tests of high-level waste (containing real radionuclides) incorporated into nepheline syenite glass and buried in contact with ground water for 15 years at Chalk River, Canada, at ambient temperature. Fletcher [26] conducted burial experiments of waste glass samples in England for up to 9 years. Although the field tests were not performed under actual repository conditions, they did provide an approximation to a potential repository. Preliminary results from burial experiments [24,25] have shown that glasses leached at much lower rates under repository-like conditions than under laboratory conditions. As an example, the observed field leach rate from the Canadian burials was over 200 times lower than the lowest leach rate reported in the laboratory [24,25]. The authors attributed about 1/5 of this difference to the lower aggressiveness of ground water over distilled water used in the laboratory experiments and to its lower temperature (6°C in the field compared to 25°C in the laboratory). The remainder of the difference was attributed to the formation of a protective surface layer.

The leaching performance of a waste glass depends on the environment under which it is tested. In a repository, the system variables ultimately controlling the environment to which the waste glass is exposed include geology, engineered waste package components, initial ground water chemistry, temperature, pressure,



radiation field, water contact time and flow rate through the repository.

The most extensive and systematic field tests began in 1982 and involve deep burial (350 meters below surface) in granite in the Stripa mine, Sweden [16-20]. The boron depletion depths of glass ABS 39\* and 41\* ranged from 0.2  $\mu\text{m}$  to 15  $\mu\text{m}$ , depending on composition and the type of material to which the glass was exposed after 1 year of burial at 90°C. At the glass/glass interface, both glasses showed a depletion of Na, Cs and B, but for the more corrosion-resistant glass, the lower depletion depth was ascribed to the formation of a thin (0.2  $\mu\text{m}$ ) coherent and dense outer layer, enriched in Mg, Ca, Sr, Ba, Zn, Al, Fe and Si, which impedes both the ion exchange and network attack of the bulk glass underneath. The presence of bentonite increased the boron depletion depth up to 1 year by a factor of approximately 5, whereas granite decreased this depth by about 2 times. This behavior is attributed to bentonite serving as a semi-infinite ion exchange medium where Ca from the bentonite is replacing Na, Li and B from the glass [19]. In contrast, the small congruent solubility of granite seems to augment the glass in reaching solubility-limited leaching [21].

Another in situ test was initiated in 1986 and involves burial in a clay formation in Mol, Belgium [22]. A number of simulated waste forms (including HLW glasses and glass-ceramics) have been, or will be, buried at the site. Their corrosion rate will be measured

---

\* Swedish alkali borosilicate (ABS) and nuclear waste glasses.



in two environments susceptible to contact the radioactive waste during its geological storage in a clay formation: host clay and a humid atmosphere loaded with clay extracts. The tests, with total exposure times of 6 years, will be carried out at various temperatures, 15, 50, 90 and 170°C.

CHAPTER III  
RESEARCH OBJECTIVES, APPROACH AND SUMMARY OF CONCLUSIONS

Research Objectives and Approach

The primary objectives of this study were (1) to evaluate the leaching behavior of selected nuclear waste glasses in a realistic repository environment, (2) to develop a characterization methodology for comparing field data with laboratory data and (3) to assess leaching mechanisms and to correlate the mechanisms observed in laboratory-leached vs field-leached specimens.

In order to achieve these objectives, both field experiments and laboratory simulation tests were conducted. The field tests involved long-term (up to 31 months) deep burial (350 m below surface) in granite in the Stripa mine in Sweden. Two configurations of samples were used. One was a 32 mm in diam. x 35-mm long minican where an alkali borosilicate glass with simulated HLW was cast into stainless steel. The second configuration was the so-called "pineapple slices," 51-mm in diam. x 5-mm thick, which resulted in a variety of glass/repository materials interfaces. Two temperatures, 90°C and the ambient temperature (8-10°C), were used to simulate the repository conditions during and after the thermal period of storage, respectively. Comparisons were made of six alkali borosilicate simulated nuclear waste glasses, including three American Savannah River Laboratory (SRL) glasses and three Swedish alkali borosilicate

(ABS) glasses. Different glass/repository materials interfaces were provided to investigate effects of these materials on glass leaching.

In the laboratory, methods were designed to consist of both static and single-pass low-flow tests, using granite rock cups as leach vessels and Stripa ground water in an attempt to closely simulate the repository-like conditions in Stripa.

Several research tools, including solid surface analysis and solution analysis techniques, were used in combination. These provided a direct evaluation of nuclear waste glass leaching under various test conditions.

### Major Conclusions

1. A significant compositional effect on glass leaching was observed under burial conditions. The leach rate expressed by the annual boron depletion depth was inversely correlated with  $(\text{SiO}_2 + \text{Al}_2\text{O}_3)/(\text{R}_2\text{O} + \text{B}_2\text{O}_3)$  wt ratio in the glasses;  $\text{R}_2\text{O}$  represents the alkali oxides.

2. Accelerated attack during the first year in the presence of bentonite appears to be a transient effect. The presence of stainless steel, Cu and Ti does not have much effect on glass leaching.

3. The leach rates of buried samples based on boron depletion at 90°C ranged from 0.3-3  $\mu\text{m}/\text{year}$  for the glass/glass interfaces investigated. These values are at least two orders of magnitude lower than those for glasses leached using MCC-1 static leaching procedures and deionized water.

4. Comparison of the laboratory simulation results with field test results indicates that glass leaching mechanisms were similar under both test conditions.

5. A model, based on glass structure and thermodynamic considerations, was proposed to better describe alkali borosilicate glass leaching than the recent model proposed by Grambow.

6. The results show that Stripa burials combined with laboratory simulations are unique experimental designs which have provided useful information regarding nuclear waste glass leaching. This work has served as a model on which design and development of the most recent burial test programs are based.

## CHAPTER IV MATERIALS AND METHODS

### Glass Compositions and Characterization

#### Burial Samples

Six alkali borosilicate simulated nuclear waste glass compositions were used in the burial experiments. They included three American SRL glasses and three Swedish ABS glasses. Their compositions are listed in Table 4-1.

Frit 131 and frit 165, which were designed to contain the Savannah River Plant (SRP) nuclear waste, were used to prepare SRL glass samples. Two glasses containing 29.8 wt% and 35 wt% TDS\* waste, respectively, were prepared from frit 131. Another SRL glass was prepared from frit 165 and contains 29.8 wt% TDS waste. ABS 39 and 41, developed and produced by Dr. T. Lakatos, Swedish Glass Research Institute, Växjö, Sweden, contain 9% by weight simulated fission product oxides. These glasses are similar to the COGEMA glass selected for vitrification of commercial HLW in LaHague, France, operations [23]. ABS 118 contains 11.25 wt% simulated fission product oxides and has a composition very close to that of the future COGEMA glass.

The glass frits were premelted from chemicals using standard procedures. The simulated SRP waste was mixed with the frit before

---

\* See the notes in Tables 4-1.

Table 4-1. Nominal Waste Glass Compositions (wt%) Used in the Stripa Burial.

Component	SRL 131 + 29.8% TDS <sup>+</sup>	SRL 165 + 29.8% TDS <sup>+</sup>	SRL 131 + 35% TDS <sup>+</sup>	ABS 39	ABS 41	ABS 118
<u>From glass frit</u>						
Na <sub>2</sub> O	12.4	9.1	11.5	12.9	9.4	9.9
Li <sub>2</sub> O	4.0	4.9	3.7	--	3.0	2.0
ZnO	--	--	--	--	3.0	2.5
MgO	1.4	0.7	1.3	--	--	--
Al <sub>2</sub> O <sub>3</sub>	--	--	--	3.1	2.5	4.9
B <sub>2</sub> O <sub>3</sub>	10.3	7.0	9.6	19.1	15.9	14.0
Fe <sub>2</sub> O <sub>3</sub>	--	--	--	5.7	3.6	2.9
La <sub>2</sub> O <sub>3</sub>	0.4	--	0.3	--	--	--
SiO <sub>2</sub>	40.6	47.7	37.6	48.5	52.0	45.5
TiO <sub>2</sub>	0.7	--	0.7	--	--	--
ZrO <sub>2</sub>	0.4	0.7	0.3	--	--	1.0
UO <sub>2</sub>	--	--	--	1.7	1.6	0.9
P <sub>2</sub> O <sub>5</sub>	--	--	--	--	--	0.3
Cr <sub>2</sub> O <sub>3</sub>	--	--	--	--	--	0.5
NiO	--	--	--	--	--	0.4
CaO	--	--	--	--	--	4.0
<u>From simulated waste</u>						
Fe <sub>2</sub> O <sub>3</sub>	13.4	13.4	15.8	--	--	--
MnO <sub>2</sub>	3.9	3.9	4.5	0.78	0.78	0.97
Zeolite**	2.9	2.9	3.4	--	--	--
Al <sub>2</sub> O <sub>3</sub>	2.7	2.7	3.2	--	--	--
NiO	1.6	1.6	1.9	0.37	0.37	0.47
SiO <sub>2</sub>	1.2	1.2	1.4	--	--	--
CaO	1.0	1.0	1.2	--	--	--
Na <sub>2</sub> O	0.9	0.9	1.0	--	--	--
Coal	0.7	0.7	0.8	--	--	--

Table 4-1.--continued.

Component	SRL 131 + 29.8% TDS <sup>+</sup>	SRL 165 + 29.8% TDS <sup>+</sup>	SRL 131 + 35% TDS <sup>+</sup>	ABS 39	ABS 41	ABS 118
Na <sub>2</sub> SO <sub>4</sub>	0.2	0.2	0.2	--	--	--
Cs <sub>2</sub> CO <sub>3</sub>	0.1	0.1	0.2	--	--	--
SrCO <sub>3</sub>	0.1	0.1	0.2	--	--	--
U <sub>3</sub> O <sub>8</sub>	1.1	1.1	1.3	--	--	--
Cs <sub>2</sub> O	--	--	--	0.89	0.89	1.11
SrO	--	--	--	0.26	0.26	0.33
BaO	--	--	--	0.46	0.46	0.58
Y <sub>2</sub> O <sub>3</sub>	--	--	--	0.15	0.15	0.19
ZrO <sub>2</sub>	--	--	--	1.29	1.29	1.62
MoO <sub>3</sub>	--	--	--	1.65	1.65	2.06
Ag <sub>2</sub> O	--	--	--	0.01	0.01	0.01
SnO	--	--	--	0.02	0.02	0.02
Sb <sub>2</sub> O <sub>3</sub>	--	--	--	0.004	0.004	0.005
La <sub>2</sub> O <sub>3</sub>	--	--	--	0.72	0.72	0.90
Nd <sub>2</sub> O <sub>3</sub>	--	--	--	1.22	1.22	1.53
Pr <sub>2</sub> O <sub>3</sub>	--	--	--	0.38	0.38	0.48
Ce <sub>2</sub> O <sub>3</sub>	--	--	--	0.76	0.76	0.95
CdO	--	--	--	0.03	0.03	0.03
<u>Total</u>	100.0	99.9	100.0	100.0	100.0	100.1

<sup>+</sup> TDS waste as received from SRL contained Fe<sub>2</sub>O<sub>3</sub>, MnO<sub>2</sub>, zeolite, Al<sub>2</sub>O<sub>3</sub>, NiO, SiO<sub>2</sub>, CaO, Na<sub>2</sub>O, Coal and Na<sub>2</sub>SO<sub>4</sub>. This waste was also doped with Cs, Sr and U.

<sup>\*\*</sup> Zeolite contains (in wt%) 67.2 SiO<sub>2</sub>, 19.3 Al<sub>2</sub>O<sub>3</sub>, 6.3 Na<sub>2</sub>O, 3.4 Fe<sub>2</sub>O<sub>3</sub>, 2.8 CaO and 1.0 MgO.



vittrification. The mixture was fused at 1150-1200°C for 2-6 hours and annealed at 500-525°C for 1 hour.

Two sample configurations were used: (1) minicans and (2) pineapple slices. The minicans were made by casting the molten glass in stainless steel rings 3 mm in diameter by 35 mm long. After annealing, a hole 200  $\mu$ m in diameter was drilled through the center of each minican. Both surfaces of the minicans were polished to a 6- $\mu$ m finish with diamond paste. Pineapple slices were prepared by casting cylinders 51 mm in diameter by 80 mm long in molds containing center carbon posts. Sections 5 mm thick were sliced from the annealed cylinders and the center posts were removed. One side of each pineapple slice was polished to a 600-grit ( $\sim 17 \mu$ m) surface finish while another side was kept in as-cut condition for easy identification of the glass interfaces after burial. Figure 4-1 shows the pineapple slices of glass, granite,\* stainless steel, Ti, Pb and compacted bentonite\*\* before burial.

Before burial, each sample was subjected to two types of surface analyses: (1) optical microscopy and (2) Fourier transform infrared reflection spectroscopy (FT-IRRS). Four to six spots on the polished surface of each pineapple slice and two spots each on both sides of the minican were analyzed using these two techniques of surface

---

\* The granite was obtained from Stripa, Sweden.

\*\* The bentonite was obtained from Wyoming. The compacted bentonite was made by means of isostatic compaction under 100 MPa of pressure. This is a so-called sodium bentonite whose main constituent (90 wt%) is montmorillonite.

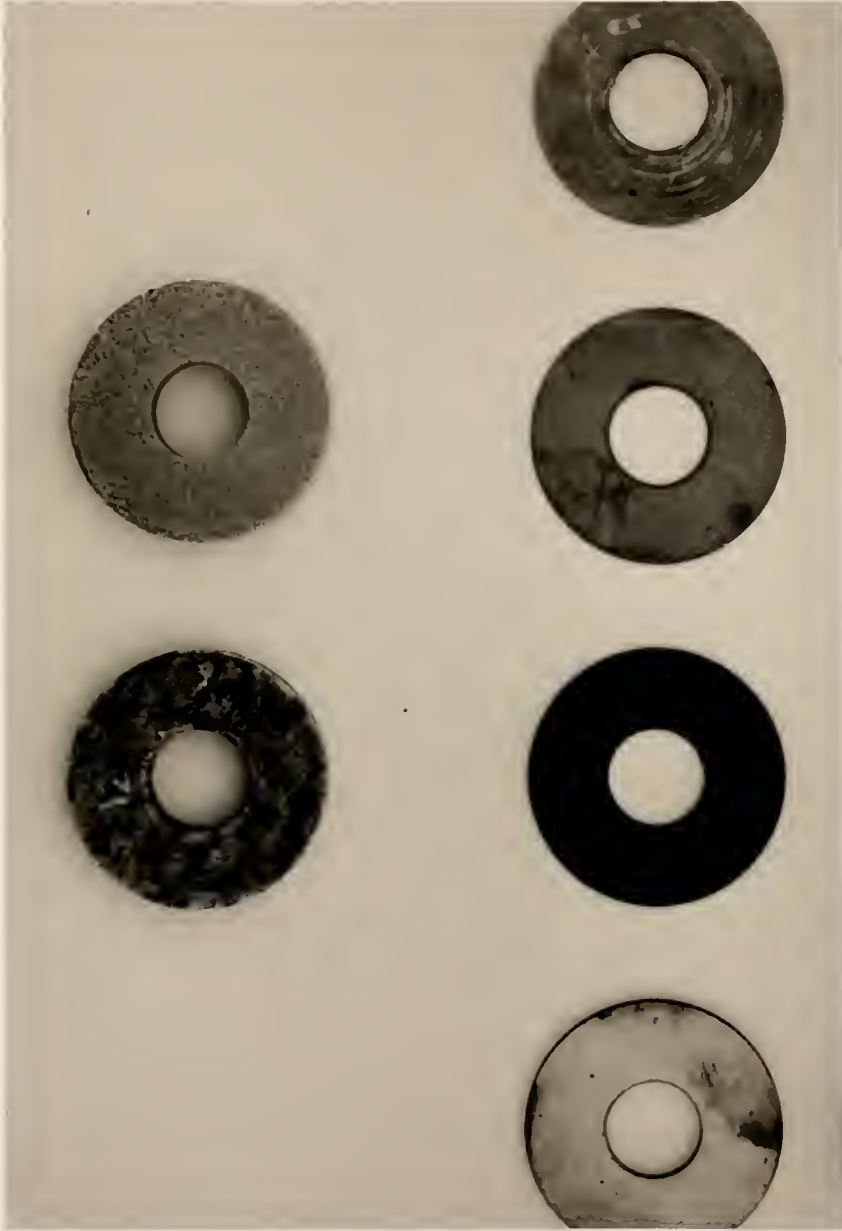


Fig. 4-1. Pineapple slices of glass, granite, stainless steel, Ti, Pb and compacted bentonite before burial.

analyses. In addition, each sample was weighed before burial. Table 4-2 is the sample matrix of the burial experiments.

#### Glass Quality

Fourier transform infrared reflection spectroscopy (FT-IRRS) was used as a nondestructive analytical tool for characterization of glass surfaces prior to the burial. One objective of this statistical analysis was to determine the relationship between the FT-IRRS spectra and glass composition used in the Stripa burial. A second objective was to check if there were any appreciable variations in composition and/or surface finish conditions among samples of the same glass formulation. SRL glass samples were used in this study. The FT-IRRS spectra were obtained on 4 to 6 spots along the diameter of each glass sample.

Table 4-3 lists the statistical variations of the FT-IRRS analysis for the SRL glasses. Figure 4-2 shows the representative spectra of SRL glass pineapple slices before burial. It is observed that both the wavenumber and the intensity (integrated area under the curve) for the broad peak containing Si-O stretching vibrations increase with increasing  $\text{SiO}_2$  content in the glass composition, i.e., in the order of SRL 131 + 35% TDS, SRL 131 + 29.8% TDS, SRL 165 + 29.8% TDS. Range of variation in peak position for the same composition was 0.4-0.8%. The standard deviation of peak position for the SRL 131 + 29.8% TDS glass slices was the largest (0.8%) due to glass heterogeneities contained in a few samples of this composition. On the other hand, the peak intensity and integrated area under the spectra vary more than peak position because peak

Table 4-2. Sample Matrix of the Stripa Burial Tests.

Time (month)	SRL 131 + 29.8% TDS	SRL 165 + 29.8% TDS	SRL 131 + 35% TDS	ABS 39	ABS 41	ABS 118
<u>Minicans*</u>						
1	90°C	90°C	--	--	--	--
3	90°C	90°C	--	--	--	--
12	90°C	90°C	--	--	--	--
24	8-10°,90°C	8-10°,90°C	--	--	--	--
<u>Pineapple Slices**</u>						
1	90°C	90°C	90°C	90°C	90°C	--
2	--	--	--	--	--	90°C
3	90°C	90°C	90°C	90°C	90°C	--
4	--	--	--	--	--	90°C
6	90°C	--	--	--	--	--
7	--	--	--	--	--	90°C
12	8-10°,90°C	90°C	90°C	90°C	90°C	90°C
24	8-10°,90°C	8-10°,90°C	8-10°,90°C	--	--	--
31	--	--	--	90°C	90°C	--

\* Including glass/glass and glass/bentonite interfaces.

\*\* In the case of SRL glasses, glass/glass, glass/bentonite, glass/granite, glass/Ti and glass/stainless steel were included with extra two interfaces, glass/Cu and glass/Pb for 1-month burial; all ABS glasses included glass/glass, glass/bentonite, glass/granite, glass/Ti, glass/Cu and glass/Pb interfaces.

Table 4-3. Variations in Spectral Characteristics of SRL Waste Glasses.

Glass	Peak* Location ( $\text{cm}^{-1}$ )	Peak* Intensity (%)	Integrated Area (Relative Value)
<u>Minicans</u>			
SRL 131 + 29.8% TDS	989 $\pm$ 4**	21.26 $\pm$ 1.67	5.22
SRL 165 + 29.8% TDS	996 $\pm$ 6	23.12 $\pm$ 1.53	5.58
<u>Pineapple Slices</u>			
SRL 131 + 29.8% TDS	980 $\pm$ 8	21.71 $\pm$ 2.42	5.16
SRL 165 + 29.8% TDS	990 $\pm$ 6	22.82 $\pm$ 2.34	5.44
SRL 131 + 35% TDS	974 $\pm$ 6	20.16 $\pm$ 2.63	4.67

\* The compound peak containing Si-O-Si stretching vibrations at 800-1200  $\text{cm}^{-1}$  was used in the statistical analysis.

\*\* Mean and standard deviation.

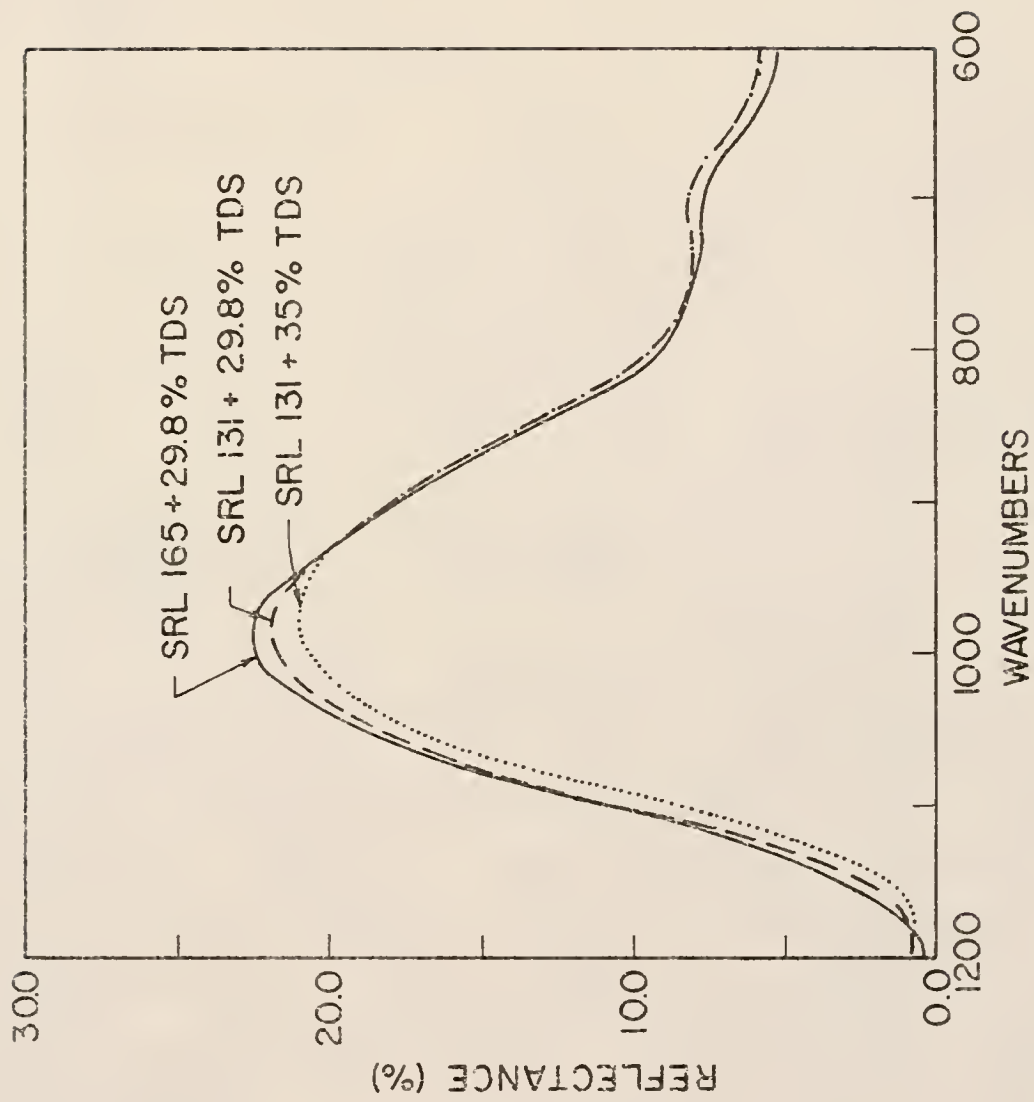


Fig. 4-2. Representative FT-IRRS spectra of SRL glass pineapple slices before burial.

intensity is sensitive to variations in the surface roughness due to polishing. All these results show that the glass samples except those containing crystallites are homogeneous compositionally but the surface polishing conditions have relatively wide variations.

#### Laboratory Samples

In laboratory simulation tests, most of the glass samples were made from two similar glass formulations, SRL 165 + 29.8% TDS and Black Frit 165-Mobay (see Table 4-4). The same melting procedures as for the burial samples were followed in making the laboratory glass. The glass melt was cast into a graphite mold. The glass bars were annealed at 500°C for 1 hour, then furnace cooled.

After cutting from glass bars, samples were polished on all surfaces up to 600 grit with SiC papers. After cleaning, each sample was subjected to two kinds of surface analyses: optical microscopy and FT-IRRS. All samples were weighed before corrosion.

#### Stripa Field Tests

##### Sample Assemblies, Minicans and Pineapple Slices

The minicans and the pineapple slices, granite slices, compacted bentonite slices, stainless steel, Ti, Pb and Cu coupons were assembled at the University of Luleå, Sweden, to provide a wide range of glass/repository materials interfaces. Minicans were designed to closely simulate a waste package in a disposal hole. Minicans and compacted bentonite coupons were stacked together to provide glass/glass and glass/bentonite interfaces (Fig. 4-3). Sleeves of Pb and Ti or Cu overpacks were placed around the steel wall of the minican and a bentonite sleeve separated the waste package from the



Table 4-4. Nominal Composition  
of Black Frit 165-  
Mobay Glass.

Component	Wt %
SiO <sub>2</sub>	55.61
Fe <sub>2</sub> O <sub>3</sub>	11.34
Na <sub>2</sub> O	10.44
B <sub>2</sub> O <sub>3</sub>	7.23
Li <sub>2</sub> O	4.82
Al <sub>2</sub> O <sub>3</sub>	4.22
MnO <sub>2</sub>	2.11
CaO	1.10
NiO	0.90
MgO	0.70
ZrO <sub>2</sub>	0.90
F	0.14
Cl	nil
Pb	nil
K <sub>2</sub> O	0.14
TiO <sub>2</sub>	0.23
BaO	0.07
ZnO	<u>0.05</u>
Total	100.00

Note: Glass was supplied by Savannah River Laboratory, Aiken, SC. This is a similar formulation to SRL 165 + 29.8% TDS. However, it contains more SiO<sub>2</sub> and less Fe<sub>2</sub>O<sub>3</sub>.



Fig. 4-3. A minican assembly.

walls of the borehole. A typical pineapple slice assembly before burial is shown in Fig. 4-4.

The SRL glasses included seven pineapple slice assemblies with different sample stacking sequences (Fig. 4-5 and Table 4-2) and five minican assemblies with the same sample stacking sequence (Table 4-2).

All the Swedish ABS glass assemblies had the same stacking sequence to provide six different interfaces (see the footnotes in Table 4-2). Thus, 35 glass/repository materials interfaces were involved in these Stripa burial tests with six alkali borosilicate simulated nuclear waste glass compositions.

#### Stripa Repository

The Stripa abandoned iron mine was chosen as an underground field laboratory where the major rock formation is a massive, grey to light red, medium-grained granite. The mine is located in central Sweden. The massive and compact nature of granite makes it very impermeable to water. The hard rock formation has great structural strength and resistance to erosion or other disruptive events. Hence, nuclear waste glass placed deep in granite is very unlikely to be disturbed by climatic or geological events, or by accidental human intrusion [58].

Table 4-5 lists the average major/minor chemical and mineral constituents of the Stripa granite. There are several fracture systems. The majority of the fractures are closed and filled mainly with chlorite but occasionally with calcite. This mine provides an environment which closely simulates an actual granite repository and



Fig. 4-4. A typical pineapple slice assembly.

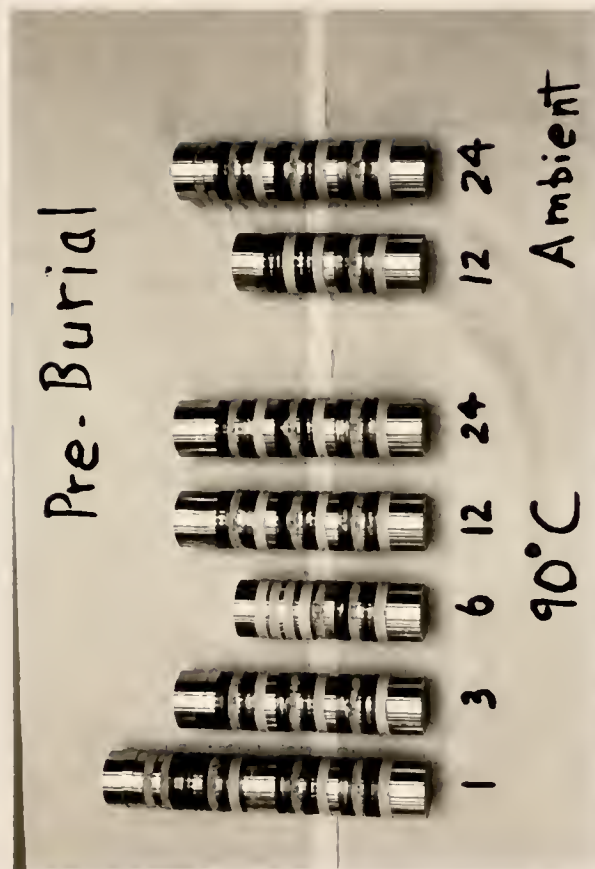


Fig. 4-5. Seven preburial pineapple slice assemblies with different sample stacking sequences for SRL simulated nuclear waste glasses.

Table 4-5. Average Major/Minor Chemical and Mineral Constituents in Stripa Granite.

Oxide	Wt %	
SiO <sub>2</sub>	74.7	
Al <sub>2</sub> O <sub>3</sub>	13.2	
Fe <sub>2</sub> O <sub>3</sub>	1.6	
FeO	NR <sup>a</sup>	
MgO	0.20	
CaO	0.6	
Na <sub>2</sub> O	4.0	
K <sub>2</sub> O	4.6	
TiO <sub>2</sub>	0.05	
P <sub>2</sub> O <sub>5</sub>	NR	
MnO	0.03	
BaO	0.02	
H <sub>2</sub> O	NR	
CO <sub>2</sub>	NR	
Mineral	Grey	Red (vol %)
Quartz	33	44
K or Na Feldspar	24	12
Plagioclase	35	39
Biotite	<1	NR
Muscovite	<1	2
Chlorite	<1	3

Adapted from [59].

<sup>a</sup> NR = not reported.

is thus ideal for conducting glass corrosion experiments. The location within the Stripa mine where the samples were buried is shown in Fig. 4-6. This is about 345 meters below the surface. The holes into which the samples were placed were about 3-m deep and 56 mm in diameter, which were filled with ground water from the mine before the samples were placed to a depth of about 2.5 m (see Fig. 4-7). The arrow indicates holes for 1-month, 90°C specimens. The ground water composition and pH prior to burial as measured in the recent study is given in Table 4-6. Table 4-7 lists the ground water composition and pH found in literature [60].

#### Burial and Retrieval

All the sample assemblies were buried in the boreholes at the 345-m level below the surface. Heater rods were placed in the center 20-mm holes on the samples designed to be maintained at 90°C (Fig. 4-6) to simulate the thermal period of ~300 years. Without the heating elements, glass samples were tested at ambient mine temperature (8-10°C), which is expected to be the temperature of a canister in a real repository after about 300 years. As shown in Fig. 4-7, a rubber seal was used to prevent water intrusion from the floor of the mine. Water entering the hole had to permeate through the granite.

Assemblies were retrieved at specific intervals over a 3-year period (see Table 4-2). After removal of the burial assemblies from the boreholes, they were wrapped in plastic until disassembled and analyzed. Water from the boreholes was analyzed prior to and after the assemblies were removed.



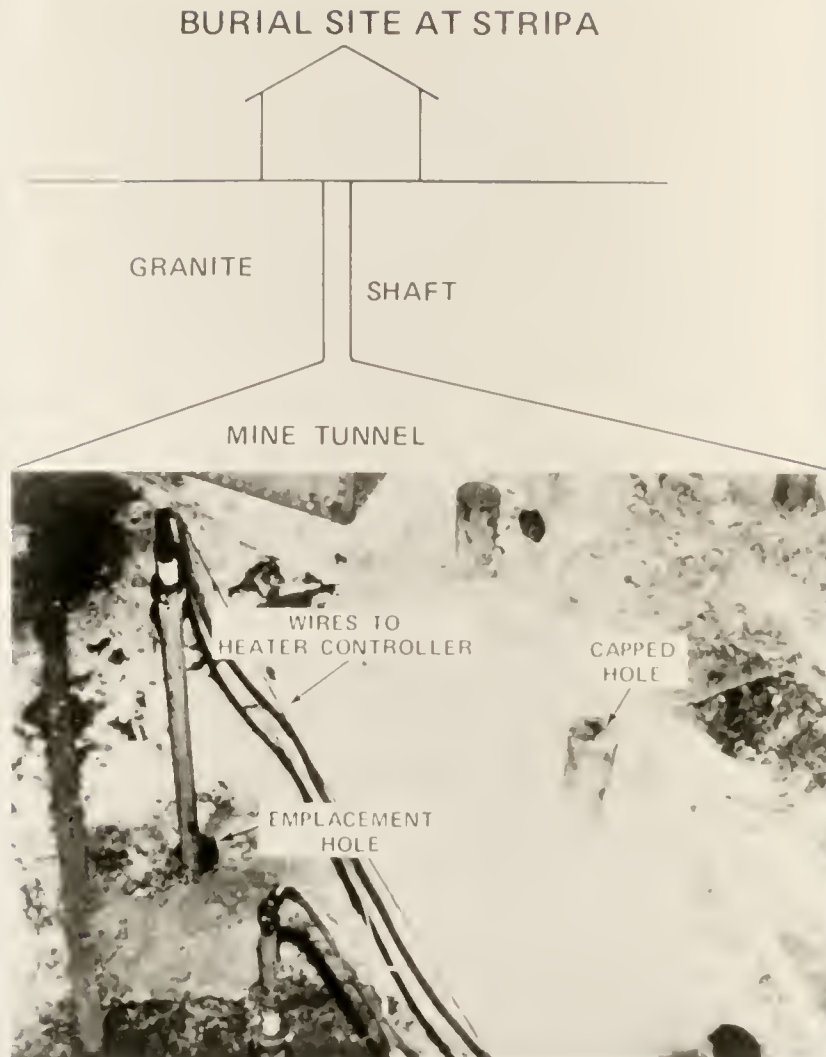


Fig. 4-6. Location within Stripa where SRL samples were buried. This is about 345 m below the surface. The holes into which the samples were placed are about 3-m deep and 56 mm in diameter. They were filled with water from the mine before the samples were emplaced. The arrow indicates holes into which the 1-month, 90°C specimens were placed. Samples were placed in the hole to a depth of about 2.5 m.

### SCHEMATIC OF BURIAL ASSEMBLY AT STRIPA

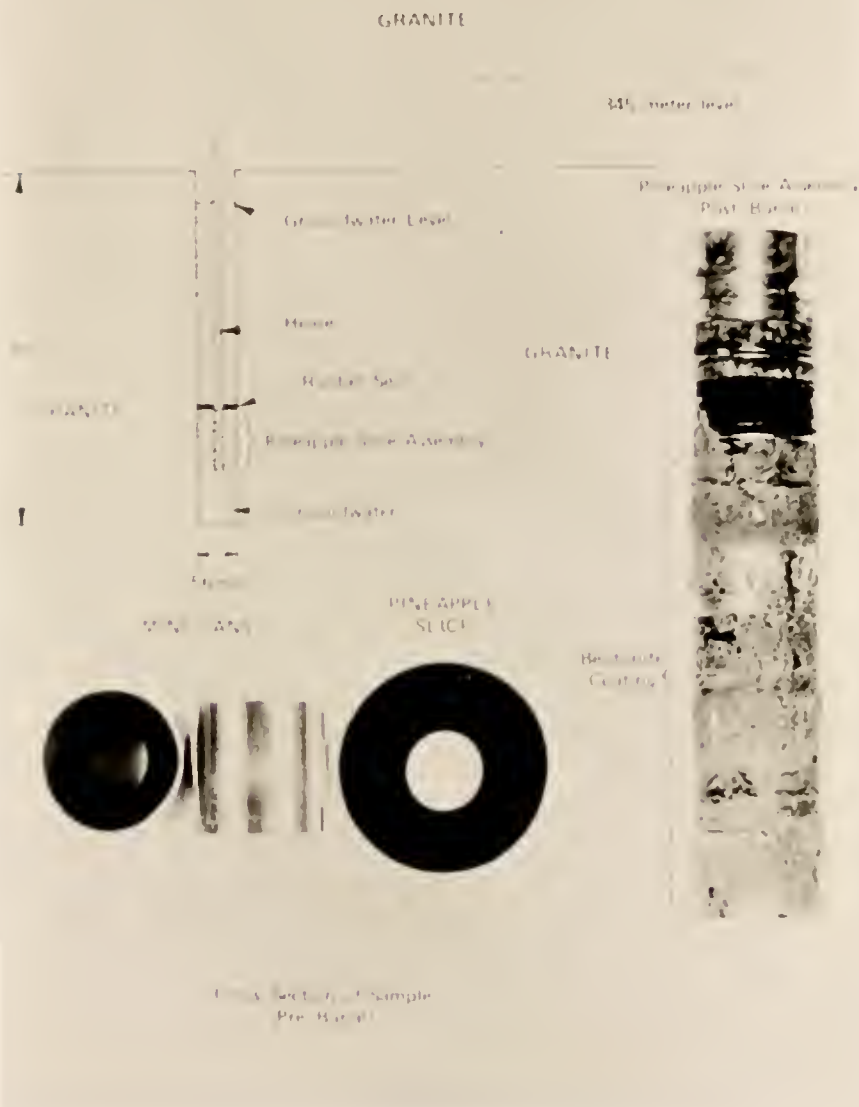


Fig. 4-7. Diagram illustrating the position of the samples in the Stripa mine during burial. A pineapple slice and minican are also shown, along with a photograph of the 1-month, 90°C assembly immediately after removal from the borehole.

Table 4-6. Ground Water Composition and pH Measured in This Study within the 1-month Test Hole at Stripa. Concentration mg/L.

	pH	Li	B	Na	Al	Si	Mn	Fe	Zn	Sr	Mo	La	Nd
Before Burial	8.1	0.16	<1	30	0.02	7.7	<0.1	<0.1	0.30	0.16	<0.01	-	-

Table 4-7. Ground Water Composition for the Stripa Granite, Literature Values.

<u>Anions</u>	<u>mg/l</u>
$\text{HCO}_3^-$	15.4-78.7
$\text{Cl}^-$	52-283
$\text{SO}_4^{2-}$	2.7-1.9
$\text{F}^-$	NR <sup>a</sup>
<u>Cations</u>	
$\text{Ba}^{2+}$	NR
$\text{Ca}^{2+}$	10-59
$\text{Fe}^{3+}$	0.02-0.24
$\text{Li}^+$	NR
$\text{Mg}^{2+}$	0.5
$\text{K}^+$	0.2-5.4
$\text{SiO}_2$	11.0-12.8
$\text{Na}^+$	43-125
$\text{Sr}^{2+}$	NR
pH	8.85-9.75
Total Dissolved	200-230 (330-410 m) <sup>b</sup> 375-510 (below 700 m) <sup>b</sup>

Adapted from [60].

<sup>a</sup> NR = not reported.

<sup>b</sup> Depth of sample below surface.

The measured flow rates through the boreholes near those where the assemblies were located were approximately 1 L/year (0.1 mL/hr) [61]. The glass surface area to ground water volume ratios (SA/V) were estimated to be  $>1 \text{ cm}^{-1}$  and were most likely different from spot to spot on some of the samples due to different water accessibility at the glass interfaces. The calculated SA/V ratios were low, about  $0.6 \text{ cm}^{-1}$  for the pineapple slices and  $0.06 \text{ cm}^{-1}$  for the minicans. This was based on the volume of water below the rubber seal and the total surface area of the glass in the hole.

The postburial procedures consisted of careful disassembling, soaking in deionized water for no more than 5 min to remove excess bentonite, if present, and two to three 5-min ultrasonic cleanings in acetone or absolute ethanol. The samples were air-dried and placed in a desiccator until analyzed.

#### Disadvantage of the Burial Test Method

The primary disadvantage of the Stripa burial is that it was not possible to calculate leach rates based on the data of solution analyses. This is because, when the samples were taken out of the borehole, the ground water above the rubber seal ran into the lower part of the borehole where the sample assembly was positioned. In addition, other contaminants may be present in the ground water. All these make the leach rate calculation based on the solution analysis data meaningless. Therefore, surface analyses had to provide the primary evaluation method for assessing glass performance and for comparing field- and laboratory-corroded specimens. As will be mentioned, the Materials Interface Interactions Tests

surface/solution analysis (MIIT-SS) effort contains an improvement over the Stripa burial in that solution analyses will be obtained [62].

#### Similar Tests Being Used in MIIT Studies at WIPP

The Materials Interface Interactions Tests (MIIT) is a series of experiments that will assess the performance of simulated SRL waste glass along with a variety of additional simulated waste glass compositions in the presence of various proposed canister, overpack and backfill components, in the salt geology at the Waste Isolation Pilot Plant (WIPP) [62]. Design and development of the MIIT tests were derived from the experience obtained through in-situ testing of over 100 simulated SRL waste glass samples buried in Stripa granite, Sweden. The MIIT in-situ testing program represents a "second generation" of the Stripa tests. The MIIT studies consist of two parts, MIIT-MI (multiple interactions), and MIIT-SS (surface/solution analysis). The MIIT-MI effort is similar to the Stripa experiments and involves glass performance as a function of a variety of proposed package components, predominantly by surface analyses. The MIIT-SS effort represents a significant improvement over the Stripa burial experiments in that solution analysis will also be obtained for simplified interactions, and time-dependent data will be obtained from single boreholes. Only pineapple slice assemblies will be utilized. All tests will be conducted at 90°C. Samples will be removed from the mine at time intervals of 6 months, 1 year, 2 years and 5 years.

### Laboratory Tests of Simulated Corrosion

In order to simulate the actual repository conditions, two sets of laboratory leaching tests were conducted. In one set, a modified MCC-1 static leach test method was used for SRL 165 + 29.8% TDS glass with two different glass surface area-to-volume of leachant (SA/V) ratios, 0.1 and 1.0 cm<sup>-1</sup>. The leachant was selected from one of the following: deionized water, Stripa ground water and Stripa ground water saturated with glass powders of the same composition as the bulk specimen at 90°C for 14 days. Prior to immersing in the leachant, each specimen was ultrasonically cleaned in either reagent grade acetone or absolute ethanol for 3 times, 5 min each. The samples were suspended inside either a PFA Teflon\* (60 ml capacity) corrosion cell and then placed inside a constant Blue M\*\* convection oven as shown in Fig. 4-8.

In another set of so-called "rock cup tests," a Stripa granite cup was placed in each PFA Teflon container to simulate granite repository conditions. The granite was obtained from boreholes in Stripa, Sweden, and the granite cups were made by Diversified Machine Works, Post Falls, Idaho. A diamond drill was used to drill a hole, 3.2 cm in diam. by 3.8 cm deep in each granite cylinder, 4.4 cm in outside diam. by 4.9 cm high. Monolithic glass samples of Black Frit 165-Mobay (see Table 4-4) were placed in the cup. A certain volume of ground water was filled both inside and outside the cup. Some of

---

\* 0102-53 MOD PFA Teflon jar, Savillex Corp., Minnetonka, MN.

\*\* Model OV-490A-2, Blue M Co., Blue Island, FL.



# ENVIRONMENTAL TESTING SYSTEM

CONSTANT TEMPERATURE OVEN  
TEMPERATURE CONTROLLER  $\pm 0.1^{\circ}\text{C}$   
OVER EXTENDED PERIODS

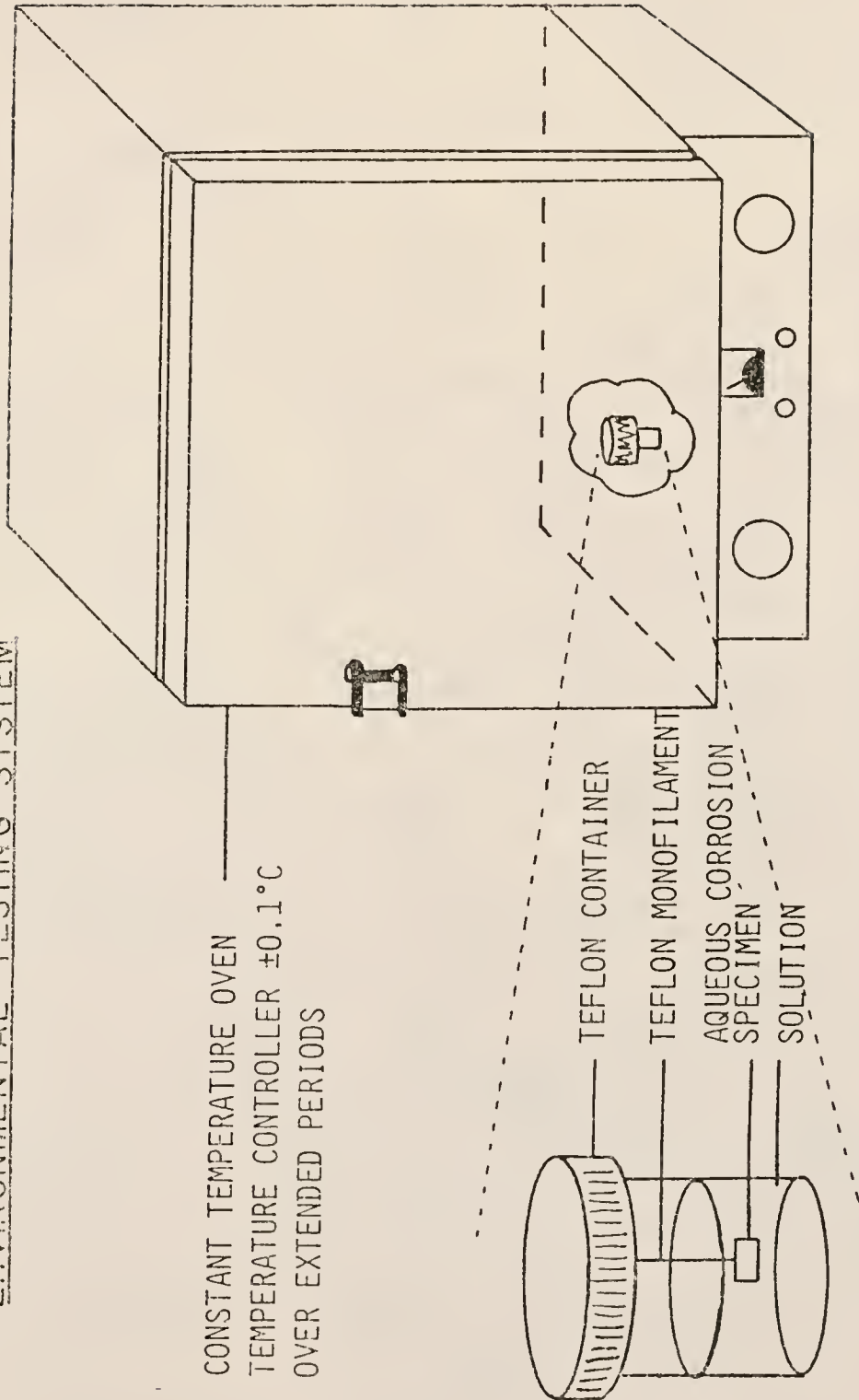


Fig. 4-8. Schematic of experimental configuration of static leach test.

the cups contained stainless steel (316 L) wires used for supporting the glass specimens. The rock cups were soaked in ground water for 2 days, then air dried.

Both static and flow test conditions were used in the rock cup tests. The SA/V ratio was  $1.0 \text{ cm}^{-1}$  in the cells. In the case of static leaching, the surface area of glass sample was about  $14 \text{ cm}^2$ . A stainless steel (316 L) wire, 0.1 cm in diameter by 18 cm in extended length was contained in the rock cup. All glass samples and stainless steel wires were cleaned ultrasonically 3 times, for 5 min before leaching with absolute ethanol. A corrosion cell for the rock cup static test is similar to that for the flow test shown in Fig. 4-9 but without the fittings in the lid of the Teflon container.

In the rock cup flow test, low flow rates, 0.1-0.3 mL/h, were used. This single pass continuous flow test method was similar to the MCC-4S procedures [27]. A stainless steel (316 L) wire, 0.1 cm in diameter x 36 cm in extended length, was contained in the rock cup. The glass surface area was about  $26 \text{ cm}^2$ . The procedures of sample preparation and granite cup cleaning were the same as in the static test. A flow leaching vessel and the experimental set-up are shown in Figs. 4-9 and 4-10. Only the leachant within the cup was forced to flow using a Peristaltic cassette pump.\* The flow rate of the ground water was controlled to  $\pm 10\%$  of the set value. The ground water was not preheated in the reservoir. Since the flow rate was low and the ground water prior to being introduced into the leaching

---

\* Made by Manostat, New York, NY.



Fig. 4-9. A corrosion cell in the flowing test.

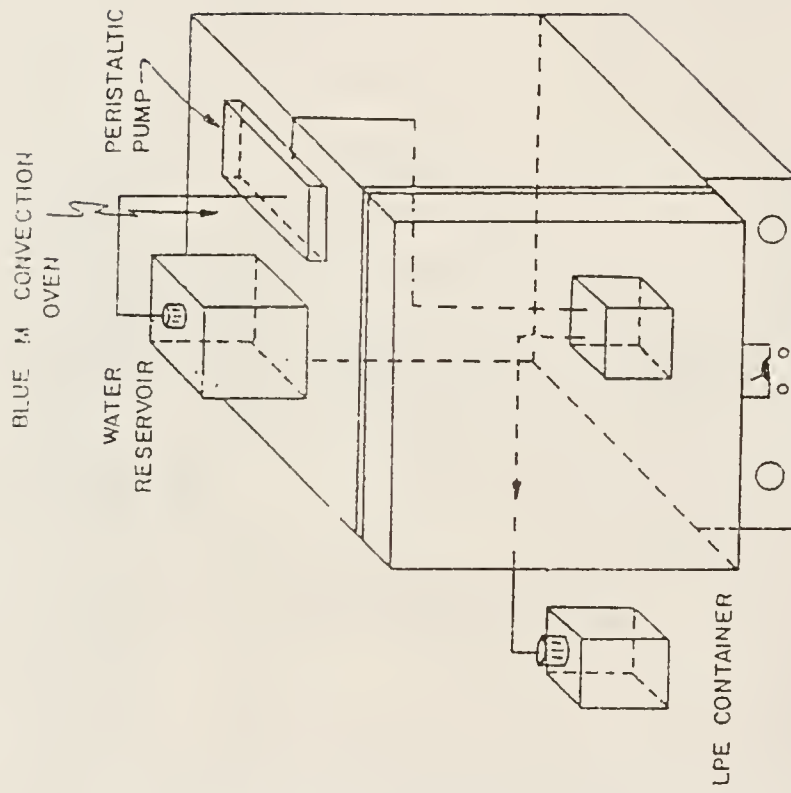


Fig. 4-10. Schematic of experimental configuration of continuous flow test.

vessel was kept at 90°C in the tubing for some time (longer than 5 min), the temperature within the leaching vessel would not be changed due to the water flow. The leachant after passage through the leach vessel was collected weekly.

All the laboratory tests were run at 90°C for up to 6 months. The sample matrix of the experiments is shown in Table 4-8.

Before leaching, each sample was weighed and examined under an optical microscope. FT-IRRS was run at 2-3 spots on each sample.

### Analytical Techniques

A combination of several analytical techniques was used for evaluating nuclear waste glass leaching. Each of the methods yields averaged information which is characteristic of a volume extending from the surface to a specific depth within the sample, as shown in Fig. 4-11 and Table 4-9. In addition, SIMS provides depth resolved concentration profiles from the surface into uncorroded bulk. As discussed earlier, all the solid surface analysis techniques in Fig. 4-11 have been used for characterizing changes on the Stripa burial glass surfaces. Solution analysis techniques including inductively-coupled plasma (ICP), atomic absorption spectrophotometry, colorimetry, and pH measurement were also used with the laboratory leached specimens.

### Solid State Analyses

#### Optical microscopy

Each sample was examined under a microscope using the reflection light mode, both prior to and after leaching. Magnification of 100X

Table 4-8. Sample Matrix of the Laboratory Tests.

---

Glass Composition*	SRL 165 + 29.8% TDS, Black Frit 165-Mobay
Temperature	90°C
SA/V	0.1 and 1.0 cm <sup>-1</sup>
Leaching Time	1, 3 and 6 months
Leaching Condition	Static and flow (0.1 and 0.3 mL/h), with and without granite cup
Leachant	deionized water Stripa ground water Stripa ground water saturated with glass powders for 14 days at 90°C

---

\* Samples were run in duplicates.

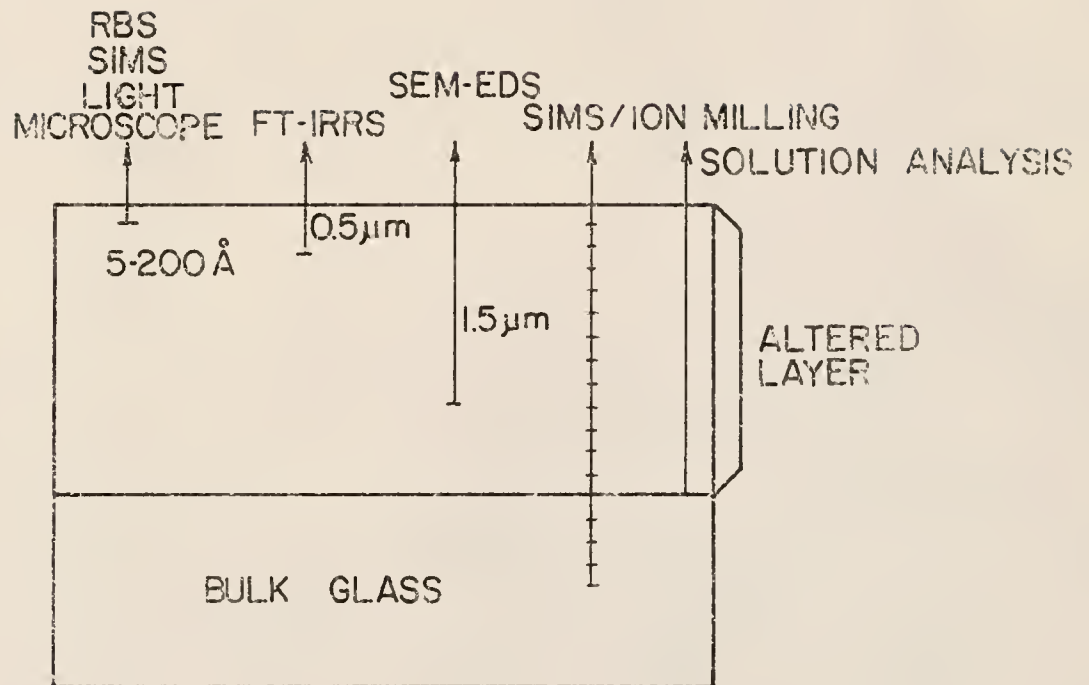


Fig. 4-11. Sampling depths with various techniques used in this study (adapted from [63,64]).



Table 4-9. Characteristics of Analytical Techniques.

	Sampling depth	Spatial resolution	Information	Detection limits(%)
Secondary ion mass spectroscopy (SIMS)	5-20Å (profiling to $\approx 10\mu\text{m}$ )	100Å- $\approx 1\mu\text{m}$	composition structure	$\leq 10^{-4}$
Fourier transform infrared reflection spectroscopy (FT-IRRS)	$\approx 0.5\mu\text{m}$	3-5mm	composition structure morphology	3
Scanning electron microscopy-energy dispersive spectroscopy (SEM-EDS)	1.5 $\mu\text{m}$	1.5 $\mu\text{m}$	morphology composition	5
Rutherford back scattering (RBS)	100 Å- $\approx 1\mu\text{m}$	1mm	composition	$\geq 10^{-3}$

was used in all cases, which permits examination of the general surface characteristics. For preleached glasses, heterogeneities, such as crystallites, can be observed (Fig. 4-12). These heterogeneities usually result when glass homogenization is not complete or the wastes have not been dissolved by the glass matrix. The glass surface finish conditions also can be checked (Fig. 4-13). In this study, glasses were polished to 600 grit or 6- $\mu$ m surface finish. Examination with an optical microscope served as a quality control for the sample conditions. For the leached glass surfaces, both surface roughening and surface precipitates can be evaluated using this simple, rapid, and inexpensive technique.

#### Fourier transform infrared reflection spectroscopy (FT-IRRS)

Fourier transform infrared reflection spectroscopy (FT-IRRS) has recently been developed as a semi-quantitative tool for characterizing the surface structure and composition of glasses both prior to and after exposure [65,66]. The important advantages of this technique include (1) it does not require vacuum and energetic electron or ion bombardment; thus it does not alter the surface of the glass as may Auger electron spectroscopy (AES), electron spectroscopy of chemical analysis (ESCA) and secondary ion mass spectrometry (SIMS); (2) it is applicable to in-situ glass surfaces of nearly any configuration and can be used for analysis of large or small areas, if desired, is relatively inexpensive and requires only standard infrared spectrometers; and (3) the FT-IRRS method can be used as an automated analytical tool and can also be coupled with solution analysis, making it especially suitable for characterization



Fig. 4-12. Light micrograph of SRL 131 + 29.8% TDS glass with crystallites (100X).



Fig. 4-13. Light micrograph of a typical glass surface after polishing to 600 grit surface finish (100X).

of surface/environment interactions [67-69]. In a spectrum of the binary soda-silica glass surface, the region where the Si-O-Si stretching peak (S) and silicon-oxygen-alkali (NS) stretching peak overlap occurs is called the coupled region. Exposure of the glass to a chemical environment alters the relative concentration of both silica and alkali ions due to preferential leaching of the alkali ions. This produces the decoupling of the S and NS peaks in the infrared reflection spectra.

Extensive surface reactions can lead to roughening of the glass surface due to formation of either pits or surface deposits. However, the wavenumber location of the S and NS peaks is not changed significantly by the surface roughening. Therefore, it is possible to use the shift of the wavenumber location of the FT-IRRS peaks to measure the change in composition of the glass surface, independent of roughening or surface deposition. The extent of surface roughening can be assessed by the decrease in intensity of the FT-IRRS peak when wavenumber location remains unchanged.

It should be noted that the FT-IRRS technique is useful for determining changes in reaction layers of  $\sim 0.5 \mu\text{m}$  thick or greater. Because of the  $0.5\text{-}\mu\text{m}$  sampling depth, the information collected by this technique within the sampling depth is averaged and accurate analysis of very thin ( $<1000 \text{ \AA}$ ) surface corrosion films is not possible. For very thick reaction layers, FT-IRRS provides an analysis of only the outer  $\sim 0.5 \mu\text{m}$  of the layer using near normal specular reflectance. This nondestructive testing technique is valuable for quick and efficient routine controls while in other

cases more detailed and usually more expensive analyses such as SIMS are necessary. Figure 4-14 shows the FT-IRRS analyses of SRL 165 + 29.8% TDS glass/glass interface prior to and after 2-year burial in Stripa at 90°C. The decoupling of the S and NS peaks in the region of 800-1150  $\text{cm}^{-1}$  and loss of peak intensity as shown in the postburial spectrum are a result of leaching.

#### Scanning electron microscopy/energy dispersive spectroscopy (SEM-EDS)

The major advantages of SEM over other techniques such as optical microscopy are that much higher magnification and a greater depth of field are possible. The specimens were usually vacuum coated with 100 Å of C or Au-Pd. The information obtained using this technique is mainly qualitative, although EDS in favorable cases may yield the average composition of the outer most few microns. Figure 4-15 shows a typical SEM\* micrograph of a glass surface after polishing to 600 grit and prior to leaching. Figure 4-16 shows the EDS data of SRL 131 + 2.98% TDS glass prior to burial.

#### Secondary ion mass spectroscopy (SIMS)

Secondary ion mass spectroscopy (SIMS) has an information depth of the order of one atomic layer combined with ionic milling (sputtering), which together with high detection sensitivity for most elements offers a unique potential in profiling. During the last several years, advances have been made by scientists at the Chalmers

---

\* Scanning electron microscope, model JSM-35CF, JEOL Ltd., Tokyo, Japan.

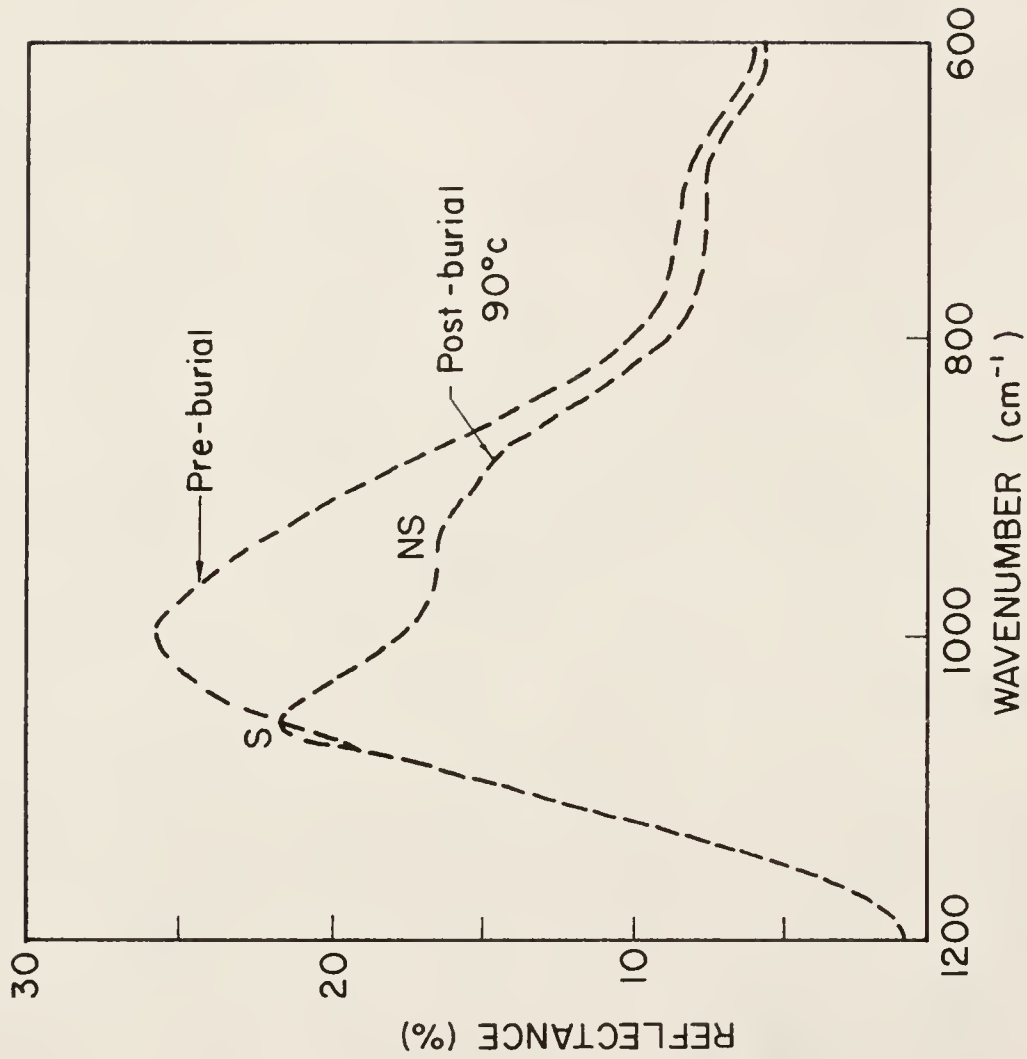


Fig. 4-14. FT-IRRS analysis of SRL 165 + 29.8% TDS glass/glass interface prior to and after 2-year burial in Stripa. The postburial spectrum shows the decoupling of the S and NS peaks in the region of 800-1150  $\text{cm}^{-1}$  and loss of peak intensity as a result of leaching.





Fig. 4-15. SEM micrograph of a typical glass surface after polishing to 600 grit prior to leaching.

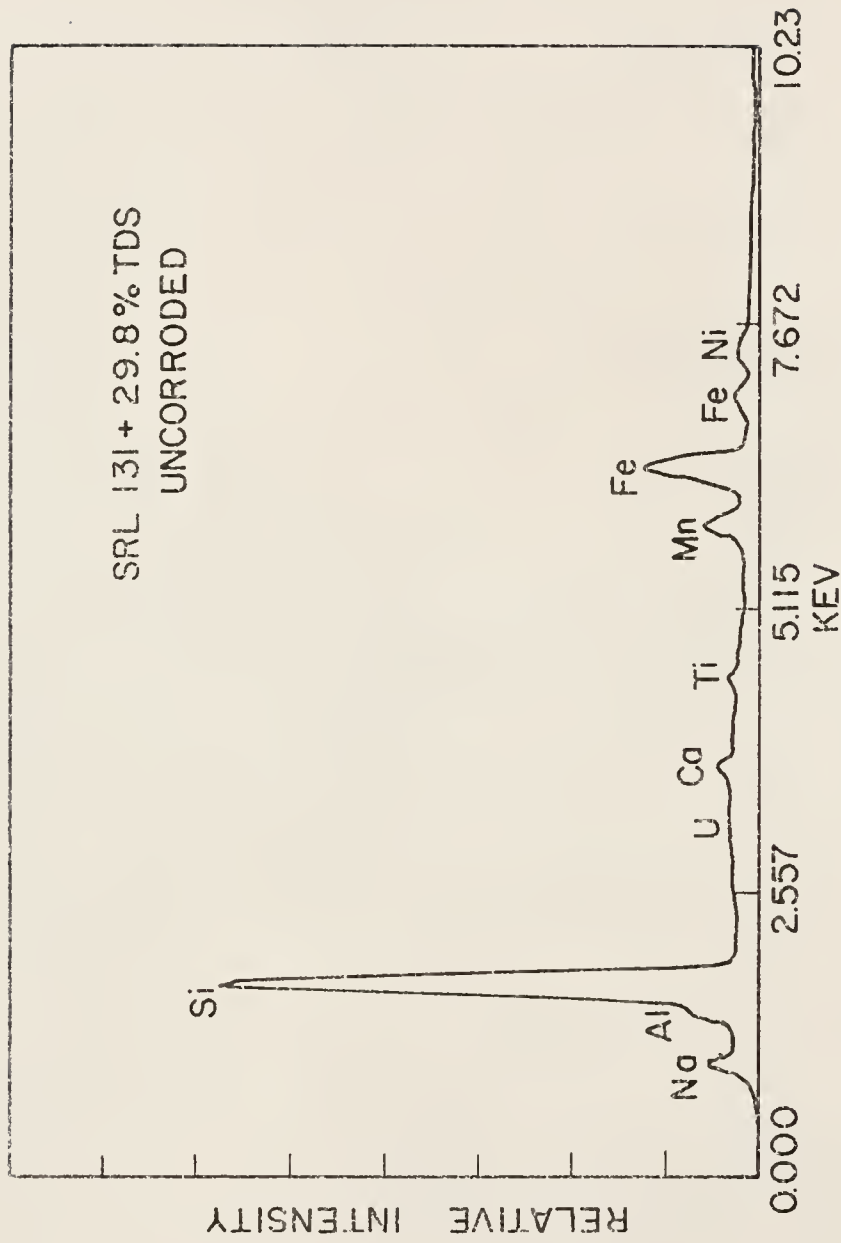


Fig. 4-16. EDS analysis of an uncorroded SRL 131 + 29.8% TDS glass surface.

University of Technology, Sweden, to develop SIMS as a sensitive and routine tool in the study of glass corrosion [70]. The glass samples were coated with a 100 Å Au film to reduce surface charging. The Cameca 3-F ion probe accelerated and focused a beam of  $O^+$  ions towards the glass sample, successively eroding the surface by sputtering, while cyclically counting the yields of sputtered secondary ions of different species which can be detected and quantified with a mass spectrometer. The raw data, processed by an on-line computer, consisted of these ionic yields vs the corresponding sputtering time. With the aid of known relative elemental sensitivity factors (RSF), the ionic yields were converted to the percent atom concentrations of all the measured elements and their sum of cations was set equal to 100 percent. Although H is measured, it is not included in the conversion calculation, because the H content of the preleached glass is unknown. The determination of relative erosion speeds at different depths of the sputtered layer permitted the conversion of sputtering time to depth. As an example, the element concentration profiles of ABS 118 glass/glass interface after 12-month, 90°C burial are shown in Fig. 4-17.

In the most recent version, the profiles were corrected to consider the elemental release and absorption during corrosion. These profiles are different from the atomic concentrations (in percent) shown in Fig. 4-17. The new profiles indicate the actual gram·atoms of each element after leaching of 100 gram·atoms of original glass, and so may be directly used in calculations of elemental losses. Due to the cation (except H) release and

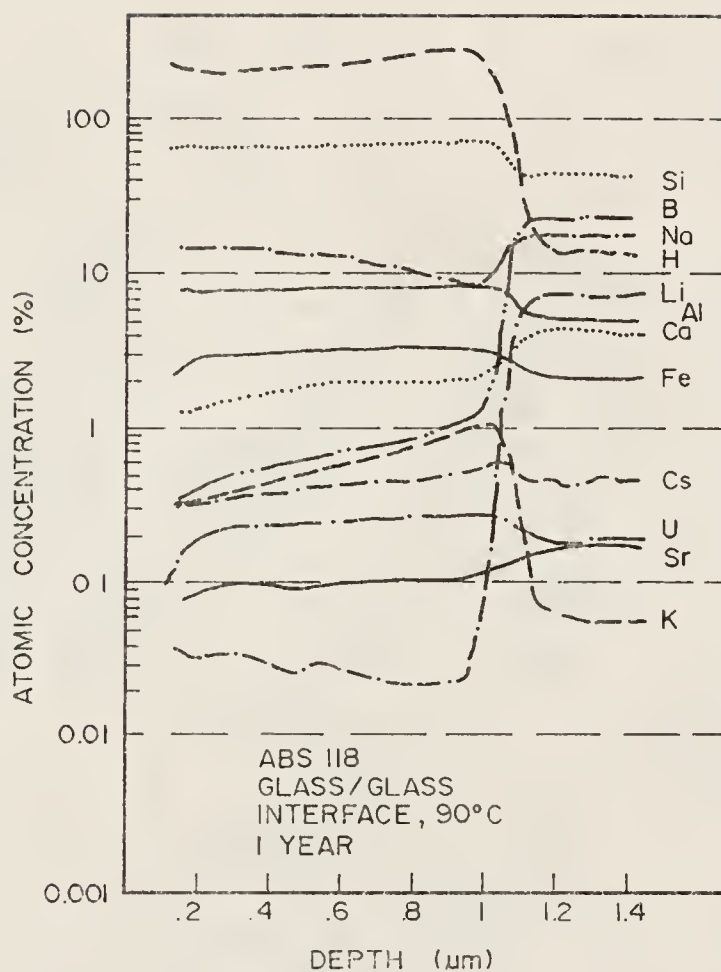


Fig. 4-17. SIMS depth profiles of ABS 118 glass/glass interface after 1-year, 90°C burial in Stripa. The atomic concentrations of all cations (except H) are summed up to 100%.

adsorption, these actual gram-atoms of various cations may not be summed up to 100 after leaching. These profiles were calculated using the least leachable elements (in most cases Al, sometimes Fe, Mn or Zr) as a standard and assuming that their actual gram-atoms remain unchanged at any time at the surface.

Taking Al as a standard element, the following equation can be written based on 100 gram-atoms of unleached glass at a specified depth in the glass surface,

$$GA_{Al,after} = GA_{Al,before} + GA_{Al,abs} - GA_{Al,leached} \quad (4-1)$$

where  $GA_{Al,after}$  = gram-atoms of Al after leaching;

$GA_{Al,before}$  = gram-atoms of Al before leaching;

$GA_{Al,abs}$  = gram-atoms of Al absorbed from solution;

$GA_{Al,leached}$  = gram-atoms of Al leached.

Since the concentrations of Al in the ground water were low both before and after leaching (see Table 5-1), neglecting the last two terms on the right side of equation (4-1) will not introduce appreciable error. Thus, we have

$$GA_{Al,after} = GA_{Al,before} \quad (4-2)$$

where  $GA_{Al,after}$  and  $GA_{Al,before}$  are the same as in equation (4-1).

Also, we can write

$$GA_{Al,after} = at.\%_{Al,after} \cdot \sum_i GA_{i,after} \quad (4-3)$$

where  $at.\%_{Al,after}$  is concentration of Al (in at.%) at a certain depth after leaching as shown in Fig. 4-17 and  $\sum_i GA_{i,after}$  is a summation of the gram-atoms of element  $i$  after leaching. Combining equations (4-2) and (4-3) gives

$$GA_{Al,before} = at.\%_{Al,after} \cdot \sum_i GA_{i,after} \quad (4-4)$$

Also

$$GA_{i,after} = at.\%_{i,after} \cdot \sum_i GA_{i,after} \quad (4-5)$$

where  $at.\%_{i,after}$  is concentration of element  $i$  (in at.%) at a certain depth after leaching, as shown in Fig. 4-17. From equations (4-4) and (4-5), we have

$$GA_{i,after} = \frac{at.\%_{i,after} \cdot GA_{Al,before}}{at.\%_{Al,after}} \quad (4-6)$$

Using equation (4-6), the actual gram-atoms of each element left based on 100 gram-atoms of unleached glass at a certain depth can be calculated. The results as obtained from the on-line computer of the SIMS instrument are given in Fig. 4-18 for the same glass specimen shown in Fig. 4-17.

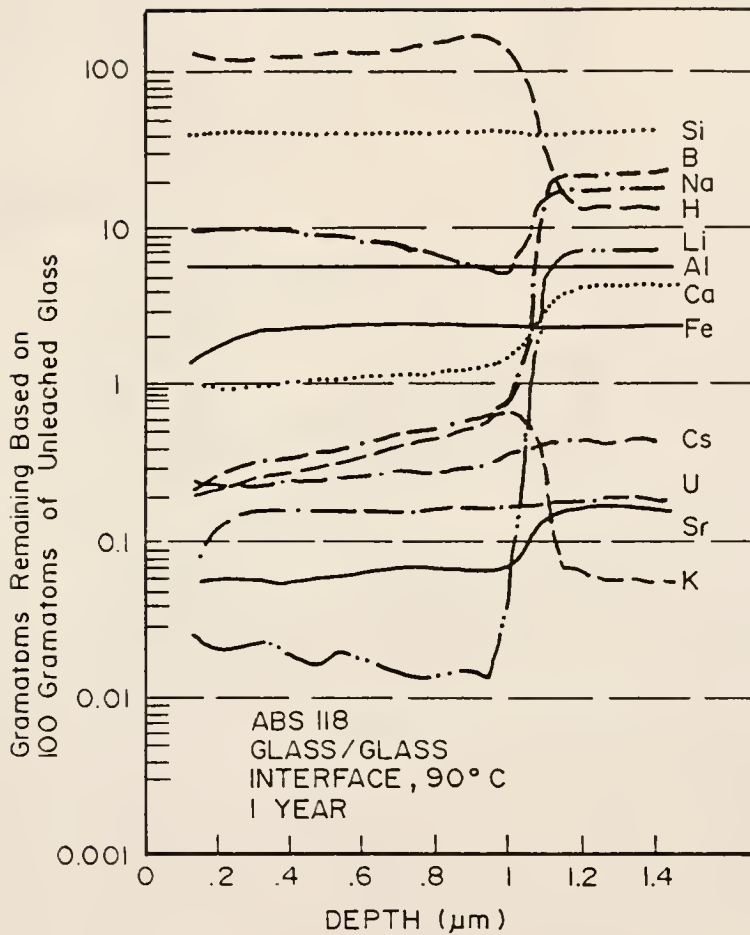


Fig. 4-18. SIMS depth profiles of ABS 118 glass/glass interface after 1-year, 90°C burial in Stripa. Data are presented as gram•atoms of various cations remaining in the leach layer at certain depth based on 100 gram•atoms of unleached glass.



Density calculation. The density of the leached surface as a function of depth was estimated using SIMS depth profiles of concentration (such as Fig. 4-17), based on conservation of matter and assuming that the volume concentration of the least-soluble species, such as Fe, Ni, Al, Zr, and Mn remain unchanged throughout the leached layer. Thus

$$\text{wt.\%}_i \cdot d = \text{wt.\%}_{i,\text{bulk}} \cdot d_{\text{bulk}} \quad (4-7)$$

where  $i$  is  $\text{Fe}_2\text{O}_3$ ,  $\text{NiO}$ ,  $\text{Al}_2\text{O}_3$ ,  $\text{ZrO}_2$  or  $\text{MnO}_2$ ;  $\text{wt.\%}_i$ , the wt% of the  $i$ th oxide;  $d$ , the density of the leached layer at a specific depth, and  $d_{\text{bulk}}$  is the glass density. From equation (4-7),

$$I_d = \frac{d}{d_{\text{bulk}}} = \frac{\text{wt.\%}_{i,\text{bulk}}}{\text{wt.\%}_i} \quad (4-8)$$

where  $I_d$  is the density index at a certain depth.

#### Rutherford back scattering surface analysis (RBS)

The Rutherford back scattering (RBS) method is a near surface analytical technique with a depth resolution of approximately 20 nm and a penetration range of up to 4000 nm [71,72]. The method is generally most effective for heavy elements in a lighter matrix. Consequently, RBS analysis may be especially useful for determining changes in uranium surface concentration during burial and in evaluating glass/metal overpack interactions such as glass/Pb interfaces. Furthermore, RBS is practically nondestructive, rapid

(15 min/spectrum) and less expensive when compared with techniques such as SIMS. The RBS technique is not ideal as a preliminary mode of analysis on complex specimens with unknown composition because mass discrimination decreases as the atomic number increases. However, it is valuable for rapid comparison of complex specimens for which basic elemental data are well established.

The RBS data were obtained using the van de Graaf generator and RBS collection system of the University of Florida's Major Analytical Instrumentation Center. The RBS analysis was performed using a 2 MeV alpha particle beam. The beam current was ~100 nA. The beam area was ~1 mm<sup>2</sup>. The scattering geometry was that of normal incidence with a scattering angle of 170°. The silicon detector had a surface area of ~20 mm<sup>2</sup> and was positioned at ~120 mm from the specimen. Only selective glass samples were run by the RBS analysis.

#### Solution Analyses

The solutions were analyzed in a variety of ways to obtain elemental concentrations and pH. These include colorimetry\*, inductively coupled plasma atomic emission spectrometry (ICP)\*\* and pH determination.\*\*\* All the solution analyses and pH measurements were done at room temperature.

---

\* Hach DR/2 Spectrophotometer, Hach Company, Loveland, CO.

\*\* Inductively coupled plasma atomic emission spectrometer, model Plasma 200, Instrumentation Laboratory, Waltham, MA.

\*\*\* Digital ionalyzer, model 801A and Ross combination electrode, model No. 810200, Orion Research, Inc., Cambridge, MA.

For most of the experiments, ICP was used for analyzing all the elements. In some cases, Si concentration was determined by using colorimetry. In an ICP, the sample solution is introduced into a spray chamber with the help of a nebulizer. The nebulizer converts the liquid sample into a fine aerosol. Argon gas flows through a quality torch which carries the smaller aerosol droplets of sample into the conical channel of plasma. The high temperature of the plasma produced by a radio frequency generator, desolvates the droplets and dissociates them into individual atoms and ions. They are excited to emit light at various wavelengths characteristic of the element, which are analyzed by a spectrometer. The spectral intensities are directly proportional to the elemental concentrations. The photomultiplier converts the light energy into electrical signals which are then digitized and processed by the instrument's computer.

## CHAPTER V TEST RESULTS

### Field Test Results

#### General Observation

When the assemblies were removed from the boreholes, there was a thin (<5 mm) coating of bentonite over their outer surfaces, as shown in Fig. 5-1. Apparently, the compacted bentonite swelled during burial and was extruded between the sides of the granite boreholes and the surfaces of the assemblies. In some instances, bentonite intrusion was observed between the minicans and the pineapple slices. For up to 1-year burial, accelerated attack was usually found on the glass surfaces exposed to compacted bentonite, or where bentonite had intruded between two samples.

Cracks were observed on many of the pineapple slices during disassembly. Two possible causes for the cracks were (1) pressure due to the swelling of the bentonite during burial, which produced a bending moment on the glass samples, and (2) large forces required to extract the assemblies from the boreholes (also due to the swelling of the bentonite), which also produced a bending moment on the glasses.

The pH changed by less than 1 unit in the boreholes from which the 1-month, 90°C minican assemblies of SRL glasses and the 31-month, 90°C pineapple slice assemblies of ABS glasses were removed.

Pineapple Slice Assembly



Post Burial - 1 Month - 90°C

Fig. 5-1. A typical assembly after burial in Stripa mine. Bentonite coating can be observed on the outer surface due to bentonite swelling.

Measured flow rates through similar holes located elsewhere in the mine were approximately 1 L/yr [61].

Several types of surface areas were observed on the postburial glass surface. As in the case of glass/glass interface shown in Fig. 5-2, these include clear, cloudy and bentonite-intruded areas. Variations in corrosion did occur from spot to spot over the same samples and this is attributed to local water accessibility, bentonite intrusion and extent of interfacial contact between the various samples. The actual SA/V ratio for the glass surfaces (including both polished and unpolished surfaces) are expected to be higher than  $0.03\text{-}0.6\text{ cm}^{-1}$ , which was calculated based on the total area of glass surface in the assembly and the volume of ground water in the corresponding borehole.

Table 5-1 shows the ground water compositions collected from the boreholes where SRL glass pineapple slice assemblies were removed. The concentration of Na increased from 40 to 255 mg/L and that of Si increased from 2.3 to 35.3 mg/L. The increased Na and Si concentration in the ground water could be due to leaching from the glass as well as release from the bentonite with the surrounding granite.

#### Results with ABS Glasses

Figure 5-3 compares the FT-IRRS spectra of the glass/glass, glass/granite and glass/bentonite interfaces for ABS 39 and 41 before and after 31-month, 90°C Stripa burial. This figures shows that the postburial spectra of ABS 41 glass/glass and ABS 41 glass/granite interfaces changed less than those of ABS 39. However, spectra of

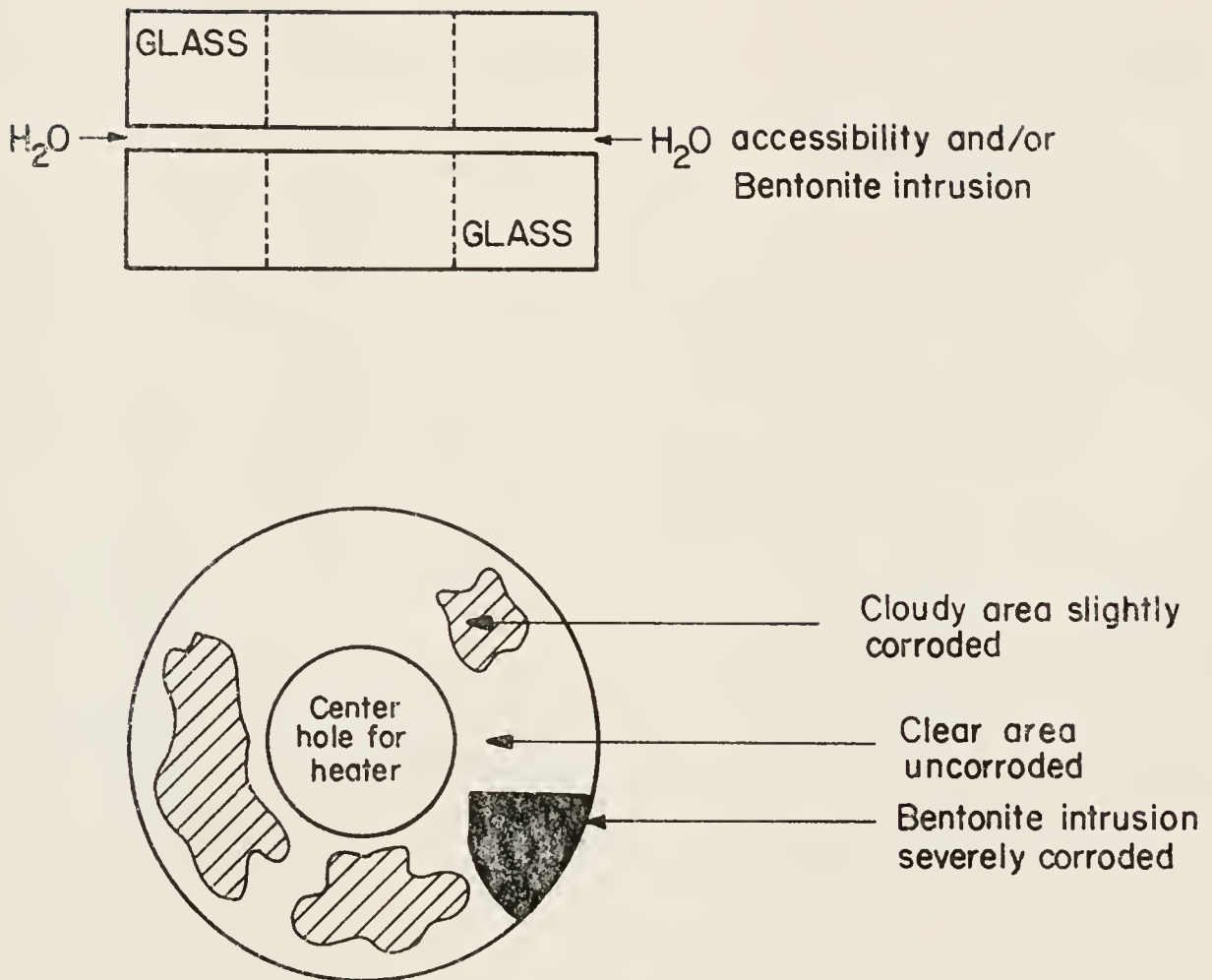


Fig. 5-2. Schematic of glass/glass interface illustrating several types of surface areas resulting from water and/or bentonite intrusion.



Table 5-1. Composition of Ground Water Collected from the Boreholes where SRL Glass Pineapple Slice Assemblies Had Been Buried. Potassium and Ca are noted but not measured.

Element	Concentration (mg/l)			
	Preburial	Postburial (months)		
		1	3	24
Na	30	70	190	147
Li	0.16	0.52	0.96	0.17
Si	7.7	10	43	14
Al	0.02	0.04	0.7	0.2
B	<1	0.9	5.48	1.26
Mo	0.16	0.35	0.29	0.25
Cr	-	-	<0.01	0.06
Fe	<0.1	<0.2	0.5	0.8
Ni	-	-	<0.01	0.11
Mg	-	-	2.13	0.77
Cu	-	-	<0.01	0.01
Zn	<0.1	<0.01	0.13	0.13
Mn	<0.1	<0.2	<0.01	0.03
La	<0.01	<0.01	<0.01	<0.01
Nd	<0.01	<0.01	<0.1	<0.1
Sr	0.30	0.20	0.19	0.38
Ba	-	-	0.20	0.07

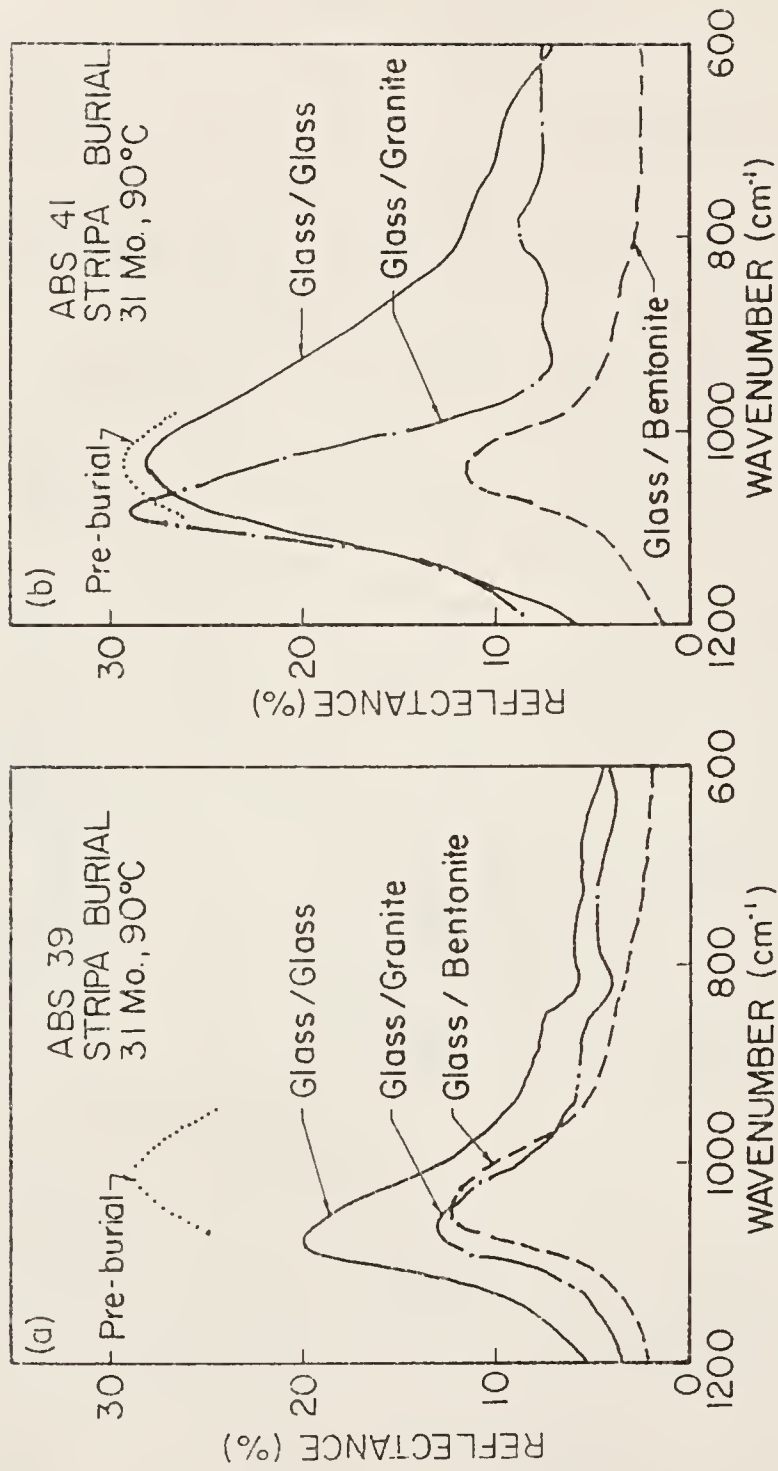
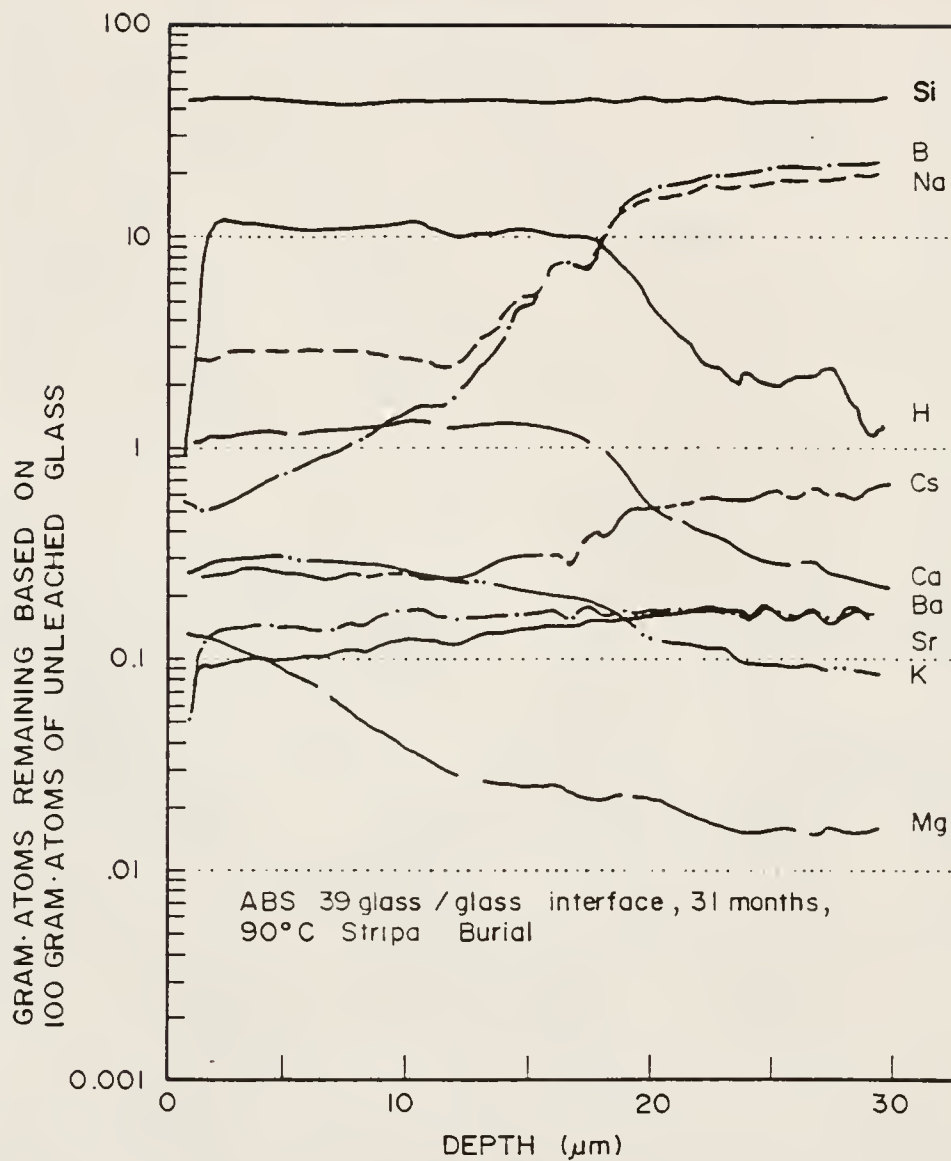


Fig. 5-3. FT-IRRS spectra of glass ABS 39 (a) and ABS 41 (b) before and after 31-month, 90°C Stripa burial.

the glass/bentonite interface did not show much difference between these two compositions.

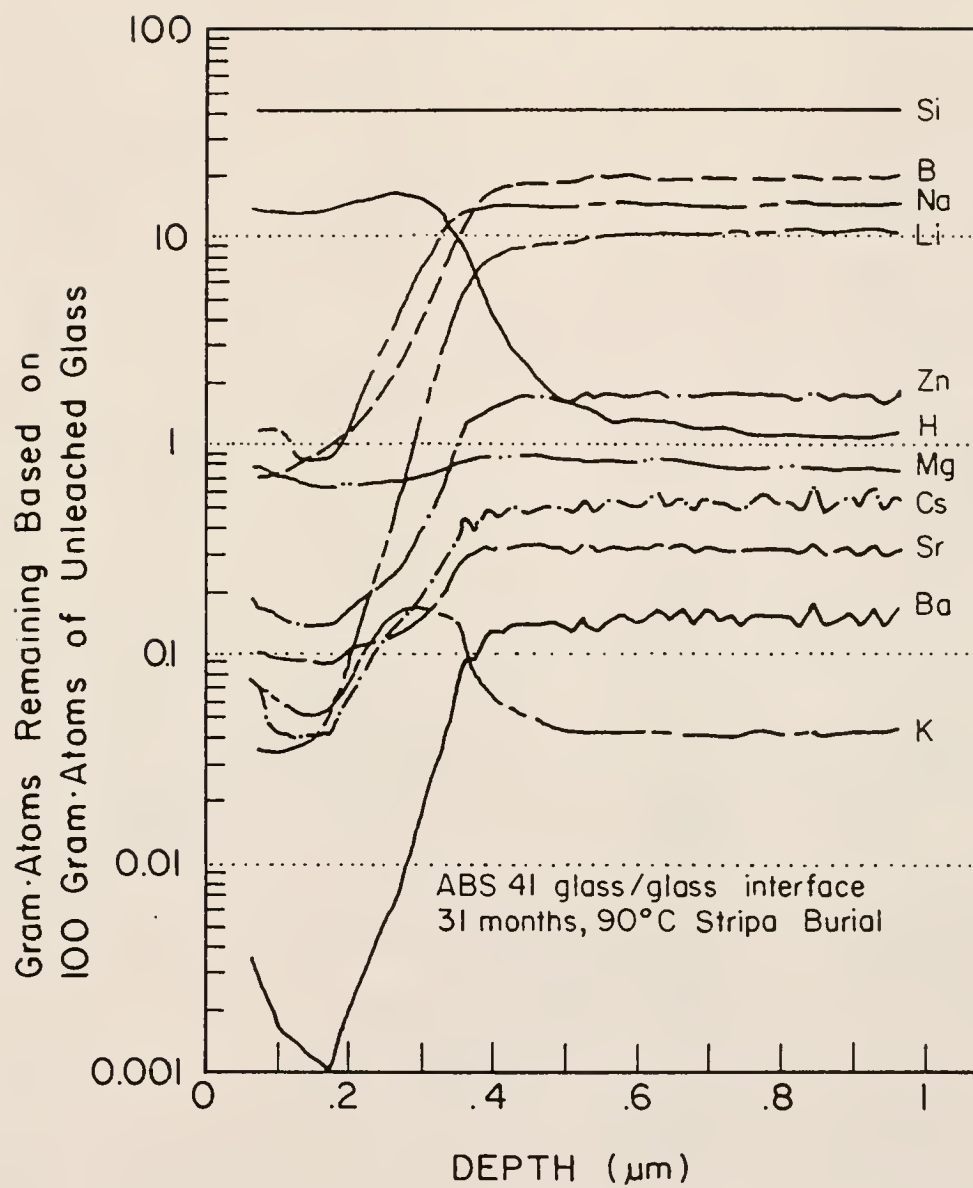
As can be seen in Fig. 5-3 (a), all three postburial spectra of ABS 39 lost considerable intensity. Based on previous FT-IRRS investigations of glass-water interactions [65,69] and the SIMS analysis shown in Fig. 5-4, this loss is due to extensive sodium and boron depletion, surface roughening and probably network dissolution. For glass/glass and glass/granite interfaces, the relative silica concentration at the glass leached layer increased, as indicated by the shifting of the peak associated mainly with Si-O-Si stretching vibrations from  $1010\text{ cm}^{-1}$  to  $1060\text{--}1070\text{ cm}^{-1}$ . For the ABS 39 glass/bentonite interface, no obvious shifting of this peak to higher wavenumbers was found.

The ABS 41 glass/glass and glass/granite interfaces behaved quite differently from those of ABS 39. For example, the FT-IRRS spectrum of the glass/glass interface almost retains the shape of the preburial spectrum, indicating very little surface attack. This is confirmed by the SIMS depth profiles. As shown in Fig. 5-4(b), the leach depth of the ABS 41 glass/glass interface is less than  $0.4\text{ }\mu\text{m}$ , which is below the sampling depth of FT-IRRS ( $\sim 0.5\text{ }\mu\text{m}$ ). In the case of the ABS 41 glass/granite interface, extensive depletion of alkali was observed, as shown by the loss in spectral intensity at the lower wavenumbers in Fig. 5-3 (b). However, the intensity of the major peak at  $1080\text{ cm}^{-1}$  of this spectrum is as high as that of the preburial one, indicating very little network dissolution and surface



(a)

Fig. 5-4. SIMS depth profiles for (a) ABS 39 (Al-corrected) and (b) ABS 41 (Si-corrected) after 31-month, 90°C Stripa burial.



(b)

Fig. 5-4.--continued.

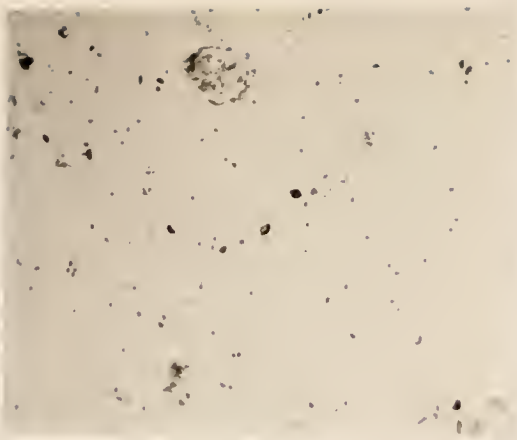
roughening. Also, the peak originally at  $1020\text{ cm}^{-1}$  in this spectrum has been shifted to  $1080\text{ cm}^{-1}$  due to an increase in the relative silica concentration at the alkali- and boron-depleted glass surface. The FT-IRRS analysis also shows that, among the three interfaces, ABS 41 glass/bentonite is the worst case with a spectrum quite similar to that of ABS 39, as discussed earlier.

The optical micrographs of the glasses with three interfaces after 31-month,  $90^{\circ}\text{C}$  Stripa burial are shown in Fig. 5-5. As can be seen from these pictures, extensive glass leaching made the ABS 39 glass surfaces very rough. In contrast, the ABS 41 glass surfaces, except those exposed to bentonite, still appear quite smooth and clear, showing very little surface attack.

It should be noted that these postburial glass surfaces are generally covered with corrosion products. For ABS 41 glass/glass and glass/granite interfaces, the surface film is very thin and in some areas the glass appears unaltered. For all three ABS 39 interfaces and the ABS 41 glass/bentonite interface, the surface films formed on the glasses are heterogeneous. Sometimes there seems to be a layer of either bentonite or superposed flakes of peeled-off reacted glass on the glass surface, as shown in the ABS 41/bentonite interface (Fig. 5-5 (f)).

The SIMS depth profiles of the two glasses reveal both the depth of leaching and the concentration of chemical species in the surface layers as in Fig. 5-4. Here, to begin with, only the results for boron will be presented, to indicate mainly the effective depths of leaching.

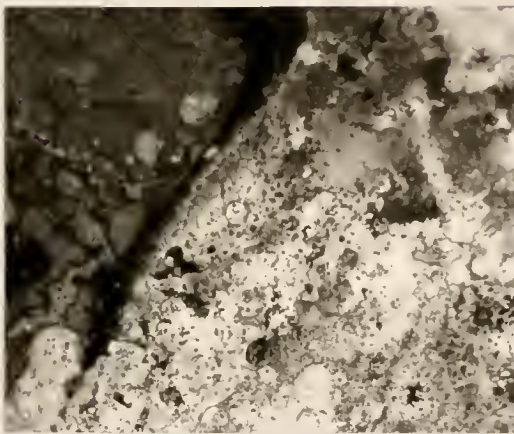




a



d



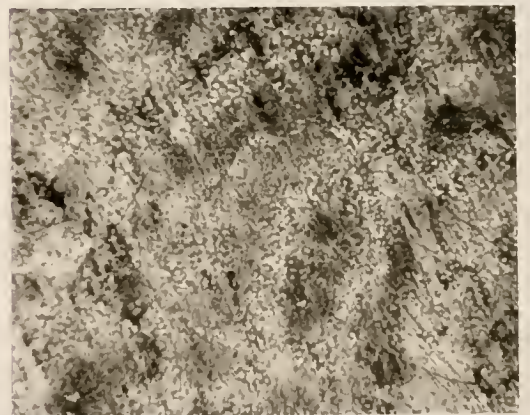
b



e



c



f

Fig. 5-5. Light micrographs (100X) of glass 39 (a) glass/glass, (b) glass/granite and (c) glass/bentonite interfaces and glass ABS 41 (d) glass/glass, (e) glass/granite and (f) glass/bentonite interfaces after 31-month, 90°C Stripa burial.



Figure 5-6 compares the boron profiles for the two glass compositions with three postburial interfaces. The reasons for selecting boron for measuring the leach depth in this dissertation are that (1) boron is one of the major glass former ions and the depth of its depletion provides a good measure of the alteration of glass network; and (2) in most cases, no phase was known to precipitate boron from solution. Therefore, its mass loss should directly indicate the amount of the glass network that had altered. The ABS 39 glass generally has thicker leached layers than ABS 41, as indicated by the depth of the boron extraction. For example, after 31 months, the leach depths of ABS 39 glass/glass and glass/granite interfaces are approximately 18 and 32  $\mu\text{m}$ , respectively, whereas those of ABS 41 are less than 1  $\mu\text{m}$ . However, the glass/bentonite interface did not show much difference in leach depth between ABS 39 and 41. In fact, ABS 41 glass leached to a depth of 20  $\mu\text{m}$  as compared with 15  $\mu\text{m}$  for ABS 39 glass when they were exposed to bentonite during the 90°C, 31-month burial. Thus, although the surface of ABS 39 exhibited a more severely attacked aspect, the long-term leaching depth of ABS 41 surprisingly exceeded that of ABS 39. In the case of glass ABS 39, however, the largest leach depth was found with the glass/granite interface, not with the glass/bentonite interface after 31-month burial at 90°C.

Figure 5-7 compares the FT-IRRS spectra of ABS 118 before and after exposure to either glass, granite or compacted bentonite during 2- and 12-month 90°C Stripa burial. As discussed earlier, selective

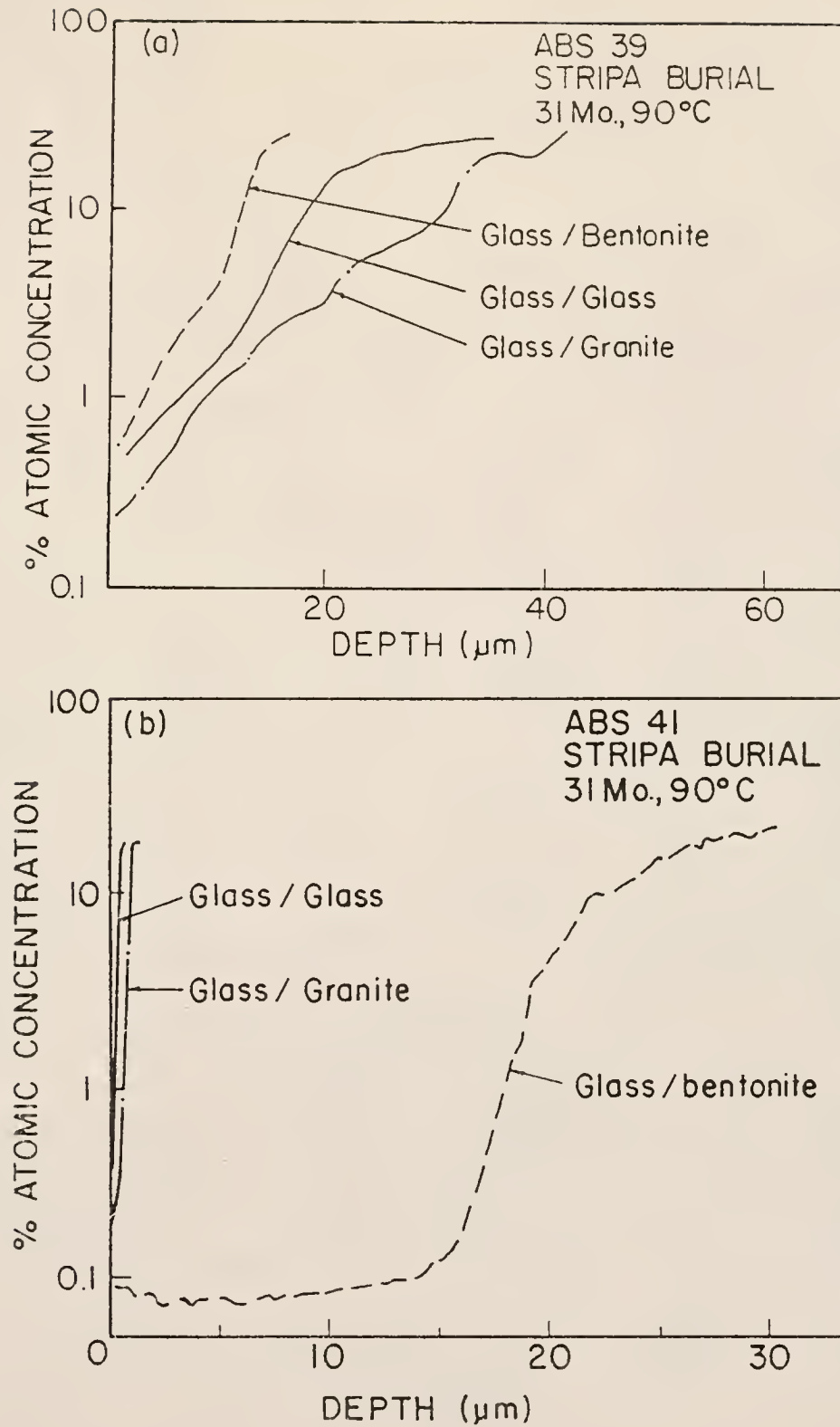


Fig. 5-6. SIMS depth profiles of boron for glass ABS 39 (a) and glass ABS 41 (b) after 31-month, 90°C Stripa burial.

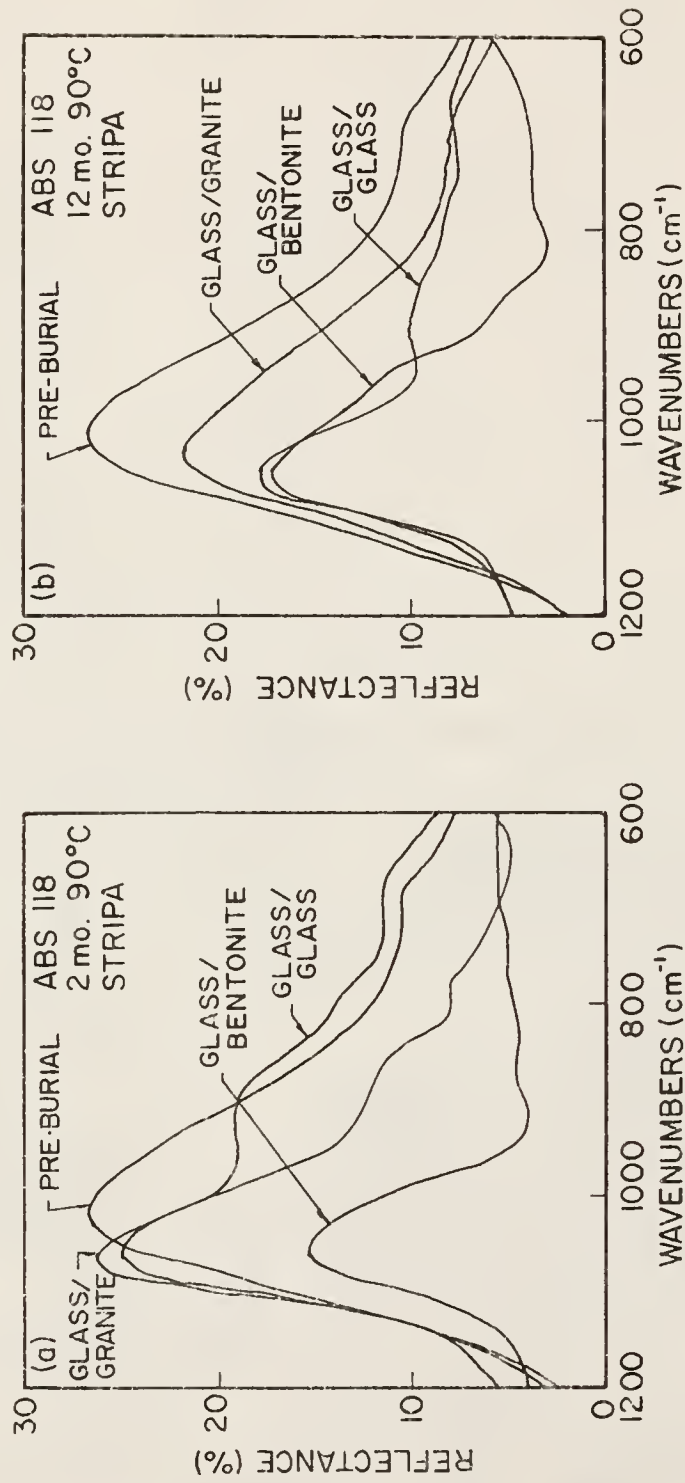


Fig. 5-7. FT-IRRS spectra of glass/glass, glass/granite and glass/bentonite interfaces for nuclear waste glass ABS 118 buried in Stripa at 90°C for (a) 2 months and (b) 12 months. Also shown is the spectrum of a preburial glass surface.

leaching of soluble species such as boron and alkalis results in an increase in the relative Si concentration at the leached surface and splitting of the broad peak at the 800-1100  $\text{cm}^{-1}$  region. The S peak then shifts to higher wavenumbers due to enrichment of  $\text{SiO}_2$ . In Fig. 5-7 (a), all the 2-month postburial spectra show the S peak at  $\sim 1060 \text{ cm}^{-1}$  for the glass/glass and glass/granite interfaces and at the  $\sim 1050 \text{ cm}^{-1}$  region for the glass/bentonite interface, as compared to the broad peak at  $\sim 1010 \text{ cm}^{-1}$  in a preburial spectrum. The high intensity of the S peak, 27% for the glass/glass and 25% for glass/granite, indicate slightly roughened surfaces as shown in Fig. 5-7 (a). The glass/bentonite interface, however, shows a rougher morphology with low S peak intensity (15%) after 2-month burial. This is consistent with the optical micrographs shown in Fig. 5-8 (a-c) for the three glass interfaces.

As regards the NS peak, the spectrum for the 2-month glass/glass interface (Fig. 5-7 (a)) shows that there still remains a considerable amount of alkalis within the  $0.5 \text{ }\mu\text{m}$  sampling depth of FT-IRRS. Actually, Si enrichment (as compared to other elements) within the altered glass surface also resulted from leaching of species other than alkalis, such as B. The SIMS data shown in Fig. 5-9 (a) confirm this concept by showing that B depletion within the  $0.5 \text{ }\mu\text{m}$  outer surface was nearly complete. For the glass/bentonite interface, the FT-IRRS analysis shows that within  $0.5 \text{ }\mu\text{m}$  depth, most alkalis have been leached out during 2-month  $90^\circ\text{C}$  Stripa burial.

After 12-month  $90^\circ\text{C}$  Stripa burial, the FT-IRRS data (Fig. 5-7 (b)) indicate that the roughness of the glass/glass interface

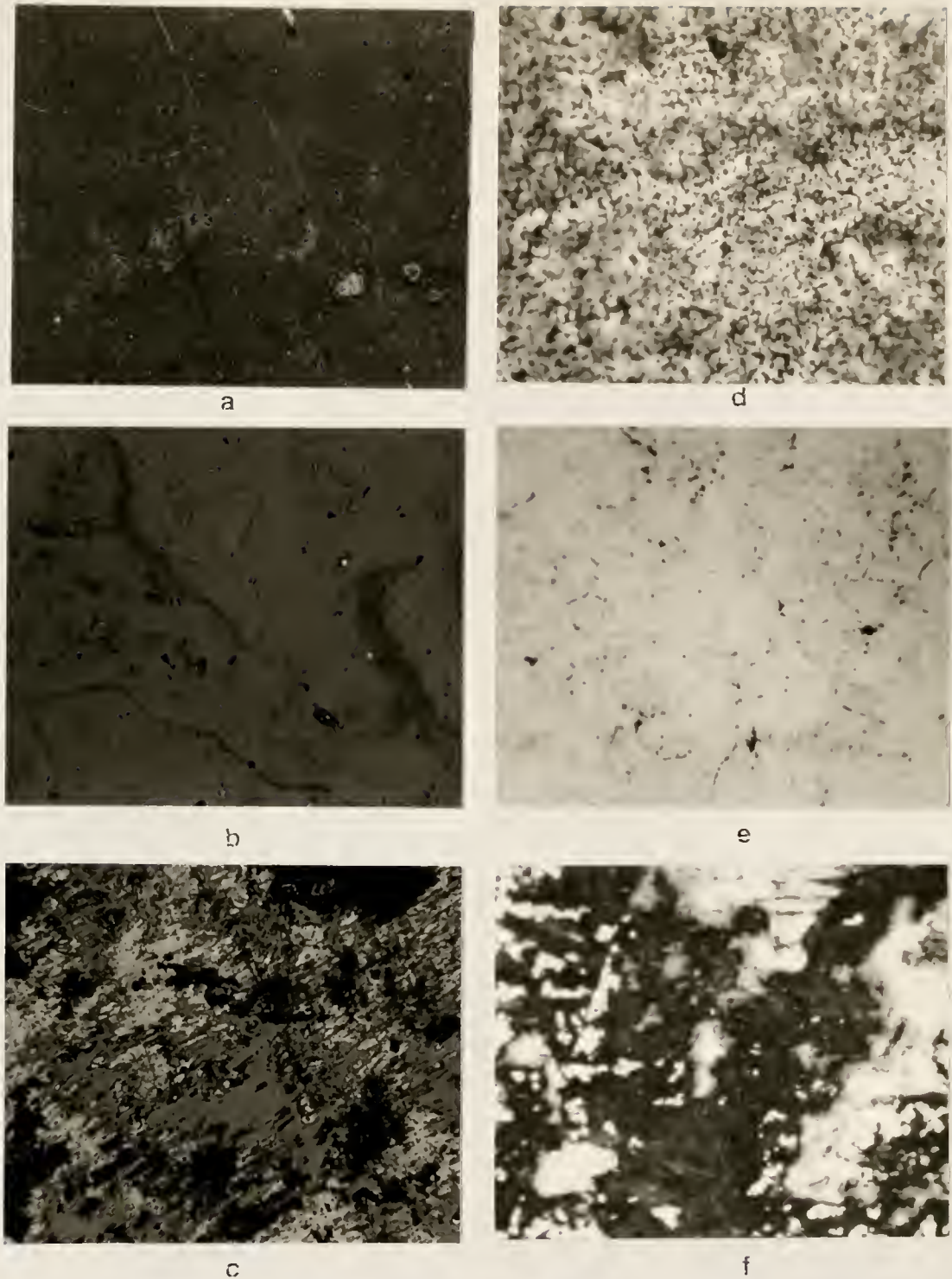


Fig. 5-8. Light micrographs (100X) of glass ABS 118 after 2-month burial, (a) glass/glass, (b) glass granite, and (c) glass/bentonite interfaces, and after 12-month burial, (d) glass/glass, (e) glass/granite, and (f) glass/bentonite interfaces at 90°C in Stripa.



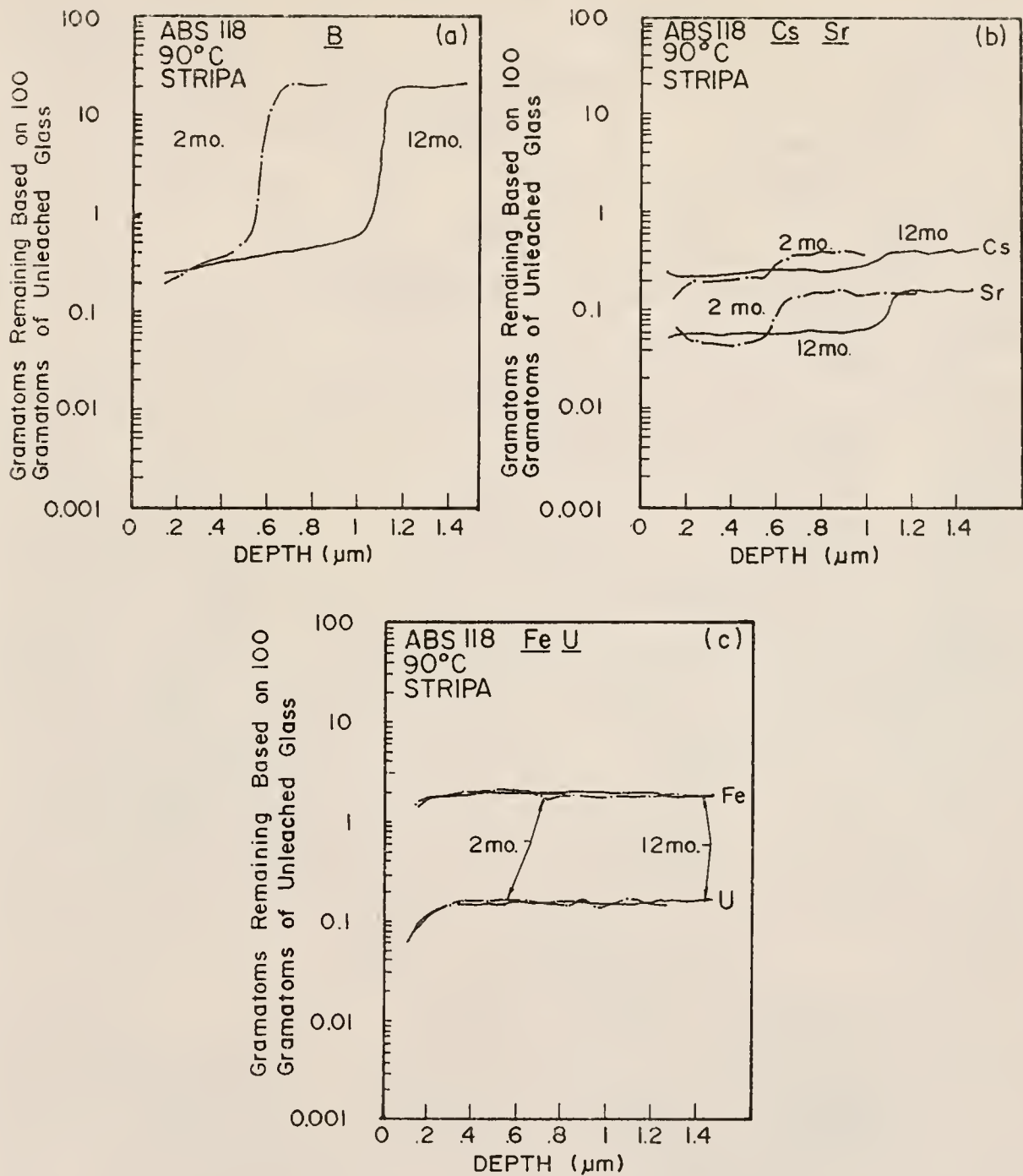


Fig. 5-9. SIMS depth compositional profiles of (a) B; (b) Cs, Sr; and (c) Fe, U for ABS 118 glass/glass interface after 2- and 12-month, 90°C burial in Stripa. Data have been corrected using Al concentration (adapted from [70]).

increased considerably. However, this interface contains a lot of alkali(s) within the altered glass surface as compared by the Na and K profiles in Fig. 5-10 (a). There is no remarkable difference between the 2- and 12-month spectra for the glass/bentonite interface. For the glass/granite interface, the 12-month spectrum shows less attack as compared to that for 2 months, although lower intensity of the 12-month spectrum suggests a rougher surface as compared to the 2-month glass sample. The optical micrographs shown in Fig. 5-8 (d-f) are consistent with the 12-month FT-IRRS data showing the order of decreasing roughness is glass/bentonite, glass/glass, glass/granite.

The SIMS compositional depth profiles of the selected elements for 2- and 12-month ABS 118 glass/glass interface are shown in Fig. 5-9. The 31-month data for ABS 39 and 41 are shown in Fig. 5-4. As estimated from the B extraction (Fig. 5-9 (a)), the leached layer thickness of ABS 118 changed from 0.65  $\mu\text{m}$  after 2-month to 1.05  $\mu\text{m}$  after 12-month burial. Thus, the leach rate of the ABS 118 glass/glass interface between 2- and 12-month burial (0.48  $\mu\text{m}/\text{yr}$ ) was smaller by a factor of 8X as compared to that during the first 2 months (3.9  $\mu\text{m}/\text{yr}$ ). One important feature observed in this figure is that B concentration dropped from 21 at % to <1 at % within 0.1  $\mu\text{m}$  thickness and that at both the "outer region" and the "gel" mid-plateau region, B is almost completely depleted (also see Table 5-2). The shoulders of Cs and Sr in the 2- and 12-month profiles (Fig. 5-9 (b)) are located nearly at the identical depth as the B



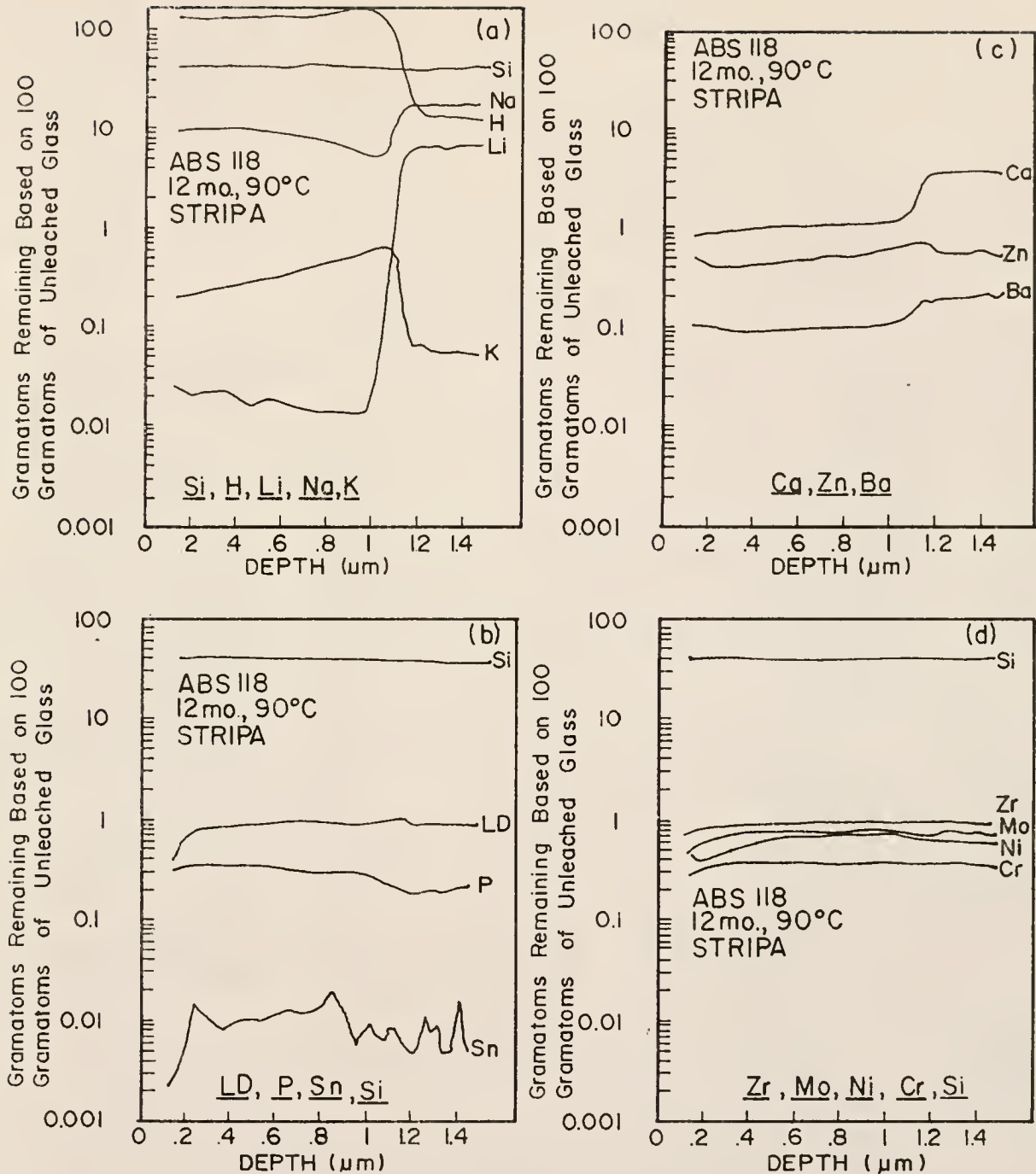


Fig. 5-10. SIMS depth compositional profiles of (a) Si, H, Na, Li, K; (b) LD (including La, Ce, Pr, Nd and Y), P, Sn; (c) Ca, Zn, Ba; and (d) Zr, Mo, Ni, Cr, Si for ABS 118 glass/glass interface after 12-month, 90°C burial in Stripa.

shoulders. However, there are not any shoulders observed in the Fe and U profiles (Fig. 5-9 (c)), suggesting that these two species are not very mobile in the glass.

As discussed in Chapter I, release of the elements such as Cs, Sr and U are the major concern since they undergo spontaneous decay and emit radioactivity. In this dissertation, the leach depths of B are used to estimate the radioactivity release. Such estimations do not take into consideration the actual levels of remaining radioactive elements as suggested by SIMS profiles of the altered layers. The estimations, therefore, represent the worst case of the fission product and actinide release.

Figure 5-10 shows the SIMS profiles of other elements of interest for the ABS 118 glass/glass interface after 12-month, 90°C burial. In Fig. 5-10 (a) for Group I elements, Li has been depleted completely while a considerable amount of Na still remains in the altered layer. Also observed was an enrichment of K probably due to the exchange of Na and Li from the glass with K from the ground water. The large difference in size between K and H would make the K/H ion exchange less probable. The H buildup at the surface layer may result from H/alkali exchange and/or hydrolysis of the glass component oxides. For Group IIA and IIB elements, the profiles (Fig. 5-10 (c)) show that Ca and Ba were depleted from the 1.05  $\mu\text{m}$  thick surface layer while very little depletion of Zn was found at the surface. The concentration of Si appears to remain almost constant (see Fig. 5-10 (b)).

The FT-IRRS spectra of ABS 118 glass/Pb, glass/Cu and glass/Ti after 2- and 12-month 90°C Stripa burial are shown in Fig. 5-11. As compared with the preburial spectrum, very little change in the shape of the spectra was observed for the glass/Pb interface for up to 12 months. First an increase then a decrease in the specular intensity for this interface indicates that the roughness of the leached glass surface first changed to a smooth one then a slightly rough one. But the thickness of this altered layer appears to be less than 0.5  $\mu\text{m}$ .

A greater extent of selective leaching, such as for B and alkalis, was observed at the glass/Cu and glass/Ti interfaces. As a result, the roughness of these glass surfaces increased. The relative  $\text{SiO}_2$  enrichment due to B and alkali depletion results in a splitting of the broad peak containing the Si-O-Si stretching (S) vibrations and Si-O-alkali stretching (NS) vibrations. However, depletion of alkalis appears to be incomplete even after 12 months burial for these two interfaces.

The optical micrographs shown in Fig. 5-12 confirm the surface morphology developed during the 2- and 12-month burial as discussed earlier. In all cases, corrosion products can be found at the glass surfaces even after short times of exposure.

The SIMS depth profiles of 23 elements as obtained at interfaces against Pb, Cu and Ti are shown in Figs. 5-13 through 5-19. Table 5-2 lists the averaged gram-atoms of each element remaining at "gel" mid-plateau and outer region of the three glass interfaces based on 100 gram-atoms of unleached glasses. The SIMS data shown here were

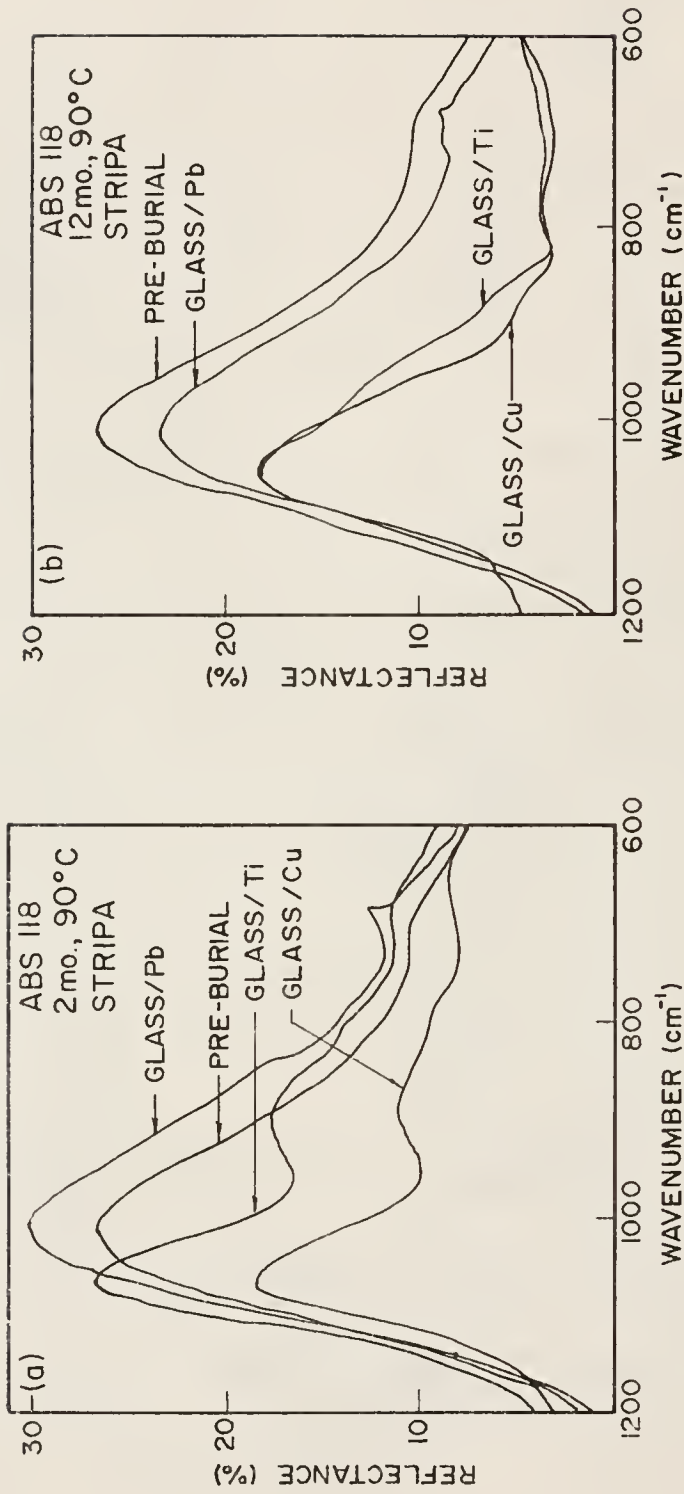


Fig. 5-11. FT-IRRS analysis of ABS 118 glass/Pb, glass/Ti and glass/Cu interfaces after (a) 2-month and (b) 12-month 90°C burial in Stripa.



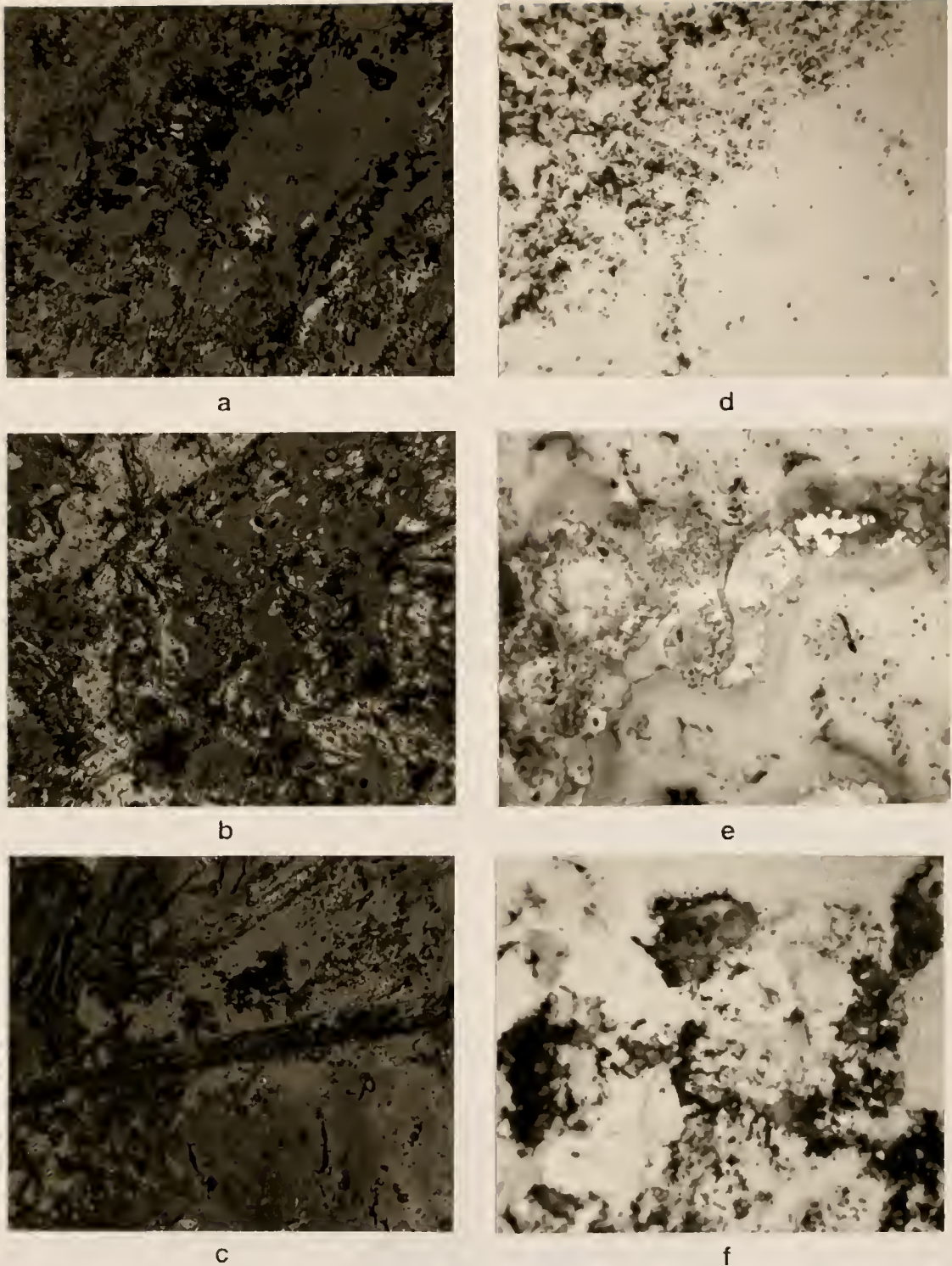


Fig. 5-12. Light micrographs of ABS 118 glass surfaces after 90°C Stripa burial for 2 months, (a) glass/Ti, (b) glass/Cu, and (c) glass/Pb interfaces, and for 12 months, (d) glass/Ti, (e) glass/Cu, and (f) glass/Pb interfaces.

the ones corrected by Al concentration, assuming that the gram-atoms of this element remain unchanged throughout the leached layer. These provide data which account for porosities and adsorbed elements. In Figs. 5-13 through 5-15, the 2- and 12-month profiles of 6 elements are compared. As shown by B extraction, the leach depth increased from 0.05  $\mu\text{m}$  to 0.4  $\mu\text{m}$  for the glass/Pb, and from 0.8  $\mu\text{m}$  to 0.85  $\mu\text{m}$  for glass/Cu between 2 and 12 months and from 0.85  $\mu\text{m}$  to 2.3  $\mu\text{m}$  for glass/Ti between 7 and 12 months.

All the glass surfaces except the glass/Pb interface show a complete depletion of B at the leach layer (Fig. 5-13). Cs and Sr leached nearly to the same depths as B (Fig. 5-14). However, Fe and U remained unchanged, except at the  $\sim 0.2$   $\mu\text{m}$  outer region where slight amounts of Fe and U have been dissolved into the ground water during burial (Fig. 5-15).

Figures 5-16 through 5-19 compare other elemental profiles of the 12-month glass surfaces for the three interfaces. Sodium, Li, Ca, Zn and Ba were depleted nearly to the same depths as B. The decrease in Si concentration at the outer surface of the glass/Pb interface (Fig. 5-16) is probably due to an enrichment of K and Pb (Figs. 5-16 and 5-18). It has been noted that almost all of the Li has been leached out of the glass surface while a considerable amount of Na still remains at the altered layer, especially for the glass/Cu case where Na concentration first decreased then increased nearly to the same concentration as that of bulk glass and finally decreased again at the outer surface region ( $< 0.2$   $\mu\text{m}$ ). There are not any

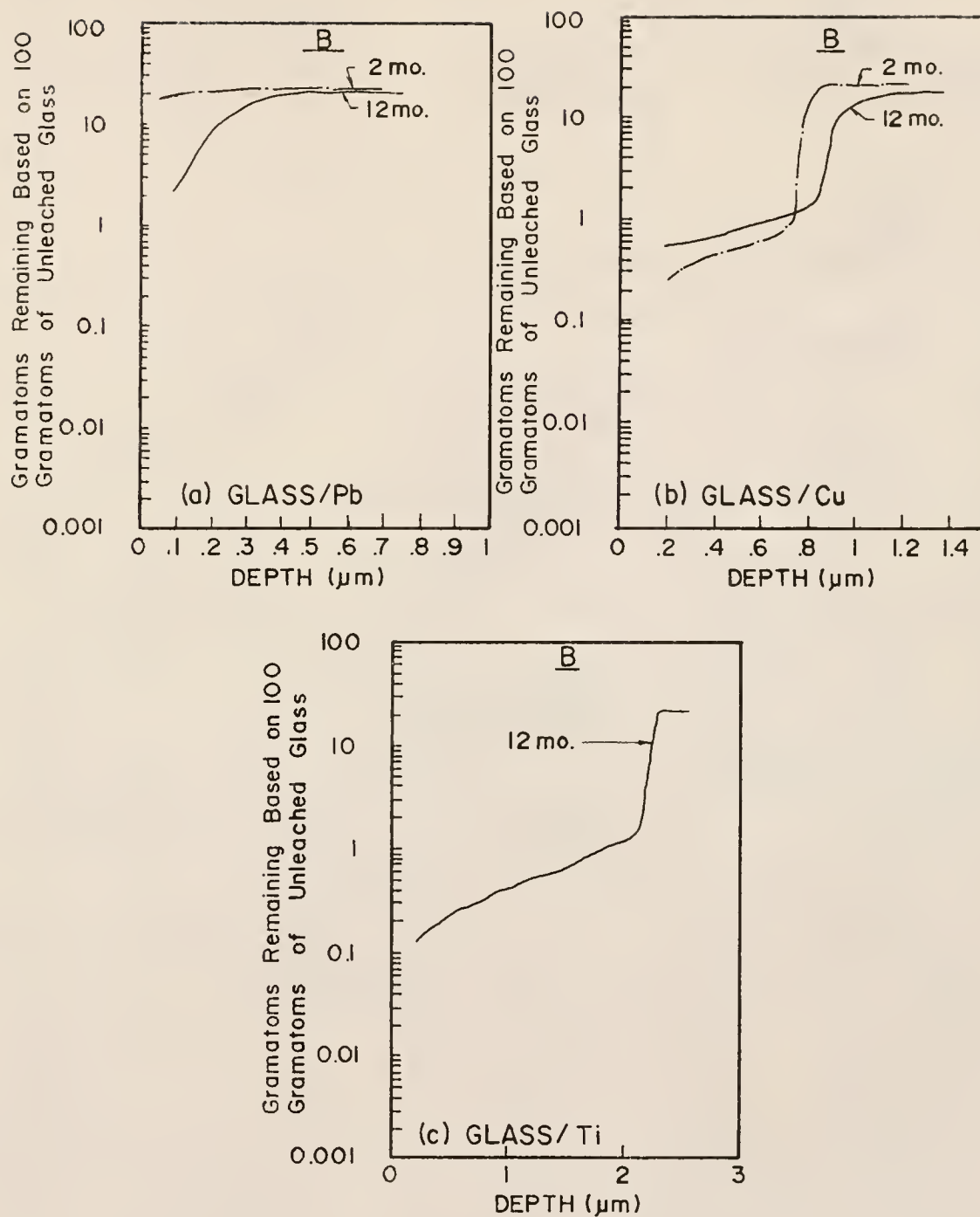


Fig. 5-13. Boron profiles of ABS 118 (a) glass/Pb, (b) glass/Cu and (c) glass/Ti interfaces after 2- and 12-month, 90°C burial at Stripa.



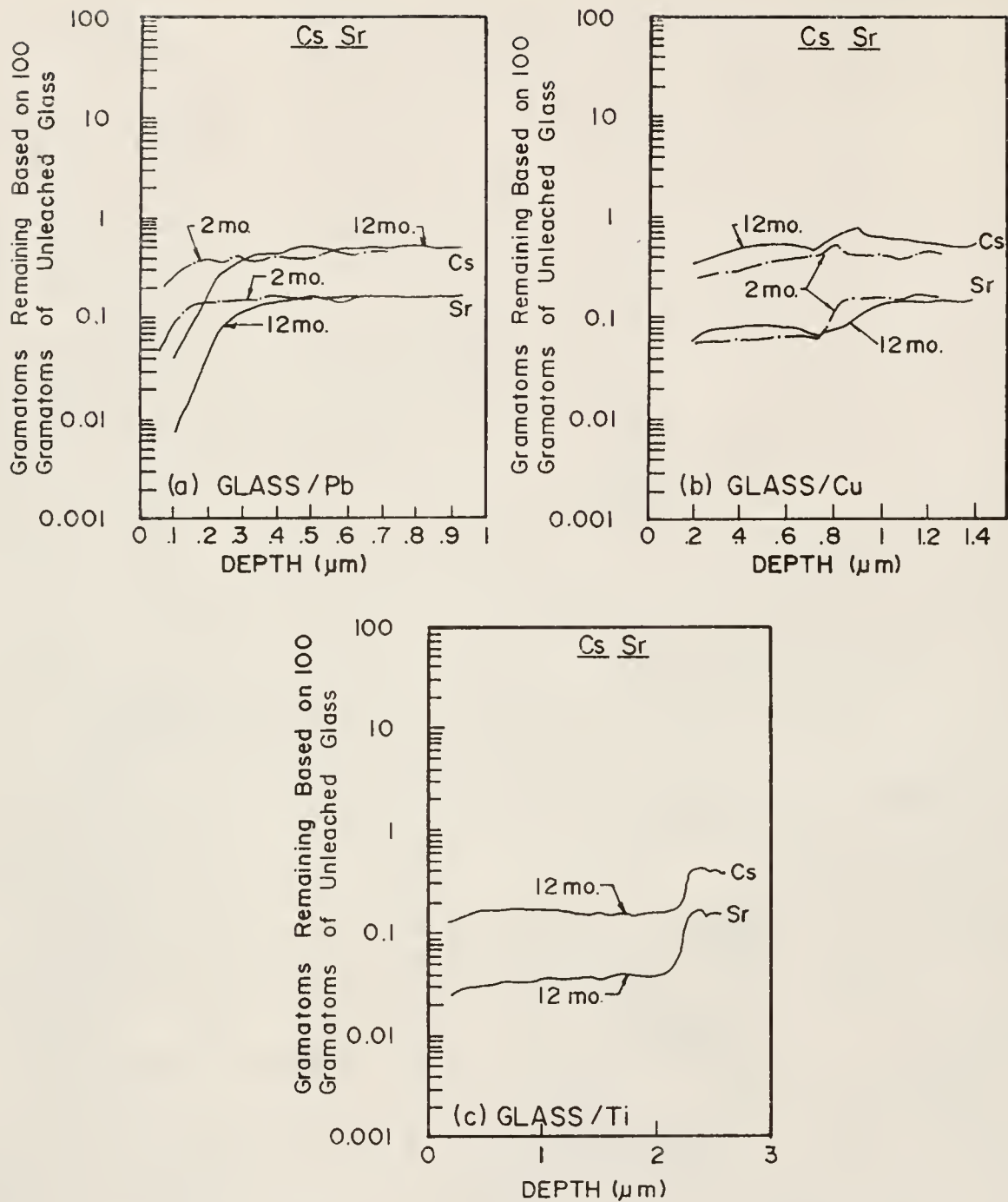


Fig. 5-14. Cs and Sr profiles of ABS 118 (a) glass/Pb, (b) glass/Cu and (c) glass/Ti interfaces after 2- and 12-month, 90°C burial at Stripa.

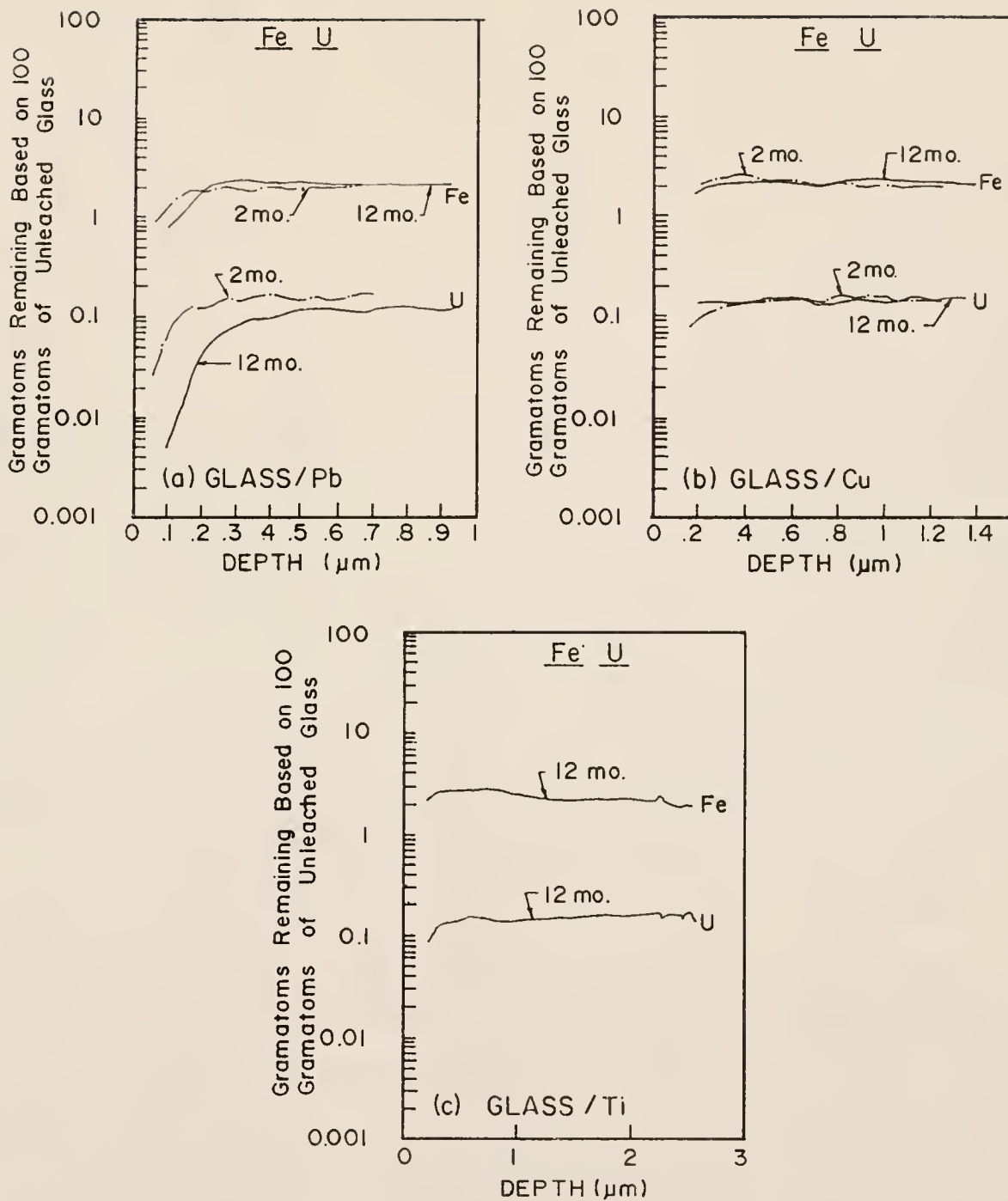


Fig. 5-15. Fe and U profiles of ABS 118 (a) glass/Pb, (b) glass/Cu and (c) glass/Ti interfaces after 2- and 12-month, 90°C burial at Stripa.

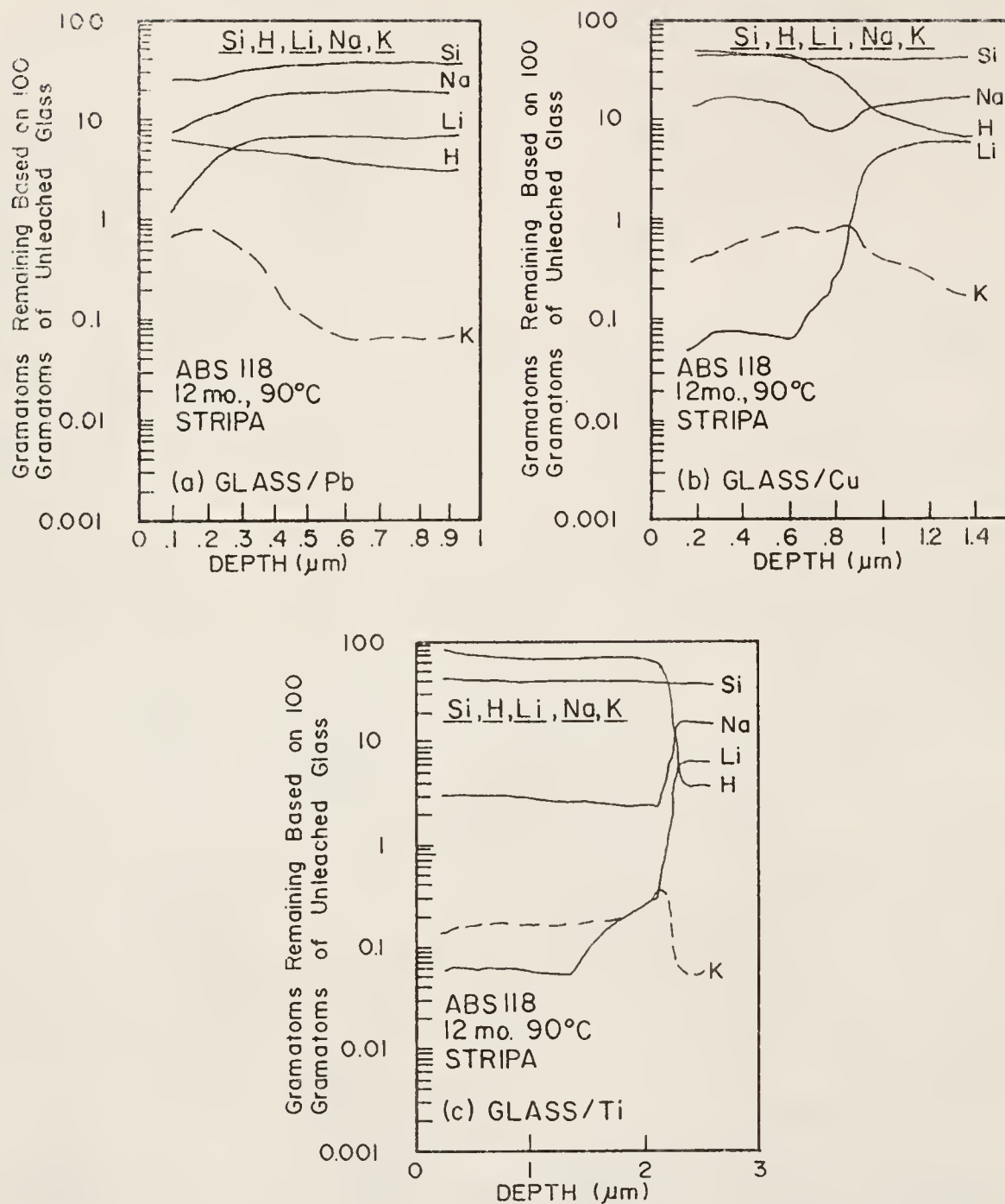


Fig. 5-16. SIMS analysis of ABS 118 (a) glass/Pb, (b) glass/Cu and (c) glass/Ti interfaces after 12-month, 90°C Stripa burial, Si, H, Li, Na and K profiles.

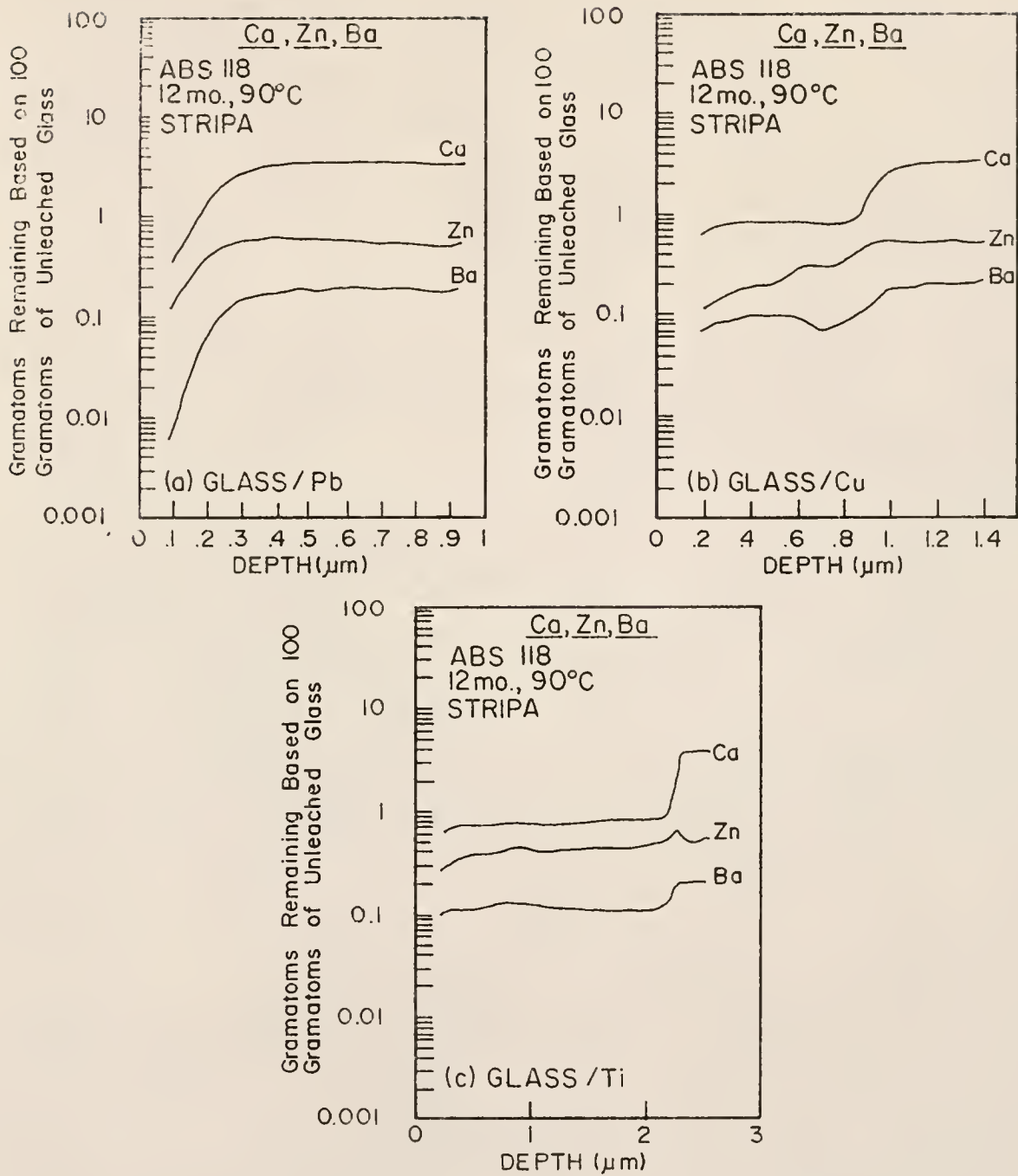


Fig. 5-17. SIMS analysis of ABS 118 (a) glass/Pb, (b) glass/Cu and (c) glass/Ti interfaces after 12-month, 90°C Stripa burial, Ca, Zn and Ba profiles.

obvious changes in the concentration of LD (including La, Ce, Pr, Nd and Y), Zr, Mo and Cr in the leached layer except at the  $\sim 0.2 \mu\text{m}$  outer region where a decrease in the concentration of these elements can be observed (Figs. 5-18 and 5-19). However, an increase in the Ni concentration was apparent at the "gel" mid-plateau region of the glass/Cu and glass/Ti interfaces after 12-month,  $90^\circ\text{C}$  burial.

It is noted that there is an apparent Pb buildup at the glass/Pb and an increase of Cu concentration at the glass/Cu interfaces (Table 5-2 and Fig. 5-18). A large peak including Pb and U in the RBS analysis for the glass/Pb interface (Fig. 5-20) confirms the buildup of Pb at this interface after 12-months of burial. The maximum mass (1 gram-atoms) of Pb was located at  $\sim 0.2 \mu\text{m}$  below the glass surface in the case of glass/Pb (Fig. 5-18 (a)) while the Cu concentration reached its maximum value at  $\sim 0.9 \mu\text{m}$  of the leach glass surface exposed to Cu during burial (Fig. 5-18 (b)).

#### Results with SRL Glasses

Figure 5-21 shows the FT-IRRS analysis of the glass/glass interface for three SRL glasses after 2-year burial in Stripa at  $8-10^\circ\text{C}$  and  $90^\circ\text{C}$ . The  $90^\circ\text{C}$  spectra suggest the depletion of alkalis and boron accompanied by the alteration of the  $\text{SiO}_2$  network within  $\sim 0.5 \mu\text{m}$  detection limit of FT-IRRS. Also shown in this figure is that the most extensive leaching occurs on SRL 131 + 29.8% TDS glass among the three SRL glasses, after 2-year burial. The spectrum of this glass surface has the lowest peak intensity and only one main peak in the  $800-1100 \text{ cm}^{-1}$  region. As regards the low temperature ( $8-10^\circ\text{C}$ ) spectrum for SRL 131 + 29.8% TDS glass/glass interface, the

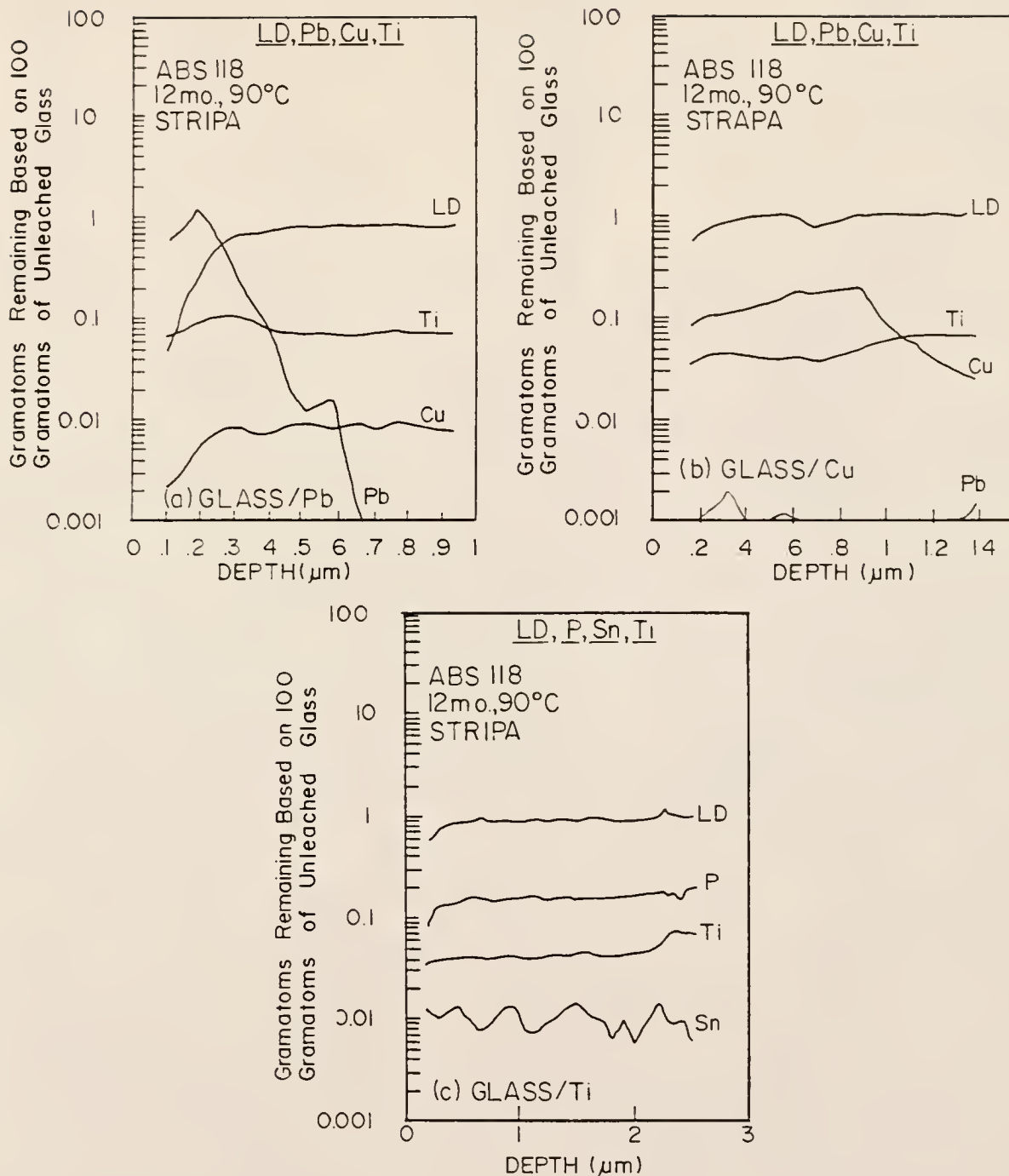


Fig. 5-18. SIMS analysis of ABS 118 (a) glass/Pb, (b) glass/Cu and (c) glass/Ti interfaces after 12-month, 90°C Stripa burial, LD, Pb, Cu and Ti profiles. LD stands for the sum of La, Ce, Pr, Nd and Y.

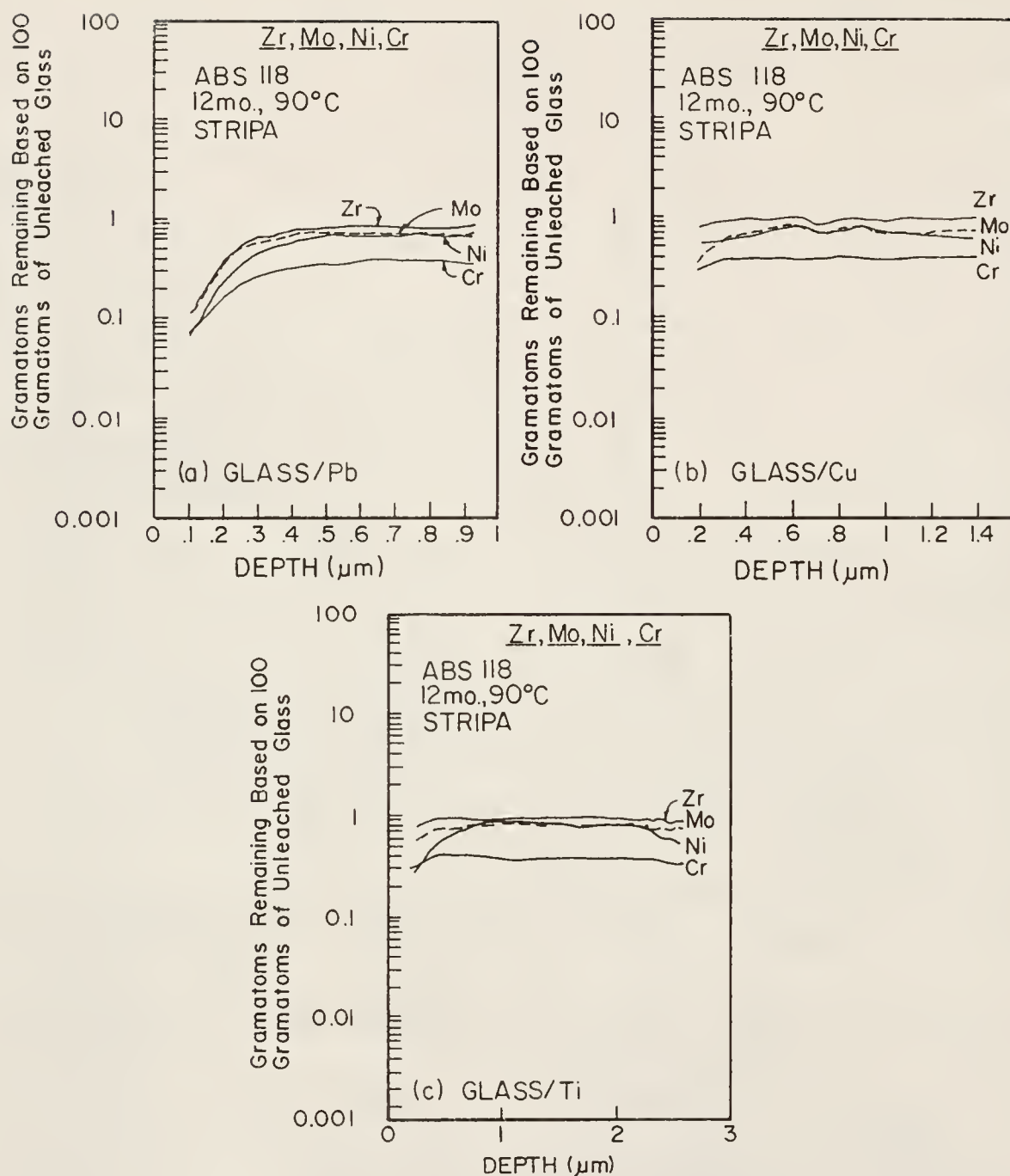


Fig. 5-19. SIMS analysis of ABS 118 (a) glass/Pb, (b) glass/Cu and (c) glass/Ti interfaces after 12-month, 90°C Stripa burial, Zr, Mo, Ni and Cr profiles.



Table 5-2. Gram-Atoms of Elements Remaining at Gel Mid-Plateau and Outer Region of the Altered Glass Surface Based on 100 Gram-Atoms of Unleached ABS 118 glass E after 12-Month, 90°C Burial in Stripa.

	Gel Mid-Plateau			Outer Region		
	Glass/Pb	Glass/Cu	Glass/Ti	Glass/Pb	Glass/Cu	Glass/Ti
Si	40					
Li	6	23	43	24	44	41
Na	16	2	0.07	1	0.05	0.5
K	0.05	9	14	7	11	3
Cs	0.4	0.8	0.6	0.7	0.3	0.11
Mg	0.05	0.1	0.5	0.04	0.3	0.11
Ca	4	0.9	0.04	0.7	0.06	0.09
Sr	0.15	0.8	0.8	0.3	0.6	0.6
Ba	0.2	0.02	0.08	0.007	0.06	0.02
Zn	0.5	0.02	0.09	0.004	0.07	0.1
B	21	0.2	0.2	0.1	0.1	0.3
Al	5.4	5	0.7	2	0.5	0.1
Mn	0.5	5.4	5.4	5.4	5.4	5.4
Fe	2	0.1	0.09	0.08	0.08	0.1
Zr	1	1.1	2	0.8	1.4	2.1
Mo	0.7	0.2	0.9	0.1	0.8	0.8
LD <sup>a</sup>	1	0.1	0.8	0.06	0.6	0.6
U	0.16	0.1	0.9	0.04	0.5	0.6
Pb	(0.007)	0.02	0.1	0.005	0.08	0.09
Cu	(0.007)	1	-	0.6	-	-
Ti	(0.07)	-	0.2	-	0.08	-
x <sub>μm</sub> <sup>b</sup>	(0.001)	0.4	0.9	-	-	0.03

<sup>a</sup> "LD" stands for the sum of La, Ce, Pr, Nd and Y.

<sup>b</sup> x<sub>μm</sub>: Approx. depth of leached layer.

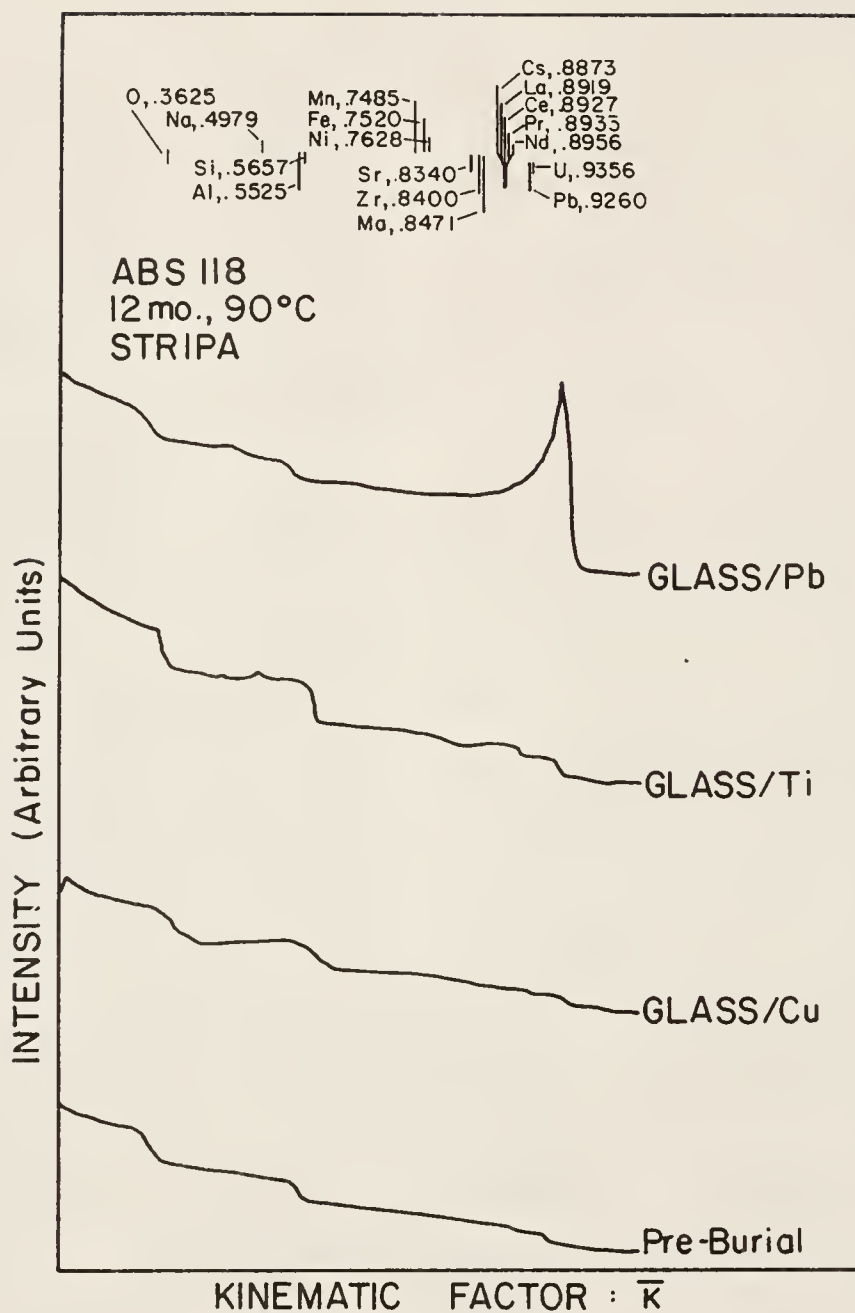


Fig. 5-20. RBS analysis of ABS 118 glass/Pb, glass/Ti and glass/Cu interfaces after 12-month, 90°C burial in Stripa.

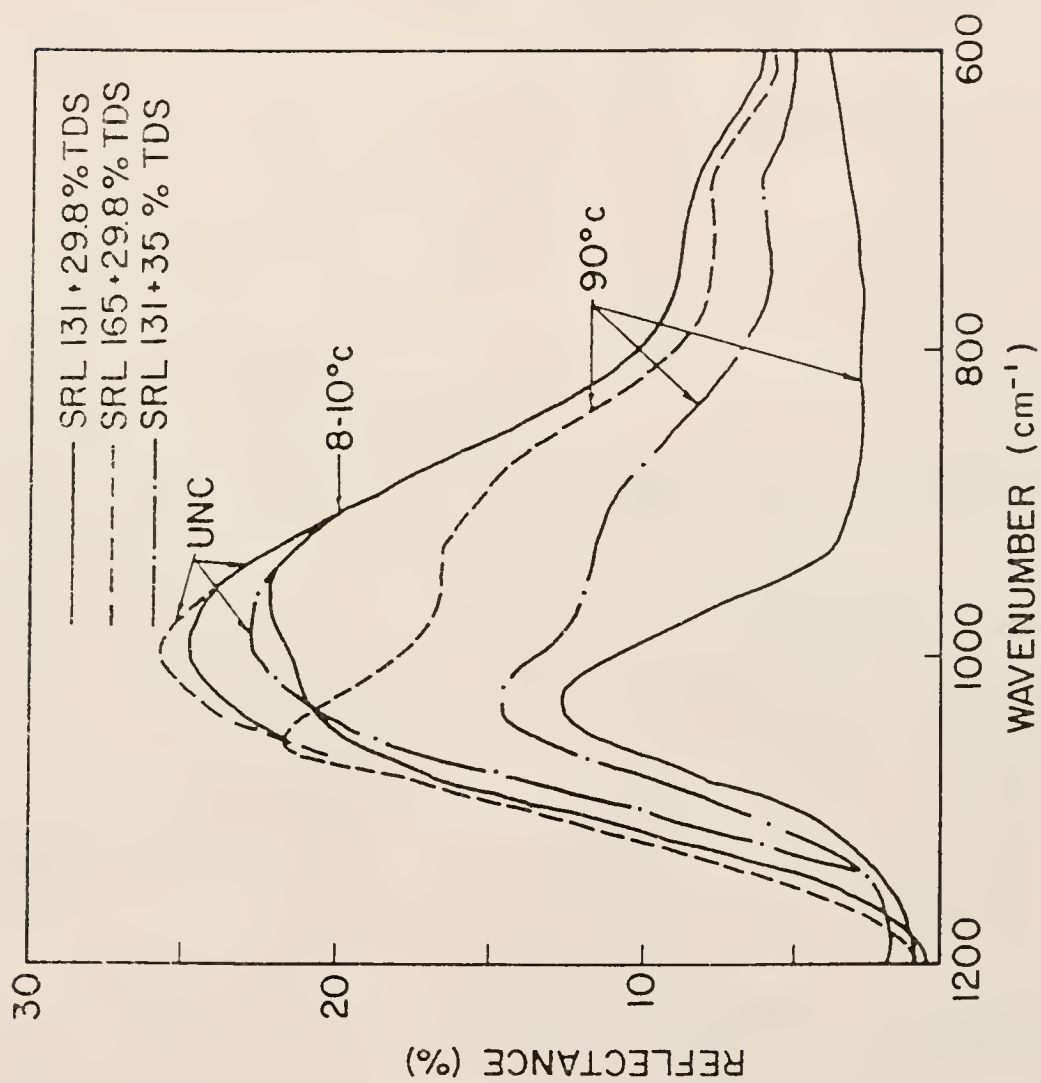


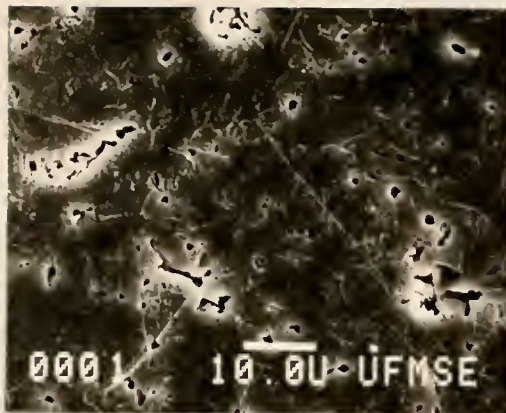
Fig. 5-21. FT-IRRS analysis of the glass/glass interface for three SRL glasses after 2 years of burial in Stripa.

intensity of the main peak containing Si-O-Si stretching vibrations decreased by only 3% as compared with a 12% (4X) decrease for the same glass buried at 90°C.

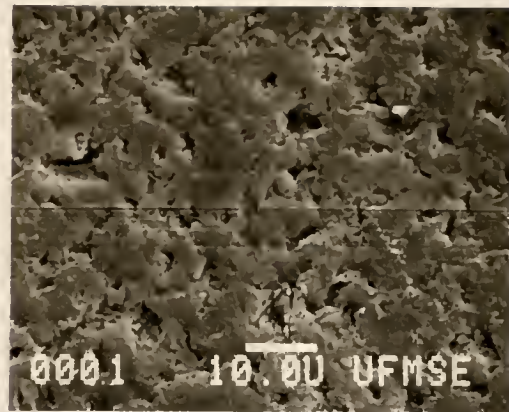
SEM micrographs of the glass/glass interface for the three SRL glasses after 2-year burial at 90°C in Stripa are shown in Fig. 5-22. These pictures provided representative views of these surfaces. Polishing scratches are clearly visible on the preburial surface (Fig. 5-22 (d)). Figure 5-22 (b) shows the vestiges of the original polishing scratches and pits on a leached SRL 165 + 29.8% TDS glass/glass interface indicating very little surface attack. On SRL 131 glasses with either 29.8% TDS or 35% TDS waste, the original polishing scratches have been removed through leaching (Fig. 5-22 (a, c)).

As revealed by SIMS analysis (Fig. 5-23 (a-c)), the leach depths of these three glasses are 3.6  $\mu\text{m}$  for SRL 131 + 29.8% TDS, 0.46  $\mu\text{m}$  for SRL 165 + 29.8% TDS and 1.85  $\mu\text{m}$  for SRL 131 + 35% TDS after 2-year, 90°C burial. These data indicate that SRL 165 frit is much better than SRL 131 and that an increase in waste loading from 29.8 wt% to 35 wt% is also beneficial (i.e., decreased the leach depth of SRL 131 glasses by 2X).

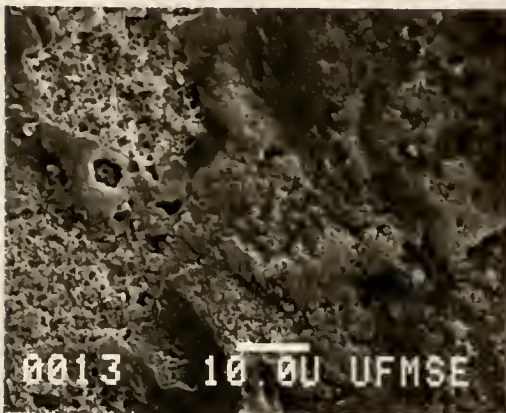
The common feature observed from the FT-IRRS and SIMS analyses is preferential leaching of alkalis and boron contained originally in the glasses. Although some dissolution of Si is observed from the SIMS compositional profiles as shown by the decrease in its gram·atoms remaining based on 100 gram·atoms of unleached glass, the



a



b



c



d

Fig. 5-22. SEM micrographs of glass surfaces in contact with glass of the same composition during 2-year burial at 90°C in Stripa: (a) SRL 131 + 29.8% TDS, (b) SRL 165 + 29.8% TDS, (c) SRL 131 + 35% TDS and (d) an uncorroded glass surface.

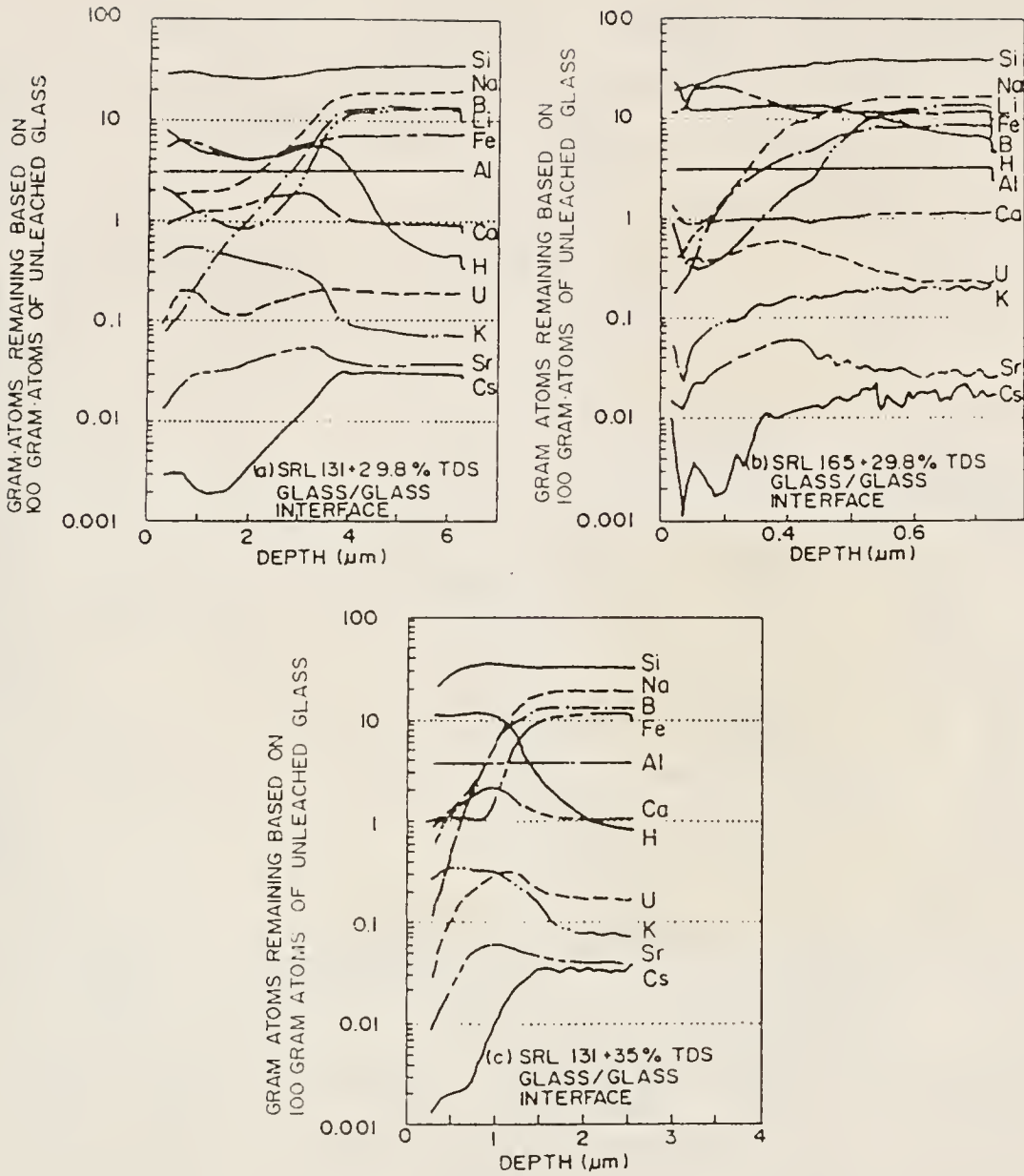


Fig. 5-23. SIMS in-depth profiles of glass surfaces after 2-year Stripa burial at 90°C.



amount of dissolved Si is small. This is mainly due to (1) that  $\text{SiO}_2$  is the glass former and the Si-O bonds are strong (106 kcal/gram·atom) and (2) the buffering effects of the ground water in the Stripa mine where pH showed less than 1 unit increase over its original value of 8.1 during the whole span of burial.

#### Effect of Glass Heterogeneities

The x-ray diffraction (XRD) pattern in Fig. 5-24 shows that some SRL 131 + 29.8% TDS glass samples contained  $\text{Fe}_3\text{O}_4$  spinel crystallites [73]. The peak at  $2\theta = 33.1^\circ$  is due to the  $\text{Fe}_2\text{O}_3$  contamination from the iron mortar during sample preparation [74]. The crystalline phase is a spinel solid solution,  $(\text{Mn}, \text{Fe}, \text{Ni})_1\text{Fe}_2\text{O}_4$ , containing small amounts of Mn and Ni, as indicated by EDS analyses for the crystal areas of a preleached heterogeneous glass shown in Fig. 5-25 (b).

The SEM-EDS analysis for SRL 131 + 29.8% TDS glass is shown in Fig. 5-25 for preleached specimens both with and without crystals. In general, the surface of the glass appears as that shown in Fig. 5-25 (a). This micrograph reveals a homogeneous surface with a few polishing scratches. Some areas of the glass surface appear as shown in Fig. 5-25 (b). The microstructure observed in these regions consists of an isolated crystalline phase within a glassy matrix. The specimens contain less than 20% crystals which are nonuniformly dispersed within the glass matrix. This value was estimated using point counts from optical micrographs obtained from a number of representative sections. Energy dispersive spectra for the crystalline area of the heterogeneous specimens are shown in



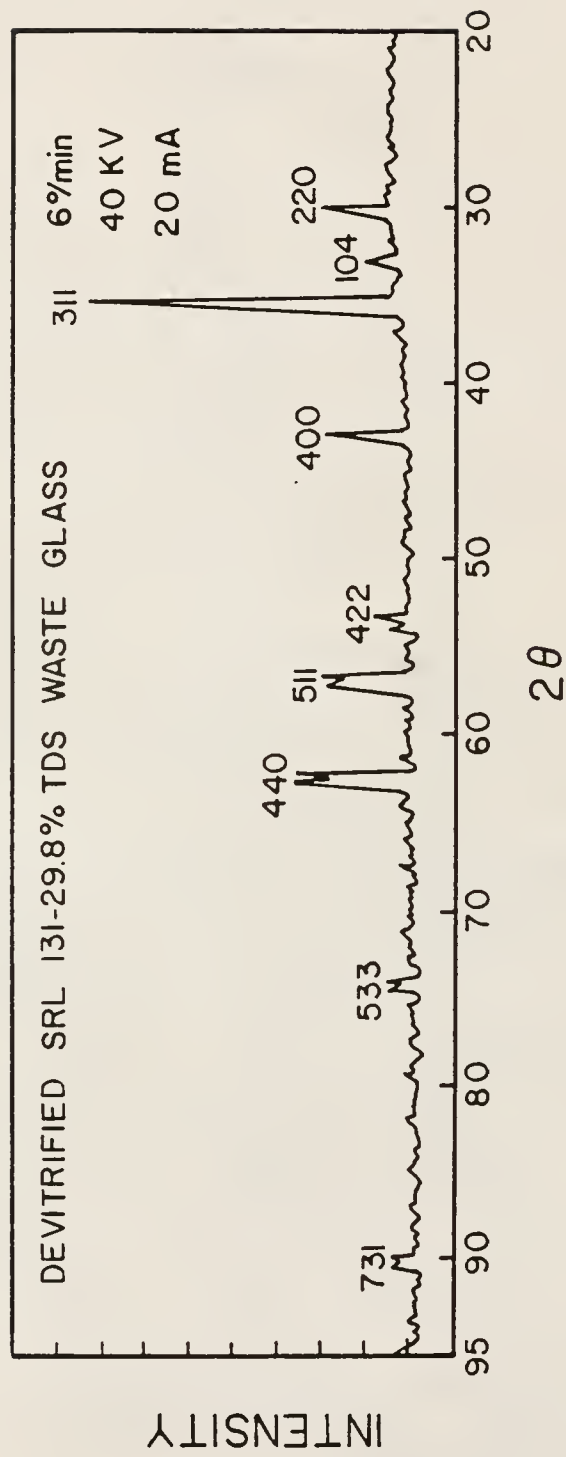
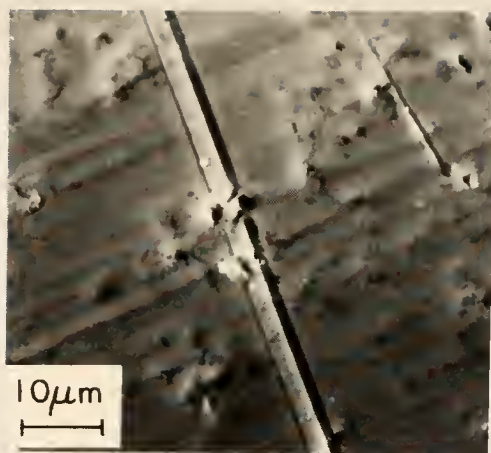
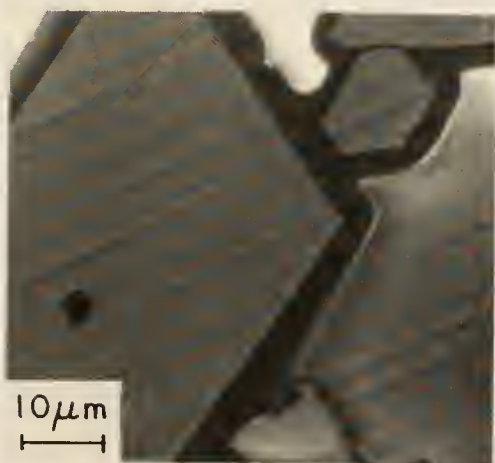
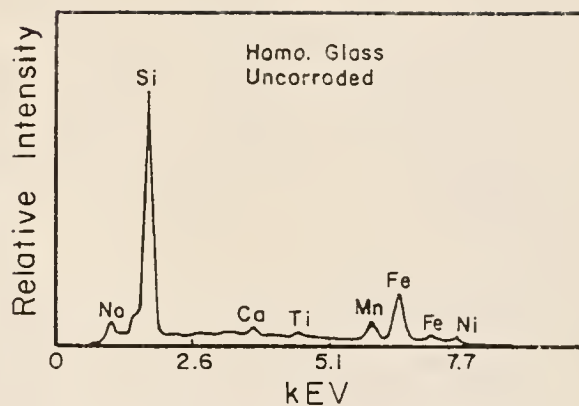


Fig. 5-24. X-ray diffraction pattern for powders prepared from devitrified SRL 131 + 29.8% TDS glass.



(a)



(b)

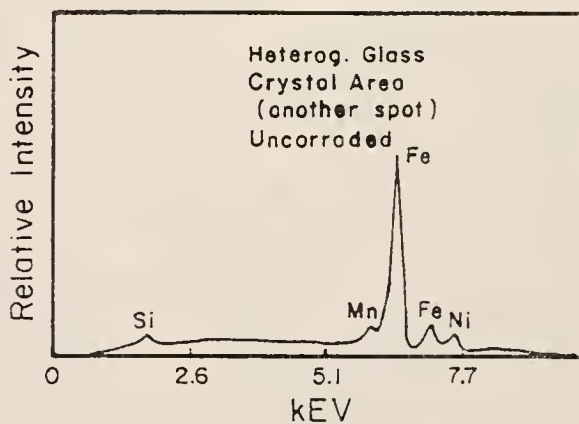
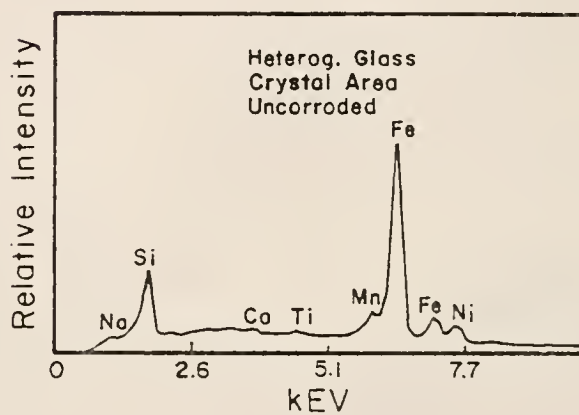


Fig. 5-25. SEM-EDS analysis of preburial SRL 131 + 29.8% TDS glass: (a) homogeneous glass surface and (b) partially devitrified glass surface.

Fig. 5-25 (b). These data reveal that the crystalline phase is rich in Fe, Ni and Mn. The presence of the Si peak is probably due to the silicate phase since the crystals are too small for isolated analysis without interference from the surrounding glass.

Uniform corrosion was observed on the homogeneous specimens buried for up to 6 months at 90°C. Figure 5-26 is the SEM of the glass surface interfaced with bentonite after 1-month burial at 90°C. This, together with EDS data in Fig. 5-28 and optical micrographs, suggests the formation of an uniformly leached surface layer.

The leaching morphology of the samples in the devitrified areas (or areas containing undissolved raw materials) appears nonuniform. The SEMS for these glass specimens after 1-, 3- and 6-month burial at 90°C are shown in Fig. 5-26 (b, c, d), respectively. The surfaces have sharply projecting crystals and deep furrows at the crystal-glass interface. These micrographs suggest that the crystalline and parent glass phases are more resistant to aqueous attack than are the interfacial regions. The extent of phase boundary attack increases during the first month of burial, but shows very little change between 3 months and 6 months. An additional feature observed on the 6-month sample is cracking of the glassy phase between the crystalline phases. The cracking is indicative of extensive leaching in these regions. Leaching occurs in the similar regions of the 1- and 3-month samples, but is apparently not extensive enough to cause cracking. Another feature shown in these micrographs is pitting,

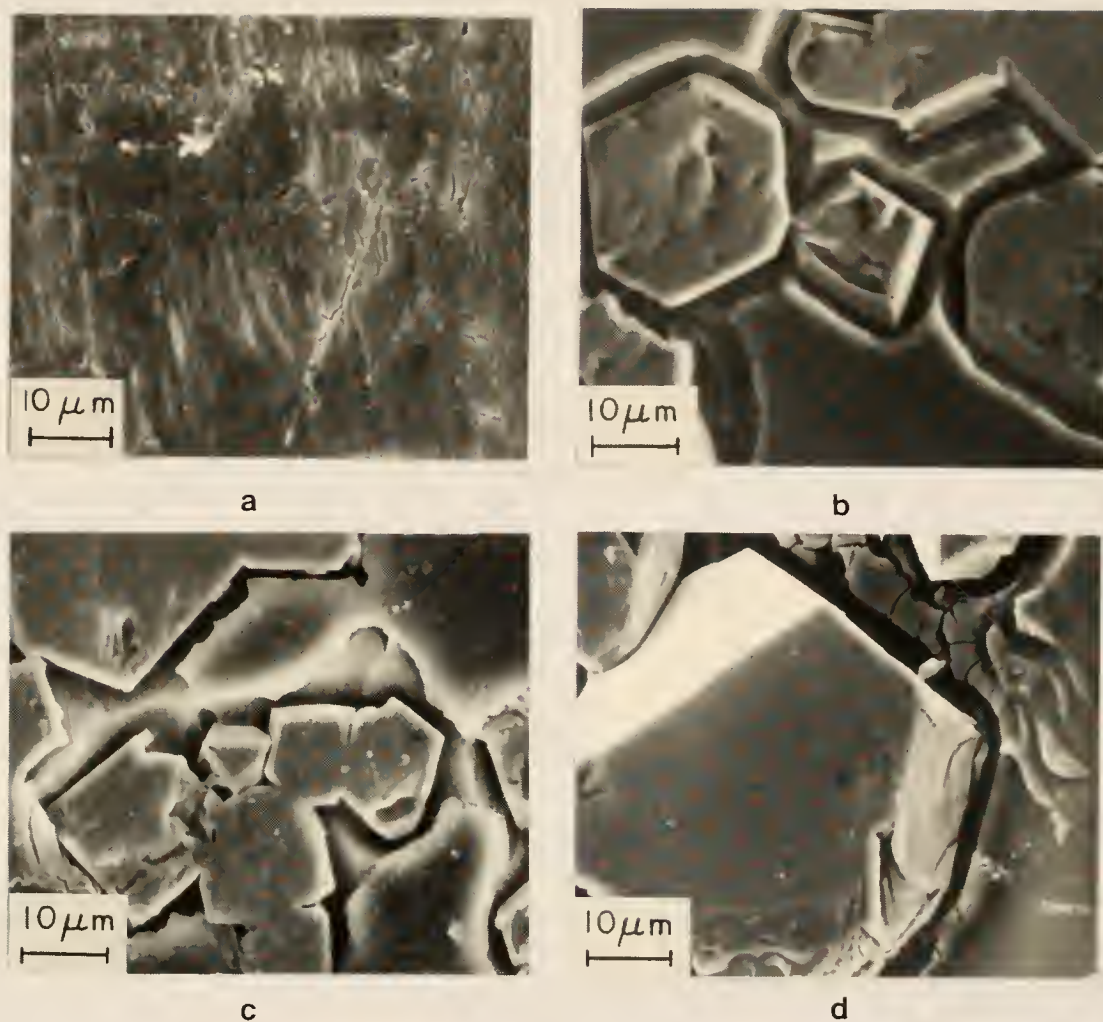
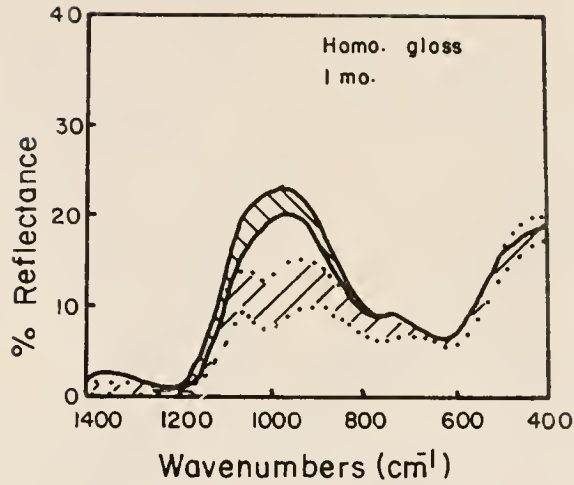


Fig. 5-26. SEM micrographs of SRL 131 + 29.8% TDS glass surfaces in contact with bentonite, Stripa burial at 90°C: (a) homogeneous glass, 1-month burial; (b) partially devitrified glass, 1-month burial; (c) partially devitrified glass, 3-month burial; and (d) partially devitrified glass, 6-month burial.

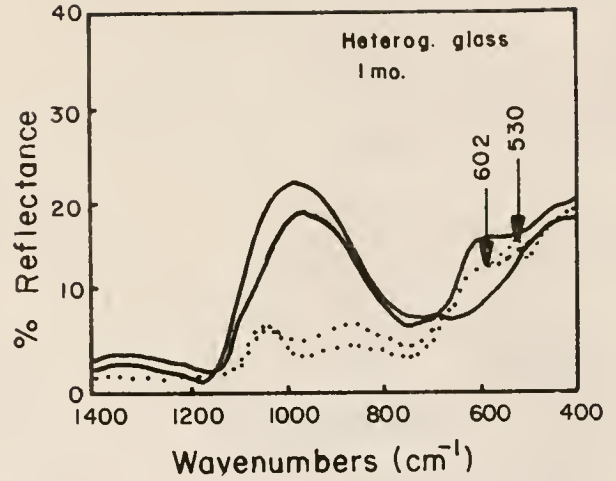
which can be seen easily within the crystalline areas for all the heterogeneous specimens buried for 1, 3 and 6 months at 90°C. These observations are consistent with the FT-IRRS spectra which show decreasing peak intensities and reduced integrated areas (Fig. 5-27 (b-d)) for longer exposure times.

The FT-IRRS spectra for homogeneous and heterogeneous glass specimens both prior to and after burial are shown in Fig. 5-27. There is comparably less change in the FT-IRRS integrated area for the homogeneous glass specimens after burial at 90°C for 1 month than for the heterogeneous glass specimens. It is also worth noting that a fine structure appears in the FT-IRRS spectra below  $700\text{ cm}^{-1}$  for the latter specimens after 1-, 3- and 6-month burial at 90°C. Two peaks, at  $602\text{ cm}^{-1}$  and  $530\text{ cm}^{-1}$ , were identified as the characteristic peaks for trevorite,  $\text{NiFe}_2\text{O}_4$ . This is consistent with the XRD [75] and EDS data showing a Fe- and Ni-rich crystal phase in the heterogeneous glass specimens. The enhancement of the fine structure of the FT-IRRS spectra due to trevorite is a consequence of a higher leach resistance of the crystalline phase than that of the glassy matrix. As a result, the crystalline phase projects out of the glass surface as time increases resulting in more of a contribution to the FT-IRRS spectra from the crystalline phase. This provides evidence for a less durable glassy matrix (as compared with the crystalline phase) and a preferential phase boundary attack of the heterogeneous samples during burial.

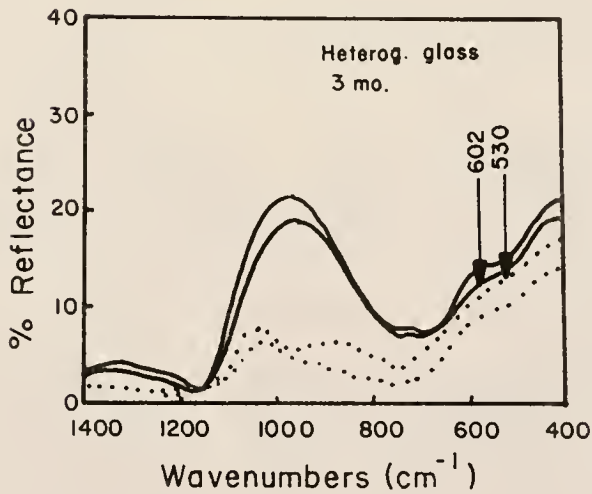




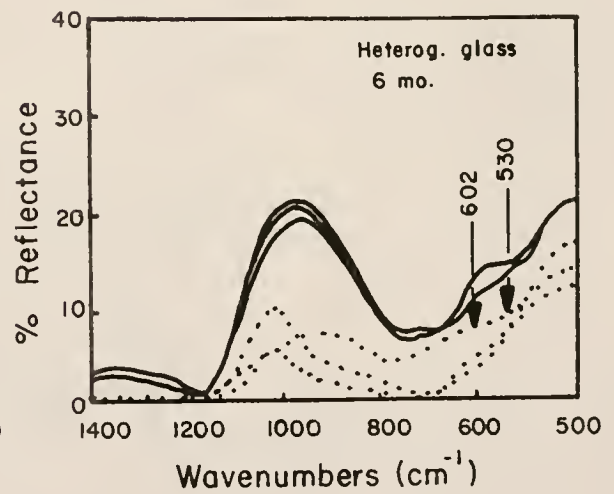
(a)



(b)



(c)



(d)

Fig. 5-27. FT-IRRS analysis of SRL 131 + 29.8% TDS glass surfaces in contact with bentonite, Stripa burial at 90°C: (a) homogeneous glass, 1-month burial; and partially devitrified glass (b) 1-month burial; (c) 3-month burial; and (d) 6-month burial.

The EDS data for homogeneous glass specimens prior to burial is shown in Fig. 5-28 (a). It was observed that the Fe:Si peak ratio increased from 1:4.7 for the uncorroded specimen (Fig. 5-25 (a)) to 1:3.7 for the burial specimen interfaced with bentonite at 90°C for 1 month. This suggests that the layer formed on the glass surface interfaced with bentonite at 90°C for 1 month burial is Fe-rich. In the case of the heterogeneous samples, the EDS data show even more Fe enrichment within the surface layer of the glassy phase (Fig. 5-28 (b)). In this case, the Fe:Si peak ratio reaches 1:3.2 indicating that crystallization favors Fe enrichment during burial. With increasing burial times, EDS data (Fig. 5-28 (c, d)) exhibit an increase in Fe:Si peak ratios (1:3.2 for 1 month, 1:1.4 for 3 months and 1:0.9 for 6 months).

The EDS data show that for uncorroded specimens, the main constituents of the crystal phase are  $\text{Fe}_2\text{O}_3$ , NiO and MnO and possibly some  $\text{SiO}_2$  (Fig. 5-25 (b)). This suggests a compositional variation of spinel solid solutions. For 3- and 6-month specimens, a small increase in Fe:Ni peak ratio can be observed (Fig. 5-29 (b, c)). These data indicate for the crystalline areas an Fe:Ni ratio of approximate 8.8:1 for 1-month, 9.5:1 for 3-month and 10:1 for 6-month burial specimens. This increase in Fe:Ni peak ratios is much smaller than the change in Fe:Si peak ratio for the glassy matrix.

Alkali ions, such as Na, are leached from the glassy surface during burial. This may be assessed from the EDS data which show lower Na peak intensities for homogeneous glass specimens buried at



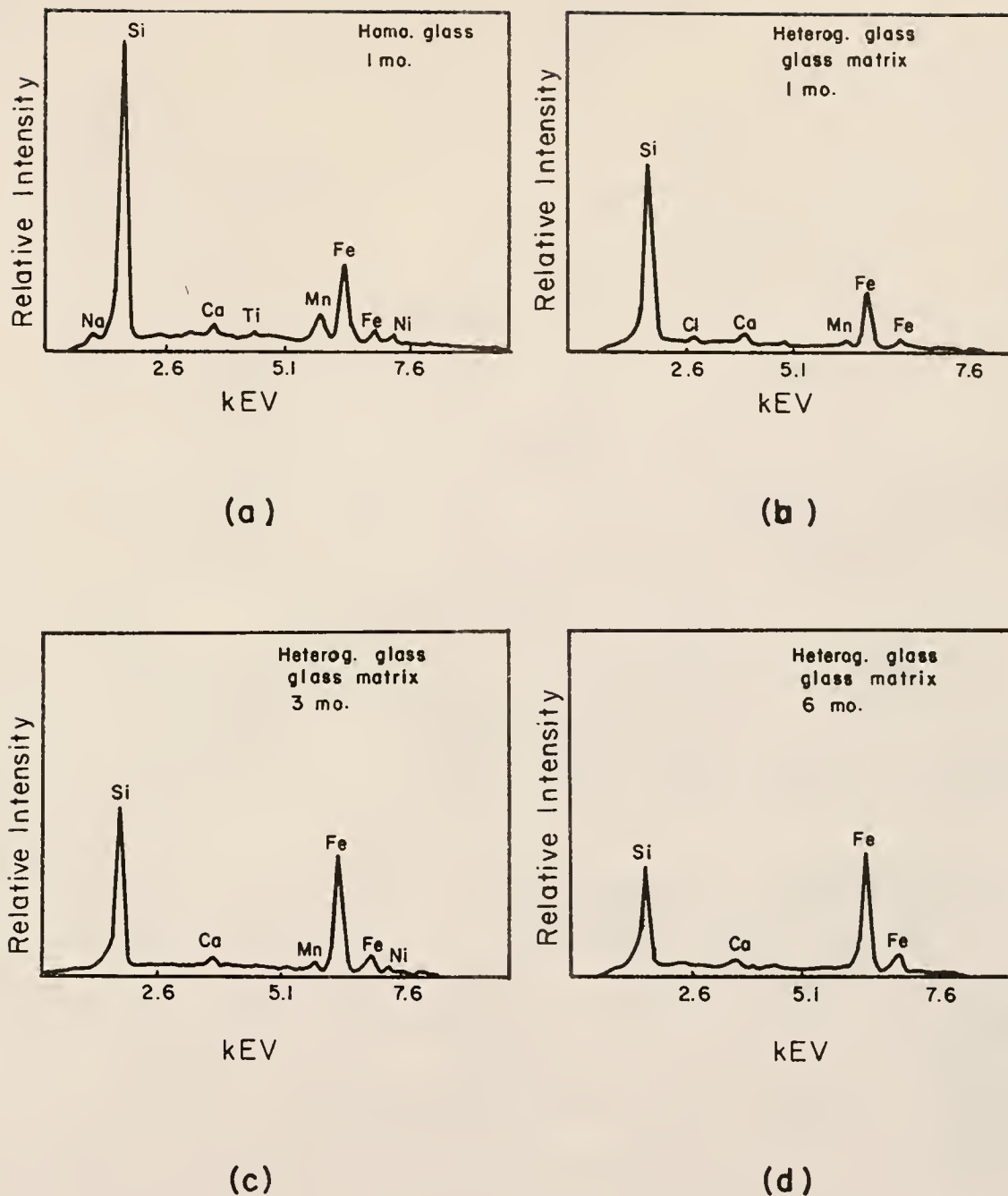


Fig. 5-28. EDS analysis of SRL 131 + 29.8% TDS glass surfaces in contact with bentonite, Stripa burial at 90°C: (a) homogeneous glass, 1-month burial; and glass matrix of partially devitrified glass, (b) 1-month burial; (c) 3-month burial; and (d) 6-month burial.

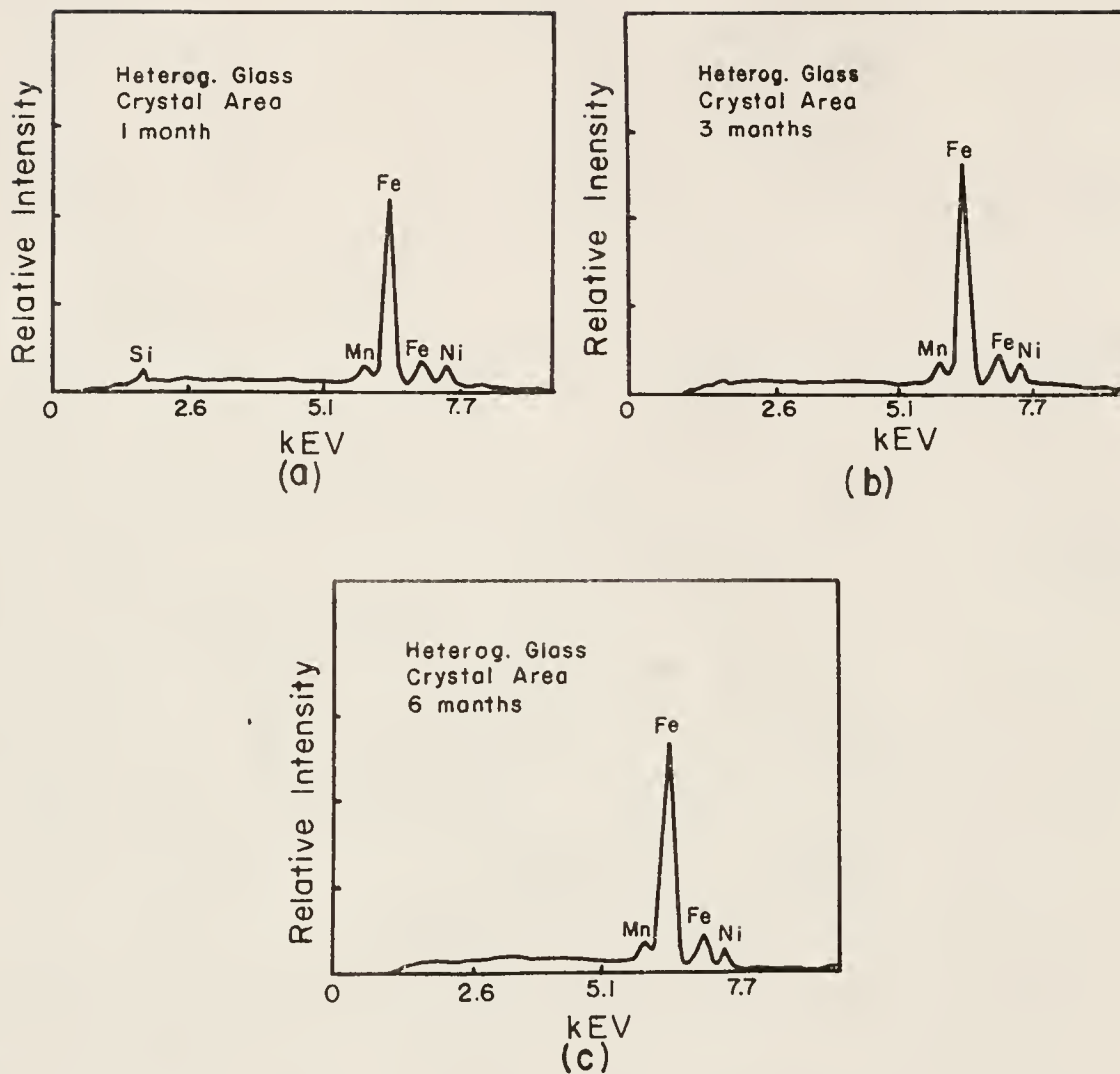


Fig. 5-29. EDS analysis of crystal areas of partially devitrified SRL 131 + 29.8% TDS glass surfaces in contact with bentonite, Stripa burial at 90°C: (a) for 1 month, (b) for 3 months and (c) for 6 months.

90°C for 1 month, and the disappearance of the Na peak for the glass matrix areas of the heterogeneous glass specimens interfaced with bentonite after 1-, 3- and 6-month burial at 90°C. On the other hand, the compositional change in the crystalline phase seems relatively small, the only exception being Si, which shows an obvious relative depletion after burial (Fig. 5-29). The Si peak shown in the spectra of the heterogeneous samples is most likely due to contributions from the surrounding glassy phase.

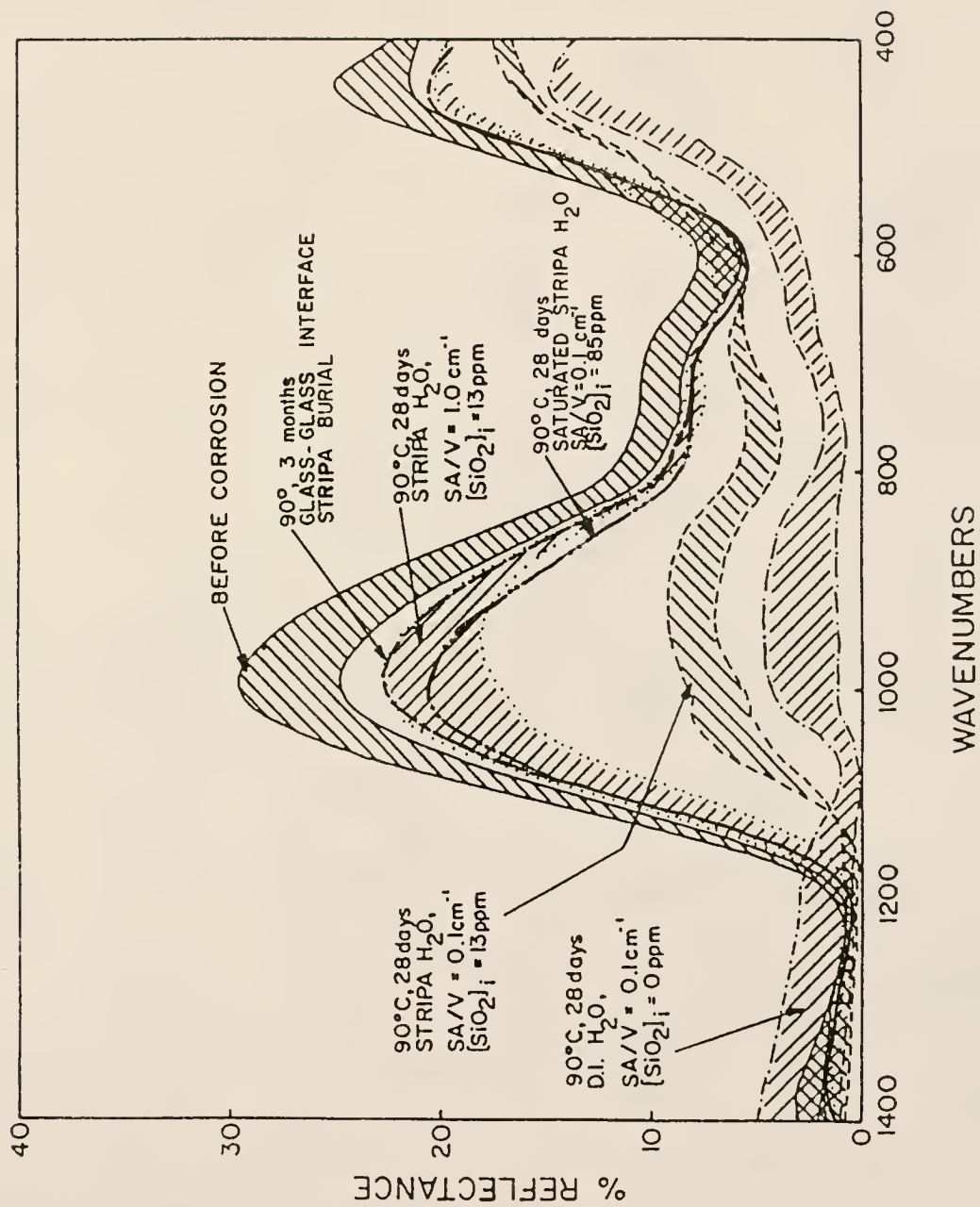
### Laboratory Test Results

#### Modified MCC-1 Static Leach Tests

Field tests were simulated in the laboratory by changing three variables. First, water from the Stripa mine was used to replace the deionized water typically used in laboratory experiments. Secondly, the SA/V was increased from  $0.1 \text{ cm}^{-1}$  (typical in lab tests) to  $1.0 \text{ cm}^{-1}$ . Although this latter value is still small compared to the SA/Vs obtained during burial, it represents a practical working value above which it is difficult to control in the laboratory when bulk glass samples are used. Thirdly, a "saturated" Stripa water was prepared by exposing regular Stripa water to a large SA/V using glass powders.

Figure 5-30 shows the FT-IRRS results of the laboratory tests for SRL 165 + 29.8% TDS glass. Three conclusions can be drawn from these results: (1) higher SA/V ratios result in less surface deterioration; (2) the extent of surface deterioration is less in ground water than in deionized water; and (3) water that already

Fig. 5-30. FT-IRRS analysis of SRL 165 + 29.8% TDS glass before and after leaching for 28 days at 90°C in (a) deionized water with SA/V = 0.1 cm<sup>-1</sup> (b) Stripa ground water with SA/V = 0.1 cm<sup>-1</sup>, (c) Stripa ground water with SA/V = 1.0 cm<sup>-1</sup> and (d) saturated Stripa ground water with SA/V = 0.1 cm<sup>-1</sup>. Also shown is a spectrum for the glass/glass interface after 3-month Stripa burial.



contains large concentrations of glass species, i.e., "saturated" Stripa water, is less aggressive than regular ground water or deionized water. The major factor contributing to the reduction in leaching is the presence of Si in solution. Si is not present in deionized water, but Stripa water contains about 13 ppm of Si and "saturated" Stripa water contains 85 ppm. As shown in Fig. 5-30, when other conditions are equivalent, including SA/V, the reduction in the FT-IRRS peak intensity is inversely related to the Si concentration in the laboratory tests. Increasing the SA/V from  $0.1 \text{ cm}^{-1}$  to  $1.0 \text{ cm}^{-1}$ , while maintaining other conditions constant, results in a decrease in the change in peak intensity. Again, this is related to the Si concentration, although the initial Si concentration is the same in both tests, i.e., when  $\text{SA/V} = 0.1 \text{ cm}^{-1}$ , the Si concentration increases more rapidly in the solution than with  $\text{SA/V} = 1.0 \text{ cm}^{-1}$ . Additionally, less Si is required to be released from the glass when  $\text{SA/V} = 1.0 \text{ cm}^{-1}$  in order to approach saturation. Therefore, less surface deterioration is expected when  $\text{SA/V} = 1.0 \text{ cm}^{-1}$ , as is confirmed by the spectra in Fig. 5-30.

SIMS analysis of SRL 165 + 29.8% TDS glass leached in the laboratory under conditions of 1 month,  $90^\circ\text{C}$  and  $\text{SA/V} = 1.0 \text{ cm}^{-1}$  is shown in Fig. 5-31. From this figure, it can be seen that B, Na, Li and U are depleted in these laboratory-leached specimens. A small amount of Si was also leached out, Ca was enriched and Fe remained almost unchanged at the surface. The depth of leaching on the glass represented in Fig. 5-31 is about  $0.5 \text{ }\mu\text{m}$ .



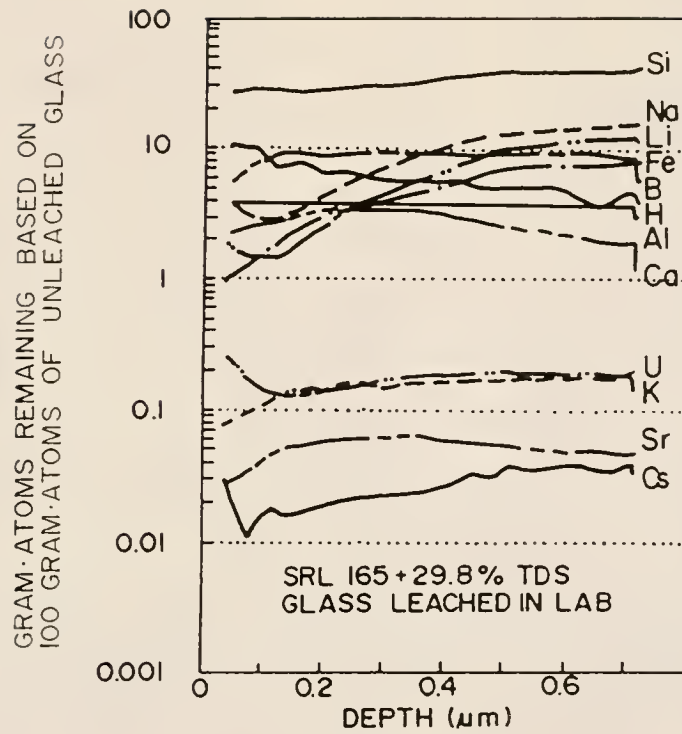


Fig. 5-31. SIMS analysis of SRL 165 + 29.8% TDS waste, laboratory-corroded, 1 month 90°C in Stripa water with SA/V = 1.0  $\text{cm}^{-1}$ .

### Single-Pass Flow Tests and Static Tests Using Rock Cups

Figure 5-32 is a plot of solution pH vs time for Black Frit 165-Mobay glass corroded under static and flow test (0.3 mL/h) conditions. The leachant was collected each week for up to 26 weeks during the flow tests and pH was measured after each collection. The original ground water pH was  $7.6 \pm 0.1$ .

In the case of flow tests, the pH changed by 0.8 unit (from 7.3 to 8.1). The pH vs time curve (Fig. 5-32) shows an initial small increase at 9-10 weeks with a maximum of 8.1, and then buffering at slightly lower pH values.

In contrast, the static leachant exhibited higher pHs (7.5-8.4). This is not surprising since under static leach conditions, the alkali ions which were leached out from the glass surface accumulated in the solution and resulted in higher pH values. However, this pH increase was small.

The ground water buffering has a strong action on glass leaching, since dissolution of the glass formers,  $\text{SiO}_2$  and  $\text{B}_2\text{O}_3$ , is highly pH-dependent. Below pH 9, the activity of  $\text{SiO}_2$  is low ( $<10^{-4}$  M for vitreous silica at  $25^\circ\text{C}$  [76] and slightly higher for borosilicate glasses). Thus, a skeleton rich in  $\text{SiO}_2$  could be preserved.

The concentrations of Si, B, Al and Li in the single pass flowing ground water as a function of leaching time, are shown in Fig. 5-33. An important feature observed in this figure is an initial increase in the solution concentration to a maximum followed by a decrease with time. Two possible reasons for this are (1) the

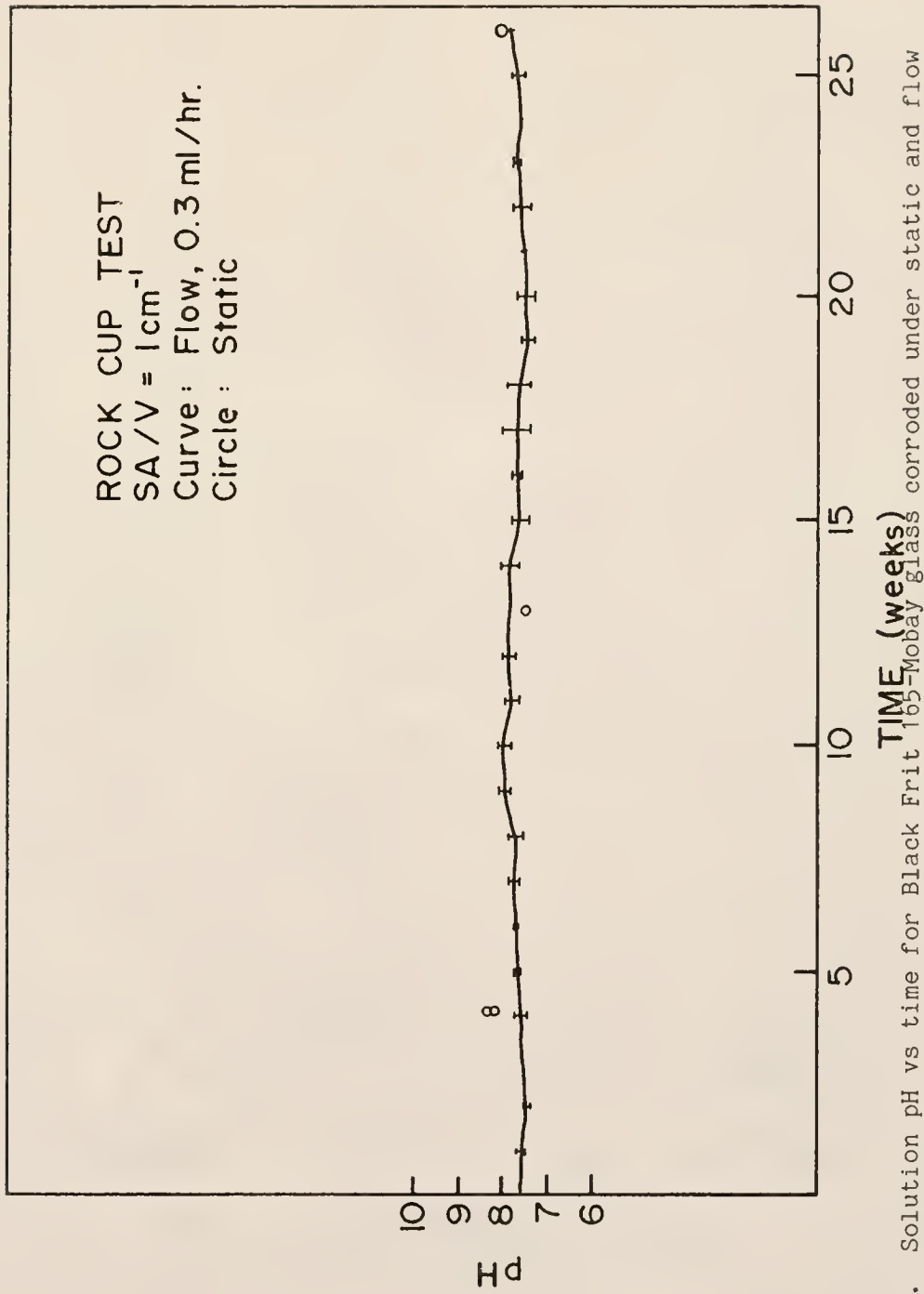


Fig. 5-32. Solution pH vs time for Black Frit 105-Mobay glass corroded under static and flow conditions.

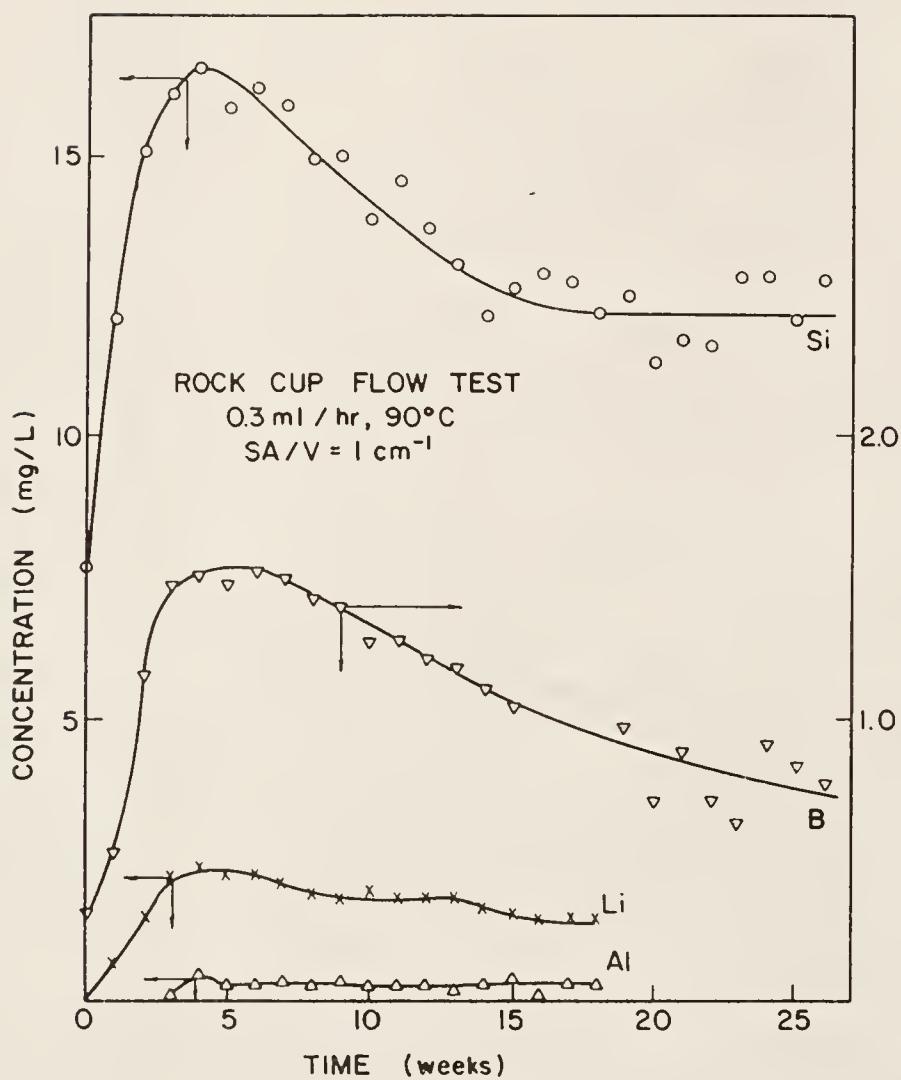


Fig. 5-33. Concentrations of Si, B, Al and Li in the single pass flowing ground water at 0.3 mL/hr as a function of leaching time for Black Frit 165-Mobay glass samples.

higher dissolution rate of edges of polishing scratches [77] and (2) as suggested by Grambow [47] a diffusion barrier established after 4-5 weeks leaching, capable of slowing down the elemental release from the inner glass.

The selective leaching of Li and B is quite visible in Fig. 5-34 where the normalized leach rates of Li, B and Si, and weight loss are plotted vs leach time. In this figure, both flow and static test results are shown. In the case of flow tests, the normalized mass loss of Li and B are larger than that of Si. Also, Li leached faster than B.

Figure 5-35 shows the EDS analysis of the Frit 165-Mobay glass surfaces prior to and after static leaching at 90°C. The peak intensity ratios to Si for various elements in the glass are listed in Table 5-3. These data confirmed the preferential leaching of alkalis as shown by the decrease in the Na to Si peak ratio vs time. The Al to Si peak ratio remained almost unchanged and the Fe to Si peak ratio increased from 0.11 to 0.16 after 6-month static leaching. These data suggest that the least-soluble species, such as Fe and Al, stay in the leached layer.

The FT-IRRS and SIMS data for Frit 165-Mobay glass leached in the granite cup tests at 90°C under static and flow conditions are shown in Figs. 5-36 and 5-37. As shown in Fig. 5-36, surface smoothening is revealed by an increase in the spectral intensity after 1-month leaching at 90°C as compared with an uncorroded surface. This is because the sharp edges of the polishing scratches have smaller curvatures and higher dissolution rates as compared to a

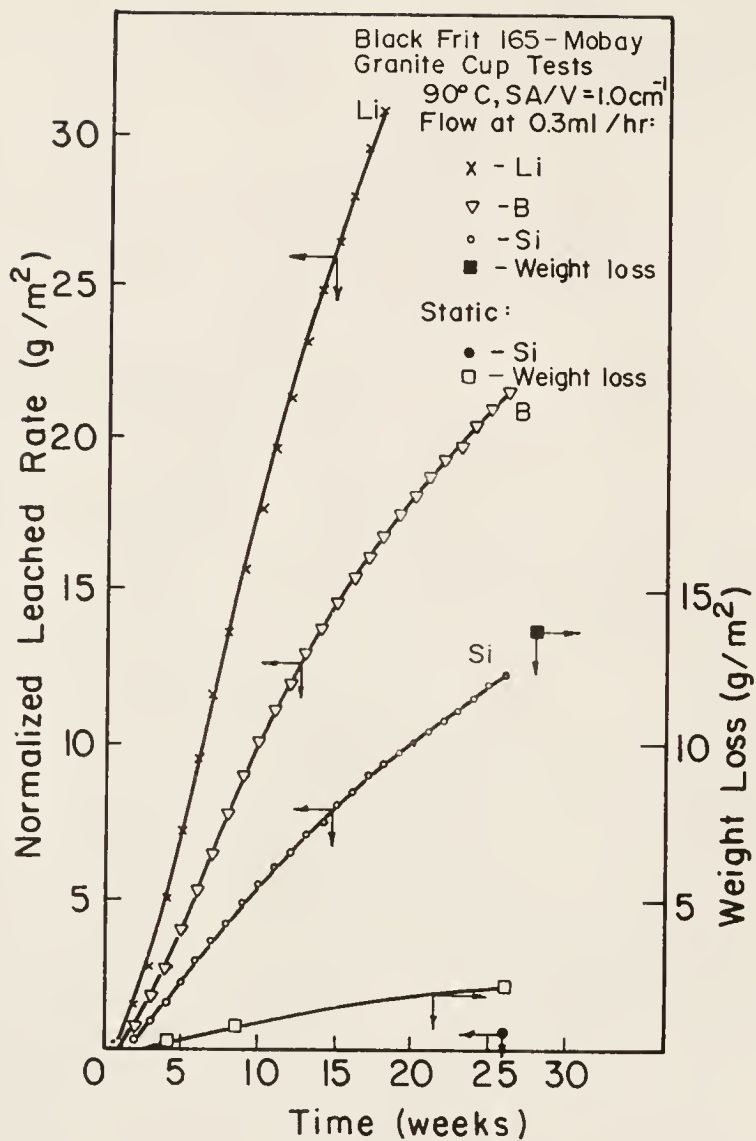


Fig. 5-34. Normalized leach rates of Li, B and Si as a function of time under flowing (at 0.3 ml/hr) conditions for Black Frit 165-Mobay glass with SA/V = 1.0 cm<sup>-1</sup>. Also shown are the weight losses for glass samples leached under static and flow conditions with SA/V = 1.0 cm<sup>-1</sup>.



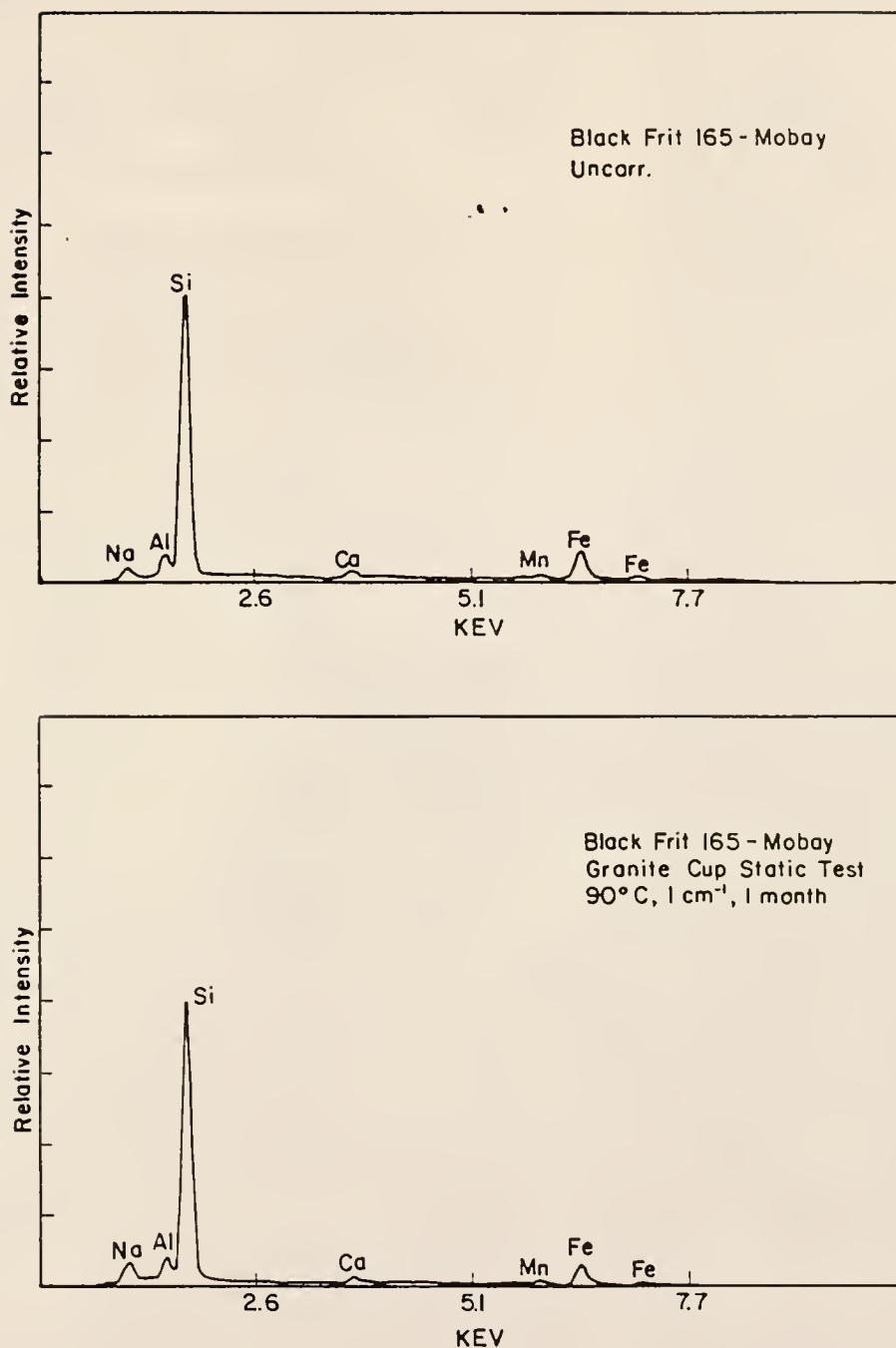


Fig. 5-35. EDS analysis of Black Frit 165-Mobay glass leached in the rock cup test at 90°C with SA/V = 1.0 cm<sup>-1</sup> in ground water under static conditions: (a) uncorroded; (b) for 1 month; (c) for 3 months; and (d) for 6 months.

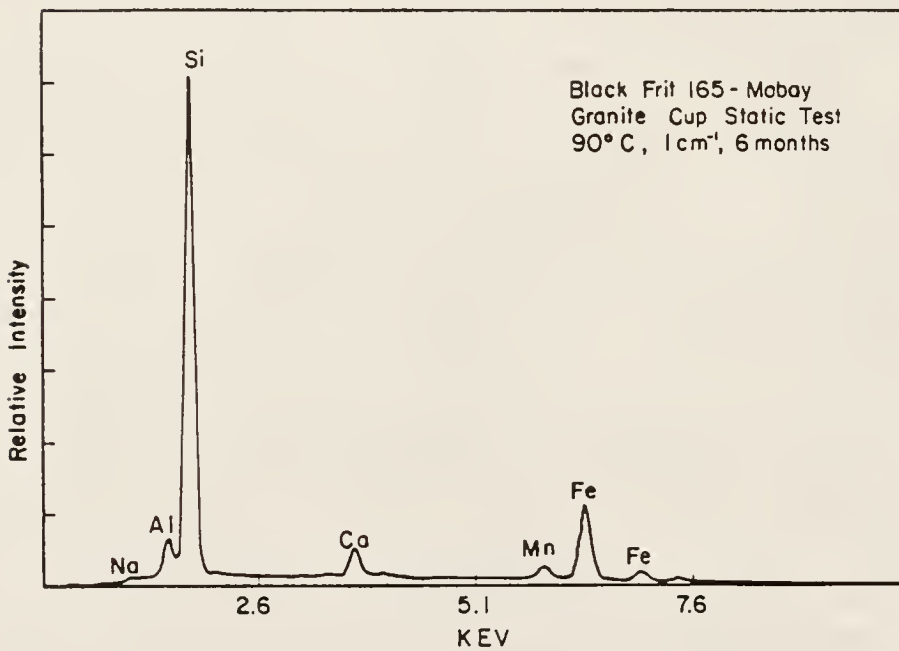
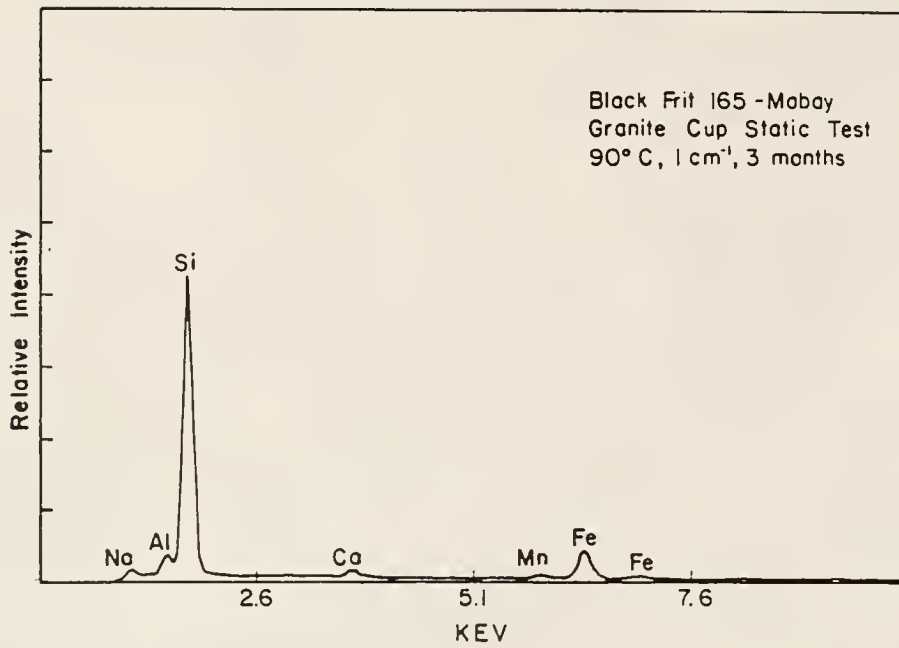


Figure 5-35.--continued.

Table 5-3. Relative Concentrations (Ratio to Si) at the Black Frit 165-Mobay Glass Surface After Static Leaching in the Rock Cup Test. Data Are from EDS Analysis.

Leach Time	Fe	Na	Al	Ca	Ti	Mn	Ni	Mg
Unc.	0.11	0.049	0.096	0.043	0.017	0.027	0.015	0.026
1 mo.	0.087	0.095	0.109	0.037	0.014	0.024	0.010	0.036
3 mo.	0.10	0.044	0.091	0.040	0.015	0.027	0.012	0.027
6 mo.	0.16	0.024	0.097	0.079	0.023	0.039	0.017	0.022

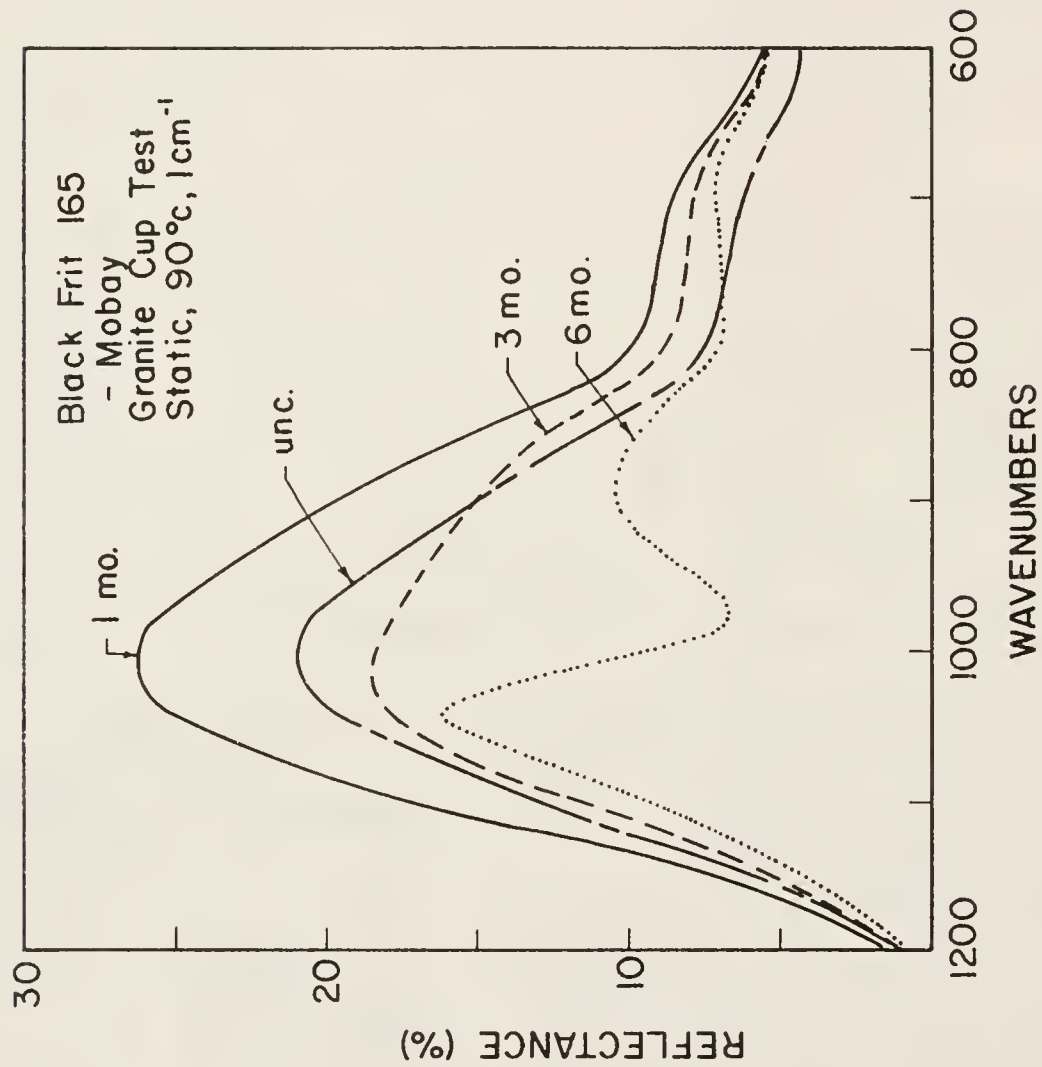
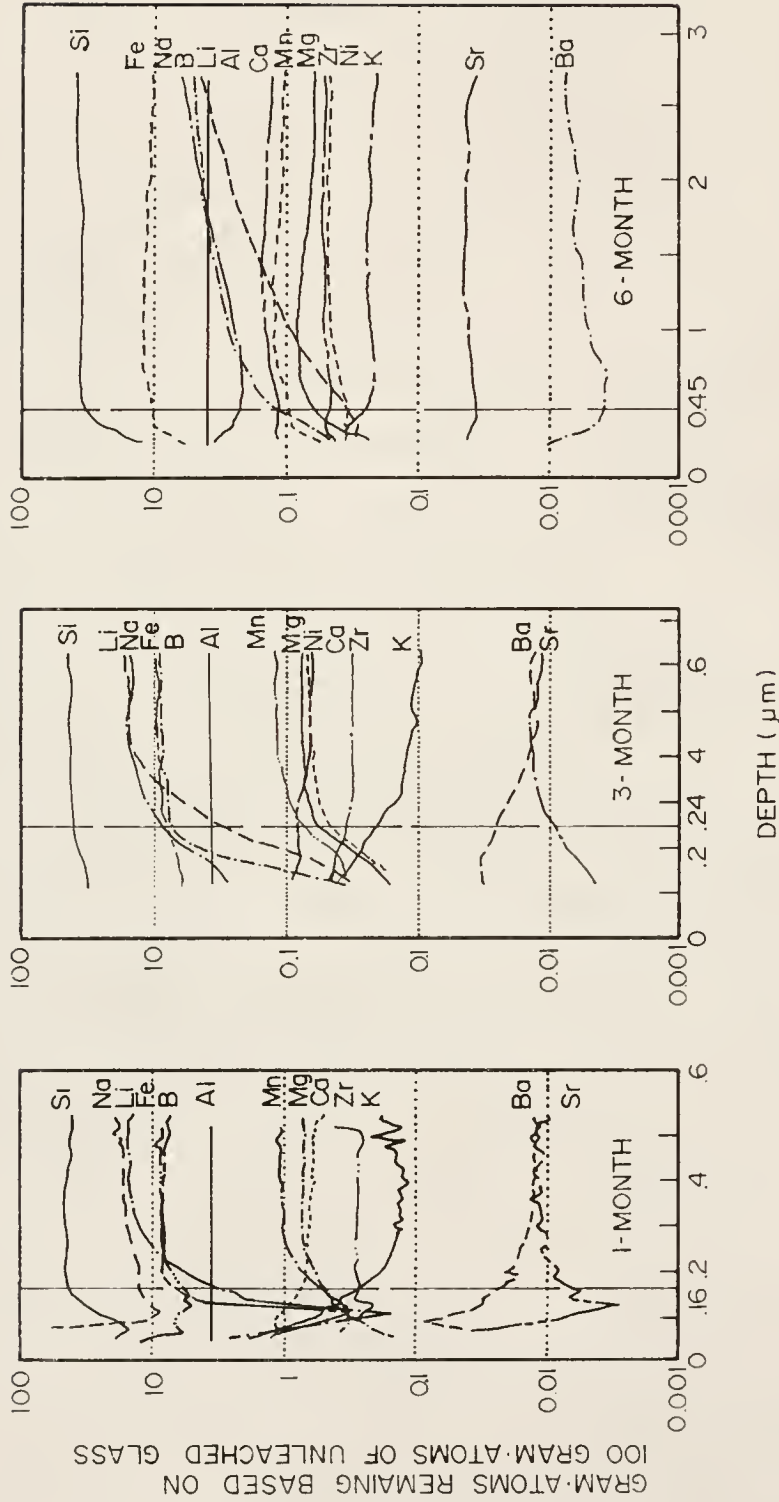


Fig. 5-36. FT-IRRS analysis of Black Frit 165-Mobay glass leached in the granite rock cup test at 90°C under static conditions with SA/V = 1.0 cm<sup>-1</sup>.

flat glass surface [77]. After 3 months, selective leaching of alkalis and boron (Fig. 5-37 (a)) caused splitting of the peak at  $800\text{--}1200\text{ cm}^{-1}$  split and resulted in a spectral intensity decrease at the same region (see Fig. 5-36). The peak position of the Si-O-Si stretching vibrations shifted to a higher wave number as a result of  $\text{SiO}_2$  enrichment within the leached glass surface. Leaching of alkali and boron also resulted in a decrease in the peak intensity of the silicon-oxygen-alkali stretching vibrations. The drop of the peak intensity for the Si-O-Si stretching vibrations is due to surface roughening through selective leaching and network dissolution after 3 months.

After 6 months, a further decrease in the spectral intensity within the region of  $800\text{--}1200\text{ cm}^{-1}$  is observed (Fig. 5-36). This roughening is basically due to further dissolution of  $\text{SiO}_2$ , the major network formers, selective leaching of  $\text{B}_2\text{O}_3$  and alkalis. Most species, such as  $\text{Fe}_2\text{O}_3$  and  $\text{Al}_2\text{O}_3$ , exhibit extremely low solubility limits in the ground water with  $\text{pH} = 7\text{--}8$  and thus stay at the glass-water interface or deposit on the walls of the corrosion pits which further roughened the glass surface (Fig. 5-37 (c)). The additional enrichment of  $\text{SiO}_2$  at the altered glass surface layer is indicated by shifting of the Si-O-Si stretching vibration peak to the higher wave numbers. Since leaching of alkalis and boron was more complete after 6 months (Fig. 5-37 (c)), the intensity of the silicon-oxygen-alkali peak decreased (Fig. 5-36). Also, separation of the two peaks became more obvious. These findings are consistent with other analytical data as discussed earlier.



(a)

Fig. 5-37. SIMS depth profiles for Frit 165-Mobay glass leached in the granite rock cup tests at 90°C with  $SA/V = 1.0 \text{ cm}^{-1}$ , (a) under static conditions and (b) under flow conditions (0.3 mL/hr).

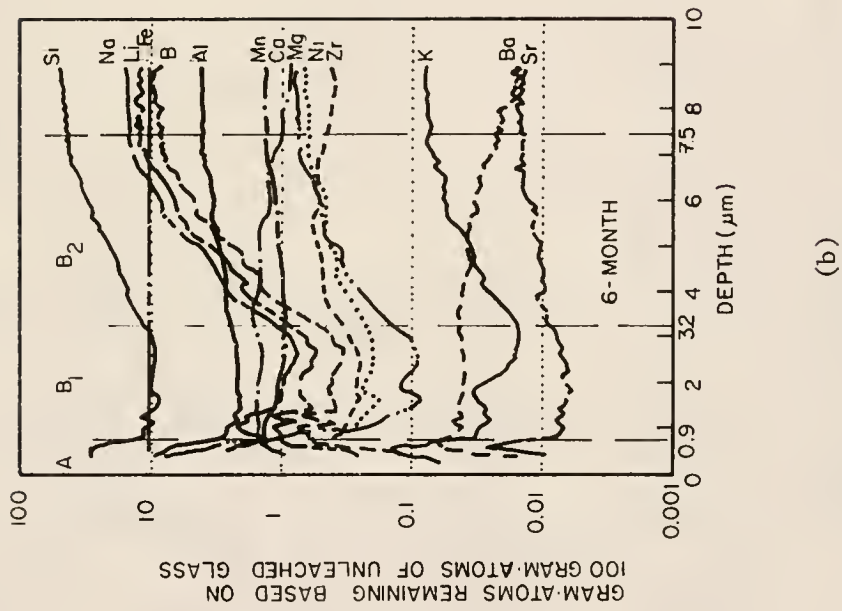


Fig. 5-37.--continued.



## CHAPTER VI DISCUSSION

### ABS Glasses

As shown by the FT-IRRS spectra, optical micrographs and SIMS depth profiles in Chapter V, the two glasses, ABS 39 and ABS 41, displayed a considerable difference in leachability during 90°C, 31-month Stripa burial. An earlier laboratory study [17-19] indicated that ABS 41 glass was three to four times more durable than glass ABS 39. The 31-month burial data confirm that glass ABS 41 is markedly superior to glass ABS 39 with respect to attack of glass/glass and glass/granite interfaces. Figure 6-1 summarizes the time dependence of the thickness of the leach layer based on boron depletion for both glasses at the glass/glass, glass/granite and glass/bentonite interfaces. As shown in Fig. 6-1 for glass ABS 41, the effect of bentonite is significant. The leached layer at this interface is 10 to 20 times thicker than those of the glass/glass and glass/granite. For this glass, the leach rate, as estimated by the slopes of the curves, was slowed down greatly after the first 1 to 3 months of burial, but the subsequent decrease in leaching rate is seen to be very moderate, if any. For example, the leachability at the ABS 41 glass/bentonite interface was 1.4  $\mu\text{m}/\text{yr}$  during the first month of burial, 7.2  $\mu\text{m}/\text{yr}$  between 1 to 3 months, but 12  $\mu\text{m}/\text{yr}$

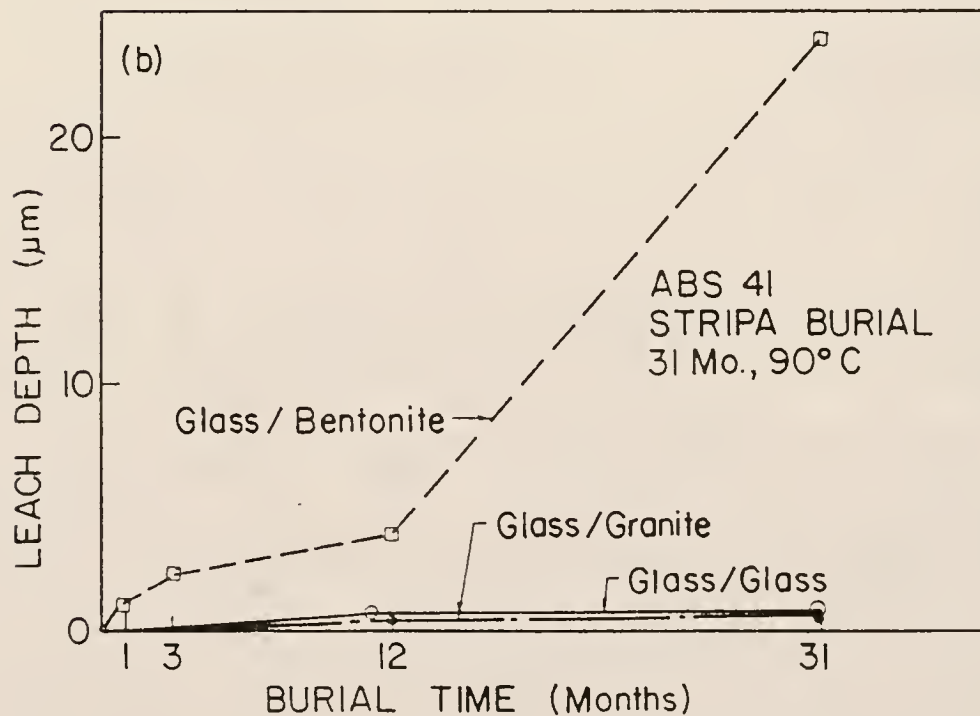
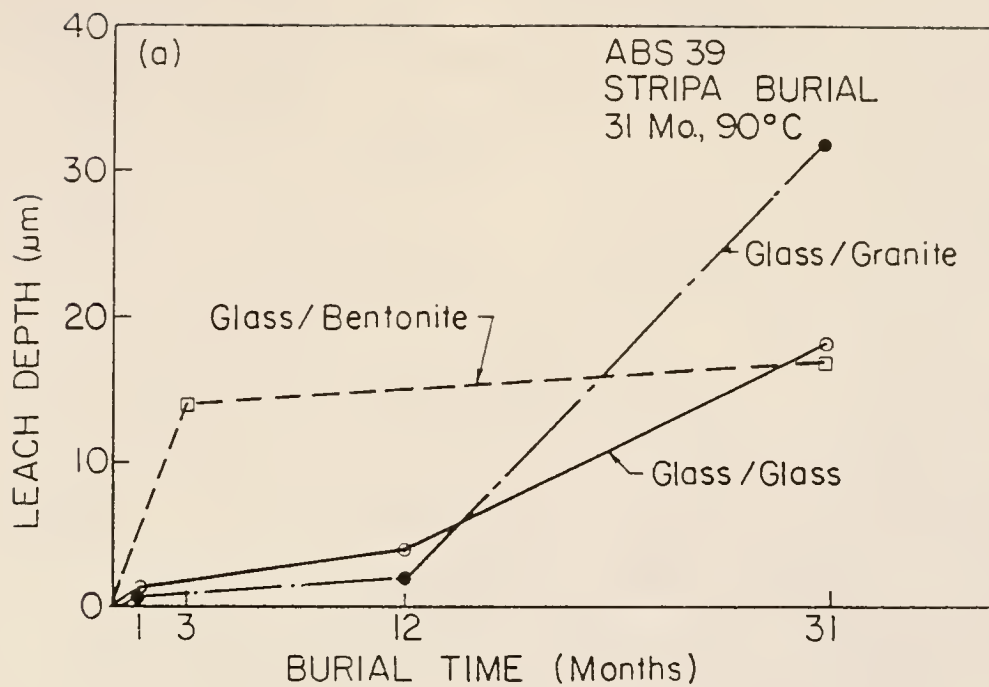


Fig. 6-1. Time dependence of reaction layer thickness for glass ABS 39 (a) and ABS 41 (b) after 31-month, 90°C Stripa burial.

between 3 to 31 months, based upon depth of boron removal. In contrast, the leachability of the ABS 41 glass/glass interface was  $0.8 \mu\text{m}/\text{yr}$  during the first 12 months and  $0.03 \mu\text{m}/\text{yr}$  for 12 to 31 months of  $90^\circ\text{C}$  burial. The leachability of the ABS 41 glass/granite interface was  $0.4 \mu\text{m}/\text{yr}$  within the first 12 months and approximately  $0.24 \mu\text{m}/\text{yr}$  between 12 and 31 months of  $90^\circ\text{C}$  burial.

Thus, during the thermal period of storage ( $\sim 300$  years), when in contact with glass of the same composition under Stripa burial conditions, ABS 41 will leach to a depth of less than  $9 \mu\text{m}$ , even if exposed to water immediately after burial. This can be compared to layer thicknesses of the order of  $2,700 \mu\text{m}$  for the glass/glass interfaces of ABS 39 (Table 6-1 and Fig. 6-1 (a)) during the same period.

For ABS 39, the presence of bentonite apparently did not appreciably accelerate glass leaching after the initial 3 months. This is a significant finding since, up to 12 months, the ABS glass/bentonite interfaces leached four times faster than the glass/glass interfaces. It is the increased leach rates at both glass/glass and glass/granite interfaces between 12 and 31 months that reduced the difference in the leach depths between these interfaces. One possible explanation is a greater exposure to water at the ABS 39 glass/glass and glass/granite interfaces. The Stripa underground laboratory is believed to provide a relevant repository environment with high SA/V ratios and low ground water flow rates. However, the actual amount of water which enters or passes through a particular interface may vary locally. Therefore, there could be an

Table 6-1. 90°C Glass Leach Rates During 12- to 31-Month Period ( $\mu\text{m}/\text{yr}$ ).

	Glass/Glass	Glass/Granite	Glass/Bentonite
ABS 39	9	19	1.3
ABS 41	0.03	0.24	12

increase in the leachability of the glass/glass and glass/granite interfaces if the ground water flow rate increased and/or the SA/V ratio decreased locally. The local attack aspect, as mentioned above, is also likely to be of importance for the accelerated leaching at prolonged times, especially at the glass/granite interfaces.

The optical micrographs indicate that this might have been the case. The rather thick and porous surface films formed on these two interfaces are evidence that these glasses leached at a low SA/V ratio or a higher ground water flow. This kind of surface film is characteristic of glass surfaces after an MCC-1 static test with  $SA/V = 0.1 \text{ cm}^{-1}$  or an MCC-4 test with a flow rate  $>0.5 \text{ mL/h}$  [78].

Based on the plot of leach depth vs burial time for the ABS 39 glass/bentonite interface, the leach rate was  $5.6 \text{ }\mu\text{m/yr}$  during the first 3 months of burial and  $1.3 \text{ }\mu\text{m/yr}$  between the 3rd and 31st month. Thus, the leach depth after the thermal period of storage ( $\sim 300$  years) can be estimated to be of the order of  $400 \text{ }\mu\text{m}$  for the ABS 39 glass/bentonite interface.

It has been shown many times, and discussed in a recent publication [79], that ABS 41 has a considerably smaller leach depth than ABS 39. This is thought to be due to a higher  $(\text{Si} + \text{Al})/(\text{alkali} + \text{B})$  ratio, and perhaps also to the coexistence of sodium and lithium in the bulk glass, i.e., a "mixed-alkali effect" which may reduce the rate of ion exchange [80,81]. Also, it has been shown [79] that the presence of divalent cations, such as zinc, may further reduce the rate of leaching through the formation of a protective zinc silicate

layer. The low depletion rate for ABS 41 is an important finding since this composition is quite close to that chosen for commercial high-level waste solidification by the French for LaHague operations. However, the observed sensitivity of ABS 41 to long-term attack at the bentonite interface is disconcerting. One contributing factor may be the presence of zinc, which, according to other evidence [79], usually enhances leaching resistance at short times, but might be less advantageous at longer exposures. This could be due to a pH effect where bentonite creates high pH environment dissolving  $\text{Zn}(\text{OH})_2$  and Zn silicates from the glass surface.

In comparing the leach rates among the three ABS glasses, the SIMS data shown in Fig. 6-2 and Table 6-2 indicate that both ABS 118 and ABS 41 are superior to ABS 39. The ABS 118 glass/glass and glass/granite interfaces leached just slightly faster than those of ABS 41, but the ABS 118 glass/bentonite interface shows a better leach resistance than ABS 41. For these three glasses, the glass/granite interfaces leached more slowly than the glass/glass interfaces.

Table 6-2 lists the SIMS surface compositional analysis of the glass/glass, glass/bentonite and glass/granite interfaces for the three ABS glasses after 12-month, 90°C Stripa burial. A common feature observed from the SIMS analysis is that, within the altered glass surfaces, almost all of boron has been depleted while a considerable amount of Na still remains in these glasses. This is probably due to the presence of Na ions in ground water before burial (Table 4-6). Thus the release of Na from glass was somewhat

Table 6-2. SIMS Compositional Analysis of Glass/Glass, Glass/Bentonite and Glass/Granite Interfaces for ABS 39, ABS 41 and ABS 118 after 12-Month, 90°C Stripa Burial (Gram-atoms Remaining Based on 100 Gram-atoms of Unleached Glass).

	ABS 39				ABS 41			
	"Gel," Mid-Plateau				"Gel," Mid-Plateau			
	Bulk	Glass/ Glass	Bentonite	Glass/ Granite	Bulk	Glass/ Glass	Bentonite	Glass/ Granite
Si	40.7	42.27	20.71	25.37	42.1	40.22	16.34	46.15
Li	(0.01)			0.02	9.8	0.94	0.17 <sup>a</sup>	0.22
Na	20.85	5.64	2.41	2.74	15.55	6.68	1.69	2.58
K	0.04	0.27	0.32	0.25	0.05	0.24	0.31	0.43
Cs	0.30	0.05	0.02	0.12	0.30	0.15 <sup>b</sup>	0.01 <sup>b</sup>	0.22
Mg	0.02	n.m. <sup>c</sup>	n.m.	0.27	0.03	0.07 <sup>d</sup>	0.56	0.31
Ca	(0.01)	0.61	0.71	0.39	0.01	0.24	0.54	0.68
Sr	0.10	0.04	0.02	0.08	0.10	0.04 <sup>b</sup>	0.02	0.04
Ba	0.15	0.01	0.04	0.01	0.15	0.15 <sup>b</sup>	0.003	0.07
Zn	-	-	-	-	1.80	1.28	0.09	1.38
B	27.45	1.28	0.13	1.09	22.2	2.98 <sup>a</sup>	0.34 <sup>a</sup>	2.46
Al	3.05	3.05	3.05	3.05	2.4	2.4	2.4	2.4
Mn	0.45	n.m.	n.m.	0.05	0.45	n.m.	n.m. <sup>d</sup>	0.22
Fe	3.60	4.30	2.57 <sup>d</sup>	2.93	1.80	2.4	1.75 <sup>d</sup>	2.4
Zr	0.55	0.55	0.59 <sup>d</sup>	0.43	0.55	0.58	0.47 <sup>d</sup>	0.49
Mo	0.80	n.m.	n.m.	0.57	0.75	n.m.	0.01	0.12
Y	0.70	0.04	0.03	0.05	0.06	0.05	0.01	0.04
La	0.20	0.15	0.05	0.07	0.20	0.18	0.02	0.12
U	0.30	0.24	0.03	0.23	0.30	0.21	0.01	0.18
X <sub>e</sub> <sup>e</sup>		4.0	14.8	1.8		1.0	3.8	0.36



Table 6-2--continued.

ABS 118									
	Bulk	"Gel," Mid-Plateau			"Outer Region"				
		Glass/ Glass	Glass/ Bentonite	Glass/ Granite	Glass/ Glass	Glass/ Bentonite	Glass/ Granite		
Si	40	41	41	34	41	39	33		
Li	6	0.02	0.01	0.3	0.02	0.01	0.4		
Na	16	8	5	6	9	2.6	6		
K	0.05	0.3	0.7	0.5	0.2	0.6	0.6		
Cs	0.4	0.2	0.03	0.05	0.2	0.02	0.03		
Mg	0.05	0.06	0.3	0.4	0.3	0.4	0.4		
Ca	4	1	0.9	0.6	0.9	0.9	0.4		
Sr	0.15	0.06	0.007	0.02	0.05	0.006	0.01		
Ba	0.2	0.1	0.04	0.01	0.1	0.03	0.01		
Zn	0.5	0.4	0.1	0.1	0.5	0.005	0.1		
B	21	0.4	0.2	1.5	0.2	0.06	1		
Al	5	5	5	5	5	5	5		
Mn	0.5	0.5	0.4	0.04	0.2	0.2	0.02		
Fe	2	2.1	2	1.3	13	1	0.8		
Zr	1	0.9	1	0.5	0.7	0.7	0.2		
Mo	0.7	0.7	0.8	0.4	0.3	0.02	0.2		
LD <sup>f</sup>	1	0.9	0.8	0.3	0.4	0.07	0.1		
U	0.16	0.1	0.1	0.05	0.06	0.01	0.01		

a Concentration increasing with depth in "gel."

b Concentration varies, minimum in "gel" zone.

c n.m.: Not measured.

d Concentration decreasing without "plateau."

e X<sub>μm</sub>: Approx. depth of leached layer.

f "LD" stands for the sum of La, Ce, Pr, Nd and Y.

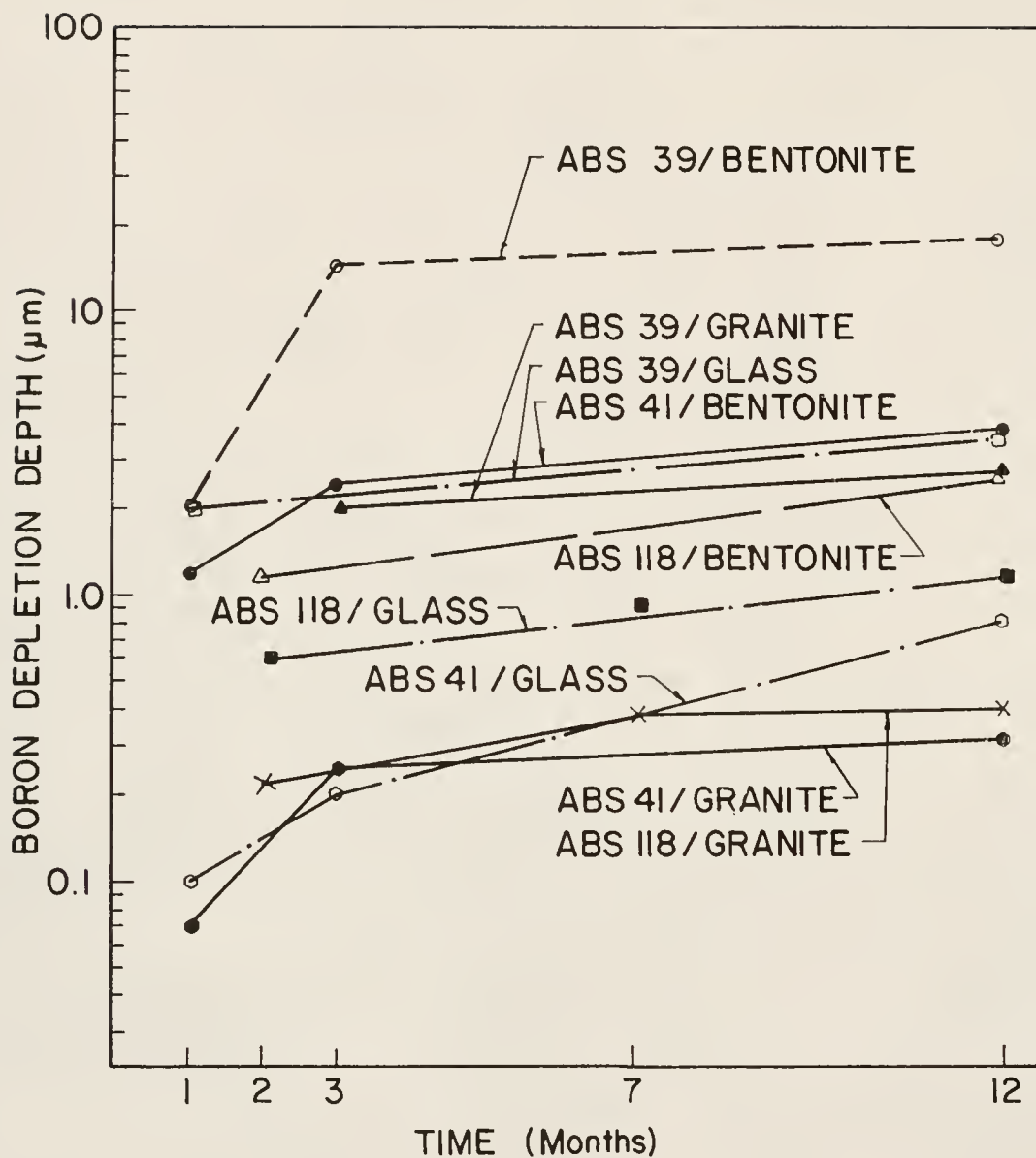


Fig. 6-2. Boron depletion depth vs burial time for the glass/glass, glass/granite and glass/bentonite interfaces. Three ABS glasses are compared.

suppressed due to a decreased concentration gradient. Data in Table 6-2 also confirm that at the ABS 41 glass/bentonite interface, more  $\text{SiO}_2$  has been dissolved from the "gel\*" mid-plateau region and Na depletion was more complete as compared to that of ABS 118. SIMS analyses also show that very little leaching of transition metals such as Zr, Mo, Ni and Cr occurred (Fig. 5-10).

### SRL Glasses

The experimental results for the three SRL glasses are summarized in Fig. 6-3 based on the boron depletion depth from the SIMS analysis. A general tendency of the time-dependence of the leach depth can be seen clearly from the figure. After an initial rapid increase, the leach rates slowed down after 1-3 months of burial.

There was an appreciable effect of composition on SRL waste glass leaching during burial. SRL 165 + 29.8% TDS was the most durable glass among the three compositions under investigation. Compared with SRL 131, SRL 165 glass frit introduced 7.1 wt% more  $\text{SiO}_2$  and 5.7 wt% less  $\text{B}_2\text{O}_3$  into the final glass composition (Table 4-1). After 2 years of burial, the SRL 165 + 29.8% TDS glass/glass interface was leached 0.5  $\mu\text{m}$  deep, as shown in Fig. 6-3, which is only 1/6 of the leach depth for SRL 131 + 29.8% TDS glass. As revealed by SIMS analysis (Fig. 6-3), the leach depths of two SRL 131 glasses are 3.6  $\mu\text{m}$  (with 29.8% TDS waste) and 1.85  $\mu\text{m}$  (with 35% TDS), respectively. These data show that SRL 165 frit is much better than

---

\* Hydrated amorphous alumino-silicate.

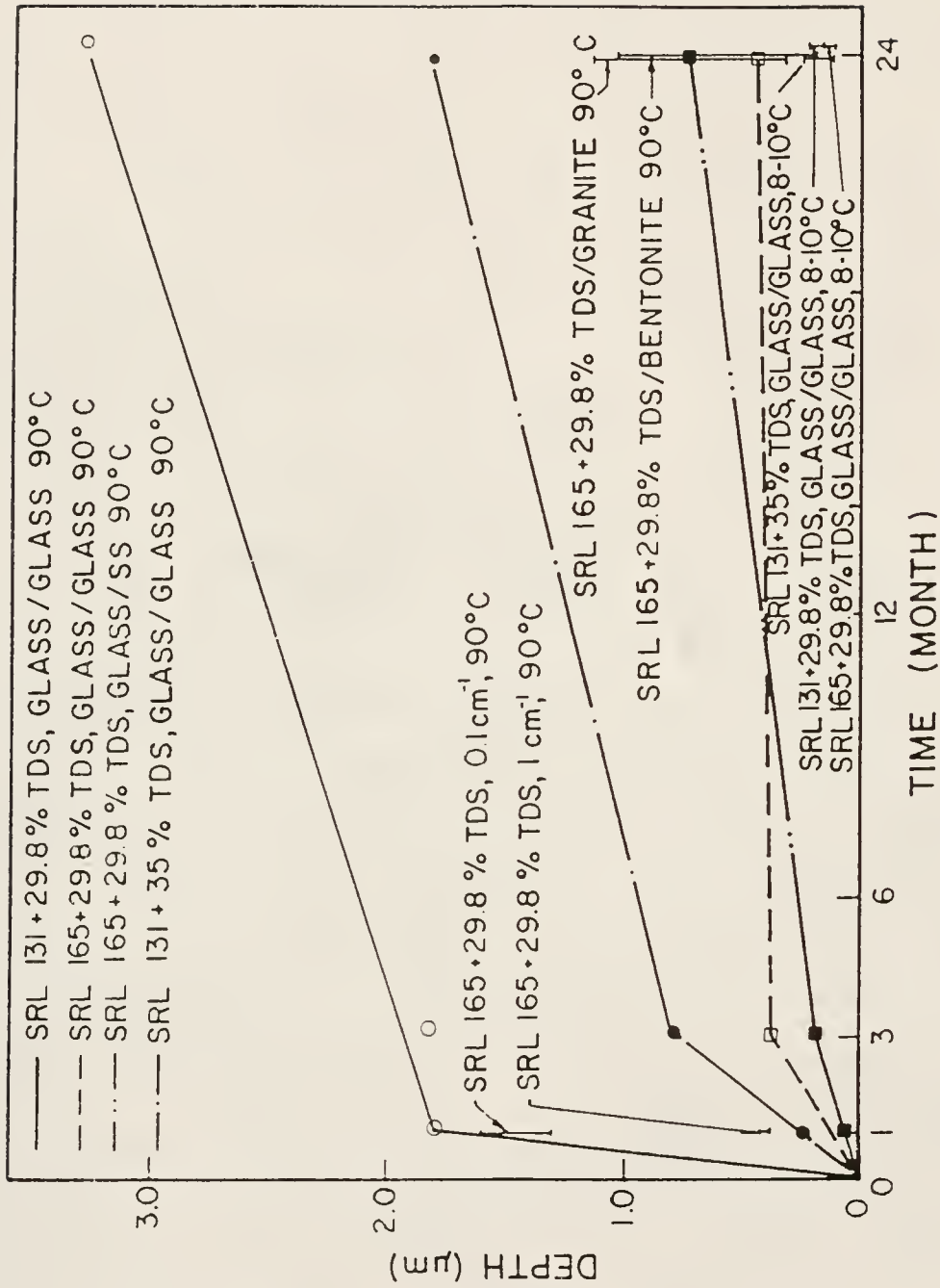


Fig. 6-3. Penetration depth as a function of leaching time for the SRL glasses either buried in contact with glass, stainless steel, granite or bentonite in Stripa mine, or leached in Stripa ground water with  $SA/V = 0.1$  or  $1.0 \text{ cm}^{-1}$  in laboratory.

SRL 131 and an increase in waste loading from 29.8 wt% to 35 wt% decreased the leach depth of SRL 131 glass by 2X.

There were no obvious effects on SRL glass leaching due to the presence of Cu, stainless steel or Ti. McVay and Buckwalter [54] have reported that a synergistic effect occurs between ductile iron and PNL 76-68 borosilicate glass: iron enhances glass dissolution and glass enhances iron corrosion. This is due to the formation of an iron silicate precipitate. The precipitate removes elements such as Si from solution and therefore inhibits the saturation effects which normally cause decreases in elemental removal rates. Thus, use of any form of iron in the repository might be a cause for concern. However, stainless steel used in these experiments exhibited excellent resistance to the laboratory and burial environments. The stainless steel (304L) used in the Stripa burial experiment belongs to group III austenitic type which possesses better corrosion resistance than the straight chromium (groups I and II) steels [82]. The stainless steel did not appear to be degraded in either the burial or laboratory experiments.

Regarding the glass/granite interface, the leach rates are different from spot to spot. As shown in Fig. 6-3, large variations are observed for SRL 165 + 29.8% TDS glass surface in contact with granite during a 2-year burial. Some areas of this glass that were in contact with granite had larger leach depths than those on the glass buried in contact with the bentonite. It should be pointed out that the most heterogeneous attack occurred on the samples buried in contact with granite for 2 years.

The presence of bentonite accelerated the attack on SRL glasses during the first year of burial at 90°C [61,83]. However, 2-year experimental results did not show any marked difference in the extent of leaching between the glass exposed to bentonite and that exposed to other types of materials (Fig. 6-3). The fact that bentonite did not significantly influence the long-term SRL glass alteration is probably due to saturation of the ion exchange capacity of the bentonite. As shown in Fig. 6-4, the Li and Na depletion depths are both larger than that of boron, obviously through an ion-exchange process in the presence of bentonite. This may be compared with the profiles at the glass/glass interface in Fig. 5-23 where the "shoulder" for B practically coincides with those for Na and Li. However, when the ion exchange sites in the bentonite structure are substituted (e.g., Al ions in the octahedral sites in bentonite are substituted by Li from the glass), the effect of bentonite on alkali extraction is reduced. The increase in the Si concentration in the leached glass surface may be also due to the presence of bentonite, since  $\text{SiO}_2$  may be transferred from the bentonite to the glass surface through a dissolution-precipitation process.

Heterogeneities can affect the corrosion behavior of alkali borosilicate simulated nuclear waste glass during burial. This work has shown that the enhanced aqueous attack of the heterogeneous nuclear waste glass can occur at the phase boundaries (see Fig. 5-26). The preferential phase boundary attack is likely to be a result of stresses surrounding the embedded crystals and/or a

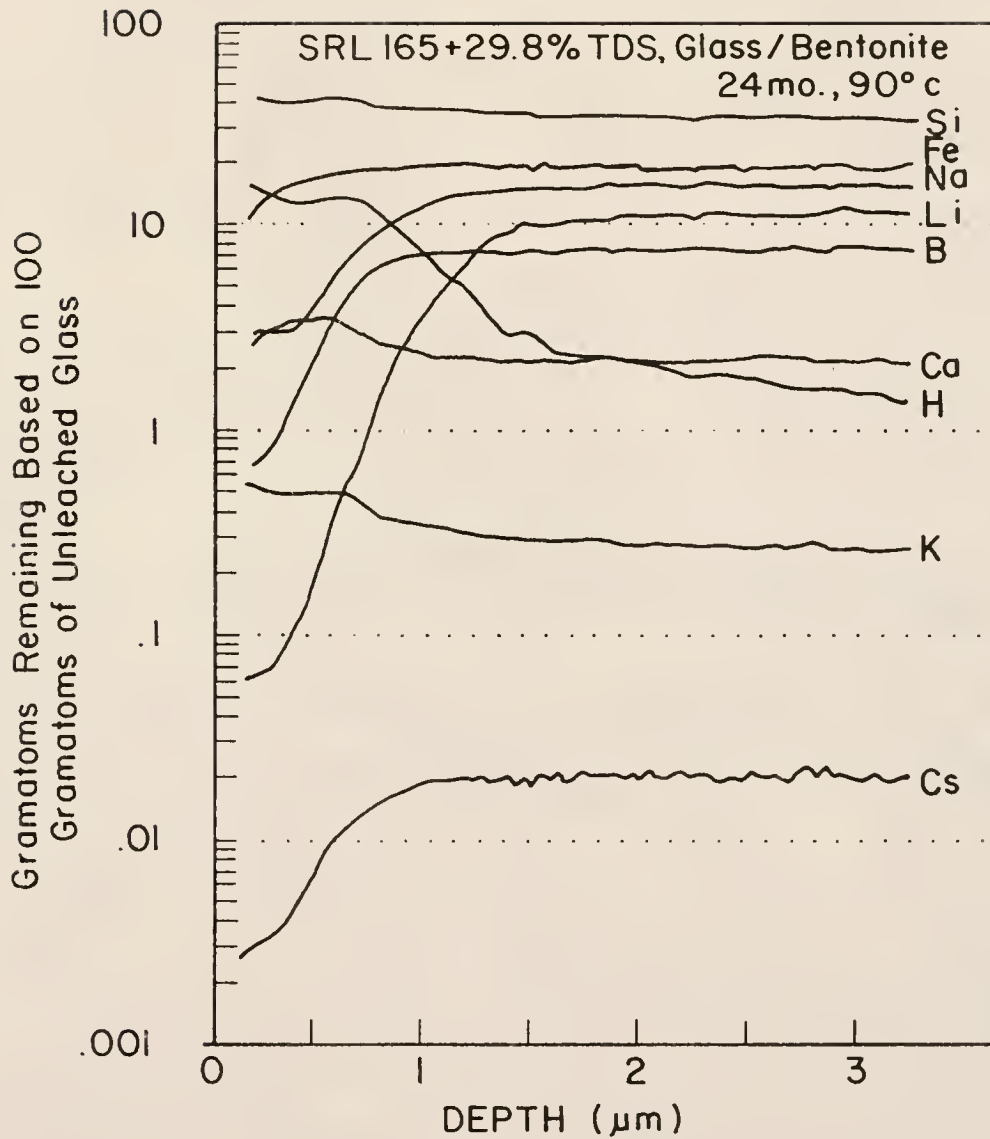


Fig. 6-4. SIMS compositional profiles of SRL 165 + 29.8% TDS glass/bentonite interface after 24-month, 90°C burial in Stripa (compare the corresponding glass/glass profiles in Fig. 5-23).



compositional gradient between the crystalline phase and glassy phase created during cooling.

For homogeneous glasses, there is only one contribution to corrosion, i.e., the glassy matrix. In the case of heterogeneous glasses, however, there are three contributions to corrosion: (1) the glass matrix, (2) the crystalline phase and (3) the interfacial regions between the two phases. The total extent of corrosion will be the sum of these contributions. In the order of decreasing durability are the crystalline phase, the glassy phase and the interfacial regions. As discussed by McCracken [84], the relative contributions to corrosion depend on the quantities of heterogeneities. When small volume fractions of crystallites are present, the improvement of chemical durability provided by the crystalline phase is less than the reduction in the chemical durability due to the creation of the interfacial regions. With large volume fraction of crystals and large grain sizes, the crystal phase will dominate the total extent of corrosion so that an improvement of chemical durability can be expected [84].

Figure 6-5 summarizes the various modes of corrosion in the heterogeneous alkali borosilicate simulated nuclear waste glass observed in the burial tests. They include (1) leaching of the glass matrix, (2) enhanced attack of the glass-crystal interface, (3) pitting of the polycrystalline phase at grain boundaries, (4) surface films enriched in the less soluble multivalent species and (5) crystallite stripping due to preferential attack of the glass crystal interface. Each of these modes of corrosion should be considered

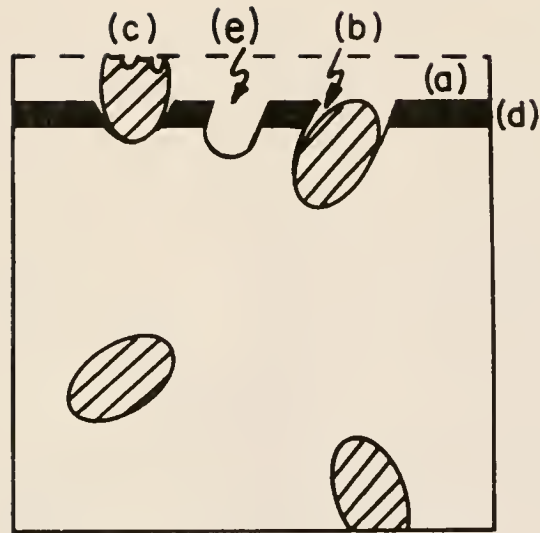


Fig. 6-5. Five modes of corrosion in partially devitrified alkali borosilicate simulated nuclear waste glass: (a) leaching of the glass matrix; (b) enhanced attack of the glass-crystal interface; (c) pitting of the polycrystalline phase at grain boundaries; (d) surface films enriched in the less soluble multivalent species; and (e) crystallite stripping.

when describing the effects of heterogeneities on glass leaching. The dominant mechanism will depend on several factors, including bulk composition and the volume fraction of heterogeneities.

### A Model of Alkali Borosilicate Glass Leaching

The concept of using glass as a host for radioactive waste is based upon the radionuclides entering into and becoming part of the random three-dimensional glass network. The structural network of the glass is provided primarily by  $[\text{SiO}_4]^{4-}$ ,  $[\text{BO}_4]^{5-}$  and  $[\text{BO}_3]^{3-}$  polyhedra. Neighboring polyhedra are bonded together by sharing strong ionic-covalent bridging oxygen bonds. Other multivalent species such as  $\text{Fe}^{+2,+3}$ , rare earths or actinides are also generally bonded within the network by bridging oxygen bonds. Low valence ions, such as  $\text{Na}^+$ ,  $\text{Cs}^+$ ,  $\text{Sr}^{+2}$ , etc., are incorporated into the network by sharing various nonbridging oxygen bonds, the bonding also depending upon size of the ions. This difference in type of bonding in the glass network is responsible for the complex leach behavior of nuclear waste glasses [15].

Three distinct features of glass leaching must be examined, understood and integrated into a coherent dynamic picture. The first of these is the mechanism of attack of the aqueous leachant on glass. The primitive processes that must be considered and elaborated include corrosion of the glass matrix and diffusion-controlled migration of mobile species through the matrix to the glass-leachant interface. The second is the control of the leaching process by the solubilities of the various glass components in the

leachant. Lastly, the impact of an altered surface layer must be evaluated. Of course, these three features are not to be regarded as independent. One must examine the interplay of all the three as they interact synergistically, to determine the behavior of glass leaching.

Table 6-3 lists the dissociation energy, coordination number and bond strength of most oxides in alkali borosilicate nuclear waste glasses. Based upon their bond strengths, which were calculated by Sun [85], oxides can be divided into three categories: (1) network formers, such as  $\text{SiO}_2$  and  $\text{B}_2\text{O}_3$ , whose bond strengths are above 80 kcal/gram·atom constitute the backbone of glass; (2) network modifiers, such as  $\text{Na}_2\text{O}$  and  $\text{Li}_2\text{O}$ , whose bond strengths are below 60 kcal/g.atom occupy random positions distributed through the structure and are located to provide local charge neutrality; and (3) intermediates, such as  $\text{Al}_2\text{O}_3$ , whose bond strengths are between 60 and 80 kcal/g.atom may contribute in part to the network structure. The values of the bond strength or dissociation energy indicate the hierarchy of energy required to break various bonds in the glass network.

In reference to the three major cations in alkali borosilicate nuclear waste glasses,  $\text{Si}^{4+}$ ,  $\text{B}^{3+}$  and  $\text{Na}^+$ , note that since Na ions are modifiers they are mobile in the glass structure and can be released through an ion-exchange process in an aqueous solution, as described by the following equation:

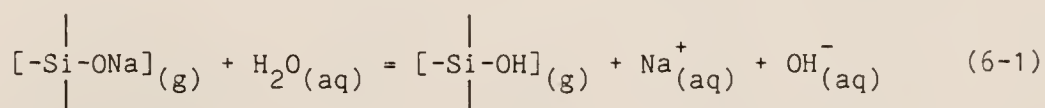


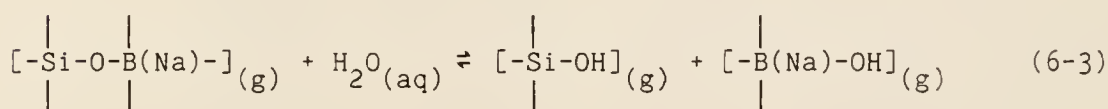
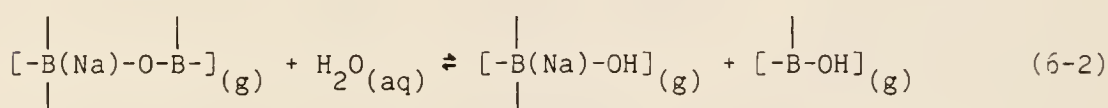
Table 6-3. Coordination Number and Bond Strength of Most Oxides in Alkali Borosilicate Nuclear Waste Glasses.

	M in MO <sub>x</sub>	Valence	Dissociation Energy per MO <sub>x</sub> (kcal/g·atom)	Coordi- nation Number	Single-Bond Strength (kcal/g·atom)
Glass formers	B	3	356	4	89
	B	3	356	3	119
	Si	4	424	4	106
	Al	3	402-317	4	101-79
	Zr	4	485	6	81
Intermediates	Al	3	317-402	6	53-67
	Zr	4	485	8	61
	Ti	4	435	6	73
Modifiers	Li	1	144	4	36
	Na	1	120	6	20
	K	1	115	9	13
	Cs	1	114	12	10
	Mg	2	222	6	37
	Ca	2	257	8	32
	Sr	2	256	8	32
	La	3	406	7	58

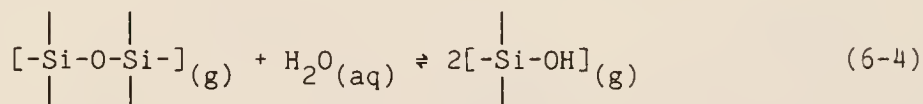
Adapted from [85]:

As a result, the solution will have a concomitant increase in pH. An introduction of a modifier oxide such as  $\text{Na}_2\text{O}$  reduces glass melting temperature, but increases the number of nonbridging oxygen bonds in the glass structure and reduces chemical durability.

Removal of B should involve breaking 3 or 4 bridging oxygen bonds associated with  $[\text{BO}_3]^{3-}$  or  $[\text{BO}_4]^{5-}$  units. The following equations represent breaking one bridging oxygen bond associated with the B structural units.



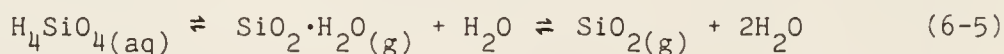
Since the dissociation energy of  $\text{SiO}_2$  (424 kcal/g·atom) is larger than that of  $\text{B}_2\text{O}_3$  (356 kcal/g·atom), release of Si is energetically less favorable. Breaking of Si-O bonds can be represented by



This is one of the reasons why all the data shown in Chapter V indicate preferential leaching of boron.

The second reason for preferential leaching of boron is the large difference in stability between boria and silica in aqueous

solutions. As pointed out by Paul and Cooke [86] and shown in Fig. 6-6, the activity of  $B_2O_3$  is several orders of magnitude larger than that of vitreous  $SiO_2$ . Thus, it is unlikely that  $B_2O_3$  reaches its solubility limit. Although it has been reported that several boron-containing silicate phases were identified on the altered glass surface, these phases were shown to be artifacts of the hydrothermal experimental method in which the leachates were allowed to evaporate in contact with the altered glass [87]. On the other hand, the silicic acid dissolved from the glass may reach saturation and precipitate to form  $SiO_2$ , as described in the equation below.



It should be mentioned that the  $SiO_2$  formed through the condensation reaction (equation (6-5)) is different from the  $SiO_2$  in the original glass, but it is still amorphous for glasses leached at temperatures not higher than 90°C and at 1 atmosphere as revealed by x-ray diffraction. The existence of strong ionic-covalent bridging oxygen bonds, especially Si-O-Si bonds, is most likely responsible for the low leachability of many nuclear waste glasses over a pH range from 4.5-9.5.

Selective dissolution of glass network formers plays an important role in glass leaching. Preferential dissolution of boron-containing units and preservation of the  $SiO_2$  network result in an altered glass surface rich in  $SiO_2$ . Such a layer may serve as a



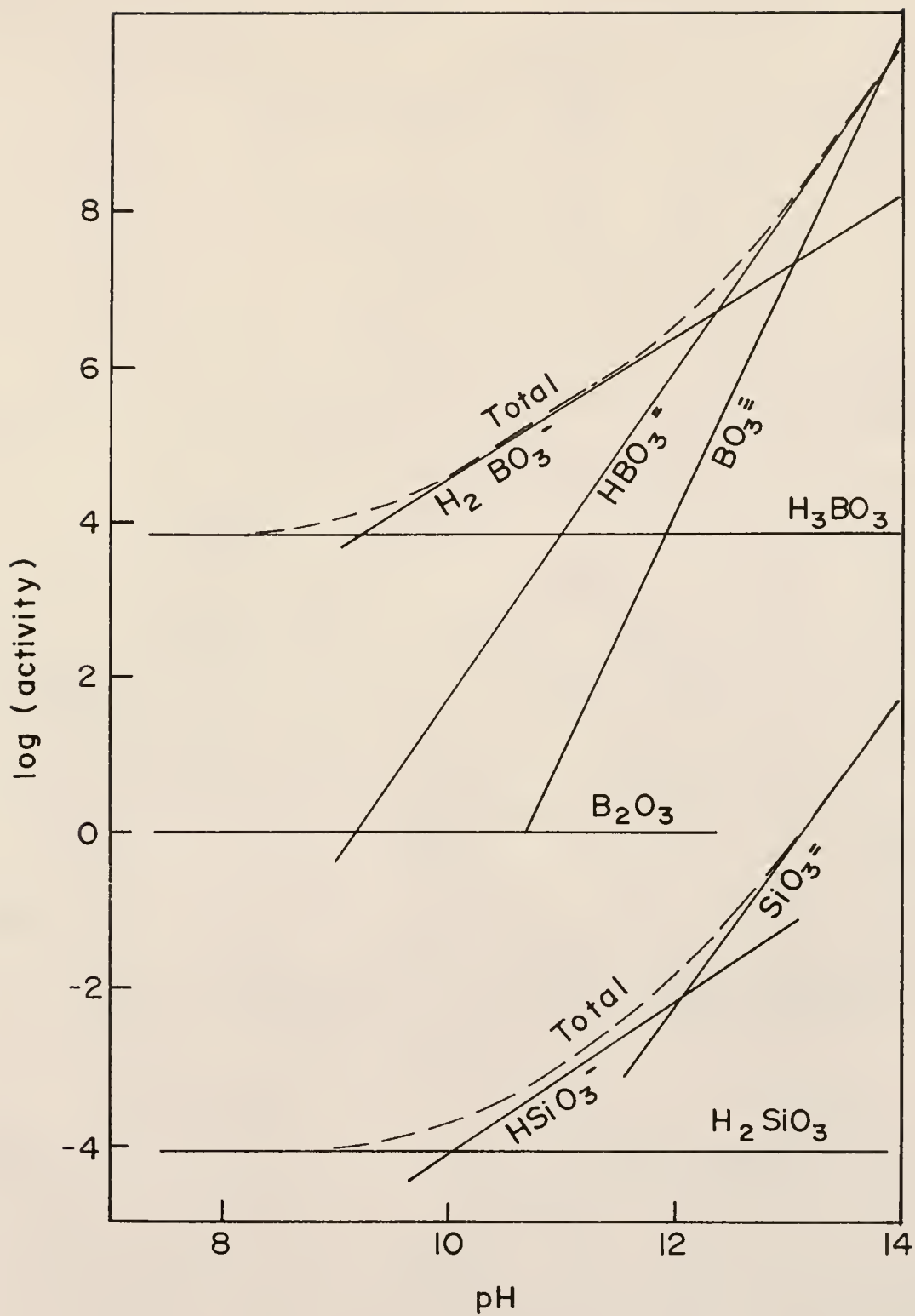


Fig. 6-6. Stability of  $B_2O_3$  and  $SiO_2$  in aqueous solution at 25°C as a function of pH (adapted from [86]).

barrier to reduce the release of other species including  $B_2O_3$  from the glass. Release of  $B_2O_3$  does not necessarily increase OH concentration as does that of  $Na_2O$  (compare equations 6-1 and 6-2). The solubility of silica is low in a solution of low pH.

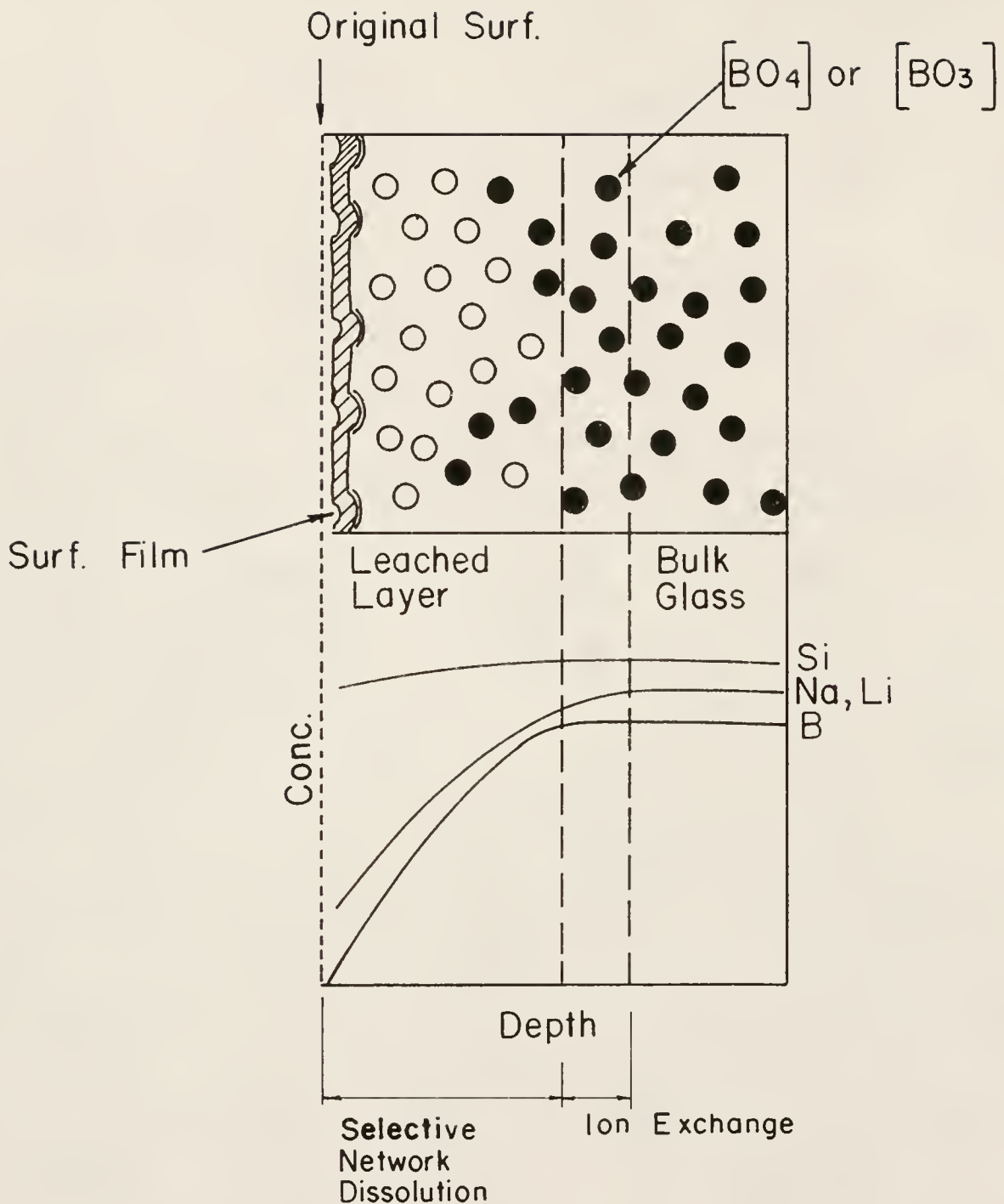
All of the alkali ions are not released through an ion exchange process. When the exchange site is  $Si-O-Na^+$ , the thermodynamics of the exchange reaction are favorable due to the high strength of the OH bond which forms. However, Na contained in  $[B(Na)O_4]^{4-}$  sites will not take part in ion exchange process since the negative charge on this site is associated with the tetrahedron rather than a particular oxygen, and unpolarizable cations such as  $H^+$  cannot effectively compensate for this charge as well as can the  $Na^+$  [88]. The thermodynamics do not favor  $H^+-Na^+$  exchange at these sites. Thus, extraction of Na from  $[B(Na)O_4]^{4-}$  sites can only occur through the release of the whole units.

Some metal ions originally contained in the ground water or released from the glass may absorb onto the glass surface and be concentrated within the altered layer. They change the solubility of silica by forming less soluble metal silicates. A good example of such metal ions is  $Al^{3+}$ . It was found that, in most cases, Al is one of the least mobile species in the glass (see the Al profile in Fig. 4-17). Aluminum ions can absorb onto the hydrated silica surface to form anionic aluminosilicate. The absorbed sites can be either on the outer surface or within the altered layer. This results in drastic reduction of the dissolution rate as well as the equilibrium solubility of the altered glass [77].

Breaking of the structural units in alkali borosilicate nuclear waste glass results in dissociation of all other species dissolved in it and linked together with less strong bonds. Then, based on the solubility limits of metal ions in aqueous solution, multiple surface layers of less soluble elements form. The onset of surface precipitation depends on the time required for various species to reach saturation in solution with respect to the surface complex. Saturation of species "i" will be a function of the initial pH, amount of alkali in the glass and rate of alkali release, temperature, initial concentration of species "i" in the solution, SA/V which influences solution concentration and flow rate which also affects solution concentration.

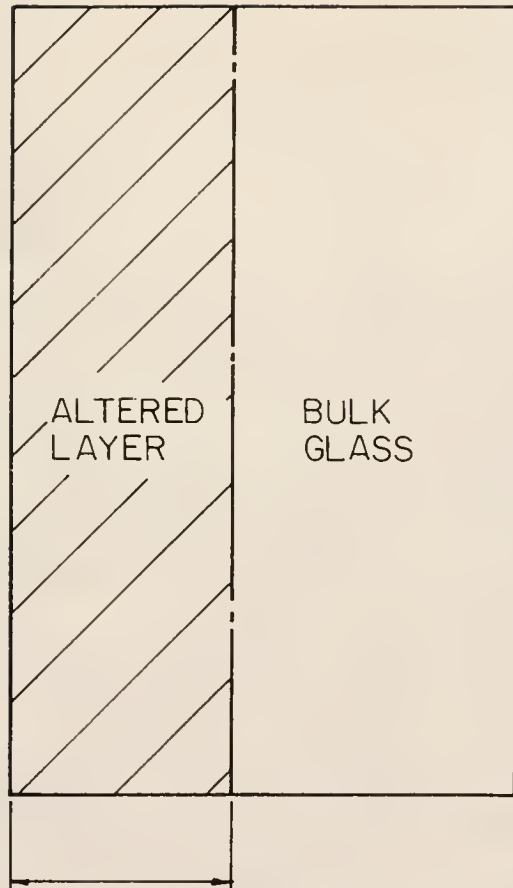
In summary the proposed model of alkali borosilicate glass leaching is based on the chemical bonding of various M-O connections and the stability of their individual oxides in aqueous solution.

Figure 6-7 (a), a schematic of this model, shows a cross-section of the altered glass surface and typical compositional profiles observed for Si, B and alkalis. It is postulated that most  $\text{SiO}_2$  in the leached layer should be embodied within an unbroken three-dimensional network. The two major network former ions, Si and B, are released at different rates, and preferential leaching of boron is obvious. The  $[\text{SiO}_4]^{4-}$  units preserved in the glass surface can hold other species contained therein, keeping them from release into solution. At the glass-water interface, boron depletion is almost complete. Leaching of alkali borosilicate glass is characterized by this selective dissolution of network formers. Preferential



(a)

Fig. 6-7. Schematics showing (a) the altered alkali borosilicate glass surface and the compositional profiles after leaching based on the model proposed in this dissertation and (b) the altered glass surface based on Grambow's model.



Complete network dissolution  
with precipitation.

(b)

Fig. 6-7--continued.

leaching of boron and preservation of the  $\text{SiO}_2$ -rich skeleton result in a honeycomb structure (in micron range) where glass density drops. The least soluble species entering solution after breaking down the Si- and B-containing units will form precipitation layers either on the outer surface or within the leached layer. The larger depletion depth of alkalis compared with that of boron is due to an ion-exchange reaction. However, high concentration of alkalis in solution may suppress the ion-exchange reactions.

As mentioned in Chapter II, Grambow proposed a model of glass leaching based on the role of metal ion solubilities. Grambow's model became the theoretical basis for understanding the surface film formation at the nuclear waste glass surface. However, Grambow did not address selective network dissolution for the borosilicate glass. In his model all the network former ions, Si and B are released at the same rate. Thus, the ratio of the normalized mass loss of B to that of Si is equal to 1 (Fig. 2-4). Current data indicate that this is not always the case. In contrast, preferential network dissolution of B is the common feature observed in static and flow leach tests. If Grambow's idea was correct, the curves shown in Fig. 5-35 should be overlapped on each other. In contradiction to the Grambow's model, the normalized leach rate of B is larger than that of Si. However, the model given in this dissertation can explain the nature of selective dissolution of the network formers quite well.

Secondly, Grambow's model assumes that all the constituents in the glass must totally dissolve into solution. This means that, in

the leaching history, the formation of the altered layer required that the glass must dissolve congruently at least once. When congruent dissolution raises solution concentration of certain elements to the level at which new solid phase form, these phases will regulate the solution concentration. Grambow's model is schematically shown in Fig. 6-7 (b). The surface films form due to precipitation only after complete network dissolution.

Figure 6-8 shows the density at the altered layer as a function of depth for the three SRL glasses after 2-year burial in Stripa at 90°C (glass/glass interface). The decrease in density is basically due to leaching of Na, Li and B. The structure of the altered layer appears more open than that of the bulk glass and contains micropores. The density drop is, therefore, directly related to the release of  $\text{Na}_2\text{O}$ ,  $\text{Li}_2\text{O}$  and  $\text{B}_2\text{O}_3$  in the glass. The number and size of these micropores may change with depth and also depend on the composition of glass and solution. The durable glasses produce a thin coherent dense surface layer which can protect the glass more effectively from further leaching. Precipitates of less soluble species on the glass surface regulates the density. This behavior is shown in Fig. 6-8 by the local increase in the density at  $\sim 0.3 \mu\text{m}$  depth of the SRL 131 + 29.8% TDS glass specimen.

#### Effect of Glass Composition

Figure 6-9 is the compositional ternary diagram showing six alkali borosilicate nuclear waste glass compositions. Three regions can be identified. These range from low leaching systems



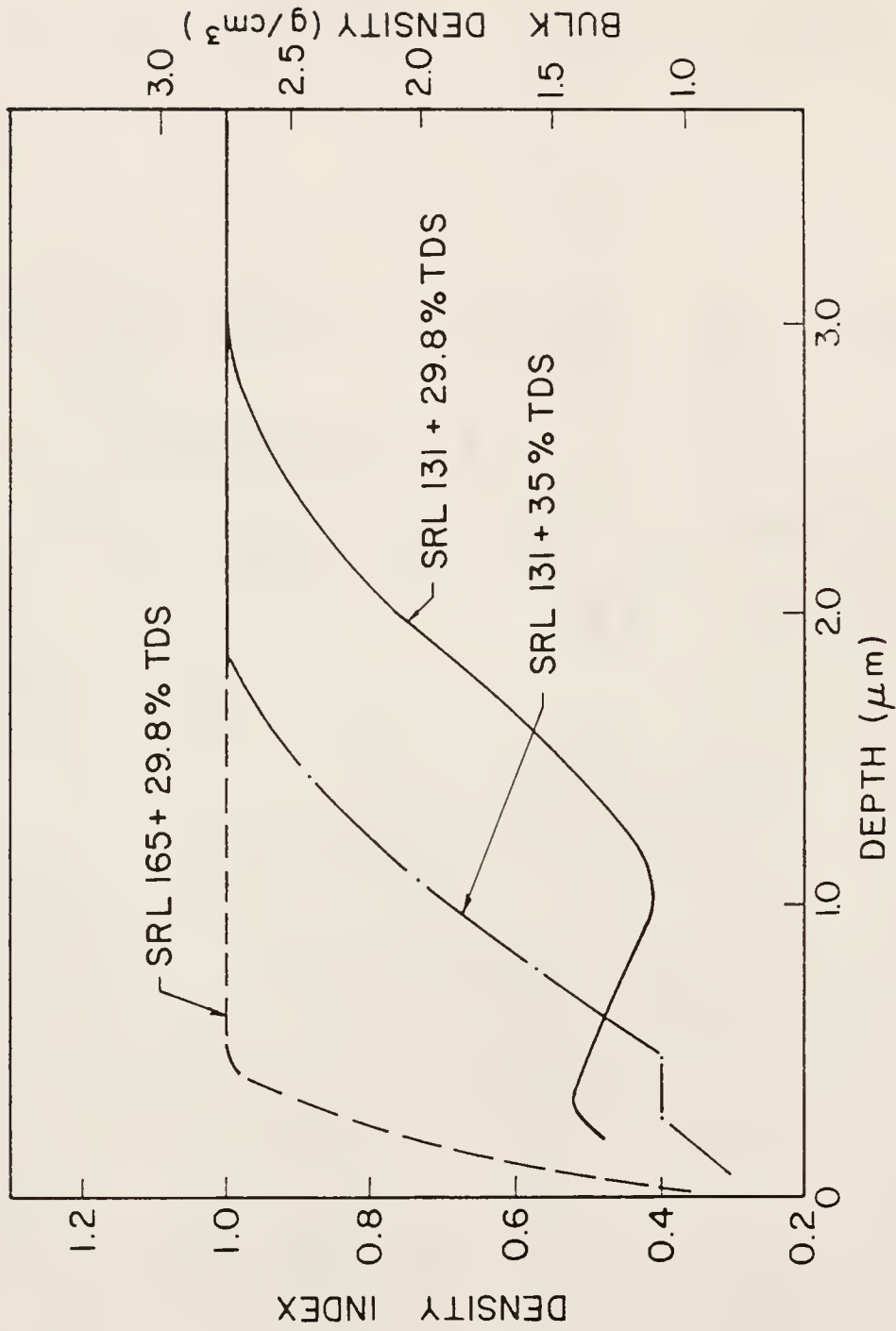
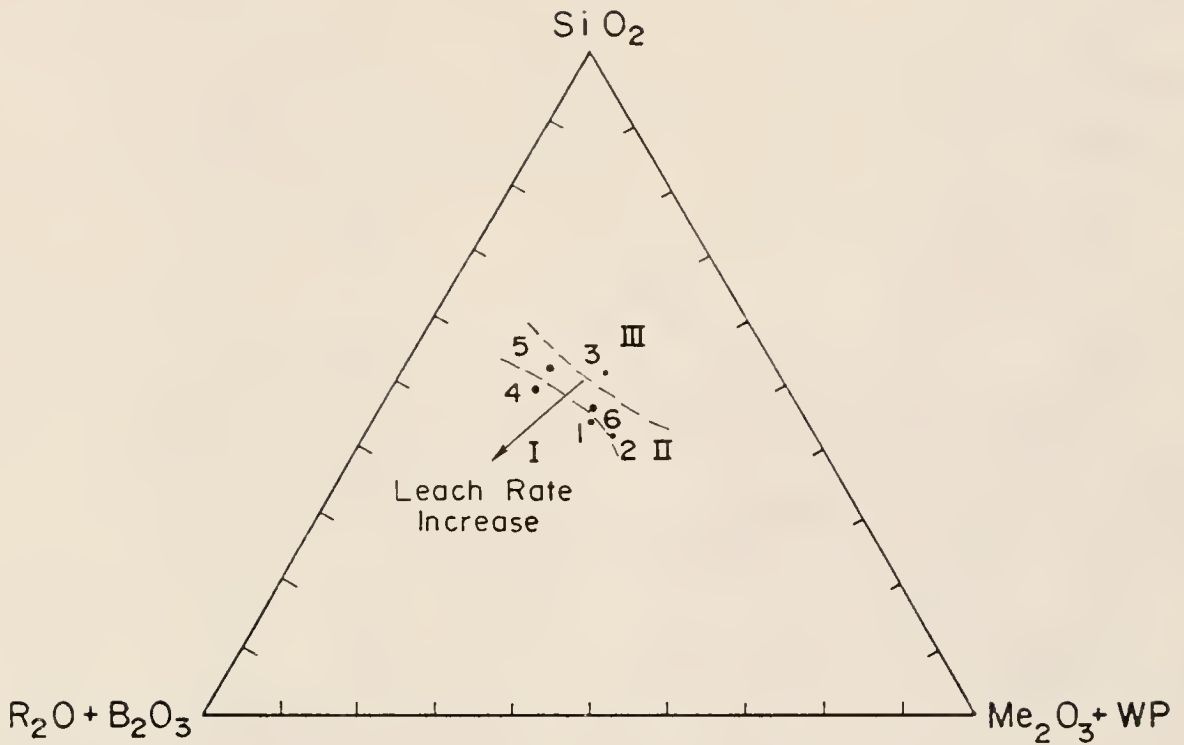


Fig. 6-8. The density index curve for three SRL glasses after 2-year burial in Stripa at 90°C.



- 1 - SRL 131 + 29.8 % TDS
- 2 - SRL 131 + 35 % TDS
- 3 - SRL 165 + 29.8% TDS
- 4 - ABS 39
- 5 - ABS 41
- 6 - ABS 118

Fig. 6-9. Compositional ternary diagram showing the direction of increasing boron depletion depth.  $\text{R}_2\text{O}$  represents alkali metal oxide,  $\text{Me}_2\text{O}_3$  represents  $\text{Al}_2\text{O}_3$  and  $\text{Fe}_2\text{O}_3$  and WP stands for waste products.

(-0.4  $\mu\text{m}/\text{year}$ ) to intermediate leaching (1-1.2  $\mu\text{m}/\text{year}$ ) to high leaching systems (2.5-3  $\mu\text{m}/\text{year}$ ), based on the boron depletion depths of the glass/glass interface for the 1-year burial samples. The leaching data were correlated with the  $(\text{SiO}_2 + \text{Al}_2\text{O}_3)/(\text{R}_2\text{O} + \text{B}_2\text{O}_3)$  wt% ratio, where  $\text{R}_2\text{O}$  stands for alkali oxides. Since preferential leaching of  $\text{R}_2\text{O}$  and  $\text{B}_2\text{O}_3$  are observed with all glass compositions and all glass/repository materials interfaces as addressed in the model, a sum of  $\text{R}_2\text{O} + \text{B}_2\text{O}_3$  is used as the denominator in the ratio. Figure 6-10 is a plot showing the boron depletion depth as a function of  $(\text{SiO}_2 + \text{Al}_2\text{O}_3)/(\text{R}_2\text{O} + \text{B}_2\text{O}_3)$  wt ratio for these glasses. It was found that leach resistance increased as this ratio increased. SRL 165 + 29.8% TDS exhibited the smallest leach depth of boron among the six waste glasses. This is not surprising since this glass composition is nearest to the  $\text{SiO}_2 - (\text{Me}_2\text{O}_3 + \text{WP})$  edge where  $\text{Me}_2\text{O}_3$  stands for  $\text{Al}_2\text{O}_3$  and  $\text{Fe}_2\text{O}_3$ , and WP, the waste products, and contains the least amount of alkali and boron with the highest  $(\text{SiO}_2 + \text{Al}_2\text{O}_3)/(\text{R}_2\text{O} + \text{B}_2\text{O}_3)$  ratio of 2.44 (see Fig. 6-10).

Glass ABS 41 is a good example to show how well the proposed model explains the leach data. Although this glass contains nearly the same amount of  $\text{SiO}_2$  and  $\text{Al}_2\text{O}_3$  (54.5%) as SRL 165 + 29.8% TDS (54.6%) and less  $\text{Na}_2\text{O} + \text{Li}_2\text{O}$ , the doubled content of  $\text{B}_2\text{O}_3$  (15.90% in ABS 41 vs 7.1% in SRL 165 + 29.8% TDS) is primarily responsible for the doubled leach rate of ABS 41 as compared to SRL 165 + 29.8% TDS. Based on Grambow's model, since these two glasses contain

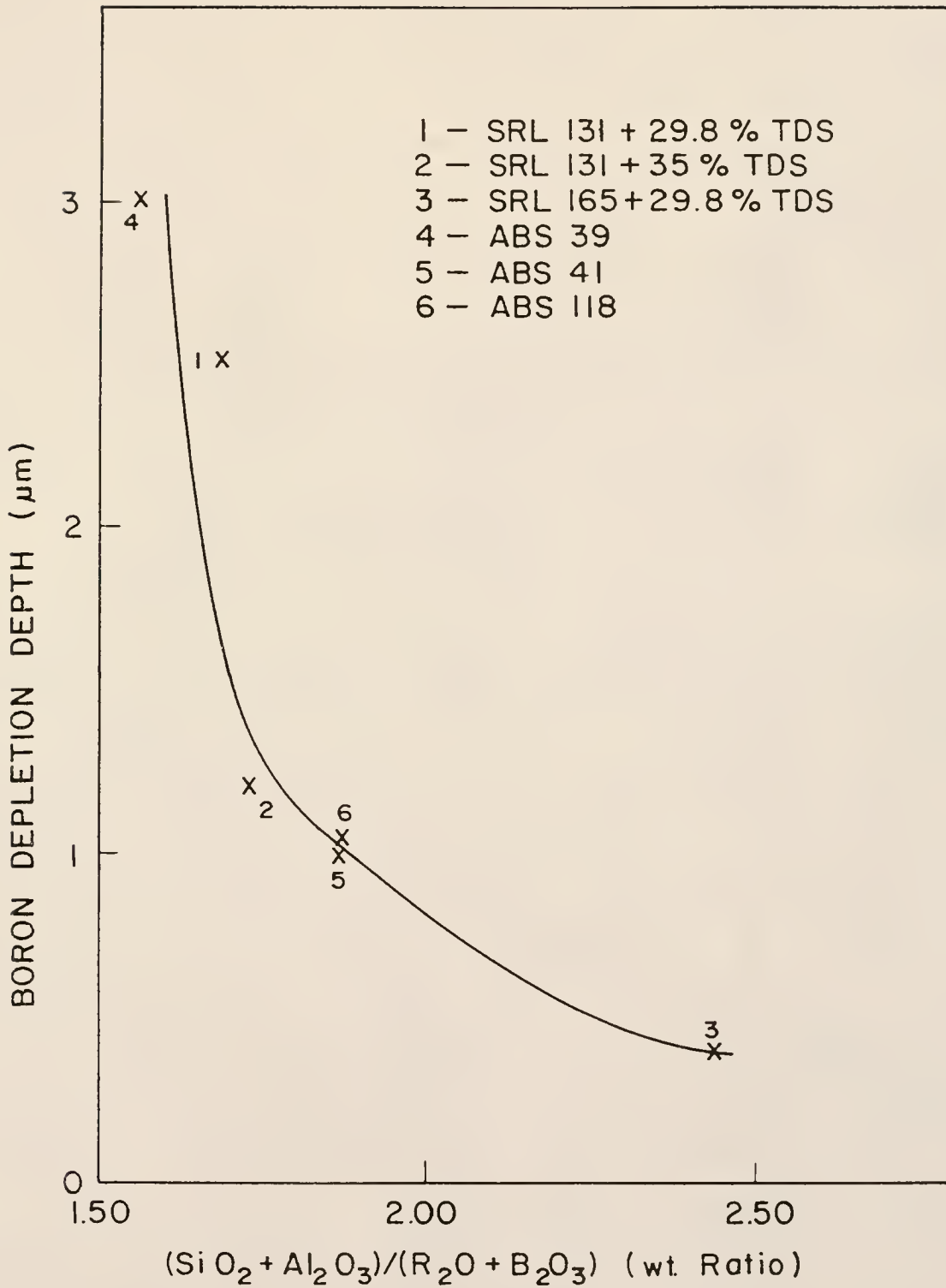


Fig. 6-10. The boron depletion depth as a function of  $(\text{SiO}_2 + \text{Al}_2\text{O}_3)/(\text{R}_2\text{O} + \text{B}_2\text{O}_3)$  wt ratio in glasses.

nearly the same amount of  $\text{SiO}_2 + \text{Al}_2\text{O}_3$ , their leach rates should be the same.

Among the six glass compositions investigated, the least durable glass was ABS 39 with the lowest  $(\text{SiO}_2 + \text{Al}_2\text{O}_3)/(\text{R}_2\text{O} + \text{B}_2\text{O}_3)$  ratio of 1.57 and the highest amount of  $\text{B}_2\text{O}_3$  (19.12%). Also, this glass contains <1%  $\text{Cs}_2\text{O}$  and no  $\text{Li}_2\text{O}$ . Therefore, a mixed alkali effect [78,80], if present, was not significant. The second least durable was SRL 131 + 29.8% TDS with a  $(\text{SiO}_2 + \text{Al}_2\text{O}_3)/(\text{R}_2\text{O} + \text{B}_2\text{O}_3)$  ratio of 1.52 (Fig. 6-10). This SRL glass contains the highest amount of  $(\text{Na}_2\text{O} + \text{Li}_2\text{O} + \text{Cs}_2\text{O})$  and second least amount of  $(\text{SiO}_2 + \text{Al}_2\text{O}_3)$ . The other two compositions, SRL 131 + 35% TDS and ABS 118, are categorized in the intermediate leaching systems together with ABS 41. Glasses ABS 118 and ABS 41 have the same  $(\text{SiO}_2 + \text{Al}_2\text{O}_3)/(\text{R}_2\text{O} + \text{B}_2\text{O}_3)$  ratio (1.87). However, ABS 41 contains 4.1% more  $(\text{SiO}_2 + \text{Al}_2\text{O}_3)$  and 2.2% more alkalis and  $\text{B}_2\text{O}_3$  as compared to ABS 118. As shown in the compositional ternary diagram (Fig. 6-9), ABS 41 is closer to the  $\text{SiO}_2 - (\text{R}_2\text{O} + \text{B}_2\text{O}_3)$  edge and slightly closer to the  $\text{R}_2\text{O} + \text{B}_2\text{O}_3$  corner than ABS 118. An improved durability of SRL 131 + 35% TDS was due to the higher waste loading, although this glass has the second lowest  $(\text{SiO}_2 + \text{Al}_2\text{O}_3)/(\text{R}_2\text{O} + \text{B}_2\text{O}_3)$  ratio (1.69). One of the major factors responsible for this improved durability is that the simulated SRP nuclear wastes consist primarily of  $\text{Fe}_2\text{O}_3$ ,  $\text{MnO}$  and  $\text{Al}_2\text{O}_3$  which have low elemental leachability. This is because these species decrease the solubility of silica in the solution by forming a coherent surface layer of less soluble metal silicates on the glass

surface [77]. Thus, in a well preserved  $\text{SiO}_2$  network, preferential leaching of boron will be more difficult. The second factor is due to the higher waste loading which lowers the absolute concentration of  $\text{B}_2\text{O}_3$  and increases the average distance between two nearest boron-containing units in the glass structure.

### Influence of Repository Variables

#### Ground Water Chemistry

Laboratory experiments (Fig. 5-30) have shown that the extent of surface deterioration is less in ground water than in deionized water and that water which already contains large concentrations of glass species is less aggressive than regular ground water or deionized water. Results also show that the major factor contributing to the reduction in leaching was the presence of Si in solution (Fig. 5-30).

As shown in equation (6-4), an increase in Si concentration will suppress the reaction in the right direction. As a result, the rate of Si dissolution will be lower in Stripa water containing 13 ppm of Si than in deionized water. This effect is illustrated schematically in Fig. 6-11 where the concentration vs time curve is shown. The leach rate of silica from the glass can be represented by the slope of the curve. The greatest slope, and hence the largest leach rate, occurs when the concentration of silica in solution is equal to zero. In a static leach test, the leach products accumulate in solution and eventually approach saturation. The leach rate of silica decreases as its solution concentration increases. When the

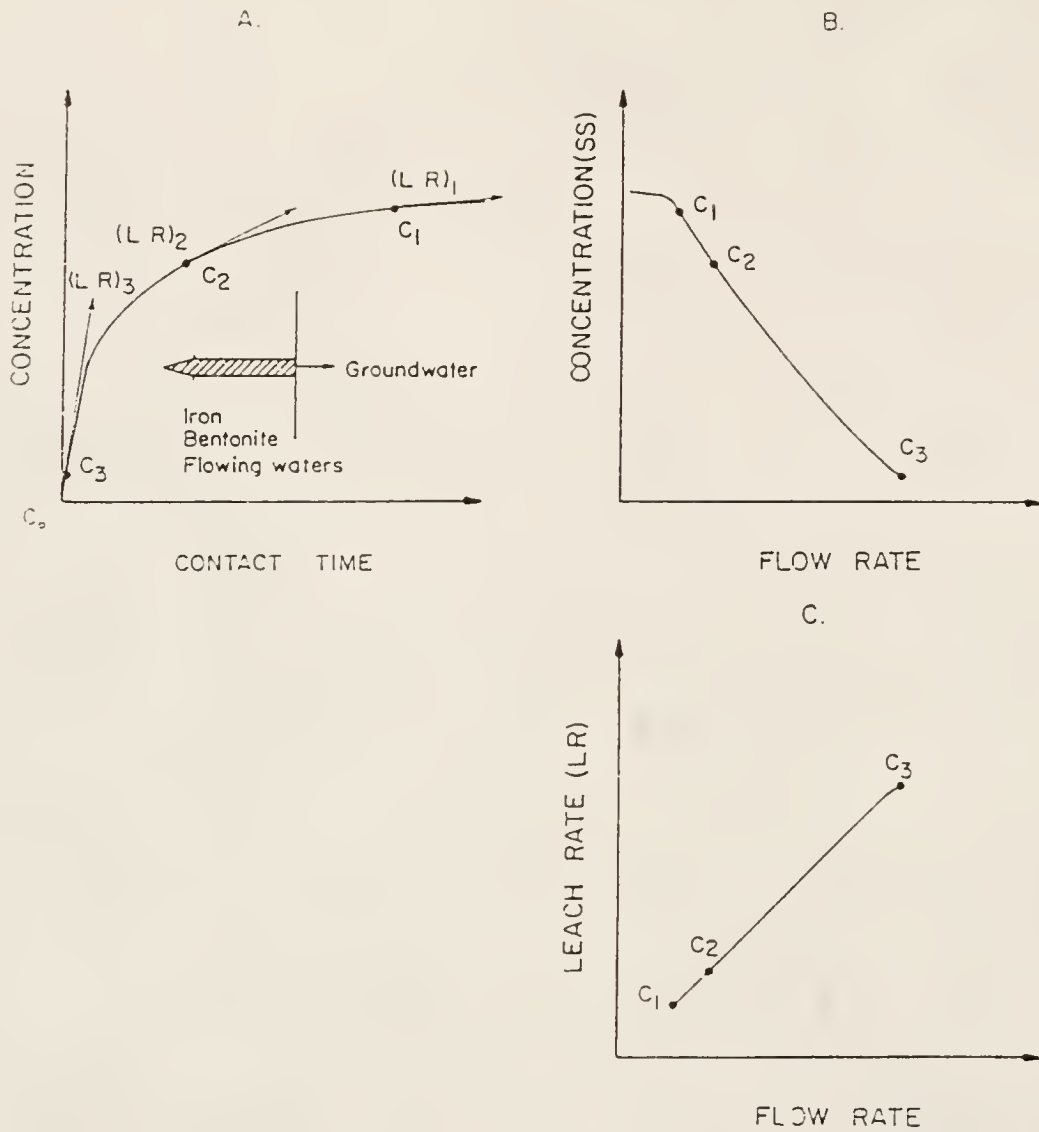


Fig. 6-11. Schematic illustrating the relationship between concentration, contact time, and leach rate (adapted from [36]).



solution becomes saturated with respect to silica, its leach rate, as measured by its change in solution concentration, will be zero.

Based on this explanation, it can be seen from Fig. 6-11 that the leach rate of silica in deionized water, where its initial concentration is zero ( $C_3$ ), will be greater than the leach rate of the same element in a leachant with an initial concentration equal to  $C_2$  or  $C_1$ . Of course, each element has a different saturation concentration, but since silica is the major structural component of the glass a reduction in its dissolution will result in concomitant reduction in dissolution of the other glass constituents.

It should be pointed out that the rate of B release depends to a large extent on the rate of  $\text{SiO}_2$  dissolution. This is due to the fact that in the glass structure,  $[\text{SiO}_4]^{4-}$ ,  $[\text{BO}_4]^{5-}$  and  $[\text{BO}_3]^{3-}$  are connected through bridging oxygen bonds into an integral three-dimensional network. Dissolution of more  $\text{SiO}_2$  structural units results in more release of  $[\text{BO}_4]^{5-}$  and  $[\text{BO}_3]^{3-}$  units, and vice versa is also true.

Secondly, a pH buffering effect of Stripa ground water has a strong effect on waste glass leaching. Stripa ground water contains weak bases and their corresponding salts such as  $\text{Ca}(\text{OH})_2$  and  $\text{CaCl}_2$ , and  $\text{Fe}(\text{OH})_3$  and  $\text{FeCl}_3$  (see Table 4-7). The  $\text{OH}^-$  ions produced as a result of alkali release from the glass can react with Ca and Fe to form corresponding bases. Therefore, during the burial tests, the ground water pH was found to increase by only 1 unit. The laboratory simulations using granite rock cups and Stripa water in both static and flow conditions (at  $<0.3$  mL/h) also show that the ground water pH

varied between 7.3 and 8.4 (Fig. 5-32). In contrast, the pH of leachant in the MCC-1 static test using deionized water reaches 9.54 after 28 days and 9.41 after 1 year [27].

Stripa ground water contains some monovalent cations such as Na and K. The existence of these monovalent cations in solution can reduce the solution pH by ion-exchange with the glass surface silanol protons [89]. The data of Shade et al. [90] show that hydrolysis of glass matrix was generally slower in brines than in deionized water, due to a lower solubility of silica at lower pH in brines. Thus, in Stripa ground water,  $\text{SiO}_2$  dissolution rate is expected to be low except in cases where the glass is highly rich in alkalis.

#### Effects of Repository Materials

Early results of the Stripa burial experiments [61,83] have shown that the presence of bentonite resulted in an accelerated attack on glasses within 1-year burial at 90°C. Recent data collected from this experiment indicate that bentonite has less effect on long-term glass leaching. This trend is best shown in Fig. 6-1 (a). When it was in contact with bentonite during burial, ABS 39 leached at a high rate during the first 3 months, then slowed dramatically and kept the same low leach rate through the 31st month.

There are several reasons which could account for more severe attack on the glass surface exposed to bentonite during an earlier period of burial:

(1) Experimental data show that the pH of bentonite-containing ground water is 0.5-1.4 units higher than without bentonite. Thus,

higher steady state concentrations of  $\text{SiO}_2$  would be expected in the presence of bentonite compared to water alone. The early surface roughening as shown by low intensity of the FT-IRRS spectra (Fig. 5-7) is indicative of an accelerated dissolution of  $\text{SiO}_2$  due to the quick rise of pH in the bentonite containing ground water. The characteristics of selective network dissolution is less apparent.

(2) Enhanced ion exchange reactions existed between glass surfaces and bentonite. Bentonite provides a solution saturated in soluble Ca-Mg, Fe, Al, etc. and a high base exchange capacity for Na [19]. As shown in Fig. 6-4, Na, Li and Cs leached up to 1-1.3  $\mu\text{m}$  deep into the surface with the Ca concentration build-up to nearly the same depth. The depletion of the alkalis is in contrast with the case of glass/glass interface (Fig. 5-23) considerably deeper than that of B.

The time-dependency of the leach depth based on boron extraction for ABS 118 glass/Pb, glass/Cu, glass/Ti, glass/glass and glass/granite interfaces after 90°C Stripa burial is compared in Fig. 6-12. Generally, very low leachability ( $\leq 3.48 \mu\text{m}/\text{yr}$ ) was found on all these glass surfaces after 12-month, 90°C Stripa burial. It is seen that glass which was in contact with Pb exhibits the smallest leach rate among the five glass interfaces. Thus after ~300 years of the thermal storage period, glass which is in contact with Ti will leach to ~1,000  $\mu\text{m}$  depth while glass in contact with Pb will leach only 40  $\mu\text{m}$ . As shown in Table 6-4, the glass/Ti interface leached by a factor of 7 faster, while both glass/Pb and glass/Cu interfaces corroded by a factor of 4 slower than the glass/glass between 7-12

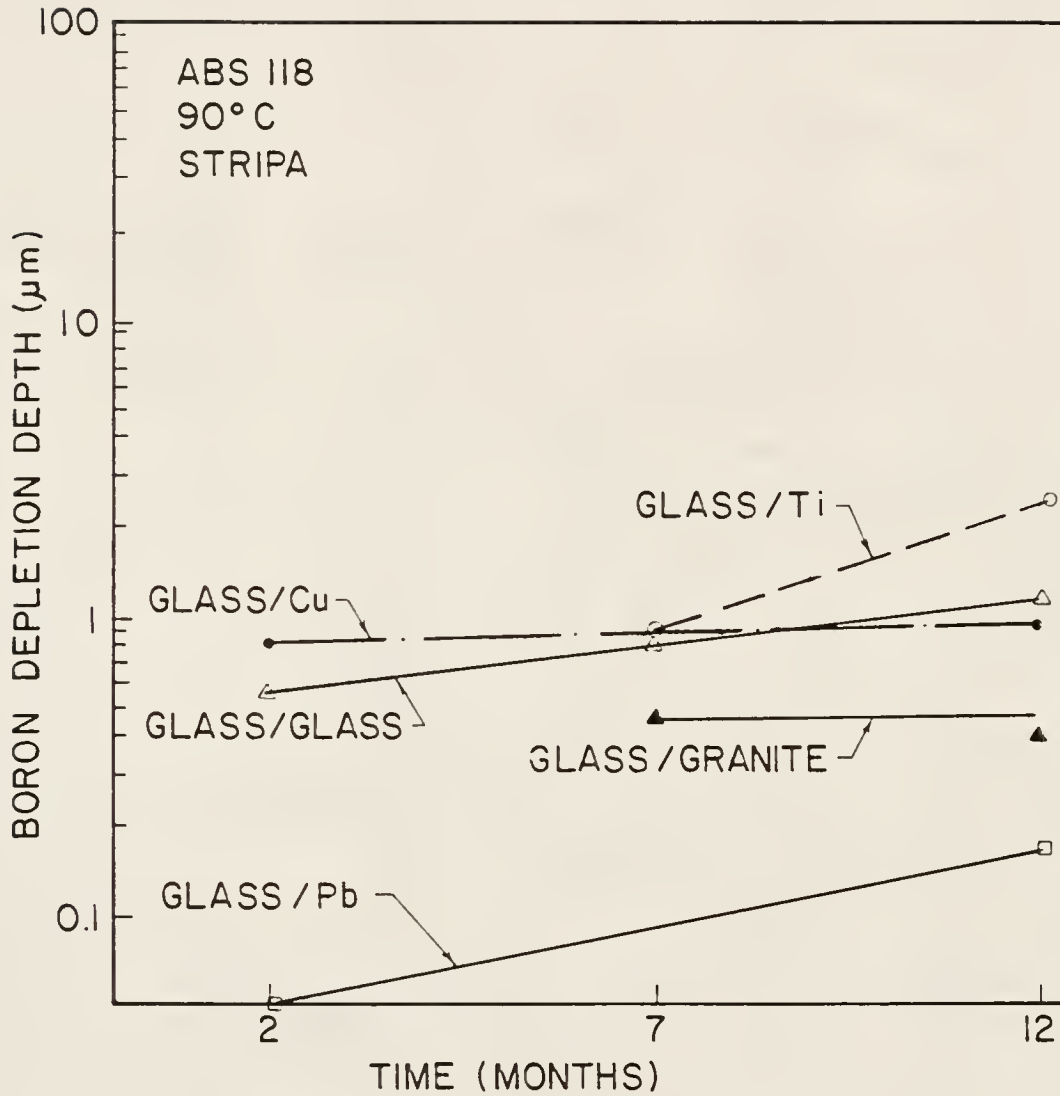


Fig. 6-12. The boron depletion depth as a function of burial time for ABS 118 glass/glass, glass/granite, glass/Pb, glass/Cu and glass/Ti interfaces after 90°C Stripa burial.

Table 6-4. 90°C ABS Glass Leach Rates During 7-12 Months Period.

Interface	Glass/Glass	Glass/Pb	Glass/Cu	Glass/Ti
Leach rate ( $\mu\text{m}/\text{yr}$ )	0.48	0.12	0.12	3.48

months of burial. The leach depths after 12-month 90°C Stripa burial are (in increasing order) glass/Pb < glass/granite < glass/Cu < glass/glass < glass/Ti.

One of the factors which may be responsible for the different leach depths with different glass/overpack metal interfaces is the difference in the tightness of the contact between the glass and various metal surfaces. Since the compacted bentonite which was used as the backfill material in the Stripa burial experiment absorbed ground water and swelled, high pressure was produced within the boreholes. The flexibility of some overpack metals such as Pb permits the metals to press tightly against the contacted glass surface under such high pressure and thus the ground water in the gaps between glass surfaces and metals was severely limited. Another possible reason why the presence of Pb may reduce glass leaching is that Pb dissolved from the metal coupon can adsorb onto the glass surface and form less-soluble lead silicate [77]. Thus, the amount of  $\text{SiO}_2$  which needs to be dissolved from the glass decreases.

As shown by the SIMS analysis (Fig. 5-16), there was no  $\text{SiO}_2$  network dissolution observed at the three glass interfaces. An apparent decrease in the Si concentration was found only at the  $<0.2 \mu\text{m}$  leached layer of the glass/Pb. This may possibly be an artifact of the SIMS data processing due to smudges of metallic Pb on the specimen surface. Considerable amounts of Na and B still remain unleached at this  $<0.2 \mu\text{m}$  surface region indicating very little surface attack.

### Effect of Temperature

Temperature influenced glass leaching significantly during burial. As regards the low temperature (8-10°C) leaching characteristics, the B depletion curves based on SIMS analysis (Fig. 6-3) indicate that the depth of the SRL 131 + 29.8% TDS glass/glass interface is approximately one order of magnitude less at 8-10°C than it is at 90°C and that the qualitative differences in B depletion depths between the three SRL glasses are very small. The SIMS data (Fig. 6-13) also shows little evidence of ion exchange at ambient temperature as revealed by the H profile. Thus, it appears that at 8-10°C, network dissolution is the predominant leach mechanism for this nuclear waste glass composition. This argument is in contradiction to that proposed by Zagar and Schillmoeller [91] which states that at temperatures below 30°C ion exchange is predominant.

### Comparison of Field and Laboratory Test Results

In order to approximate the Stripa burial conditions laboratory tests were conducted using Stripa ground water, granite rock cups and higher SA/V ratios. Results show that the Stripa repository conditions could be approximated in the laboratory using  $SA/V \geq 1.0 \text{ cm}^{-1}$  and static or low flow ( $\leq 0.1 \text{ mL/h}$ ) conditions. An increase in the flow rates from 0.1 to 0.3 mL/h resulted in a 6X increase in the leach rates based on the mass loss data shown in Fig. 5-34. The SA/V ratio in the Stripa burial test at glass/glass interfaces was probably  $>5 \text{ cm}^{-1}$  depending upon the ground water accessibility and the extent of bentonite intrusion.



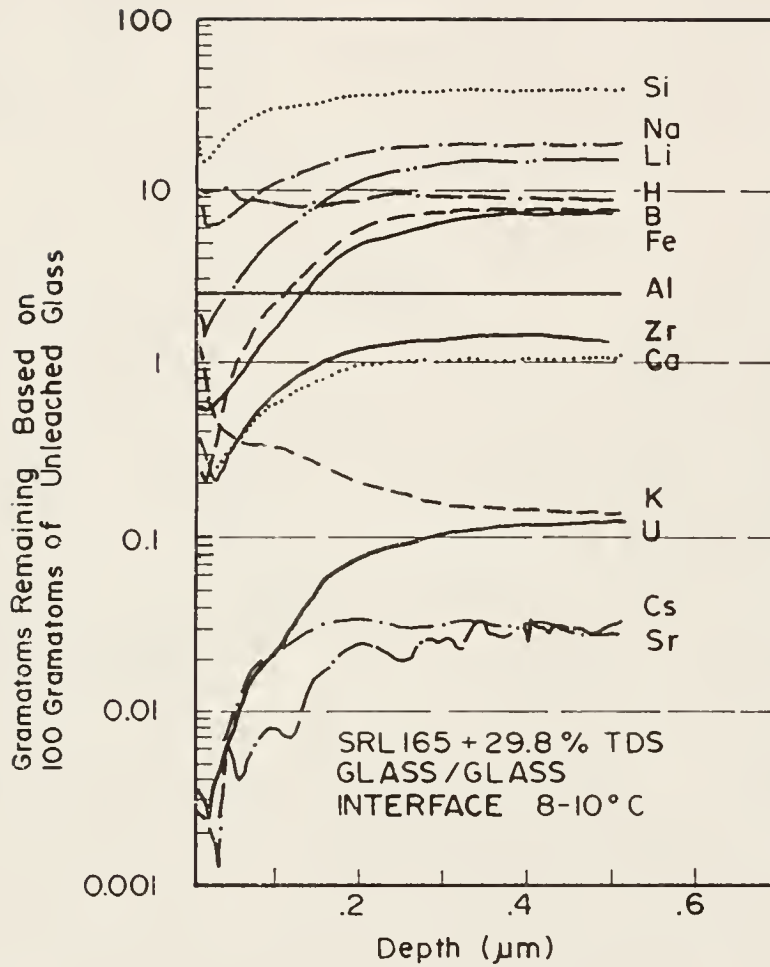


Fig. 6-13. SIMS compositional profiles of SRL 165 + 29.8% TDS glass/glass interface after 8-10°C Stripa burial for 2 years.

The SIMS depth profiles shown in Fig. 5-23 (b) for SRL 165 + 29.9% TDS glass buried for 2 years in Stripa at 90°C, and Figs. 5-31 and 5-37 for the similar glass leached statically in the laboratory in ground water with  $SA/V = 1.0 \text{ cm}^{-1}$ , suggest that the glass leached through similar corrosion mechanisms in the field as in the laboratory. These profiles indicate that depletion of alkalis and boron, and to a more limited extent silica, had occurred in both the laboratory- and field-leached glasses. At the outer surface, the concentrations of Na, Li, B and Si were significantly depleted with respect to the unleached glass. Within the inner region, the alkalis and boron had been leached to a greater extent than silica, and B appears to have been leached to a lesser extent than the alkalis, such as Li. In addition, the curves for the same elements in these two cases assume nearly the same shapes, suggesting that the leach mechanisms under the field and laboratory conditions are most likely the same.

Regarding the leaching kinetics, the granite rock cup tests simulated the Stripa granite repository much better than the laboratory test in which granite cup was not used. As indicated by the boron depletion, the leach depths after 1-, 3- and 6-month leaching under the granite rock cup test conditions are 0.16, 0.24 and 0.45  $\mu\text{m}$  (Fig. 5-37). The boron depletion depth of the 1-month laboratory sample leached in absence of granite is 0.46  $\mu\text{m}$ . This indicates that glass leaches at a lower rate in an environment containing granite. It is expected that if a higher SA/V ratio is

used ( $\approx 5 \text{ cm}^{-1}$ ) in the granite rock cup test, glass leach rate will be closer to that observed in Stripa burial tests. Data from both field- and laboratory-corroded glass samples confirm very well the validity of the proposed model of glass leaching.

The weight loss of a SRL 165 burial glass slice calculated from Fig. 6-8 is approximately  $0.31 \text{ g/m}^2$ , as compared with  $0.25 \text{ g/m}^2$  (based on sample weight) for a 28-day laboratory-leached sample using ground water with  $\text{SA/V} = 1.0 \text{ cm}^{-1}$  at the same temperature.

## CHAPTER VII SUMMARY

Burial experiments with three SRL and three ABS simulated nuclear waste glasses were conducted to evaluate the resistance of these glasses to ground water attack under repository-like conditions. Glass samples were buried in the boreholes at a level of ~350 meters below the surface in the Stripa granite at either ambient mine temperature (8-10°C) or 90°C. Included in the same boreholes were potential waste package components. Two sample configurations, pineapple slices and minicans, were used. Glasses were also leached in the laboratory using the Stripa ground water and granite rock cups to simulate the Stripa repository.

The leached surfaces were characterized using SEM-EDS, FT-IRRS, SIMS, RBS and optical microscopy in combination. Solution analytical techniques were also used wherever possible.

The leaching behavior of six nuclear waste glasses including three American defense HLW glasses and three Swedish glasses containing commercial HLW in realistic repository conditions was evaluated. A leaching model for the alkali borosilicate nuclear waste glasses was proposed to elucidate the mechanisms of borosilicate glass leaching. The model is based on the considerations of the bond strengths for different oxides contained in the glass structure and stability of these oxides in aqueous

solution, which could explain the observed preferential leaching of boron and preservation of the  $\text{SiO}_2$  honeycomb network. This model is different from Grambow's model which assumes complete dissolution of all glass constituents followed by precipitation based on the solubility limits of various oxides in the glass [39].

A significant compositional effect on glass leaching was observed with the six simulated nuclear waste glasses under burial conditions. The leach rate expressed by the annual boron depletion depth was inversely correlated with  $(\text{SiO}_2 + \text{Al}_2\text{O}_3)/(\text{R}_2\text{O} + \text{B}_2\text{O}_3)$  wt ratio in these glasses which can be considered in line with either model. Glass SRL 165 + 29.8% TDS was the most durable composition among the six. An increase in waste loading of SRL 131 from 29.8% to 35% decreased its leachability by 2X. These results agree with the earlier work on the compositional dependence of nuclear waste glass leaching [92,93].

Accelerated attack during the first year in the presence of bentonite appears to be a transient effect. The time when this alleviation of the bentonite effect occurs is dependent on glass composition and may be disturbed by the local effects such as variation in the effective SA/V ratio.

Little difference in leach depths was observed between glass/glass, glass/stainless steel and glass/Cu interfaces. The glass surfaces which were in contact with granite showed smaller or larger leach depths than glass/glass interface, and heterogeneous attack was usually found on the glass/granite interface. The rock cup tests show that the presence of granite resulted in a reduction

in leach rates. The slowest leach rate was found at the glass surface which was in contact with Pb. Pb provided an intimate contact between the glass and Pb surface after bentonite swelling, resulting in a high SA/V environment and reduced leaching.

Results of the Stripa burial tests show that glass specimens containing crystallites exhibit preferential attack of the interface between crystalline and glassy phases. The crystalline phase, identified as spinel solid solution, exhibits better chemical resistance than the glassy phase. These results are consistent with the laboratory leach results [94-98]. The degradation of the leach rates of the partially devitrified glasses is due to preferred attack at the glass-crystal phase boundaries.

There is no obvious effect of sample configuration (minicams vs pineapple slices) on glass leaching since the stainless steel rings are chemically inert.

Temperature significantly influenced glass leaching during burial. Based on SIMS depth profiling, glass leaching was 3X to 10X as fast at 90°C as at 8-10°C, depending upon the glass compositions. It appears that, at low temperatures, network dissolution is the predominant leach mechanism.

Short-term laboratory static tests using ground water and high SA/V ratios ( $\geq 1.0 \text{ cm}^{-1}$ ) can approximate the Stripa burial environment. The SIMS in-depth profiles of glass surfaces after Stripa burial and laboratory simulation tests reveal that glass leached by the similar mechanisms, but more slowly under burial conditions than

under the laboratory-controlled environment. This is attributed to the difference in the SA/V, the burial glass samples being leached with SA/V  $\geq 5 \text{ cm}^{-1}$ . Surface composition and morphology are nearly identical for glasses leached under laboratory and burial conditions.

Using the slopes in the boron depletion depth vs burial time curves, the leach depths of the glasses can be extrapolated up to 300 years of storage (the thermal period) from the 90°C SIMS data and to  $10^5$  years of storage from both 90°C and 8-10°C data. Tables 7-1 and 7-2 list the results of calculations. It is shown that, except for the ABS 39 glass/glass and glass/granite interfaces and ABS 41 glass/bentonite interface, the boron depletion depths are less than 1,000  $\mu\text{m}$  after 300 years of storage assuming these glasses are exposed right after the disposal sites are closed and the stainless steel canisters are assumed to be breached right away. The estimated boron depletion depths of the three SRL nuclear waste glasses, which are in contact with glass of the same composition during  $10^5$  years of burial would be less than 10 mm (Table 7-2).

All these results show that Stripa burials combined with laboratory simulations are unique experimental designs which have provided useful information regarding leach performances of nuclear waste glasses. This work has served as a model on which design and development of the MITT tests are based. Over 1,000 samples from 8 countries are involved in WIPP tests, which is thought to be the "second generation" of the Stripa tests.



Table 7-1. Estimated Boron Depletion Depths ( $\mu\text{m}$ ) after 300 Years of the Thermal Period of Storage for the Six Nuclear Waste Glasses. It is assumed that glasses will be in contact with ground water right after the repository is closed and leach at constant 90°C. Therefore, such kind of estimation only represents the upper limits of glass leaching.

Glass Composition	Glass/Glass	Interfaces					
		Glass/ Granite	Glass/ Bentonite	Glass/ Stainless Steel	Glass/Pb	Glass/Cu	Glass/Ti
SRL 165 + 29.8% TDS	10	<20	<20	100	-	-	-
SRL 131 + 35% TDS	200	-	-	-	-	-	-
SRL 131 + 29.8% TDS	300	-	-	-	-	-	-
ABS 39	2,700	5,700	400	-	-	-	-
ABS 41	10	70	3,600	-	-	-	-
ABS 118	300	10	700	-	40	40	1,000

Table 7-2. Estimated Boron Depletion Depths ( $\mu\text{m}$ ) after  $10^5$  Years of Storage for the Glass/Glass Interfaces of SRL Simulated Nuclear Waste Glasses. It is assumed that glasses will be in contact with ground water right after the repository is closed and leach at constant  $90^\circ\text{C}$ . Therefore, such kind of estimation only represents the upper limits of glass leaching.

Glass Composition	Depth
SRL 165 + 29.8% TDS	6,300
SRL 131 + 35% TDS	8,800
SRL 131 + 29.8% TDS	9,600

## REFERENCES

1. W.R. Gilmore, ed., Radioactive Waste Disposal, Low and High Level, Noyes Data Co., Park Ridge, NJ (1977).
2. A.S. Subo and D.J. Rose, "Disposal of Nuclear Wastes," Science, 182, 1205 (1973).
3. G.K. Oertel and R.D. Walton, Jr., "Management of Defense High-Level Waste in the United States," p. 1 in Advances in Ceramics, Vol. 8, G.G. Wicks and W.A. Ross, eds., American Ceramic Society, Columbus, OH (1984).
4. M.S. Abdelhamid, P.C. Newsom and L.E. Rykken, "In Situ Characterization of the High-Level Waste Sludge at West Valley," p. 124 in Advances in Ceramics, Vol. 8, G.G. Wicks and W.A. Ross, eds., American Ceramic Society, Columbus, OH (1984).
5. L.L. Hench and B.F. Zhu, An Overview of Nuclear Waste Immobilization, University of Florida, Gainesville, FL (1984).
6. Engineered Waste Package System Design Specification, ONWI-423, Office of Nuclear Waste Isolation, Battelle Memorial Institute, Columbus, OH (1983).
7. J.F. Kircher, D.P. Moak, and D.E. Clark, Waste Package Materials Testing for a Salt Repository: 1982 Status Report, ONWI-490/UC-70, Office of Nuclear Waste Isolation, Battelle Memorial Institute, Columbus, OH (1983).
8. A Method for Product Performance Evaluation of Candidate Waste Forms for Immobilization of High-Level Radioactive Wastes, DOC/TIC-11612, United States Department of Energy, Interface Working Group on High-Level Waste Form Selection Factors, Washington, DC (1982).
9. J.B. Dunson, A.M. Eisenberg, and R.L. Schuyler, Du Pont Engineering Department, T.H. Gould, J.L. Butler, and J.B. Pickett, Savannah River Laboratory, Assessment of Processes, Facilities, and Costs for Alternative Solid Forms for Immobilization of SRP Defense Waste, DP-1625, Savannah River Laboratory, Aiken, SC (1982).

10. The Evaluation and Review of Alternative Waste Forms for Immobility of High-Level Radioactive Wastes, Report Number 3, DOE/TIC-11472, United States Department of Energy, Alternative Waste Form Peer Review Panel, Washington, DC (1981).
11. T.A. Bernadzkowski, ed., The Evaluation and Selection of Candidate High Level Waste Forms, USDOE/TIC-11611, National Technical Information Service, Springfield, VA (1982).
12. C. Sombret, "The Status of French High-Level Radioactive Wastes Solidification," p. 50 in The Treatment and Handling of Radioactive Wastes, A.G. Blasewitz, J.M. Davis and M.R. Smith, eds., Battelle Press, Columbus, OH (1983).
13. A Review of the Swedish KBS-II Plan for Disposal of Spent Nuclear Fuel, Committee on Radioactive Waste Management, Subcommittee for Review of the KBS-II Plan, Commission on Natural Resources, National Research Council, National Academy of Science, Washington, DC (1980).
14. N.J. Magnani and J.W. Braithwaite, "Corrosion-Resistant Metallic Canisters for Nuclear Waste Isolation," p. 377 in Scientific Basis for Nuclear Waste Management, Vol. 2, C.J.M. Northrup, Jr., ed., Plenum, New York (1980).
15. L.L. Hench, D.E. Clark, and J. Campbell, "High Level Waste Immobilization Forms," Nucl. Chem. Waste Management, 5, 149 (1984).
16. L.L. Hench, A. Lodding, and L. Werme, "Analysis of One Year In Situ Burial of Nuclear Waste Glasses in Stripa," p. 310 in Nuclear Waste Management, Advances in Ceramics, Vol. 8, G.G. Wicks and W.A. Ross, eds., American Ceramic Society, Columbus, OH (1984).
17. L.L. Hench, L. Werme, and A. Lodding, "Nuclear Waste Glass Interfaces after One Year Burial in Stripa, Part 3: Glass/Granite," J. Nucl. Materials, 126, 226 (1984).
18. L.L. Hench, L. Werme, and A. Lodding, "Nuclear Waste Glass Interfaces after One Year Burial in Stripa, Part 1: Glass/Glass," J. Nucl. Materials, 125, 273 (1984).
19. A. Lodding, L.L. Hench, and L. Werme, "Nuclear Waste Glass Interfaces after One Year Burial in Stripa, Part 2: Glass/Bentonite," J. Nucl. Materials, 125, 280 (1984).
20. L.L. Hench and M.J.R. Wilson, "Nuclear Waste Glass Interfaces after One Year Burial in Stripa, Part 4: Comparative Surface Profiles," J. Nucl. Materials, 136, 218 (1985).

21. L.L. Hench, A.R. Jurgenson, A. Lodding, and L. Werme, "Effect of Granite on Nuclear Waste Glass Surface Behavior," to be published in J. Nucl. Materials.
22. P.V. Iseghem, W. Timmermans, W. Debruyn, J. Dresselaers, and B. Neerdael, "In Situ Testing of Nuclear Waste Forms in an Underground Laboratory in Clay," to be published in Advances in Ceramics, 20.
23. Radioactive Glasses: Research and Testing, CEA Group, Paris (1982).
24. W.F. Merritt and P.J. Parsons, "The Safe Burial of High-Level Fission Product Solutions Incorporated into Glass," Health Phys., 10, 655 (1964).
25. W.F. Merritt, "High Level Waste Glass: Field Leach Tests," Nucl. Technol., 32, 88 (1977).
26. W.W. Fletcher, "The Chemical Durability of Glass, Progress Report on Burial Experiments at Ballidon and Warsham, England," unpublished (1974).
27. Materials Characterization Center, Nuclear Waste Materials Handbook, DOE/TIC-11400, Pacific Northwest Laboratory, Richland, WA (1981).
28. Materials Characterization Center, Materials Characterization Center Test Methods--Preliminary Version, PNL-3990, Pacific Northwest Laboratory, Richland, WA (1981).
29. M.J. Plodinec, C.M. Jantzen, and G.G. Wicks, "Thermodynamic Approach to Prediction of the Stability of Proposed Radiowaste Glasses," p. 491 in Nuclear Waste Management, Advances in Ceramics, Vol. 8, G.G. Wicks and W.A. Ross, eds., American Ceramic Society, Columbus, OH (1984).
30. R.G. Newton and A. Paul, "A New Approach to Predicting the Durability of Glasses from Their Chemical Compositions," Glass Technol., 21, 307 (1980).
31. R.C. Ewing, "Natural Glasses: Analogues for Radioactive Waste Forms," p. 57 in Scientific Basis for Nuclear Waste Management, Vol. 1, G.J. McCarthy, ed., Plenum, New York (1979).
32. C.M. Jantzen and M.J. Plodinec, "Thermodynamic Model of Natural, Medieval, and Nuclear Waste Glass Durability," J. Non-Cryst. Solids, 67, 207 (1984).

33. D.M. Strachan, "Results from a 1-Year Leach Test: Long-Term Use of MCC-1," p. 181 in Scientific Basis for Nuclear Waste Management, Vol. 5, W. Lutze, ed., Elsevier, New York (1982).
34. J.K. Bates, J.L. Daniel, and M.J. Steindler, "Extended Leach Studies of Actinide-Doped SRL 131 Glass," p. 183 in Scientific Basis for Nuclear Waste Management VI, Vol. 15, D.G. Brookins, ed., Elsevier, New York (1983).
35. D.M. Strachan, B.O. Barnes, and R.P. Turcotte, "Standard Leach Tests for Nuclear Waste Materials," p. 347 in Scientific Basis for Nuclear Waste Management, Vol. 3, J.G. Moore, ed., Plenum Press, New York (1981).
36. Final Report of the Defense High-Level Waste Leaching Mechanisms Program, PNL-5157 UC-70, Pacific Northwest Laboratory, Richland, WA (1984).
37. M.J. Plodinec, G.G. Wicks, and N.E. Bibler, An Assessment of Savannah River Borosilicate Glass in the Repository Environment, DP-1629, Savannah River Laboratory, Aiken, SC (1982).
38. L.L. Hench, "Survey Lecture for the XI Intl. Cong. Glass," p. 343 in Glass '77, A Survey of Contemporary Glass Science and Technology, J. Gotz, ed., Prague, Czechoslovakia (1977).
39. L.L. Hench and D.E. Clark, "Physical Chemistry of Glass Surfaces," J. Non-Cryst. Solids, 28, 83 (1978).
40. L.L. Hench, "Glass Surfaces--1982," J. Phys. Colloque, C9, Suppl., 625 (1982).
41. B. Grambow, "The Role of Metal Ion Solubility in Leaching of Nuclear Waste Glasses," p. 93 in Scientific Basis for Radioactive Waste Management, Vol. 6, W. Lutze, ed., Elsevier, New York (1982).
42. G.G. Wicks, Proceedings of Waste Management 1981 Conference, Tucson, AZ.
43. L.L. Hench and D.E. Clark, Surface Properties and Performance Prediction of Alternative Waste Forms, NUREG/CR-3472, Vol. 2, U.S. Nuclear Regulatory Commission, Washington, DC (1986).
44. B. Grambow, "A General Rate Equation for Nuclear Waste Glass Corrosion," p. 15 in Scientific Basis for Nuclear Waste Management VIII, Vol. 44, C.M. Jantzen, J.A. Stone, and R.C. Ewing, eds., Materials Research Society, Pittsburgh, PA (1985).



45. P. Aagaard and H.C. Helgeson, "Thermodynamic and Kinetic Constraints on Reaction Rates among Minerals and Aqueous Solutions. I. Theoretical Considerations," Am. J. Sci., 282, 237 (1982).
46. R. Adiga, "Leaching Behavior of Nuclear Waste Glass under Laboratory Simulated Repository Conditions," Master's Thesis, University of Florida, Gainesville, FL (1984).
47. B. Grambow, H.P. Hermansson, I.K. Björner, H. Christensen, and L. Werme, "Reaction of Nuclear Waste Glass with Slowly Flowing Solutions," to be published in Advances in Ceramics, 20, American Ceramic Society, Columbus, OH (1987).
48. G.G. Wicks, B.M. Robnett, and W.E. Rankin, "Chemical Durability of Glass Containing SRP Waste-Leachability Characteristics, Protection Layer Formation, and Repository System Interactions," p. 15 in Scientific Basis for Nuclear Waste Management, Vol. 5, W. Lutze, ed., Elsevier, New York (1982).
49. D.E. Clark and C.A. Maurer, "Waste Glass/Repository Interactions," p. 71 in Scientific Basis for Nuclear Waste Management, Vol. 5, W. Lutze, ed., Elsevier, New York (1982).
50. H.P. Hermansson, H. Christensen, D.E. Clark, and L. Werme, "Effects of Solution Chemistry and Atmosphere on Leaching of Alkali Borosilicate Glass," p. 143 in Scientific Basis for Nuclear Waste Management, Vol. 6, D.G. Brookins, ed., Elsevier, New York (1983).
51. G. Malow, "The Mechanisms for Hydrothermal Leaching of Nuclear Waste Glasses: Properties and Evaluation of Surface Layers," p. 347 in Scientific Basis for Nuclear Waste Management, Vol. 5, W. Lutze, ed., Elsevier, New York (1982).
52. T.D. Chickalla and J.A. Powell, Nuclear Waste Management Quarterly Progress Report, Oct.-Dec. 1980, PNL-3000-8/4C-70, Pacific Northwest Laboratory, Richland, WA (1981).
53. D. Savage and J.E. Robbins, "The Interaction of Borosilicate Glass and Granodiorite at 100°C, 50 MPa: Implications for Models of Radionuclide Release," p. 145 in Scientific Basis for Nuclear Waste Management, Vol. 5, W. Lutze, ed., Elsevier, New York (1982).
54. G.L. McVay and C.Q. Buckwalter, "Effect of Iron on Waste-Glass Leaching," J. Am. Ceram. Soc., 66, 170 (1983).
55. G.L. McVay and L.R. Pederson, "Effects of Gamma Radiation on Glass Leaching," J. Am. Ceram. Soc., 64, 154 (1981).



56. G.L. McVay, W.J. Weber and L.R. Pederson, "Effects of Radiation on the Leaching Behavior of Nuclear Waste Forms," Nucl. Chem. Waste Manage., 2, 103 (1981).
57. Japanese, Swiss and Swedish Project (JSS) Report Phase I: A Summary of Work Performed at Studvik Energiteknik AB and at Swiss Federal Institute for Reactor Research (EIR), 84-03, Swedish Nuclear Fuel and Waste Management Co., Stockholm, Sweden (1984).
58. Geological Disposal of Radioactive Waste, In Situ Experiments in Granite, Proceeding of the Nuclear Energy Agency Workshop, Stockholm, Sweden (1982).
59. A. Olkiewicz, J.E. Gale, R. Thorpe, and B. Paulsson, "Geology and Fracture System at STRIPA," Swedish-American Cooperative Program on Radioactive Waste Storage in Mined Caverns in Crystalline Rock, LBL-8907, SAC-21, Lawrence Berkeley Laboratory, Berkeley, CA (1979).
60. P. Fritz, J.F. Barker, and J.E. Gale, "Geochemistry, Origin, and Age of Groundwater in the Stripa (Sweden) Test Mine," p. 543 in Scientific Basis for Nuclear Waste Management, Vol. 2, C.J.M. Northrup, Jr., ed., Plenum Press, New York (1980).
61. D.E. Clark, B.F. Zhu, R.S. Robinson, and G.G. Wicks, "Preliminary Report on a Glass Burial Experiment in Granite," p. 324 in Advances in Ceramics, Vol. 8, G.G. Wicks and W.A. Ross, eds., American Ceramics Society, Columbus, OH (1984).
62. G.G. Wicks, WIPP/SRL In-Situ and Laboratory Testing Programs-- Part 1: MIIT Overview, Non-radioactive Waste Glass Studies, DP-1706, UC-70, Savannah River Laboratory, Aiken, SC (1985).
63. L.L. Hench, D.B. Spilman, and A.D. Buonaquisti, "Rutherford Back Scattering Surface Analysis of Nuclear Waste Glasses after One Year Burial in Stripa," Nuclear Chem. Waste Management, 5, 75 (1984).
64. D.E. Clark, C.G. Pantano, Jr., and L.L. Hench, Corrosion of Glass, Magazines for Industry, Inc., New York (1979).
65. S.A. Anderson, "Investigation of Structure of Glasses by Their Infrared Reflection Spectra," J. Am. Ceram. Soc., 33, 45 (1950).
66. L.L. Hench and D.E. Clark, "Physical Chemistry of Glass Surfaces," J. Non-Cryst. Sol., 28, 83 (1978).
67. D.M. Sanders, W.B. Person, and L.L. Hench, "New Methods for Studying Glass Corrosion Kinetics," Appl. Spectrosc., 26, 530 (1972).

68. D.M. Sanders, "Structure and Kinetics of Glass Corrosion," Ph.D. Dissertation, University of Florida, Gainesville, FL (1973).
69. D.M. Sanders and L.L. Hench, "Mechanisms of Glass Corrosion," J. Am. Ceram. Soc., 56, 373 (1973).
70. A. Lodding, D.E. Clark, E.U. Eugstrom, L. Werme, and G.G. Wicks, "SRL Glass Leached in Burial Environment: SIMS Study of Element Distributions," to be published in Advances in Ceramics, 20.
71. W.K. Chu, J.W. Mayer, and M.-A. Nicolet, Backscattering Spectrometry, Academic Press, New York (1978).
72. W.D. Mackintosh, "Rutherford Scattering," p. 403 in Characterization of Solid Surfaces, P.F. Kane and G.B. Larrabee, eds., Plenum Press, New York (1974).
73. Powder Diffraction File, Card No. 19-629, Joint Committee on Powder Diffraction Standards, Swarthmore, PA.
74. Powder Diffraction File, Card No. 24-72A, Joint Committee on Powder Diffraction Standards, Swarthmore, PA.
75. Powder Diffraction File, Card No. 10-325, Joint Committee on Powder Diffraction Standards, Swarthmore, PA.
76. A. Paul, "Chemical Durability of Glasses: A Thermodynamic Approach," J. Mater. Sci., 12, 2246-2268 (1977).
77. R.K. Iler, The Chemistry of Silica, John Wiley & Sons, Inc., New York (1979).
78. D.E. Clark, H. Christensen, H.P. Hermanson, S.B. Sundvall, and L. Werme, "Effects of Flow on Corrosion and Surface Film Formation on an Alkali Borosilicate Glass," p. 19 in Advances in Ceramics, Vol. 8, G.G. Wicks and W.A. Ross, eds., American Ceramic Society, Columbus, OH (1984).
79. D.E. Clark, A. Lodding, H. Odellius, and L. Werme, "Elemental Analysis of Swedish Nuclear Waste Glasses: Leachability vs. Composition," accepted for publication in J. Mater. Sci. Eng.
80. M.F. Dillmore, D.E. Clark, and L.L. Hench, "Chemical Durability of  $\text{Na}_2\text{O-K}_2\text{O-CaO-SiO}_2$  Glasses," J. Am. Ceram. Soc., 61, 439 (1978).
81. J.R. Hendrickson and P.J. Bray, "A Theory for the Mixed Alkali Effect in Glasses. Part 1," Phys. Chem. Glasses, 13, 43 (1972).

82. M.G. Fontana and N.D. Greene, Corrosion Engineering, McGraw-Hill, New York (1978).
83. B.F. Zhu, D.E. Clark, L.L. Hench, G.G. Wicks, and L. Werme, "One-Year Leaching of Three SRL Glasses in Granite," p. 187 in Scientific Basis for Nuclear Waste Management VIII, Vol. 44, C.M. Jantzen, J.A. Stone, and R.C. Ewing, eds., Materials Research Society, Pittsburgh, PA (1985).
84. W.J. McCracken, D.E. Clark, and L.L. Hench, "Aqueous Durability of Lithia-Disilicate Glass Ceramics," J. Am. Ceram. Soc., 61, 1218 (1981).
85. K.H. Sun, "Fundamental Conditions of Glass Formation," J. Am. Ceram. Soc., 30, 277 (1947).
86. A. Paul and D. Cooke, "Chemical Stability of Boron-Containing Glass Enamels with Special Reference to Lead Release," p. 509 in Proceedings of the Conference on Boron in Glass and Glass Ceramics, Materials Research Society, Vol. 12, L.D. Pye, V.D. Frechette, and N.J. Kreidl, eds., Plenum Press, New York (1978).
87. B.E. Schaetz, W.P. Freeborn, D.K. Smith, C. Anderson, M. Zolensky, and W.B. White, "The Role of Boron in Monitoring the Leaching of Borosilicate Glass Waste Forms," p. 129 in Scientific Basis for Nuclear Waste Management VIII, Vol. 44, C.M. Jantzen, J.A. Stone, and R.C. Ewing, eds., Materials Research Society, Pittsburgh, PA (1985).
88. L.D. Pye, V.D. Fréchet, and N.J. Kreidl, eds., Borate Glasses, Structure, Properties, Applications, Materials Science Research, Vol. 12, Plenum, New York (1978).
89. Long-Term Performance of Materials Used for High-Level Waste Packaging, NUREG/CR-3900/ BMI-2127, Vol. 4, Battelle's Columbus Laboratories, Columbus, OH (1985).
90. J.W. Shade, L.R. Pederson, and G.L. McVay, "Waste Glass-Metal Interactions in Brines," p. 358 in Advances in Ceramics, Vol. 8, G.G. Wicks and W.A. Ross, eds., American Ceramic Society, Inc., Columbus, OH (1984).
91. L. Zagar and L. Schillmoeller, "Ueber die physikalisch-chemischen Vorgaenge bei der Wasserauslaugung von Glasoberflaechen," Glastechn. Ber., 33, 109 (1960).
92. A.A. Hench and L.L. Hench, "Computer Analysis of Compositional Effects in Nuclear Waste Glass Leaching," to be published in Nucl. Chem. Waste Manage.

93. G.G. Wicks, W.D. Rankin, and S.L. Gore, "International Waste Glass Study--Composition and Leachability Correlations," p. 171 in Scientific Basis for Nuclear Waste Management VIII, Vol. 44, C.M. Jantzen, J.A. Stone, and R.C. Ewing, eds., Materials Research Society, Pittsburgh, PA (1985).
94. M.B. Robnett and G.G. Wicks, Effect of Devitrification on the Leachability of High-Level Radioactive Waste Glass, DP-MS-81-60, Savannah River Laboratory, Aiken, SC (1981).
95. C.M. Jantzen, D.F. Bickford, and D.G. Karraker, "Time-Temperature-Transformation Kinetics in SRL Waste Glass," p. 30 in Advances in Ceramics, Vol. 8, G.G. Wicks and W.A. Ross, eds., American Ceramic Society, Columbus, OH (1984).
96. C.M. Jantzen and D.F. Bickford, "Leaching of Divitrified Glass Containing Simulated SRP Nuclear Waste," p. 135 in Scientific Basis for Nuclear Waste Management VIII, Vol. 44, C.M. Jantzen, J.A. Stone, and R.C. Ewing, eds., Materials Research Society, Pittsburg, PA (1985).
97. N.E. Bibler, "Characterization of Borosilicate Glass Containing Savannah River Plant Radioactive Waste. 2. Microstructure and Durability," Glasstechn. Ber., 56K, 736 (1983).
98. L.L. Hench and D.E. Clark, Surface Properties and Performance Prediction of Alternative Waste Forms, NUREG/CR-3472, Vol. 2, U.S. Nuclear Regulatory Commission, Washington, DC (1986).

## BIOGRAPHICAL SKETCH

BingFu Zhu was born June 22, 1946, in Shanghai, China. He received his elementary education in Shanghai and was graduated from Xianming Middle School in 1962. He entered the East China University of Chemical Technology, Shanghai, in September 1962, and received his diploma from the Department of Inorganic Industry in September 1968.

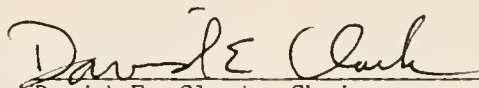
He was an engineer in Wanshan Cement Works, China, from September 1968 through September 1975. Subsequently, he joined the faculty of the Department of Silicate Technology, Wuhan Institute of Building Materials, China, for 3 years. In September 1978, he returned to the East China University of Chemical Technology to pursue an M.S. in glass science and received the degree from the Department of Inorganic Materials in February 1982. In March 1982, he entered the University of Florida to start working for a Ph.D. in materials science and engineering.

He has published papers on chemical strengthening of glasses and glass corrosion. He is a member of American Ceramic Society and National Institute of Ceramic Engineers.

He married JiSi Wang on October 14, 1981.



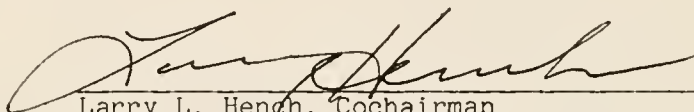
I certify that I have read this study and that in my opinion it conforms to acceptable standards of scholarly presentation and is fully adequate, in scope and quality, as a dissertation for the degree of Doctor of Philosophy.



---

David E. Clark, Chairman  
Professor of Materials Science and  
Engineering

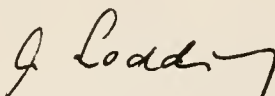
I certify that I have read this study and that in my opinion it conforms to acceptable standards of scholarly presentation and is fully adequate, in scope and quality, as a dissertation for the degree of Doctor of Philosophy.



---

Larry L. Hench, Cochairman  
Graduate Research Professor of Materials  
Science and Engineering

I certify that I have read this study and that in my opinion it conforms to acceptable standards of scholarly presentation and is fully adequate, in scope and quality, as a dissertation for the degree of Doctor of Philosophy.



---

Alexander Lodding  
Professor of Materials Physics, Chalmers  
Institute of Technology, Sweden

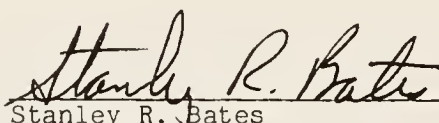
I certify that I have read this study and that in my opinion it conforms to acceptable standards of scholarly presentation and is fully adequate, in scope and quality, as a dissertation for the degree of Doctor of Philosophy.



---

Christopher D. Batich  
Associate Professor of Materials Science  
and Engineering

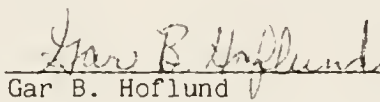
I certify that I have read this study and that in my opinion it conforms to acceptable standards of scholarly presentation and is fully adequate, in scope and quality, as a dissertation for the degree of Doctor of Philosophy.



Stanley R. Bates

Associate Engineer of Materials Science  
and Engineering

I certify that I have read this study and that in my opinion it conforms to acceptable standards of scholarly presentation and is fully adequate, in scope and quality, as a dissertation for the degree of Doctor of Philosophy.



Gar B. Hoflund

Professor of Chemical Engineering

This dissertation was submitted to the Graduate Faculty of the College of Engineering and to the Graduate School and was accepted as partial fulfillment of the requirements for the degree of Doctor of Philosophy.

May 1987



Dean, College of Engineering

\_\_\_\_\_  
Dean, Graduate School



UNIVERSITY OF FLORIDA



3 1262 08554 1695